



Università degli Studi di Torino

Doctoral School of the University of Torino

PhD Programme in Technology Driven Sciences for Cultural Heritage:

T4C XXXIV Cycle

**Comprehensive Archaeometric Study of Ayla-
Aksum Amphorae from Adulis, Red Sea Coast of
Eritrea**

www.tech4culture.unito.it



TABLE OF CONTENTS

1. Introduction	9
2. Overview of Pottery Materials.....	13
2.1. Clay and Pottery Materials.....	13
2.2. Bibliography.....	17
3. Overview of Ceramic Archaeometry and Research Questions.....	24
3.1. Themes on Archaeometric Study of Pottery	25
3.1.1. The Question of Typological Classification.....	25
3.1.2. Themes on Provenance.....	26
3.1.3. Themes On Technology of Production.....	32
3.1.4. Themes on Use.....	35
3.2. Research Questions.....	39
3.2.1. Sampling.....	41
3.3. Bibliography.....	46
4. Archaeological and Geological Context.....	53
4.1. Archaeological Context.....	53
4.1.1. The Archaeological site of Adulis.....	53
4.1.2. The Archaeological site of Zafar.....	56
4.1.3. The Archaeological site of Ayla.....	57
4.2. Geological Context.....	58
4.3. Bibliography.....	60
5. Provenance.....	64
5.1. Materials and Methods.....	64
5.1.1. Optical Microscopy (OM).....	64
5.1.2. Scanning Electron Microscopy- with Energy Dispersive X-ray Analysis (SEM-EDX)	64

5.1.3. Inductively Coupled Plasma- Optical Emission Spectrometry (ICP-OES)	65
5.2. Results and Discussion.....	67
5.2.1. Petrographic Observations.....	67
5.2.1.1. Ayla-Aksum Amphorae.....	67
5.2.1.2. Late Roman Amphora 1.....	70
5.2.1.3. Late Roman Amphora 1(?).....	71
5.2.1.4. Local Pottery and Clayey Materials.....	73
5.2.1.5. Dolia.....	78
5.2.1.6. Red Slipped Ware.....	79
5.2.1.7. Undetermined Class.....	79
5.2.2. Areal Micro-chemical analysis of Ceramic Bodies by SEM-EDX.....	81
5.2.3. ICP-OES.....	84
5.3. Archaeological Implications.....	97
5.4. Bibliography.....	99
6. Technology of Production.....	101
6.1. Materials and Methods.....	101
6.1.1. Sampling.....	101
6.1.1. Analytical Methods.....	102
6.1.2.1. X-ray Powder Diffraction (XRPD).....	102
6.1.2.2. Scanning Electron Microscopy (SEM).....	102
6.2. Results and Discussion.....	103
6.2.1. SEM-Micro-structural Features.....	103
6.2.2. XRPD Phase Analysis.....	118
6.3. Archaeological Implications.....	128
6.4. Bibliography.....	129
7. Organic Residues Analysis.....	131
7.1. Materials and Methods.....	131

7.1.1. Sampling.....	131
7.1.2. Analytical Methods.....	132
7.1.2.1. Fourier Transform- InfraRed (FT-IR)	132
7.1.2.2. Gas Chromatography- Mass Spectrometry (GC-MS)	133
7.2. Results and Discussion.....	134
7.2.1. FT-IR Analysis.....	134
7.2.2. GC-MS.....	137
7.3. Archaeological Implications.....	143
7.4. Bibliography.....	144
8. Conclusions.....	146
Appendix 1. Photos of Samples Considered in the Study.....	151
Appendix 2. Drawings of Representative Samples.....	155
Appendix 3. List of Samples and Analytical Methods Applied.....	157
Appendix 4. The Petrographic Information of studied potsherds and briquettes	160
Appendix 5. Photomicrographs from Petrographic Observations	161
Appendix 6. XRPD Data of Representative Samples	168
Appendix 7. BSE SEM Images of Polished Thin Sections	176
Appendix 8. SEM Images of Fractures.....	181
Appendix 9. FT-IR Spectra of Extracts	185
Appendix 10. SEM-EDX Chemical Data on the Bulk.....	192
Appendix 11. SEM-EDX Chemical Data on the Matrices.....	193
Appendix 12. ICP-OES Data of Major, Minor and Trace Elements.....	194
Appendix 13. Information on Loss of Ignition (L.O.I.) of Samples.....	197
Appendix 14. Appendix 12: ICP Data on Certified Materials.....	200

List of Abbreviations and Acronyms

LRA1- Late Roman Amphora 1

ND- Undetermined

XPL- Cross- Polarised Light

PPL- Plane-Polarized Light

FTIR – Fourier Transform InfraRed (Spectroscopy)

CV- Continuous Vitrification

GC-MS- Gas Chromatography- Mass Spectrometry

ICP-OES – Inductively Coupled Plasma Optical Emission Spectrometry

IV- Initial Vitrification

LOD – Limit of Detection

LO I.- Loss of Ignition

NV- Non-Vitrified

OM – Optical Microscopy

PCA – Principal Component Analysis

PPM- Parts Per Million

REE – Rare Earth Element

SD – Standard Deviation

SEM-EDX – Scanning Electron Microscopy with Energy Dispersive X-Ray Analysis

XRPD – X-Ray Powder Diffraction

BSE- Back-Scattered Electrons

SE- Secondary Electrons

Acknowledgements

A word of gratitude is extended to several people and institutions from the planning of this study to supervision of the PhD study and mentorship from different expertise. I would like to express my deepest gratitude first for the Commissioner of Culture and Sports of the State of Eritrea, H.E. Ambassador Zemedede Tekle, for endorsing the PhD project and providing significant assistance in terms of the bureaucratic support from the government of Eritrea. The facilitation from Dr. Tsegai Medin, head of Archaeological Heritage Research branch at the Commission of Culture and Sports of Eritrea and Mr. Yohannes Gebreyesus, Director of Culture in the Northern Red Sea Region of Eritrea, during the fieldwork and authorisation of the export of samples for my research is also greatly appreciated. The support from Eastern Desert Research Centre (Ce.R.Do.) under the scientific coordination of prof. Serena Massa is equally acknowledged. I would also like to thank the Office of the Executive Director of the National Higher Education & Research Institute (NHERI) of the State of Eritrea for their facilitation during the PhD study.

In terms of the scientific work, which involved supervision and mentorship from a wider multidisciplinary expertise, I would first like to thank my supervisor prof. Alessandro Lo Giudice for arranging such a platform and guiding me in all aspects related to planning the laboratory analysis, secondment visits and dissemination of the research results. The support and mentorship from prof. Monica Gulmini and Dr. Patrizia Davit (Department of Chemistry, University of Turin) and prof. Lara Maritan (Department of Geosciences, University of Padua) encompassed their wide-ranging expertise in the study of pottery materials, and I highly value their expertise, patience, and time to help me learn the different aspects in the archaeometric study of pottery. The much-needed support from prof. Serena Massa (Catholic University of Milan) in arranging field work campaigns, selection of samples and helping refine the archaeological context of the study is highly appreciated. The help provided by prof. Roberto Giustetto (Department of Earth sciences, University of Turin) in terms of X-ray Diffraction analysis is also greatly acknowledged. I would also like to thank prof. Ericka Ribeckini and prof. Jannette Lucejko (Department of Chemistry and Analytical Chemistry, University of Pisa) and Dr. Anna Piccirilo (Conservation and restoration Center La Venaria Reale), for providing all the data and information on organic residue analysis. The support from prof. Alessandro Re (Department of Physics, University of Turin) in terms of assistance

in supervision, Dr. Laura Guidorzi (Department of Physics, University of Turin) who helped me in the treatment of geo-chemical data with statistical tools and interpretation, and archaeologist Chiara Mandelli, whose indispensable help in the typological classification of imported pottery at Adulis are also acknowledged. Each of these colleagues have contributed to the writing of the thesis through their respective expertise.

Finally, a mention of gratitude to the assistance from Leonardo Tauro (Department of Geosciences, University of Padua) and Nadia Curetti (Department of Earth Sciences, University of Turin) in their respective laboratories is essential.

On a personal note, I would like to thank my parents and family as well as my friends for their support during this marathon but stimulating experience.

Abstract

Current archaeological excavations in the ancient port of Adulis, on the Red Sea coast, in present-day Eritrea have yielded a large *corpus* of imported and local pottery. These wares come from contexts dated from the 5th to the 7th century CE, during which this port was intensely occupied. Imported pottery from the Eastern Mediterranean, the Levant, Indian Ocean and Arabian Peninsula dominated the assemblages, testifying the importance of the site in inter-regional trade. Moreover, a local pottery production also flourished, equally significant to understand the culture- history of the site. At present, only scarce archaeometric information is available about the pottery assemblages excavated from Adulis. The main focus of this research is on the ‘Ayla-Aksum’ amphorae – dominating the Adulis assemblages – which have been investigated here with a multi-analytical archaeometric approach, together with local pottery, Late Roman Amphora 1, *dolia* samples, and slipped ware.

Petrographic, Scanning Electron Microscopy with Energy Dispersive X-ray Analysis and Inductively Coupled Plasma -Optical Emission Spectrometry analyses allowed the distinction of fabrics and compositional groups, significant to provide information on the provenance and helpful in completing the ceramic sequence at Adulis. Moreover, data from mineralogical (X-ray Powder Diffraction) and micro-structural (Scanning Electron Microscopy) viewpoints are discussed to highlight different technologies of production and micro-structural features relevant to complement information on provenance in as much as a discussion on organic residue analysis on some samples by Fourier Transform InfraRed Spectroscopy (FT-IR) and Gas Chromatography Mass Spectrometry (GC-MS). By considering the typological classification presented in this study, corroborated by mineralogical and geo-chemical information, this research represents the first comprehensive archaeometric investigation of pottery assemblages from Adulis.

1. Introduction

The reconstruction of different aspects of pottery production, distribution, or consumption provides the basis for interpretation of the behaviour of the people who produced, distributed, or used the pottery in the past. The archaeometric questions ultimately reside on tackling how pottery production or distribution was organised and the driving reason/s for technological innovation and technological choice/s and thus require a scientific paradigm to understand different scales of social processes.

The role of physical sciences in the reconstruction of the provenance, technologies of pottery production, use and their distribution is a well-established frontier in as much as the development of multi-disciplinary paradigm together with archaeologists to tackle these questions. A full account of the cultural and environmental processes which contribute to the pottery life cycle attest to the different stages of the chaîne opératoire and are, therefore, intertwined in the archaeometric research. Embarking from these premises, the essay discusses how archaeometric approaches can help build the ceramic sequence for the archaeological site of Adulis on the Red Sea Coast of Eritrea by emphasising the need to corroborate traditional archaeological methods with the state-of-the art permeating different avenues of the physical sciences.

A large corpus of pottery assemblages has been recovered from excavations at the archaeological site of Adulis, on the Red Sea coast of Eritrea. Adulis was the most important port for trade in the northern Horn of Africa during antiquity linking the early urban settlements of the Eritrean and Ethiopian highlands and of the coastal people (Peacock and Blue 2007; Zazzaro *et al* 2014).

The discussion on local versus imported pottery has become prevalent in the archaeological research at Adulis while the development of ceramic sequence constitutes a great deal of the current studies on the site. Levantine ceramic forms, and particularly the Ayla-Aksum amphora represent the most tangible evidence of the trade contacts of Adulis with major ports in the Red Sea world in Late antiquity. The wider distribution of these amphorae over the Red Sea has compelled some researchers to postulate, perhaps other production centres elsewhere than Ayla in the present-day Jordan. The Ayla-Aksum amphorae contribute to the

debate on local versus imported pottery at Adulis and are, therefore, studied here from archaeometric perspectives.

Other pottery classes which include Late Roman Amphora 1, *dolia* and the red slipped ware represent the wider classes of Levantine and Indian Ocean varieties found at Adulis and are also studied to provide comparative parallels in as much as the pottery representing local production at Adulis. These pottery classes attest to the most tangible evidence of ancient trade involving the archaeological site of Adulis. The knowledge of mineralogical composition and chemical tracers can shed light into provenance, ancient exchange networks and towards understanding cycles in raw materials exploitation strategies that perhaps include changes in the exploitation of clay deposits during occupation at the site.

In this respect, the main goal of this study is the characterization of a group of Ayla-Aksum Amphora from Adulis together with local pottery, Late Roman Amphora 1, *dolia* and red slipped ware based on chemical and mineralogical information. The study of organic residues on a set of samples presumed to be Late Roman Amphora 1 (?) from macroscopic observations was also included in the research to facilitate their proper identification and provenance. In these samples secure identification of the typology was limited due to a few diagnostic attributes and the combination of petro-mineralogical, geochemical, and organic residue studies proved crucial to advance their classification. A multi analytical approach which includes the study of mineralogical composition through Optical microscopy (petrography) and X-ray Powder diffraction as well as chemical composition via Inductively Coupled Plasma-Optical Emission Spectrometry and Scanning Electron Microscopy with Energy Dispersive X-ray Analysis has been integrated for purposes of this study. Moreover, Fourier Transform Infrared Spectroscopy (FT-IR) and Gas Chromatography Mass Spectrometry (GC-MS) have been used for the characterization of organic residues.

The thesis is divided into sections where subsequent chapters have been framed to provide insight into the conceptual and methodological foundations as well as the results and discussions drawn from the study. The emphasis on the archaeological and geological contexts, on the other hand, is provided in a way to highlight the significance of Adulis by providing parallels from sites in the Red Sea world and to provide a comprehension of the availability of potential raw materials or geological basins for pottery production respectively. Similarly, a synopsis into the major themes around ceramic materials, the complexities of typological classification, the provenance postulate, technology of production

and pottery use considering the coating materials on ancient ceramics, is given in the subsequent chapters of the essay to make sense of the issues constituted in archaeometric study of pottery.

A departure from what merits a complete typological classification lays the basis to assess how the subject should be dealt in building a ceramic sequence in a site as complex as Adulis, where the production of what can be termed as “local pottery” is found together with a variety of imported transport and common wares from across the Red Sea world and wider Eastern Mediterranean and Indian ocean, often poses a complexity. A great deal of the samples considered for the study have been attributed to specific typological classes on the basis of diagnostic features while, on the other hand, superficial resemblance of fabrics macroscopically yielded difficulties and deficiencies to securely link them to a specific typological attribution. In this respect, it can be said that the archaeometric approach becomes a crucial component to the definition of fabrics combining macroscopic observations and petro-mineralogical and geo-chemical studies.

Moreover, different approaches to tackle provenance are outlined, in order to provide a glimpse into how different postulates can be related to the human component behind ceramic production and use. The mere fact that data from mineralogical and geo-chemical studies needs to consider a variety of aspects linked to cultural processes and human behaviour is highlighted by integrating different levels of the provenance postulate. The rationale to use different statistical tools to treat data in light of the aforementioned aspects of cultural processes is equally interweaved to formulate the conceptual framework of this work. On a similar account, the need to incorporate micro-structural studies as well as phase identification analytical approaches is justified to corroborate information on provenance by exploring different aspects related to the technology of production of ceramics.

The rationale for organic residues analysis is further postulated to make sense of how such an information can be utilized to complement information on provenance and technology of production and thus constituted a major part of the work. In this respect, it is highlighted in that an overview of provenance, technology of production and patterns of ceramic use can be integrated in a multi-analytical approach in an attempt to formulate the basis of building a ceramic sequence at Adulis.

Similarly, subsequent chapters highlight the catalogue of samples chosen for the study and the analytical methods adopted on one hand, and the results on provenance, technology of

production and use on the other. The chapters on the results of this study are framed to treat the information in light of specific themes and the concomitant analytical methods to extract data relevant for each specific theme addressed. The delimitation of the future directions of research to complete the ceramic sequence at Adulis is also drawn by highlighting the gaps that exist and the potential venues that can be explored

2. Overview on Pottery Materials

Pottery is certainly a key material in the archaeological heritage. In archaeological sites, pottery findings are considered the most important source of information due to their large distribution. Pottery production is one of the most ancient industries and the invention of pottery is the learning result of two main processes: the handling of clay and its transformation by means of fire (Rye 1981; Rice 1987).

Archaeological pottery sherds contain three categories of mineral phases: (1) primary minerals are linked to the clay source, are present in the original clay body and remain in the sherd after the firing and deposition processes; (2) firing phases form from reactions that occur during the firing process; and (3) secondary minerals form when the sherd is subjected to burial or other use and post-use processes (Rye 1981; Orton and Hughes 2013).

2.1. Clay and Pottery

Archaeological potteries are made from a circumstantial or deliberately prepared mixture of clay, other solid materials known by the generic name of fillers or temper, and water. When a wet mixture of clay and fillers is formed into a desired shape, then dried and finally heated to high temperature (above 600°C), it becomes consolidated into pottery. In every ceramic manufacture, potters learned empirically which clays yield the best result as a ceramic, then passing on their experience as a cultural teaching process. Irrespective of how specialised, the issue of prospecting and collecting good clay is of major importance (Rye 1981; Sillar and Tite 2000; Roux 2017).

Clays which form the primary component of pottery, evokes the knowledge of humans of the properties of earthy materials. The usage of the term clay is often made in reference to a clay source, clay body, or clay mineral and accordingly definitions of the term account for the characteristics of depositional situation, granulometry, chemical composition and mineralogy (Rice, 1987; Wagner and Hermann 2009; Gualtieri 2020; Eramo 2020).

Clay minerals are viewed as components of sedimentary deposits and comparatively recent accumulations of weathering and disintegration products of parent rocks (Pollard and Heron

2008; Gualtieri 2020). In this respect, the depositional situation of clays (location of decomposed material relative to the parent rock) allows their classification as primary or secondary clays. The knowledge of the parent rock/s from which the primary clays are derived, particularly allows attribution to a geological context that in turn can give clues for shed light into provenance studies.

Similarly, a granulometric definition of clays entails a particle size grade concomitant of specific particle-size range (Pollard and Heron 2008; Rice 1987). Accordingly, clays refer to particles smaller than 2 micrometres in diameter.

Chemically, clays are the end-product of weathering of silicate rocks and can therefore be represented as primarily composed of silica and alumina (Goffier 2007; Pollard and Heron 2008). Most clays are also described as hydrous aluminium silicates and the relative percentage of the chemical formula (alumina, silica, and water) varies considerably in different types of clays. Iron and aluminium hydrous oxides also fall into the frame of a chemical definition of clays.

Mineralogically, clay minerals or mineral groups fall into a category of layered silicates or phyllosilicates. The phyllosilicates consist of a regular ordering of layers of silica and alumina structural components. Differences in the arrangement of the layers as well as substitutions of aluminium and silicon by various cations provide the basis for classification of clay minerals (Pollard and Heron 2008; Neese 2000). Accordingly, kaolinite and halloysites are two layered clays, having a layer of silica tetrahedrons and a layer of alumina octahedrons. Illites as well as smectites and vermiculites on the other hand belong to three-layer clays where one layer of alumina octahedrons is sandwiched between two sheets of silica tetrahedrons. The chlorite group constitutes another sub-division where alternating layers of different types are stacked on top of each other (Goffier 2007).

The clay minerals have the property of being able to exchange certain cations and anions in an aqueous solution (Goffier 2007; Pollard and Heron 2008). The commonest exchangeable cations are Ca^{2+} , Na^+ , K^+ , Mg^{2+} , and H^+ . Ion exchange is important because the physical properties of clay materials frequently depend on the exchangeable ions carried by the clay.

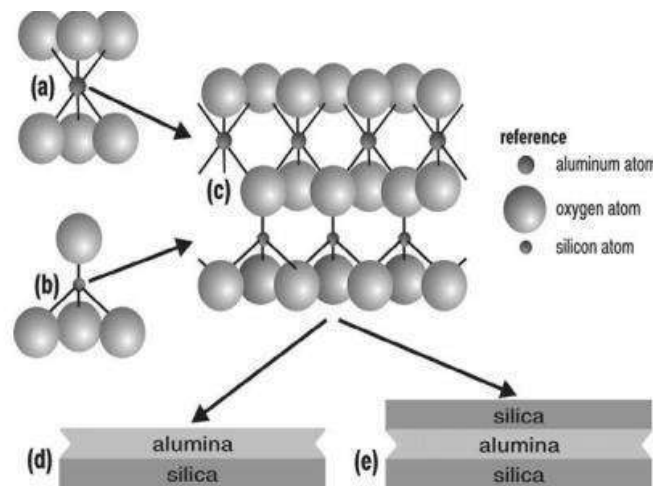


Fig. 4.1 The structure of clays.

Clays are the end products of the weathering of rocks and minerals; their main components include silicon and aluminum, within an octahedral coordination by oxygen (a), the silicon is in a tetrahedral coordination (b). Structural studies show that in most clays the silicon and aluminum are arranged in layers superposed on each other: atoms of oxygen of are shared by the superposed layers (c). The distinctive character of each different clay is due to cations of sodium, potassium, calcium, or magnesium occupying positions in and between the sheets. Kaolinite and halloysite, two clays that are suitable for making ceramic materials, have a two-layer (also designated as 1:1) structure, in which one layer of alumina is bound to one of silica (d). Other clays have a three-layer (or 2: 1) structure, made up of one layer of alumina between two of silica (e). (Goffier, 2007).

Figure1: The Structure of Clays (Goffier 2007)

For a particular clay/s used in ceramic production, it should be workable and plastic. The addition of water to dry clay produces a clay–water mixture that, within a narrow range of water content, has *plastic properties* (Rice 1987; Eramo 2020; Gualtieri 2020). Wet clay mixtures can, therefore, be modelled, molded, or otherwise made to acquire a shape that will be retained after the forming operations. Water-poor mixtures are not plastic, however, and excess water results in mixtures, known as *slips*, that are too fluid to retain a shape (Rye 1981; Eramo 2020; Gualtieri 2020). The plasticity of clay–water mixtures is due principally to three factors: the crystal structure of clay minerals, the shape of the clay particles and their small size (Gualtieri, 2020). In general, clays need to be suitable to be shaped and thus workable and this is attained by plasticity among other factors. The paste refers to the end product of the compositional/textural processing and homogenization applied to the starting

clay (Gualtieri 2020; Eramo 2020). If unsatisfactory in the natural state, clays should be processed to meet expected physical characteristics, that is workability, drying shrinkage, firing behaviour and firing properties (Rye 1981; Orton and Hughes 2013). Several ethnographic cases have demonstrated that clay mixing was done to change clay properties and/or colour (De Boer and Lathrap 1979; Rice 1987; Matson 1989; Gualtieri 2020; Eramo 2020). On the other hand, the mixing of two or more clays of different composition and texture to form a paste was done to improve workability and firing behaviour of the single clays. The processing choices, as well as other techno-functional traits, are the results of a tradition of learning from avoiding failures in the different stages in manufacturing, handed down from one generation to the next (Gosselain and Livingstone Smith 2005; Fowler 2017). A suitable paste recipe is, thus attained through material subtraction, addition and homogenisation (see Eramo 2020 for detailed discussion).

The other essential component of most wet clay mixtures are the *non-clay materials*, which are also known by a variety of other names, such as *fillers*, *non-plastic fillers*, *non-plastic materials*, *inclusions*, *temper*s, and *additives*. The term temper is used for non-plastic material intentionally added to the clay (Rye 1976; Rice 1987; Gualtieri 2020). Considered as one of the first major innovations of pottery technology, tempering entails a techno-cultural implication. It can be accomplished by adding natural or artificial materials, of mineral, plant and animal origin (Rye 1981; Rice 1987; Gualtieri 2020; Eramo 2020). In general, temper is added to the clay to improve workability, enhance strength, minimize shrinkage, and help the drying of the paste. The amount of temper material is thus relevant in terms of the physical changes it may bring about in the paste at the plastic state or after firing (Rice 1987).

Natural mineral tempering materials are probably the most documented ones, both archaeologically and ethnographically (Rye 1981; Rice 1987; Kilikoglou *et al* 1998; Heidke and Miksa 2000; Gosselain and Livingstone Smith 2005). Many kinds of rock and natural sands were used as tempers, depending on the available sources (Heidke *et al* 2002; Sterba *et al* 2009). Tempering materials differ with respect to the effect they render on the texture and strength of the paste, in their reactions during firing, and the procedures required for their preparation (Gualtieri 2020; Eramo 2020). Quartz, heavy minerals, chert, muscovite, microcline, orthoclase, plagioclase, hornblende, biotite, pyroxene and olivine represent the most frequently used terrigenous materials (Tucker 2009; Eramo 2020).

Sands of volcanic origin as temper in transport amphorae are well-documented in the Mediterranean area and represent an important proxy for provenance studies, given their petrographical/geochemical fingerprints (Thierrin Michael 1990; Whitbread 1995; Katsarou *et al* 2002; Olcese and Thierrin Michael 2007; Palumbi *et al* 2014). Calcareous rock fragments and spathic calcite were also extensively used as tempers throughout history (Muntoni *et al* 2009; Fabbri *et al* 2014; Albero 2014; Tenconi *et al* 2016) in as much as the Argillaceous rock fragments (ARFs) (Potter *et al* 1980; Whitbread 1986).

The presence of vegetal temper in pottery was also attested in different archaeological contexts (Mariotti Lippi and Pallecchi 2017; Gualtieri 2020; Eramo 2020). On the other hand, animal tempers consisting of hard parts (e.g., bones, shells), hairs and excrements are reported (London 1981; Rye 1981; Rice 1987; Abbink 1999; Quinn *et al* 1998; Stilborg 2001; Quinn and Day 2007; Maritan *et al* 2007; Feathers 2006; Perttula *et al* 2011). Diatomaceous earth, sponge spicules and feathers account for other alternatives of animal tempers (Shepard 1964; Matiskainen and Alhonen 1984; Skibo *et al* 1989; Mariotti Lippi and Pallecchi 2017; Gilmore *et al* 2018;). Furthermore, artificial grog and chamotte(which indicate recycled crushed ceramic used as temper in new ceramic paste) represent a widely used class of tempers(Cuomo Di Caprio and Vaughan 1993; Hamer and Hamer 2004; Braekmans and Degryse 2017; Eramo 2020) Finally, organic materials of different origin that are used to improve workability of paste and coatings are considered as additives (Rice 1987; Skibo 1989; Jeffra 2008; Shahack 2011; Kulkova and Kulkov 2016; Kiryushin *et al* 2012). Having provided a sketch of ceramic materials, the next chapter addresses major aspects in ceramic archaeometry studies, and the research questions addressed in this study.

2.2. Bibliography

Abbink A A. (1999) Make it and break it: the cycles of pottery. A study of the technology, form, function, and use of pottery from the settlements at Uitgeest-Groot Dorregeest and Schagen-muggenburg. PhD, Leiden University. Leiden, Netherlands.

Albero Santacreu D. (2014) Identifying spathic calcite recipe in archaeological ceramics: possibilities and limitations. *Cerâmica* 60:379–391. <https://doi.org/10.1590/S0366-69132014000300009>.

Braekmans D, Degryse P. (2017) Petrography: optical microscopy. In: Hunt AM (ed) The Oxford handbook of archaeological ceramic analysis. Oxford University Press, Oxford, England, 233–265.

Cuomo di Caprio N, Vaughan S J. (1993) An experimental study in distinguishing grog (chamotte) from argillaceous inclusions in ceramic thin sections. *Archeomaterials* 7:21–40.

DeBoer W R, Lathrap D W. (1979) The making and breaking of Shipibo Conibo ceramics. In: Kramer C (ed) *Ethnoarchaeology: implications of ethnography for archaeology*. Columbia University Press, Guildford, pp 102–138.

Dickinson W R, Shutler R. (2000) Implications of petrographic temper analysis for Oceanian prehistory. *J World Prehist* 14:203–266.

Eramo G. (2020) Ceramic technology: how to recognize ceramic processing, *Archaeol Anthropol Sci*. <https://doi.org/10.1007/s12520-020-01132-z>

Fabrizi B, Gualtieri S, Shoal S. (2014) The presence of calcite in archeological ceramics. *J Eur Ceram Soc* 34:1899–1911. <https://doi.org/10.1016/j.jeurceramsoc.2014.01.007>.

Feathers J K. (2006) Explaining shell-tempered pottery in prehistoric Eastern North America. *J Archaeol Method Theory* 13:89–133. <https://doi.org/10.1007/s10816-006-9003-3>.

Fowler K D. (2017) Ethnography. In: Hunt AM (ed) The Oxford handbook of archaeological ceramic analysis. Oxford University Press, Oxford, England, pp 469–486

Gilmore Z I, Sassaman K E, Glascock M D. (2018) Geochemical sourcing of fiber-tempered pottery and the organization of late archaic Stallings communities in the American Southeast. *J Archaeol Sci* 99:35–46. <https://doi.org/10.1016/j.jas.2018.08.009>.

Gliozzo E. (2020) Ceramics investigation. Research questions and sampling criteria *Archaeol Anthropol Sci*. 12, 202. <https://doi.org/10.1007/s12520-020-01128-9>.

Goffe Z. 2007. *Archaeological Chemistry*. Second Ed. John Wiley & Sons, Inc., Hoboken, New Jersey.

Gosselain O P, Livingstone Smith A. 2005. The source: clay selection and processing practices in sub-Saharan Africa. *Pottery manufacturing processes: reconstruction and interpretation*. BAR International Series 1349:33–47.

Grimshaw R W. 1980. *The Chemistry and Physics of Clays*, McGraw-Hill, New York.

Gualtieri S. (2020) Ceramic raw materials. How to establish the technological suitability of a raw material. *Archaeol Anthropol Sci.* 12, 183. <https://doi.org/10.1007/s12520-020-01135-w>.

Hamer F, Hamer J. 2004. *The potter's dictionary of materials and techniques*. University of Pennsylvania Press.

Heidke J, & Miksa E. (2000). Correspondence and discriminant analyses of sand and sand temper compositions, Tonto basin, Arizona. *Archaeometry*, 42 (2), 273-29. <https://doi.org/10.1111/j.1475-4754.2000.tb00882.x>

Heidke J, Miksa E, and Wallace, H D. (2002) A Petrographic Approach to Sand-Tempered Pottery Provenance Studies: Examples from Two Hohokam Local Systems. In *Ceramic Production and Circulation in the Greater Southwest: Source Determination by INAA and Complementary Mineralogical Investigations*, edited by Donna, M. Glowacki and Hector, Neff, pp. 152–178. The Cotsen Institute of Archaeology Monograph 44. University of California, Los Angeles

Heimann R, Maggetti M. 2014. *Ancient and historical ceramics: materials, technology, art and culinary traditions*. Schweizerbart and Bortraeger science publishers, Stuttgart, pp 550.

Hoard R J, O'Brien M J, Khorasgany M G, Gopalaratnam V S. (1995) A materials-science approach to understanding limestone-tempered pottery from the Midwestern United States. *J Archaeol Sci* 22: 823–832. [https://doi.org/10.1016/0305-4403\(95\)90011-X](https://doi.org/10.1016/0305-4403(95)90011-X).

Jeffra C. (2008) Hair and potters: an experimental look at temper. *World Archaeology* 40: 151–161. <https://doi.org/10.1080/00438240801889431>.

Katsarou S, Sampson A, Dimou E. (2002) Obsidian as temper in the Neolithic pottery from Yali, Greece. In: Kilikoglou V, Maniatis Y, Hein A (eds) *Modern trends in scientific studies on ancient ceramics*. BAR International Series 1011:111–120.

Kilikoglou V, Vekinis G, Maniatis Y, Day P M. (1998) Mechanical performance of quartz tempered ceramics: part I, strength and toughness. *Archaeometry* 40:261–279. <https://doi.org/10.1111/j.1475-4754.1998.tb00837.x>.

Kiryushin K Y, Kiryushin Y F, Glushkov I G. (2012) The use of animal hair in ceramic manufacturing at the Tytkesken-2 Neolithic Site, Western Siberia. *Archaeol Ethnol Anthropol Eurasia* 40:41–50.

Kulkova M, Kulkov A. (2016) The identification of organic temper in Neolithic pottery from Russia and Belarus. *The Old Potter's Almanack* 21:2–12. <https://doi.org/10.11588/opa.2016.1.33496>.

London G. (1981) Dung-tempered clay. *J Field Archaeol* 8:189–1. <https://doi.org/10.2307/529413>.

Maggetti M. (2010) Neolithic pottery from Switzerland: Raw materials and manufacturing processes. In: *From mine to microscope, advances in the study of ancient technology*. Oxbow Books, Oxford, pp 29–42.

Mariotti L M, Pallecchi P. (2017) Organic inclusions. In: Hunt AM (ed) *The Oxford handbook of archaeological ceramic analysis*. Oxford University Press, Oxford, England, pp 565–581.

Matiskainen H, Alhonen P. (1984) Diatoms as indicators of provenance in Finnish sub-neolithic pottery. *J Archaeol Sci* 11:147–157. [https://doi.org/10.1016/0305-4403\(84\)90049-9](https://doi.org/10.1016/0305-4403(84)90049-9).

Matson F. (1989). *Ceramics: The hub of ancient craft interplay*. In P. McGovern & M. Notis (Eds.), *Cross-craft and cross-cultural interactions on ceramics: Ceramics and Civilization Vol. 4*, (pp. 12-28). Westerville: American Ceramic Society.

Montana G. (2017) Ceramic raw materials. In: Hunt AM (ed) *The Oxford handbook of archaeological ceramic analysis*. Oxford University Press, Oxford, England, pp 87–100.

Muntoni M, Eramo G, Laviano R. (2009). Production of Mid-late Neolithic Serra d'Alto' ware in the bardic trough (Southeastern Italy). In K. Biró, V. Szilágyi, A. Kreiter (Eds.), *Vessels: inside and outside Proceedings of the 9th European Meeting on ancient ceramics* (pp. 53-62). Budapest: Hungarian National Museum

Müller N S, Kilikoglou V, Day P M, Vekinis G. (2010) The influence of temper shape on the mechanical properties of archaeological ceramics. *J Eur Ceram Soc* 30:2457–2465. <https://doi.org/10.1016/j.jeurceramsoc.2010.04.039>.

- Nesse W D. 2000 Introduction to Mineralogy. Oxford University Press, New York.
- Newman A. (ed.), 1987. Chemistry of Clays and Clay Minerals, Longmans, London.
- Olcese G, Thierrin Michael, G. (2009). Graeco-Italic amphorae in the region of Ostia: archaeology and Archaeometry, in: K.T. Birò, V. Szilagyí, A. Kreiter (Eds.), Vessels: Inside and Outside. Proceedings of the 9th European Meeting on Ancient Ceramics (EMAC '07) (Budapest, October 24-27, 2007), Budapest 2009, pp. 159-164, ISBN: 9789637061424.
- Orton C and Hughes M. 2013 (2nd edn). Pottery in Archaeology. Cambridge: Cambridge University Press, 2013. Pp. xx + 340, illus. isbn9781107008748 (bound); 9781107401303 (paper)
- Palumbi G, Gratuze B, Harutyunyan A, Chataigner C. (2014) Obsidian tempered pottery in the southern Caucasus: a new approach to obsidian as a ceramic-temper. *J Archaeol Sci* 44:43–54. <https://doi.org/10.1016/j.jas.2014.01.017>.
- Perttula T K, Beth Trubitt M, Girard J S. (2011) The use of shell-tempered pottery in the Caddo area of the Southeastern United States. *Southeast Archaeol* 30:242–267. <https://doi.org/10.1179/sea.2011.30.2.004>.
- Pollard A M, Batt C M, Stern B, Young S M M. 2007. Analytical chemistry in archaeology. Cambridge University Press, New York.
- Pollard M and Heron C. 2008. Archaeological Chemistry, Royal Society of Chemistry, Cambridge, UK.
- Potter P E, Maynard J B, Pryor W A. 1980. Sedimentology of shale: study guide and reference source. Springer Science & Business Media
- Quinn P, Alaimo R J, Montana G. (1998) Calcareous nannofossil analysis of ceramics and probable raw materials from an ancient Punic kiln site on the island of Mozia, western Sicily. *J Nannoplankton Res* 20: 85–87.
- Quinn P S, Day P M. (2007) Ceramic micropalaeontology: the analysis of microfossils in ancient ceramics. *J Micropalaeontol* 26:159–168. <https://doi.org/10.1144/jm.26.2.159>.
- Rice P M. 1987. Pottery analysis: a sourcebook. University of Chicago Press, Chicago.

Roux V. 2019 *Ceramics and society: a technological approach to archaeological assemblages*. Springer, Berlin.

Rye O S. (1976) Keeping your temper under control: materials and the manufacture of Papuan pottery. *Archaeology & Physical Anthropology in Oceania* 11:106–137. <https://doi.org/10.1002/j.1834-4453.1976.tb00245.x>.

Rye O S. 1981. *Pottery technology: Principles and Reconstruction*. Taraxacum, Washington, DC.

Shahack-Gross R. (2011) Herbivorous livestock dung: formation, taphonomy, methods for identification, and archaeological significance. *J Archaeol Sci* 38:205–218. <https://doi.org/10.1016/j.jas.2010.09.019>.

Shepard A O. (1964) Temper identification: “Technological Sherd Splitting” or an unanswered challenge. *Am Antiq* 29:518–520. <https://doi.org/10.2307/277999>

Sillar B. (2000) Dung by preference: the choice of fuel as an example of how Andean pottery production is embedded within wider technical, social, and economic practices. *Archaeometry* 42:43–60. <https://doi.org/10.1111/j.1475-4754.2000.tb00865.x>.

Sillar B, Tite M S. (2000) The challenge of ‘technological choices’ for materials science approaches in archaeology. *Archaeometry* 42:2–20. <https://doi.org/10.1111/j.1475-4754.2000.tb00863.x>.

Skibo J M, Schiffer M B, Reid K C. (1989) Organic-tempered pottery: an experimental study. *Am Antiq* 54:122–146. <https://doi.org/10.2307/281335>.

Sterba J H, Mommsen H, Steinhauser G, Bichler M. (2009) The influence of different tempers on the composition of pottery. *J Archaeol Sci* 36:1582–1589. <https://doi.org/10.1016/j.jas.2009.03.022>.

Stilborg O. (2001) Temper for the sake of coherence: analyses of bone-and chaff-tempered ceramics from Iron Age Scandinavia. *Eur J Archaeol* 4:398–404. <https://doi.org/10.1179/eja.2001.4.3.398>

Tenconi M, Maritan L, Mazzoli C. (2016) Textural changes in speleothem inclusions during firing: a useful tool to estimate temperature in speleothem-bearing pottery. *Archaeometry* 58:39–53. <https://doi.org/10.1111/arc.12238>.

Thierrin-Michael G. (1991), Roman wine amphorae: production sites in Italy and imports to Switzerland, in *Archaeometry '90. International symposium on archaeometry*, Heidelberg, 2–6 April 1990 (eds. E. Pernicka and G. A. Wagner), pp.523–32.

Tite M S. 2008. Ceramic Production, Provenance and Use – A Review. *Archaeometry* 50, 2: 216-231. University of Oxford. <https://doi.org/10.1111/j.1475-4754.2008.00391.x>

Tucker M E. 2009. *Sedimentary petrology: an introduction to the origin of sedimentary rocks*. John Wiley & Sons, New York.

Velde B, Druc I C. 1999. *Archaeological ceramic materials: origin and utilization*. Springer Science & Business Media, Berlin Heidelberg.

Wagner B and Herrmann G A. (eds). 2009. *Natural Science in Archaeology*. Springer-Verlag. Berlin, Heidelberg.

Whitbread I. (1995). *Greek Transport Amphorae: A Petrological and Archaeological Study*. British School at Athens. Fitch Laboratory Occasional Paper, 4. Athens: The British School at Athens.

Whitbread I. (1986). The characterization of argillaceous inclusions in ceramic thin sections. *Archeometry*, 28 (1), 79-8

3. Overview of Archaeometric Study of Pottery and Research Questions

Ceramic objects are rich sources of information and constitute a large part of the memory of past and present human activities (Rice 1987; Albero 2014; Gliozzo 2020a). These objects are valuable indicators of technological and socio-economic processes related to specific epoch/s of human history.

A multitude of questions can be constituted in archaeometric research on archaeological pottery and yet can be mainly linked to the study of production techniques, provenance, age, use and conservation state (Tite 1999; Hunt 2016; Gliozzo 2020a). In this respect, the scientific analysis of archaeological pottery is significant to provide the mineralogical and chemical characterization as well as understand morphological and micro-structural features of these artifacts.

The manufacture of ceramics is tied to a specific socio-cultural context and response to certain needs of communities within a specific area or wider region/s. Social, ideological, economic, and political factors shape the choices made by potters. In this respect, the actions of the potter, namely the selection and mining of clay sources, manipulation of the clays (in terms of washing and mixing them and adding of tempers), forming, and shaping of the vessel, decorating it and applying surface treatments and eventually firing the vessel attest the sequence in ceramic material culture studies (Roux 2017; Schlanger 1994). Archaeological pottery thus entails complex patterns of material culture, and their study intrinsically needs the application of multidisciplinary approaches. Archaeological, historical, environmental, ethnographic, experimental, technological, and compositional studies are necessary to contribute to the study of archaeological pottery to assess factors that possibly contribute to and/or affected by the specific nature of the ceramic assemblages under investigation (Albero 2014; Maritan 2019; Gliozzo 2020a). Modern analytical methods allow to solve broad and/or specific questions related to studies of archaeological ceramics (Hunt 2016; Maritan 2019; Gliozzo 2020a) and multi-disciplinary linkages enable to develop a common interface among archaeologists, physicists, chemists, Earth scientists and all the various expertise that are needed to the overall investigation of pottery studies. Therefore, typological classification and chronological sequencing, chemical and mineralogical characterization as well as technological investigations are, thus, intertwined in a multi-analytical framework.

Considering that ceramic research project needs to be planned from the inception to include archaeological and analytical knowledge, a sketch of key aspects of the themes of typological classification, provenance, technology of production and use is provided below to relate them to the research questions tackled by this study.

3.1. Themes on Archaeometric Study of Pottery

3.1.1. The Question of Typological Classification

The issue of typological classification in ceramic studies has been an ongoing discussion for decades. The notion of classification as has been noted in the literature resonates around the recognition of differences and similarities among phenomena (Bortolini 2017; Gliozzo 2020a). The variables that are used to ascribe differences or similarities, thus, determine the meaning and viability of a typological classification. Yet, the inherent limitations of typological classification pose problems to define variable selection (Gliozzo 2020a). Limited information of the original form or function of the ceramic artefact is discerned from sherds of broken vessels, which are often used by archaeologists to build typological classification, while detailed typologies and over-classification can produce information that can be difficult to connect to aspects of cultural behaviour (Gliozzo 2020a). The limitations of typological classification have been discussed widely and are particularly quite visible in the study of amphorae assemblages (Keay 1984; Reynolds 2005). Our understanding of ceramic traditions, production and distribution systems of amphorae assemblages, therefore, cannot rely solely on typological evidence based on stylistic and typo-chronological sequencing.

It is noted that a major deficiency of morpho-stylistic classification of ceramics lies in the attribution of which features can be considered adequate to discriminate ceramic styles and identify regional variations or distinct ceramic traditions (Gliozzo 2020a). The extent of variation between prototypes belonging to the same cultural traditions and stylistic attributes can be also fuzzy from this point of view.

Reynolds (2005) has indicated the problems regarding the attribution of amphorae including whole fabric groups to their sources due to different variants of the same ceramic tradition. The diversity of production might entail evolution in specific regions and need to be linked to geological sources, a feature which cannot be solely approached from stylistic classification. Reynolds (2005) has also enumerated the difficulties and pitfalls of working with rims and fragments of handles and bases than complete vessels, which hindered the construction of a

typology for amphorae in a wide range fossil shell and limestone fabrics which have a variable degree of volcanic and argillaceous material. This problem is quite noticeable in Late Roman coarse wares and the complexities of typological analysis of Levantine amphorae from Cilicia to Gaza and their regional production trends from the 1st to 7th centuries is extensively discussed. This aspect concerns the classes of imported transport amphorae and common wares from Levantine that were found in excavations at Adulis and need to be considered as per se.

Given these limitations of typological classifications, it has been argued that the use of a series of descriptive parameters involving macroscopic and microscopic approaches can constitute a secure frame for ceramic typology (Gliozzo 2020a). Different schools have established different criteria to approach the macroscopic classification of ceramic bodies and propose numerous features to be considered. While the criteria mostly emphasizing typological classification based on morphological and stylistic attributes hinder secure descriptions, Gliozzo (2020a) has further extended the discussion recently to encompass two levels of descriptions, namely the morphological-stylistic and micro-textural and compositional levels to address how an accurate typological classification can be possible by integrating archaeologists and scientists in a multidisciplinary team. The ‘M(acro)-typology’ described by Gliozzo (2020a) encompasses ‘information on the archaeological context of the finds and the morphological-stylistic attributes of the ceramic body and refrains from identifying mineralogical phases based on their visual appearance.’ This classification forms the basis of classification for the materials sampled for archaeometric analysis. A second level of typological classification has also been suggested by Gliozzo (2020a) to encompass what is termed as ‘M (acro and) M(icro)-typology’ to allow the characterization of ceramic body to answer questions of production, use and distribution. The second level of typological classification thus will provide a chemical, mineralogical and petrographic characterization. Notwithstanding how the concept of typological classification is addressed and refined in its evolution of the current knowledge, it is important to constitute the input from archaeological and analytical frontiers.

3.1.2. Themes on Provenance

Provenance studies are widely discussed in archaeometric research applied on ceramic materials. The study of provenance implies the determination of a production site useful to understand how the raw materials and sources were utilized as well as the acquisition of

information on technological aspects to reconstruct production, distribution, and patterns of trade in the past (Tite 1999; Gliozzo 2020a). The provenance postulate entails association to different scales of geographical scope that allow identification and location of the supply basins of raw materials used to produce ceramics. The question of provenance involves both the raw materials that were used to produce ceramics and the ceramic artefacts found at the production and the distribution sites (Gliozzo 2020a; Hein and Kilikoglou 2020; Montana 2020). The distribution of workshops and kilns, trade routes, movement of people, cultural contacts and intra-site and inter-site relationships are thus considered to draw conclusions.

There are different approaches to attribute provenance to archaeological ceramics and accordingly different levels of provenance classification should be considered to link them to socially and/or geographically verifiable scale. Ceramics of known provenance, such as kiln wasters, can be analysed in comparison with ceramics from other locations on one hand (Mommsen 2011; Gliozzo 2020a) or large quantities of ceramics from a single site on the other hand can be analysed in order to establish compositional groups, of which the largest group is assumed to be local (Bishop *et al* 2017; Holmsqvist 2019). Alternatively, chemical compositions of ceramics can be analysed in comparison with natural clays in the area to pinpoint clay sources (Kilikoglou *et al* 1988; Tite 1999; Gliozzo 2020a; Hein and Kilikoglou 2020; Montana 2020). It should be noted that each of these approaches presents specific limitations and are worthy to be discussed to highlight the complexities in provenance postulations.

As for pottery, a widely used approach in provenance studies relies on the use of reference group, which assumes that the largest compositional group is local to the site in question as a result of the use of specific raw materials and manufacturing techniques (Bishop *et al* 1982; Montana *et al* 2018; Hein and Kilikoglou 2020). In other words, it is postulated with this approach that there is less variation within a single clay or temper source than there is between different sources.

The chemical fingerprint is provided from elemental composition, where numerous samples must be analysed to form pottery groups according to similarities in chemical data (Bishop *et al* 1982; Blackman *et al* 1993; Neff and Glascock 1995; Stoner 2016; Hein and Kilikoglou 2020). These results can be linked to the clay sources and therefore allow to establish the production area or site and make inferences if the materials were locally produced or imported. For provenance studies, it may be possible to match raw clay sources and the

composition of archaeological pottery if the manufacture process does not involve significant manipulation by mixing of clays or adding of tempering materials (Gliozzo 2020a). Yet, the manipulation of the potters due to cultural practices of manufacture makes it difficult to compare ceramics to clays and tempers in a ‘one-to-one manner’; thus, the composition of pottery is the sum of the various chemical and cultural components (Arnold *et al* 1991 Montana 2020; Hein and Kilikoglou 2020). In this respect, prior treatments of the raw materials and the potential changes in composition during firing and/or burial must be considered.

Problems with the reference group approach may arise if the results are based only on bulk chemical data and the clay paste composition and mineralogical inclusions are not analysed (Bishop, 1982; Holmqvist 2019). The variation of coarsely tempered ceramics produced in the same workshop using the same raw materials may, in some cases, result in their categorisation to different groups in statistical analysis unless the clay paste composition is taken into consideration (Buxeda i Garrigós *et al* 2003; Hein and Kilikoglou 2020). The paste composition thus needs to be selectively analysed in ceramic provenance studies, as it is more directly linked to the original clay source than the possibly processed ceramic fabric (Hein and Kilikoglou 2020, Montana 2020). Differences in the added amounts of tempers also create problems even when ceramics produced using the same clay are analyzed. Elemental concentrations are affected, and samples will be clustered differently in multivariate statistical analysis (Holmqvist 2019; Hein and Kilikoglou 2020). Moreover, potters might have manipulated their clays and temper raw materials in as much as firing temperatures affect the composition of ceramics. It is crucial, therefore, to consider the human factor behind ceramic manufacture while sampling possible raw material sources (Hein and Kilikoglou 2020; Gliozzo 2020a). It needs to be postulated in provenance studies that there is no mixing of raw materials in the production, or it can be recognized using appropriate analytical methods. It is also important to assume that the chemical compositions of the raw materials should remain unchanged or can be predictably comparable in the finished product.

Moreover, the knowledge of local geology and maps are important for ceramic provenance studies. Geological surveys and maps can offer information on the potential sources of tempers. Sampling of clay deposits for provenance studies is a successful approach and requires intensive geological surveys (Montana 2020; Gliozzo 2020a). Ethno-archaeometric approaches furthermore, prove to be indispensable to understand raw materials exploitation strategies.

The exploitation of raw materials by different production centers or workshops should further be sought in provenance studies. It is noteworthy to mention that different production centers might have exploited the same source areas or ceramics produced in one workshop, in contrast might have been produced from different recipes or source areas (Hein and Kilikoglou 2020). As far as patterns of exchange are concerned, raw material exchange might have also existed between different production centers or workshops (Bishop *et al* 1982; Eramo 2020; Montana 2020). When intra-site and inter-site exploitation of raw materials is considered, it is assumed in provenance studies that the chemical fingerprint is different between sources and can be analytically characterized in the object with precision to discriminate between different potential raw material sources (Kilikoglou *et al* 1988; Mommsen 2011; Montana 2020; Hein and Kilikoglou 2020). In general, pottery produced using the same raw materials, technology and by the same community should have the same chemical composition. It should also be noted that the groups made based on ceramic analysis can correspond to different ‘recipes’, but not necessarily to different geological sources (Eramo 2020; Hein and Kilikoglou 2020). The manipulation of raw materials, particularly temper addition/ subtraction, clay mixing, and homogenization and the like should be considered when comparisons are made with raw clay sources and similarly the analytical data should be interpreted according to the pottery manufacturing practices (Adan-Bayewitz and Perlman 1985; Montana 2020). On other account, post-depositional enrichment, or dilution of composition needs to be considered while comparing archaeological pottery to potential raw material sources (Buxeda i Garrigós *et al* 2001; Maritan and Mazzoli 2004; Maritan 2020). In such cases, it becomes apparent to assess whether post-depositional variation is noticeable or not and it is assumed that such variation can be comprehended analytically.

Moreover, Gliozzo (2020a), has indicated that a production group can serve as the best reference for a provenance investigation if it is geographically, technologically, and chronologically well defined. The study of provenance of specific classes of pottery can be approached, when suitable production groups have been published in the literature, for instance. As Gliozzo (2020a) puts it, the collection should first be typologically investigated (including both morphology and composition) and the composition should then be compared against the composition of known production groups as well as finally, ascribed to specific production/supply areas, regions, districts or, at least, to specific sites. On-line databases and repositories featuring petrographic and geo-chemical information, thus are important to

exploit for comparative parallels. Provenance studies will become complex, on the other hand, when no suitable production groups can be found in the literature for comparisons (Gliozzo 2020). In the absence of established production groups and/or known production sites, as Gliozzo (2020a) puts it, the collection considered for investigation will not constitute a production group as the geographical scale of reference would be quite wider and thus will constitute a distribution/ consumption group. From an archaeometric point of view, these groups can provide information related to production diversity.

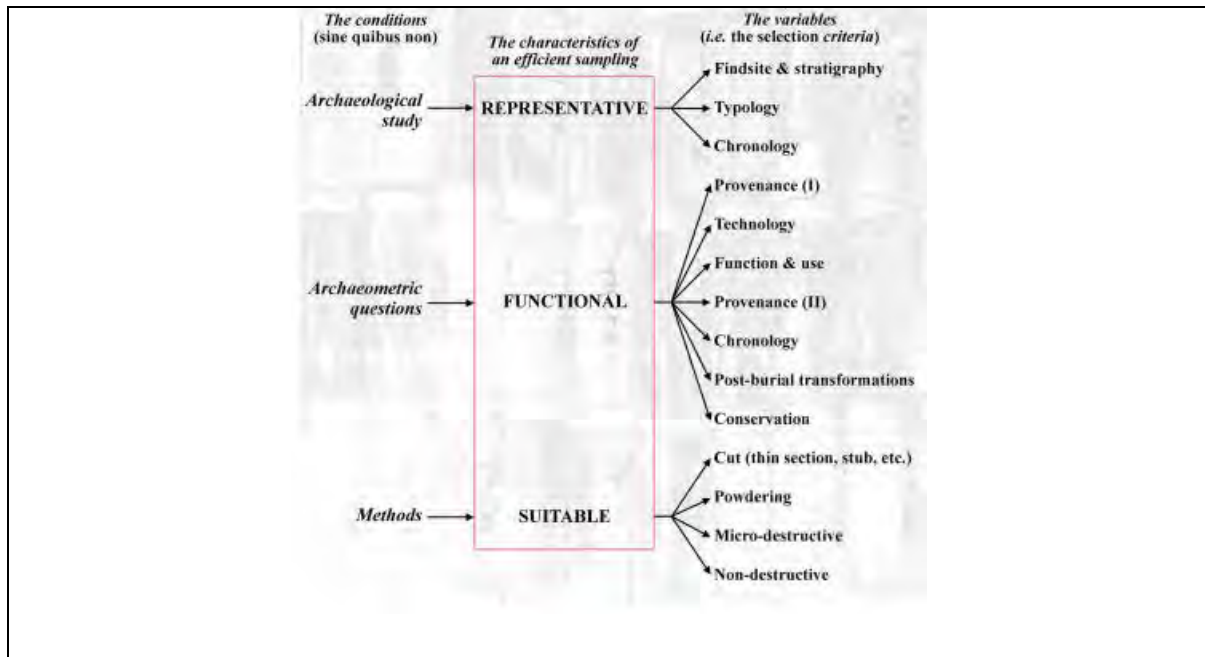


Figure 2: Ceramic archaeometry research steps and guide for a proficient sampling (Gliozzo 2020)

As regards provenance study of ancient ceramics, sampling procedure is another recurring theme. The selection of samples by consent between archaeologists and scientists is the best approach to consider archaeological issues related to technological features of the ceramic artifacts and the desirable methodological and analytical probes (Albero 2014; Gliozzo 2020a). It should be noted that the requirements of analytical techniques to study archaeological pottery are different from those applied in conventional laboratory analysis and the type of analytical approach must be designed with respect to the specific archaeological question (Maritan 2019). Therefore, for a proper sampling adequate knowledge of the archaeological study/site, clear formulation of the archaeometric research questions and the definition of the experimental procedure are important. A proficient sampling strategy should entail a representation of typological, stratigraphic, and chronological framework necessary for a complete archaeological study, needs to be functional to specific questions of provenance to approach the archaeometric questions and

constitute suitable methods and approaches to extract information (for a detailed review see Gliozzo 2020a). The schematic representation above provides research steps and requirements for a proficient sampling (see Gliozzo 2020a).

Finally, the use of statistical tools and requirements for data treatment in provenance studies should be considered. A large amount of information on chemical and mineralogical signatures of archaeological pottery is obtained from archaeometric studies. The chemical elements that are meaningful for provenance analysis can vary depending on the analyzed ceramic materials. In some cases, variation in one element can be considered adequate to identify a difference in the raw material utilized, but generally several elements should be considered, preferably showing clear differences of concentrations in different ceramic types, and relatively small differences in ceramics of the same type (Baxter 1994; Baxter 2001; Papageorgiou 2018 and 2020). Handling and modelling data are necessary by using sophisticated mathematical and statistical approaches to identify composition groups. In archaeometric research, multivariate data analyses are often used and accordingly Principal Component Analysis (PCA), Cluster Analysis (CA) as well as Classification and Discriminant Analyses (DA) have found tremendous application for provenance studies (Aitchison 1986; Baxter 2001, 2009 and 2015; Baxter *et al* 2008; Papageorgiou 2020). These statistical tools are used to highlight variation and show patterns in a dataset by visualizing the similarity or differences between ‘‘ compositional groups’ (Papageorgiou 2020). In addition to interpreting the analytical data, it is important to review the archaeological questions around the provenance, technology of production and chronology with appropriate level of certainty (Tite 1999; Papageorgiou 2020). Papageorgiou (2020) gives a detailed review of statistical approaches applied in archaeometric study of ceramics with emphasis on the rationale to use specific data treatment procedures and the complexities that have to be taken into account.

In conclusion, it is often debated whether chemical or mineralogical-petrographic analysis are better suited in archaeometric studies of ceramic provenance (Tite 1999; Maritan 2019; Gliozzo 2020a; Hein and Kilikilgou 2020). Today it is agreed upon that a systematic characterization of a ceramic object should constitute chemical and mineralogical-petrographic analyses. Maritan (2019), has enumerated the spectrum of analytical techniques which can be used for ceramic archaeometric studies considering the latest advancements and specific requirements. It is, thus, crucial to combine bulk chemical analysis with microscopic analysis, such as scanning electron microscopy or petrographic microscopy. Therefore, in

addition to the bulk chemical composition of a ceramic sherd, the ceramic paste and mineralogical inclusions can be analysed separately, and the question of intentionally added non-plastic, coarse-grained materials should be considered to form meaningful compositional groups for provenance studies (Tite 1999). A multi-analytical approach that constitutes chemical, mineralogical-petrographic and microstructural studies is thus imminently desirable (Tite 1999; Maritan 2019; Gliozzo 2020a).

3.1.3. Themes on Technology of Production

The reconstruction of the technology of production is one of the several issues addressed by archaeometric studies of ancient ceramics. The entire production cycle, from manipulation of the raw materials to the finishing of the object are studied using analytical approaches. Eramo (2020) states that the compositional/textural (i.e., levigation, tempering, clay mixing), mechanical (i.e., kneading, forming), and thermal (i.e., firing, use) transformation of the clayey raw materials yields typical man-made microstructures and requires specific descriptive strategies. The technological choices made to attain paste plasticity and desired product in different stage of manufacture are studied in as much as considering different aspects of clay processing in the forming stages and the effects of mineral, vegetal and/or animal tempers on the paste and the fired body (Heinmann and Maggetti 2014; Gliozzo 2020a; Eramo 2020).

The processing of raw clay concerns one of the features of the study of technology of production (Ingold 2012; Roux 2017 and 2019; Gliozzo 2020a; Thér 2020). A schematic representation of clay processing has been provided by Eramo (2020) as seen in Fig.3.

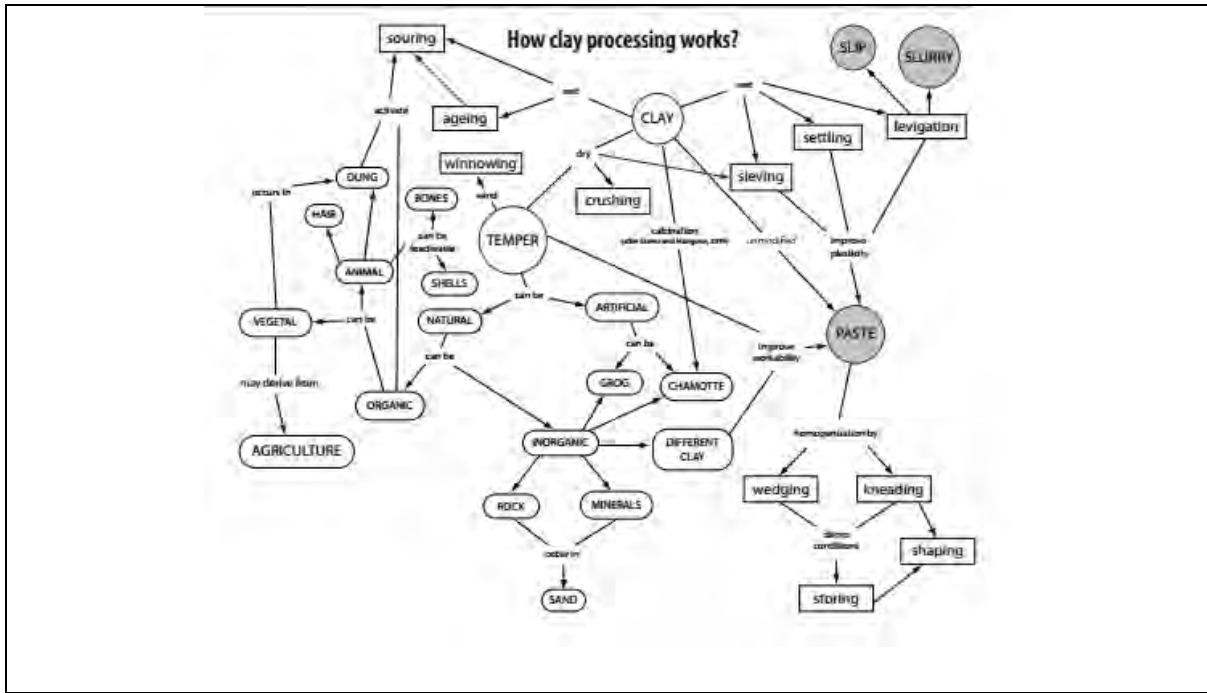


Figure 3: Concept map of clay processing (Eramo 2020)

In a similar vein, the process involving the modelling of the paste and related surface features are addressed in morphological and micro-structural studies (Thér 2020 and Ionescu and Hoeck 2020). Moreover, surface treatments (for eg. if the ceramic was covered with a slip or glaze), beg analytical probes to answer a series of questions regarding composition, material sourcing and related production. The comprehension of the technologies used to produce slips and gloss bodies, sigillata, and different glazes from different periods require specific background knowledge and analytical strategies (Aloupi Siotis 2020; Sciau *et al* 2020; Gliozzo 2020a; Pradell and Molera 2020).

A great deal of archaeometric works have focused on comprehension of the firing regimes of ancient ceramics (Tite and Maniatis 1981; Maggetti 1982; Fabbri *et al* 2014; Nodari *et al* 2004 and 2007; Trindade *et al* 2009; Heimann and Maggeti 2014; Montesana *et al* 2019; Gliozzo 2020b). The effectiveness of the firing treatments, the atmosphere as well as temperature reached in firing structures and firing cycles performed are central to these discussions (see Gliozzo 2020b). It is known that during firing, clay minerals decompose and react with temper minerals to form new microcrystalline mineral phases, with the latter depending mainly on the composition of the raw clay-rich material, its granulometry, additives, the firing temperature as well as the kiln atmosphere conditions (Tite and Maniatis 1981; Maggetti, 1982, Maritan *et al* 2006 and 2007; Nodari *et al* 2004 and 2007; Chatfield,

2010; Trindade *et al* 2009 ; Gliozzo 2020b). Therefore, discussion of thermo-dynamics and kinetics of reactions occurring during firing is important.

During firing, disequilibrium conditions dominate the reaction behavior of temper grains and clay matrix which are characterized by the presence of different reacting sub-systems (Heimann and Maggetti 2014; Gliozzo 2020b). The reaction subsystems are compositionally defined and correspond to specific mineral phases in mutual contact. The nucleation and growth of new mineral phases as well as reactions corresponding to compositional variations of phases represent different aspects of the processes in firing and can help to assess the role played by exerted temperature as well as bulk and mineralogical compositions (Nodari *et al* 2004 and 2007; Gliozzo 2020b). Moreover, microtextural relationships among firing phases result from transformations occurring in the clay matrix, in mineral phases and at boundaries between clay matrix and mineral phases (Trindade *et al* 2009 and 2010; Gliozzo 2020b). The progressive fusion between clay matrix and mineral temper grains, shape changes of mineral phases as well as increase of the aggregation rate within the clay matrix and the formation of secondary porosity (inter-granular bridges) phenomena are produced by increasing the firing temperature and account for the micro-textural relationships (Maggetti 1982; Maritan *et al* 2006 and 2007; Nodari *et al* 2004 and 2007; Gliozzo 2020b).

It is known that a series of reactions occur within clay mineral structures with increasing temperature (Rice, 1987: 86-93; Gliozzo, 2020b). At 200-300°C surface-adsorbed water turns to vapor and is driven off while dehydroxylation occurs as water between lattice planes is driven off and temperature gradient is dependent up on clay mineral type (Heimann and Maggetti 2014). Major alterations take place around 600°C and the lattice structure for all clay minerals collapses irreversibly by around 900°C. Finally, at even higher temperatures (1275-1460°C from kaolinite) new minerals (such as cristobalite, sillimanite and kyanite) form (Gliozzo 2020b). Changes that occur during firing include carbonate decomposition, dehydroxylation of clay minerals (loss of hydroxyls), and the formation of firing minerals such as gehlenite, anhydrite, anorthite, pyroxenes, wollastonite, melilite and the like (Trindade *et al* 2009; Heimann and Maggetti 2014; Gliozzo 2020b). Recently, Gliozzo (2020b) has made an extensive review of the reconstruction of the firing process considering the thermal behaviour of several mineralogical phases. In this case, the behaviour of calcite and dolomite; quartz and cristobalite; K-feldspar and plagioclase; rutile and anatase; haematite, maghemite, hercynite and metallic Fe; illite, muscovite, biotite and chlorite; wollastonite, melilite, anorthite and monticellite; diopside and kaolinite is central to account

for the study of changes during firing in calcareous and non-calcareous matrix. The effects of firing in the development of amorphous/vitrified components, matrix and porosity, colour, and variations in chemical composition are further indicated (for detailed information see Gliozzo 2020b).

The state-of-the-art in reconstruction of the firing process allows to establish a technological correlation between the type of ceramic to be produced and the firing temperature within a broad temperature interval (Tite and Maniatis 1981; Heimann and Maggetti 2014; Chatfield 2010; Mentessana *et al* 2019; Gliozzo 2020b; Xanthopoulou *et al* 2021). In a similar perspective, a review of archaeometric works propose a broad range of temperatures as the maximum temperature to have been reached and yet the heating rate, soaking and cooling times are difficult to determine. It should be noted therefore, that determination of firing temperature is linked to the approximation of equivalent firing temperature as indicated in the literature while the broader technological studies cannot be limited to determination of maximum temperature only (Gliozzo 2020b). The information on the maximum temperature, as has been indicated in some studies (Trindade *et al* 2009 and 2010; Gliozzo 2020b) can be linked to technological assessments when the use of a particular type of clay, the production of a specific class of materials or the activity of a specific workshop are considered. As Gliozzo (2020b) puts it, this aspect is not evenly reached in all parts of the firing structure and could have been diachronically modified during the span of a ceramic workshop. The role of experimental research is paramount in these frontiers. Moreover, adequate sampling and archaeometric investigations are needed in as much as the study of both production and firing structures.

In conclusion, there are many alternative clays, tempers and firing temperatures that can be used in production and, thus, the resulting pottery adequately satisfies the strength, toughness, thermal shock resistance and permeability requirements in use (Tite 2008; Heimann and Maggetti 2014; Muller 2017; Eramo 2020; Gliozzo 2020b). The technological choices made will depend on the overall environmental, technological, economic, social, political, and ideological context of production, which need to be accounted for in archaeometric studies.

3.1.4. Themes on Use

Ceramics have been used for varied functions over time. The reconstruction of the intended use of a ceramic vessel has been central to discussions of the study of production cycles in

response to social, economic, and technological dynamisms of ancient societies (Rice 1987). Developments in organic residue analysis of ancient materials have greatly benefited from advances in chromatographic and mass spectrometric instrumentation. The analysis of lipids (i.e., fats, waxes and resins) preserved in ceramic bodies has begun since the 1970s and proved to be versatile to comprehend pottery use with a high degree of specificity (Evershed *et al* 2008; Stern *et al* 2008; Stacey *et al* 2010; Roffet-Salque *et al* 2017). Recent developments in analytical chemistry and bio-molecular sciences, on the other hand, hallmark refinements and sophistication in terms of extraction methods and the scale of analytical breadth, allowing lipid analyses of tens to hundreds of potsherds representing archaeological assemblage/s. The determination of biomarkers, namely the structures of compounds, or suite(s) of compounds, originating from plant and animal sources, in sediments, ceramics and other matrices, substantially widens the available evidence for archaeology and archaeometric studies (Evershed 2008; Stacey 2009). Coupled with studies of isotopic composition, it is also possible from lipid residue analysis to have information on environmental and climatic phenomena in as much as exploring insights into past lifestyles from several proxies.

It should be noted, however, that organic residue analysis in ceramics is not without complexities and challenges. The comprehension of problems related to the preservation of extant residues and the complexities they pose in analytical methods, thus, should be significantly addressed. Visible organic residues could derive from burnt residues, soot, etc., deposited by heating of the vessel over fire, or from materials used as decoration, sealants or adhesives (Evershed 2008; Roffet-Salque *et al* 2017). These residues adhere to the interior or exterior surfaces of the vessel and become of interest to archaeologists to probe function. Yet, residues are susceptible to post-burial degradation/loss and post-excavation contamination as well as loss. Such phenomena create complexity for analytical procedures. Hence, absorbed organic residues in the walls of pottery sherds, that generally originate from the original contents or were either stored or processed in the vessels as a result of single use or multiple events of the vessel's lifetime, are favored in organic residue analysis (Stacey 2009; Roffet-Salque *et al* 2017).

On other accounts, the complexity of analytical methods and extraction methods needs to be considered. A review from the early attempts to extract and analyze absorbed residues to the recent developments targeting specific class of residues is provided in many archaeometric studies (Evershed *et al* 2008; Stacey *et al*, 2010; Cramp and Evershed 2015; Roffet-Salque *et*

al 2017). Traditionally lipids have been extracted from visible residues and powdered fabric using organic solvent mixtures (Evershed 2008; Roffet-Salque *et al* 2017). High-throughput and higher recoveries of lipids from archaeological potsherds are possible from recent protocols involving the direct hydrolysis and methylation of lipids (Evershed 2008), while the examination of sherds using solvent extraction is widely used to compensate for the loss of compositional information when complex lipids are hydrolysed (Roffet-Salque *et al* 2017). Gas chromatography and mass spectrometry allow the microgram (μg) to nanogram (ng) amounts of compounds to be detected and identified due to their higher sensitivities. The possibility of extracting stable isotope information from individual biomarker structures is also realized thanks to the advent of gas chromatography–combustion–isotope ratio mass spectrometry (GC-C-IRMS) in the 1990s introduced, which allowed to explore a range of new avenues in the application of organic residue analysis in archaeology (Mottram *et al* 1999; Colombini *et al* 2005; Stacey 2009; Cramp and Evershed 2015; Roffet-Salque *et al* 2017). These analytical methods allow amorphous and invisible organic materials to be detected and identified, further providing answers to complex archaeological questions in time and space.

As regards to the archaeological questions tied to organic residue analysis, trade in exotic goods and their distribution from specific site/s to regional scales has become the widely discussed subject in the study of transport amphorae and/or transport jars. Insights into production technology suitable for function/use and repair can be obtained from the analysis of organic residues from pottery. Specific aspects of use, repair as well as decoration can be approached along these frontiers from organic residue analysis. To date, a range of sealants such as waxes, resins and bituminous materials have been identified on archaeological ceramics, dating back as far as the Neolithic. A review of known sealants or coating materials is provided from several archaeometric works (Connan *et al* 2008 and 2020; Stern *et al* 2008; Stacey *et al* 2010). The use of FTIR and GC-MS has allowed to characterize organic residues present on transport vessels in as much as the study of the coating materials used to seal the walls of transport vessels to be suitable to transport liquids and/or foodstuff (Roffet-Salque Salque *et al* 2017). The versatility of these approaches has allowed to shed light on trade involving different regions.

In conclusion, archaeometric research on pottery, as well as on all cultural heritage materials, exploits analytical techniques generally used in other research fields for the study of organic and inorganic materials. The sampling strategy can influence interpretation, extent of

methodological and analytical techniques (Hunt 2016; Maritan 2019; Gliozzo 2020a). Analytical techniques applied in archaeometric studies of ceramic materials are defined by the sampling strategy (non-destructive and destructive techniques); solicitation sources used to investigate the sample (photons, electrons, protons, etc.) and the information needed to address the specific archaeological questions related to provenance, dating, production technology and conservation state (Tite 1999; Maritan 2019; Gliozzo 2020a). The nature of the information obtained (chemical, physical, mineralogical, micro-structural features), the cost of the analyses required, the availability of the instruments, the amount of the sample needed, and the time needed for analysis are generally considered in ceramic provenance studies.

Chemical analysis of minor and trace elements by INAA account for the first attempts to approach ceramic provenance studies (Arnold et al 1991; Mommsen 2011; Maritan 2019; Gliozzo 2020a;). Methods for elemental analysis, such as Optical Emission Spectroscopy (OES), Inductively Coupled Plasma Mass Spectrometry (ICP-MS), Energy-Dispersive X-ray spectroscopy (EDS, EDX) and XRF are widely applied to determine major and minor elements in the ceramic matrix and are used till the present days (Hein and Kilikoglou 2020). On the other hand, mineralogical studies of the ceramic matrix enable understanding of features such as the nature of raw materials used and firing conditions to investigate the production technology (Maritan 2019, Tite 1999, Quinn 2013).

Mineralogy of the pottery is usually studied by X-ray Diffraction (XRD), thin section petrography, Thermogravimetric analysis (TGA/DSC), Fourier-Transform Infrared Spectroscopy (FT-IR), Raman Spectroscopy, as well as Scanning Electron Microscope with Energy-Dispersive X-ray (SEM-EDS) (Tite 1999; Froh 2004; Maritan 2019; Gliozzo 2020a). The effects of firing conditions are also observed on the morphology and microstructure of the final product. These features are investigated by means of SEM, petrographic microscopy, and porosity analyses (Maritan 2019; Gliozzo 2020a).

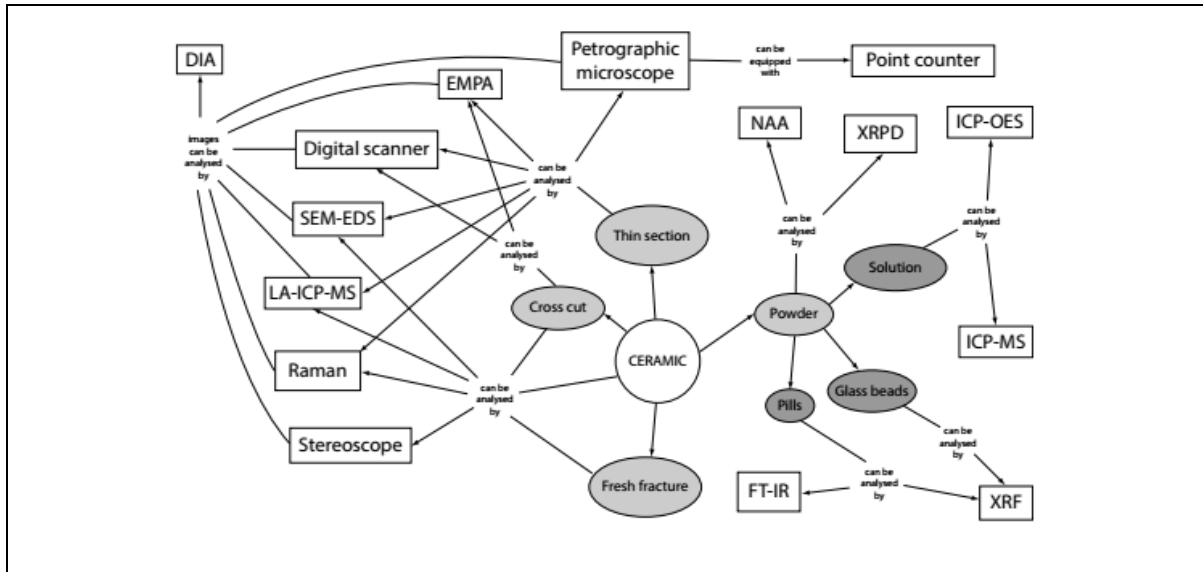


Figure 4: Analytical methods for ceramic archaeological analysis including sampling requirements (Eramo 2020)

Moreover, the use of FT-IR has proven to be a useful tool to screen the presence of organic residues in much as the versatility of chromatographic techniques and mass spectrometry to thoroughly study extant residues preserved in ceramic sherds (Derrick 1989; Font *et al* 2007; Dimitrakoudi *et al* 2011; Roffe Salque *et al* 2017; Nardella *et al* 2019; Connan *et al* 2020).

Having outlined the major themes around the archaeological study of pottery, a discussion of the research questions tackled in this study is provided next.

3.2. Research Questions

This archaeological research primarily focuses on the archaeological study of the Ayla-Aksum amphorae recovered from the on-going excavations at Adulis, in the Red Sea Coast of Eritrea. The amphorae are widespread over much of the Red Sea world and the frequency of their findings in Aksum and Adulis prompted archaeologists to coin the term Ayla-Aksum amphorae, further posing hypothesis on multiple production centres in the Red Sea world apart from the Ayla kilns. To date, little information exists on the archaeological study of the Ayla-Aksum pottery complex and its distribution in the 1st millennium CE from the African Red Sea shore. The gap that exists in terms of tackling the question of their provenance stimulated this archaeological work, which intended to provide petro-mineralogical as well as geo-chemical information to tackle the question of their provenance on one hand, and the study of the technology of their production by providing micro-structural and morphological information as well as the comprehension of mineralogy and phase identification on the

other. A full-fledged multi-analytical approach to the study of the Ayla-Aksum amphorae complex is provided at present from the sites of Ayla in Jordan and Zafar in Yemen (see Raith *et al* 2013). Archaeometric study of the Ayla-Aksum pottery from as archaeological sites in Southern Transjordan and the Negev is also provided by Holmqvist (2019) to understand production and exchange of late Byzantine and early Islamic pottery in the region. The previous studies laid the comparative basis for the archaeometric study of the Ayla-Aksum amphorae from the site of Adulis and interpretation was made based on the parallels with the existing literature.

Although this archaeometric research is framed on the study of Ayla-Aksum amphorae, the sampling of other ceramic classes including local pottery, Late Roman Amphora 1, *dolia samples* and red slipped ware was also considered for a comparative purpose¹. The selection of representative samples belonging to local production, particularly is quite crucial to see whether similarities/differences in petro-fabrics, mineralogy, geo-chemical information and micro-structural as well as morphological features can allow inferences on the question of the provenance and distribution of the Ayla-Aksum amphorae and the technology of their production. The study of imported transport and common wares (namely the Late Roman Amphora 1, *dolia* and red Slipped ware) is also equally important to provide comparative parallels as well as help build the ceramic sequence at Adulis, which has been primarily based on morpho-stylistic typological classification. Therefore, besides the comprehension of the provenance and distribution of the Ayla-Aksum amphorae samples recovered from the excavations at Adulis, the questions of provenance and technology of production of the different classes of pottery are equally tackled.

Moreover, samples which have been macroscopically classified as LRA 1(?) and characterized by a presence of a superficial coating material/residues and have been considered for organic residue analysis, in order to determine their possible content. Although these samples are possibly imported vessels and do not correspond to the main ceramic class analysed here, the organic residue analysis is considered due to the real chance of sampling such interesting materials from the on-going excavations at Adulis. Ceramics have largely

¹ The local pottery refers to a wide range of fabrics presumed to have been produced in Adulis. The Late Roman Amphora 1 (LRA 1) on the other hand is a long-lived (fourth to seventh century CE) family of medium-sized transport vessels ranging from 50 to 58 cm in height and 30 to 31 cm in length and were made in many production centers in the eastern Mediterranean, including Rhodes, western Anatolia, the Cilician coast, and Cyprus (Reynolds 2005). Finally, the *dolia* and red slipped ware also represent classes of imported pottery at Adulis and become relevant to understand pottery production exchange.

contributed to our understanding of the trade involving the Mediterranean, Red Sea, and Indian Ocean worlds and studies on the extent of these trade networks are growing by the study of organic contents preserved in different transport vessels. The Late Roman Amphora 1 and the Torpedo jars, which were produced in contemporary times, are excellent proxies for understanding the Indian Ocean trade during the 1st millennium CE and the distribution of these transport vessels over much of the Indian Ocean and Red Sea provides a comparative parallel. In this respect, the study of the coating materials present in these samples was intended to make inferences within these themes. The samples were also included within the wider questions of provenance and technology of production tackled in this study.

3.2.1 Sampling

The sampling procedure for the selection of Ayla-Aksum amphorae, local pottery, LRA1, *dolia* and red slipped ware fragments followed a protocol based on the evaluation of their diagnostic attributes. Fabric variability was preliminary defined from macroscopic observations and considered the representativeness of these materials in the various stratigraphic contexts of the excavated sectors at Adulis (Fig. 5). A large amount of the fragments considered for this study comes from contexts dated to 5th -7th CE. In few cases of fragments with insignificant diagnostic features, the attribution to specific typological classifications was problematic. The interpretation of petrographic fabrics and compositional groups pertaining to these samples is, thus, treated cautiously². Similarly, six raw clay samples have been selected from the vicinity of the archaeological site of Adulis to draw parallels in terms of petrographic, mineralogical, and geo-chemical proxies for the locally produced assemblages.

Samples which have been macroscopically classified as LRA 1(?) due to a few diagnostic features and characterized by a presence of a superficial coating material/residues have also been considered for organic residue analysis, in order to determine their possible content.

The samples considered in this study were obtained during the excavations in 2019 and 2020 at Adulis, where assistance was provided for typological classification by archaeologists. The attribution of different typologies for pottery uncovered from the excavations at Adulis is an on-going process and consequently samples have been ascribed by the researcher to suit the needs of this specific archaeometric work, while reference is also made to the sample ID

² Few samples posed a problem in terms of secure typological classification and were included in the sampling to see parallels with the classes considered and include samples 2.4, 2.9, 4.3 and 4.4.

provided in the Adulis database (see table 1). In a few cases, sample ID in the Adulis database is not provided as detailed work is on-going. Therefore, interpretation is made by referring to the sample names provided by the researcher and the specific classes of typologies pertaining to each sample studied. The list of the samples and related information on typology and stratigraphic contexts is provided in table 1.

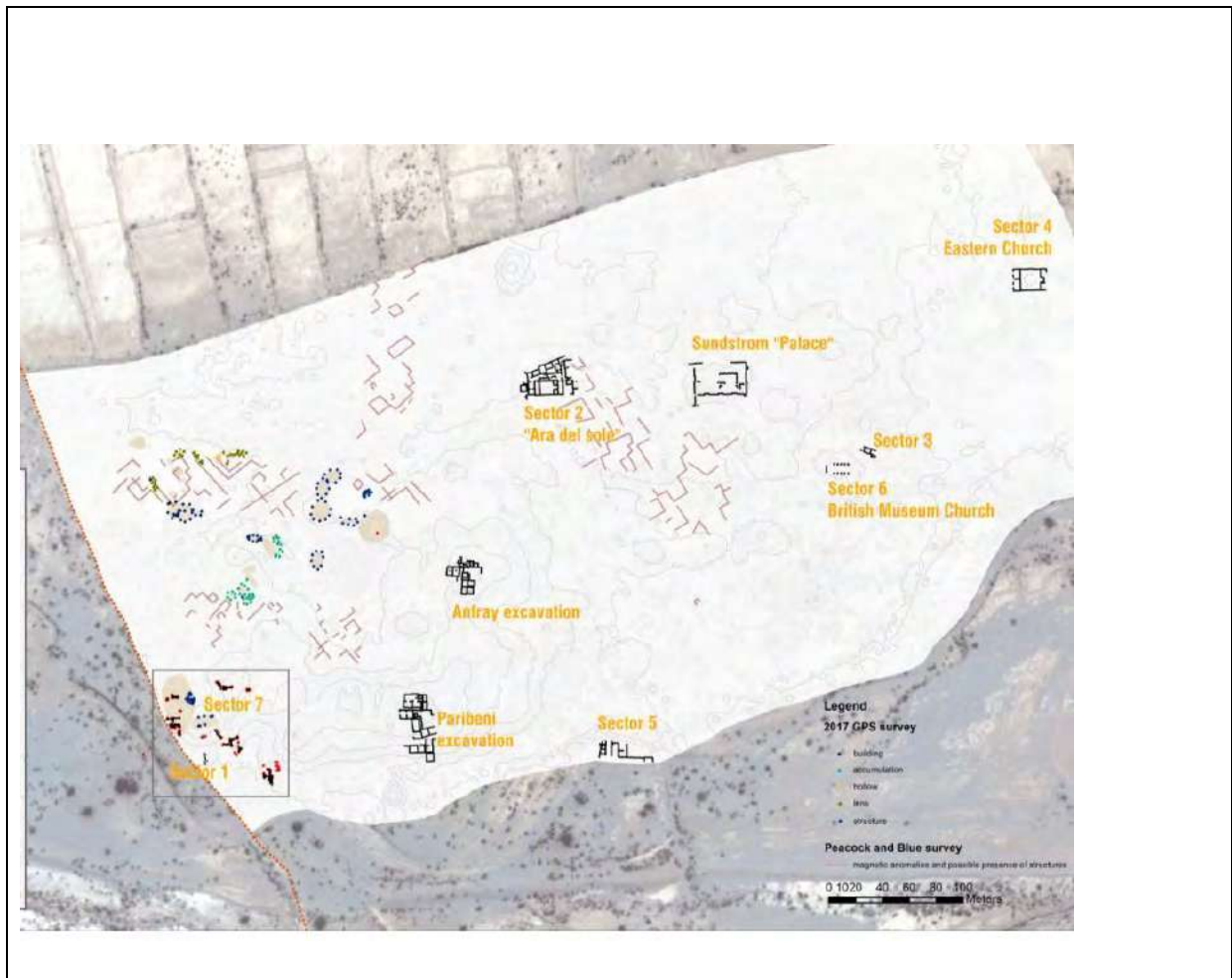


Figure 5: Map showing the sectors of excavation at Adulis (*Adulis Archaeological Project Reports, 2011-2018.*) Samples have been obtained from these sectors

Moreover, a comprehensive survey of on-line database repositories of the Roman amphorae digital resource (University of Southampton)³ and the Levantine Ceramic Project⁴ also enabled to make comparative parallels, particularly on imported pottery. The description of the samples considering their stratigraphic contexts and typological classification is provided in table 1. In summary, while the study of the Ayla-Aksum amphorae fragments in

³ https://archaeologydataservice.ac.uk/archives/view/amphora_ahrb_2005/

⁴ <https://www.levantineceramics.org/>

comparison to the rest of the pottery classes helped to tackle the question of their provenance, more generally this sampling choice provided data on petro-fabrics and compositional groups that will help establish the ceramic sequence for pottery excavated from Adulis.

Table 1: Description of samples considered in this study

Class	Sample	Year	Sector/locality	Associated SU	Description of SU	ID-Adulis database
Ayla	1.1	ADU '12	1	1035	Abandonment phase of collapsed basalt stones	None
	1.2	ADU'18	2	2513	southern wall of the staircase adjacent to the south perimeter of the church, phase 2	18.16- 18.17
	1.3.1	ADU '12	1	1001	surface layer	None
	1.3.2	ADU'12	2	1001	surface layer	None
	1.4.1	ADU '18	2	2178	collapse or accumulation north of 2116	18.66
	1.4.2	ADU '18	2	2178	collapse or accumulation north of 2116	18.66
	1.5	ADU '18	2	2173	deposit layer north of 2116	
	1.6	ADU '18	1	2123(B)	collapse east of 2116	18.11-18.14
	1.7.1	ADU '18	2	2177(B)	same as 2178	18.50-18.52
	1.7.2	ADU '18	2	2177(B)	same as 2178	18.50-18.52
	1.8	ADU '18	2	2518(B)	pit	
	2.0	ADU '14	5	5035	river sediment	
	3.3	ADU '19	2	2524=2527	collapse	19.20
	3.4	ADU '19	2	2524=2527	collapse	19.17
	3.5	ADU '19	2	2524=2527	collapse	19.18
	3.6	ADU '19	2	2524=2527	collapse	19.15
	3.7	ADU '19	2	2524=2527	collapse	19.14
	3.8	ADU '19		6033	eastern wall of the church	19.50
	C01	ADU '19	2	2524=2527	collapse	
	C04	ADU '19	2	2185	accumulation of ceramic fragments north of 2186	
C05	ADU '19	6	6036			
Local	2.5	ADU '18	2	2513	collapse / rubble covering the southern staircase	2513(4)
	2.6	ADU'18	2	2173	deposit layer north of 2116	2173(18)

Class	Sample	Year	Sector/locality	Associated SU	Description of SU	ID-Adulis database
	2.7	ADU '18	2	2173	deposit layer north of 2116	2173(9)
	2.8	ADU '18	2	2513	collapse / rubble covering the southern staircase	2173(2)
	CW01	ADU '20	3	3101A	collapse of the building near to the cathedral	CW01
	CW02	ADU '20	3	3101A	collapse of the building near to the cathedral	CW02
	CW03	ADU '20	3	3101A	collapse of the building near to the cathedral	CW03
	CW05	ADU '20	3	3101A	collapse of the building near to the cathedral	CW05
	CW07	ADU '20	3	3101A	collapse of the building near to the cathedral	CW07
	CW08	ADU '20	3	3101A	collapse of the building near to the cathedral	CW08
	CW09	ADU '20	3	3100	collapse of the building near to the cathedral	CW09
	CW11	ADU '20	3	3100	collapse of the building near to the cathedral	CW 11
	CW16	ADU '20	3	3101B	collapse of the building near to the cathedral	CW 16
	CW18	ADU '20	3	3101B	collapse of the building near to the cathedral	CW 18
	CW19	ADU '20	3	3101B	collapse of the building near to the cathedral	CW 19
	CW20	ADU '20	3	3101B	collapse of the building near to the cathedral	CW 20
	CW21	ADU '20	3	3101B	collapse of the building near to the cathedral	CW 21
Bricks	4.10	ADU '19	2	2532 A 1 st level	filling of 2532	
	4.11	ADU '19	2	2524=2527	collapse	
Raw Clay	H1	ADU '20	Afta	15°18'35''N 39°37'33''E	Halenga River	
	H2	ADU '20	Afta	15°18'35''N 39°37'33''E	Halenga River	
	F1	ADU '20	Foro	15°15'53''N 39°37' 11'' E	Foro Dam	
	F2	ADU '20	Foro	15°15'53''N 39°37' 11'' E	Foro Dam	
	M1	ADU '20	Zula	15°14'35''N 39°39' 53'' E	Merghena, Zula	

Class	Sample	Year	Sector/locality	Associated SU	Description of SU	ID-Adulis database
	M2	ADU'20	Zula	15°14'35''N 39°39' 53'' E	Merghena, Zula	
LRA1	1.9	ADU'18	2	2513	southern wall of the staircase adjacent to the south perimeter of the church, phase	18.32-18.37
	2.1	ADU '18	2	2123	collapse east of 2116	18.9 IP
	2.2	ADU '14	3	3058	Clay-silt stratum, ascribable to period 1, phase 2(5th -late 6th c.CE.	
	2.3	ADU '17	4	4110	Massive earthen layer, rich in charcoal and ceramic finds	17.9-17.16
	3.0	ADU '19	2	2522		19.37
	3.1	ADU '19	2	2522		19.38
	3.2	ADU '19	2	2524=2527	collapse	19.24
LRA1 (?)	C02	ADU'19	2	2176	small portion of a wall delimiting the grave 2175	
	C03	ADU'19	2	2525	collapse/accumulation	
	C06	ADU '19	2	2528	backfilling of the cut 2529	
	C07	ADU'20	6	6076	collapse of the room South to the apse of the "British Church"	
	C08	ADU'20	6	6076	collapse of the room South to the apse of the "British Church"	
	CO9	ADU'20	6	6076	collapse of the room South to the apse of the "British Church"	
	3.9	ADU '19	2	2528	backfilling of the cut 2529	19.77
<i>Dolia</i>	1.0	ADU'12	2	2116	Wall facing E-W orientation	None
	4.0	ADU '19	6	6011	Abandonment layer of pastophorion	19.71
	4.8	ADU '19	2	2524=2527	collapse	
	4.9	ADU '19	2	2533		19.88
Red Slipped	4.5	ADU '19	6	6037		19.70
	4.6	ADU '19	2	2524=2527	collapse	19.34

Class	Sample	Year	Sector/locality	Associated SU	Description of SU	ID-Adulis database
ND	2.9	ADU'18	2	2173	southern wall of the staircase adjacent to the south perimeter of the church, phase	2173(16)
	2.4	ADU '18	2	2513	southern wall of the staircase adjacent to the south perimeter of the church, phase	IP 5
	4.1	ADU '19	6	6038		19.86
	4.3	ADU '19	2	2524=2527	collapse	19.27
	4.4	ADU '19	6	6036		19.59

Moreover, the analytical methods used in this study constitute an approach to gain information on fabric description, petrographic mineralogical, and chemical signatures, morphological and micro-structural features as well as to evaluate the characterisation of the organic residues. A brief description of the analytical methods is provided in subsequent chapters, and the summary of the analytical approaches applied on each sample is provided in appendix 2.

3.3. Bibliography

Aloupi-Siotis E. (2020) Ceramic technology. How to characterise black Fe-based glass-ceramic coatings. *Archaeol Anthropol Sci.* <https://doi.org/10.1007/s12520-020-01134-x>.

Albero Santacreu D. 2014. Materiality, Techniques and Society in Pottery Production: The Technological Study of Archaeological Ceramics through Paste Analysis. Warsaw, Poland: De Gruyter Open Poland. <https://doi.org/10.2478/9783110410204>

Arnold D E, Neff H, Bishop R L. (1991) Compositional analysis and “sources” of pottery: an ethnoarchaeological approach. *Am Anthropol* 93(1):70–90. <https://doi.org/10.1525/aa.1991.93.1.02a00040>.

Aitchison J. 1986. The statistical analysis of compositional data. Chapman & Hall, London.

Baxter M J. (1994). Stepwise Discriminant Analysis in Archaeometry: A Critique, *Journal of Archaeological Science*, Volume 21, Issue 5, Pages 659-666, <https://doi.org/10.1006/jasc.1994.1065>.

Baxter M J. (2001) Statistical modelling of artefact compositional data. *Archaeometry* 43(1):131–147. <https://doi.org/10.1111/1475-4754.00008>.

Baxter M J. (2009) Archaeological data analysis and fuzzy clustering. *Archaeometry* 51(6):879–1054. <https://doi.org/10.1111/j.1475-4754.2008.00449.x>.

Baxter M J. 2015. Notes on quantitative archaeology and R. Research Gate, Nottingham.

Baxter M J, Beardah CC, Papageorgiou I, Cau MA, Day PM, Kilikoglou V. (2008) On statistical approaches to the study of ceramic artefacts using geochemical and petrographic data. *Archaeometry* 50(1):142–157. <https://doi.org/10.1111/j.1475-4754.2007.00359.x>

Bishop R L, Rands R L, Holley G. (1982) Ceramic compositional analysis in archaeological perspective. In: Schiffer MB (ed) *Advances in archaeological method and theory*, Vol. 5, 1982. Academic Press, New York.

Bortolini E. 2017. Typology and Classification. In A. M. W. Hunt (ed.), *The Oxford Handbook of Archaeological Ceramic Analysis*: 651–670. Oxford, Oxford University Press.

Buxeda I Garrigos J, Cau Ontiveros MA, Kilikoglou V. (2003) Chemical variability in clays and pottery from a traditional cooking pot production village: testing assumptions in Pereruela. *Archaeometry* 45(3):1–17. <https://doi.org/10.1111/1475-4754.00093>.

Buxeda i Garrigós J. (1999) Alteration and contamination of archaeological ceramics: the perturbation problem. *J Archaeol Sci* 26(3):295– 313. <https://doi.org/10.1006/jasc.1998.0390>.

Buxeda i Garrigós J, Kilikoglou V, Day P M. (2001) Chemical and mineralogical alteration of ceramics from a late bronze age kiln at Kommos, Crete: the effect on the formation of a reference group. *Archaeometry* 43(3):349–371. <https://doi.org/10.1111/1475-4754.00021>.

Chatfield M. (2010). Tracing firing technology through clay properties in Cuzco, Peru, *Journal of Archaeological Science*, Volume 37, Issue 4, <https://doi.org/10.1016/j.jas.2009.11.003>.

- Colombini MP, Giachi G, Modugno F, Ribechini E. (2005). Characterisation of organic residues in pottery vessels of the Roman age from Antinoe (Egypt) *Microchem J* 79:83–90. <https://doi.org/10.1016/j.microc.2004.05.004>.
- Eramo G. (2020) Ceramic technology. How to recognize clay processing. *Archaeol Anthropol Sci.* 12, 164. <https://doi.org/10.1007/s12520-020-01132-z>
- Evershed R P. (2008). Organic residue analysis in archaeology: the archaeological biomarker revolution. *Archaeometry* 50, 895–924. <https://doi.org/10.1111/j.1475-4754.2008.00446.x>.
- Fabbri B, Gualtieri S, Shoval S. (2014) The presence of calcite in Archaeological ceramics. *J Eur Ceram Soc* 34(7):1899–1911. <https://doi.org/10.1016/j.jeurceramsoc.2014.01.007>
- Froh J. 2004 *Archaeological Ceramics Studied by Scanning Electron Microscopy*. Hyperfine interactions 154: 159-176. Kluwer Academic Publishers.
- Gliozzo E. (2020a) Ceramic technology. How to reconstruct the firing process. *Archaeol Anthropol Sci.* 12, 260. <https://doi.org/10.1007/s12520-020-01133-y>
- Gliozzo E. (2020b). Ceramic technology. How to reconstruct the firing process. *Archaeol Anthropol Sci* **12**, 260. <https://doi.org/10.1007/s12520-020-01133-y>
- Heimann R, Maggetti M. 2014. *Ancient and historical ceramics: materials, technology, art and culinary traditions*. Schweizerbart and Bortraeger science publishers, Stuttgart, pp 550.
- Hein A, Kilikoglou V. (2020) Ceramic raw materials. How to recognize them and locate the supply basins *Chemistry. Archaeol Anthropol Sci.* 12, 180. <https://doi.org/10.1007/s12520-020-01129-8>
- Holmqvist-Sipilä E. 2019. *Ceramics in Transition: Production and Exchange of Late Byzantine-Early Islamic Pottery in Southern Transjordan and the Negev*. Archaeopress. ISBN 978-1-78969-225-9 (e-Pdf).
- Hunt A M W. 2016. *The Oxford handbook of archaeological ceramics analysis*. Oxford University Press, Oxford. ISBN: 9780199681532.
- Ingold T. (2012) Toward an ecology of materials. *Annu Rev Anthropol* 41:427–442. <https://doi.org/10.1146/annurev-anthro-081309-145920>.

Ionescu C, Hoeck V. (2020) Ceramic technology, How to investigate surface finishing. *Archaeol Anthropol Sci* <https://doi.org/10.1007/s12520-020-01144-9>.

Keay S J. 1984. Late Roman amphorae in the Western Mediterranean. A typology and economic study: the Catalan evidence. Oxford: British Archaeological Reports International Series.

Kilikoglou V, Maniatis Y, Grimanis A P. (1988) The effect of purification and firing of clays on trace element provenance studies. *Archaeometry* 30(1):37–46. <https://doi.org/10.1111/j.1475-4754.1988.tb00433.x>.

Maggetti M. (1982) Phase analysis and its significance for technology and origin. In: Franklin AD, Olin JS (eds) *Archaeological ceramics*. Smithsonian Institution Press, Washington, pp 121–133.

Maritan L, Nodari L, Mazzoli C, Milano A, Russo U. (2006) Influence of firing conditions on ceramic products: experimental study on clay rich in organic matter. *Appl Clay Sci* 31(1-2):1–15. <https://doi.org/10.1016/j.clay.2005.08.007>

Maritan L, Mazzoli C, Freestone I C. (2007) Modelling changes in mollusc shell internal micro-structure during firing: implication for temperature estimate in shell-bearing pottery. *Archaeometry* 49:529–541. <https://doi.org/10.1111/j.1475-4754.2007.00318.x>

Maritan, L. (2019) Archaeo-ceramic 2.0: investigating ancient ceramics using modern technological approaches. *Archaeol Anthropol Sci* 11:5085–5093. <https://doi.org/10.1007/s12520-019-00927-z>.

Maritan L. (2020) Ceramic abandonment. How to recognise post depositional transformations. *Archaeol Anthropol Sci*. 12, 199. <https://doi.org/10.1007/s12520-020-01141-y>.

Maritan L, Mazzoli C. (2004) Phosphates in archaeological finds: implications for environmental conditions of burial. *Archaeometry* 46(4): 673–683. <https://doi.org/10.1111/j.1475-4754.2004.00182.x>.

Mentesana R, Kilikoglou V, Todaro, S V, & Day, P M. (2019). Reconstructing change in firing technology during the Final Neolithic–Early Bronze Age transition in Phaistos, Crete.

Just the tip of the iceberg? *Archaeological and Anthropological Sciences*, 11, 871-894.
<https://doi.org/10.1007/s12520-017-0572-8>.

Mommsen H. (2011) Provenancing of pottery. In: *Nuclear Techniques for Cultural Heritage Research*. International Atomic Energy Agency (IAEA), Vienna, pp 41–70.

Montana G. (2020) Ceramic raw materials. How to recognize them and locate the supply basins. *Mineralogy, petrography. ArchaeolAnthropol Sci.* 12, 175
<https://doi.org/10.1007/s12520-020-01130-1>.

Müller N S. 2017. Mechanical and thermal properties. In: Hunt AM (ed) *The Oxford handbook of archaeological ceramic analysis*. Oxford University Press, Oxford, England, pp 603–624.

Neff H, Glascock M D. (1995). The state of nuclear archaeology in North America. *Journal of Radioanalytical and Nuclear Chemistry, Articles 196*, 275–286
<https://doi.org/10.1007/BF02038045>.

Nodari L, Maritan L, Mazzoli C, Russo U. (2004) Sandwich structures in the Etruscan-Padan type pottery. *Appl Clay Sci* 27:119–128. <https://doi.org/10.1016/j.clay.2004.03.003>.

Nodari L, Marcuz E, Maritan L, Mazzoli C, Russo U. (2007) Hematite nucleation and growth in the firing of carbonate-rich clay for pottery production. *J Eur Ceram Soc* 27:4665–4673.
<https://doi.org/10.1016/j.jeurceramsoc.2007.03.031>.

Papageorgiou I. (2018) Cluster analysis. In: *The SAS Encyclopaedia of Archaeological Sciences*. John Wiley & Sons. <https://doi.org/10.1002/9781119188230.saseas0099>.

Papageorgiou I. (2020) Ceramic investigation. How to perform statistical analyses. *Archaeol Anthropol Sci.* 12, 210. <https://doi.org/10.1007/s12520-020-01142-x>.

Pradell T, Molera J. (2020) Ceramic technology. How to characterise ceramic glazes. *Archaeol Anthropol Sci* <https://doi.org/10.1007/s12520-020-01136-9>.

Quinn P S. 2013. *Ceramic petrography: the interpretation of archaeological pottery and related artefacts in thin section*. Archaeopress, Oxford.

Reynolds P. (2005). *Levantine amphorae from Cilicia to Gaza: a typology and analysis of regional production trends from the 1st to 7th centuries*. Conference: LRCWI. Late Roman

Coarse Wares, Cooking Wares and Amphorae in the Mediterranean: Archaeology and Archaeometry at: Barcelona, 14-16th March 2002 Volume: British Archaeological Reports, International Series 1340.

Roffet-Salque M, Dunne J, Altoft D T. Emmanuelle Casanova Lucy J. Smyth J Whelton, H.L. Evershed R P (2017) From the inside out: Upscaling organic residue analyses of archaeological ceramics, *Journal of Archaeological Science: Reports*, Volume 16, pp. 627-640, <https://doi.org/10.1016/j.jasrep.2016.04.005>.

Roux V. 2017. Ceramic manufacture. The chaîne opératoire approach. In: Hunt AM (ed) *The Oxford handbook of archaeological ceramic analysis*. Oxford University Press, Oxford, England, pp 101–113.

Schlanger N. (1994) Mindful technology: unleashing the chaîne opératoire for an archaeology of mind. In: Renfrew C, Zubrow EBWE (eds) *the ancient mind: elements of cognitive archaeology*. Cambridge University Press, pp 143–151.

Sillar B, Tite M S. (2000) The challenge of ‘technological choices’ for materials science approaches in archaeology. *Archaeometry* 42(1):2–20. <https://doi.org/10.1111/j.1475-4754.2000.tb00863.x>

Stacey R. (2009). *Organic Residues: Origins, Analysis and Scope — An Overview for the Archaeological Ceramicist*. *The Old Potter's Almanack*. 14, 1–8.

Stern B, Connan J, Blakelock E, Jackman R, Coningham, R A E, Heron C. (2008). From Susa to Anuradhapura: reconstructing aspects of trade and exchange in bitumen coated ceramic vessels between Iran and Sri Lanka from the third to the ninth centuries AD. *Archaeometry* 50, 409–428. <https://doi.org/10.1111/j.1475-4754.2007.00347.x>.

Stoner D W. (2016) The analytical nexus of ceramic paste composition studies: A comparison of NAA, LA-ICP-MS, and Petrography in the Pre-Hispanic Basin of Mexico, *Journal of Archaeological Science*, Volume 76, pp. 31-47, <https://doi.org/10.1016/j.jas.2016.10.006>.

Thér R. (2020) Ceramic technology. How to reconstruct and describe pottery-forming practices. *Archaeol Anthropol Sci*. 12, 172. <https://doi.org/10.1007/s12520-020-01131-0>.

Tite M S. (1999) Pottery production, distribution, and consumption—the contribution of the physical sciences. *J. Archaeol Method Theory* 6(3):181–233. <https://doi.org/10.1023/A:1021947302609>.

Tite M S, Maniatis Y. (1981) Technological examination of Neolithic-Bronze Age pottery from central and southeast Europe and from the Near East, *Journal of Archaeological Science*, Volume 8, Issue 1. pp. 59-76. <https://doi.org/10.1038/257122a0>.

Trindade M J, Dias M I, Coroado J, Rocha F. (2009) Mineralogical transformations of calcareous rich clays with firing: a comparative study between calcite and dolomite rich clays from Algarve, Portugal. *Appl Clay Sci* 42:345–355. <https://doi.org/10.1016/j.clay.2008.02.008>

Xanthopoulou V, Iliopoulos I, Liritzis I. (2021) Mineralogical and Microstructure Analysis for Characterization and Provenance of Ceramic Artifacts from Late Helladic Kastrouli Settlement, Delphi (Central Greece). *Geosciences*, 11,36. <https://doi.org/10.3390/geosciences11010036>

4. Archaeological and Geological Context

4.1 Archaeological Context

The archaeological context of this study provides a synopsis of the occupation phases of the archaeological site of Adulis by highlighting the importance of the site in the Red Sea, Indian Ocean, and Mediterranean commerce. Since the archaeometric work is situated particularly within the study of the Ayla-Aksum amphorae, a brief glimpse of the sites of Ayla and Zafar is also incorporated from where archaeometric studies of the Ayla-Aksum amphorae have been reported.

4.1.1. The Archaeological Site of Adulis

The site of Adulis lays in the bay of Zula, on the Eritrean coast. Adulis was the most important port for trade in the northern Horn of Africa during antiquity linking the early urban settlements of the Eritrean and Ethiopian highlands and of the coastal people (Peacock and Blue 2007; Schimdt *et al* 2008; Zazzaro *et al* 2014). The origins and the demise of the ancient port city of Adulis remain debated. Earliest phases of occupation have been suggested from the discovery of levels of occupation containing ceramics that may correspond to possible 2nd – 1st millennium BCE (Manzo 2010). Yet, current knowledge of the direct contacts of the ancient port of Adulis with peoples from the western Mediterranean and of the western Indian Ocean, particularly, since the latest centuries BCE to the early 7th century CE comes from literary sources and archaeological evidence uncovered from this site and other archaeological sites in the Red Sea basin, Eastern Mediterranean, and Indian Ocean. Featuring both in Classical and Byzantine sources, the development and history of Adulis has been connected to other Red Sea ports such as Berenike, Myos Hormos, Clysma and Ayla (Peacock and Blue 2007; Zazzaro 2013; Seland 2014) In this respect, the connections of Adulis to Berenike and Myos Hormos (the main ports of Romans in the Red Sea) is evinced in the 1st and 2nd centuries CE, while the northern Red Sea ports of Ayla and Clysma became directly linked to Adulis from the 4th century CE, and particularly at the end of 5th -early 6th century. These phenomena attest to the role of Adulis in the articulation of the Roman, Aksumite and Byzantine commerce from the first centuries BCE to Late Antiquity.

First mentions of Adulis date back to the 1st century AD. Pliny the Elder, when describing the eastern coast of Africa, mentions an *oppidum Aduliton*, NH (6.34). The relevance of the site in the international trade is clearly attested by Pliny as he defined Adulis as the most important emporium for the people of Trogydytica and Aethiopia (*maximum hic emporium Trogydytarum, etiam Aethiopum*). The *Periplus of the Red Sea* also refers to the settlement as an emporium mainly for the ivory, obsidian, and turtle shells (*Periplus Maris Erythraei* 23; Casson 1989). It has been mentioned that Adulis appears to have been an independent port in its earlier stages (Peacock and Blue, 2007; Zazzaro 2013; Zazzaro *et al* 2014). Adulis, however, as a port of the Aksumite Empire came to prominence to the western sources after the 4th century CE. The rise to prominence of Aksum as a regional power is partly related to the loosening of the control of the western side of the Red Sea by the Romans (Phillipson 2000; Zazzaro *et al* 2014; Fattovich 2019). A long period of political and military instability that occurred during the 3rd century CE culminated in the weakening of the Roman Empire and favoured the rise of a regional power in the Horn of Africa. Aksum's involvement in the Mediterranean-Indian Ocean trade was possible through Adulis and its military control over the southern Red Sea. Aksumite ventures to seize control of the opposite coast of the Red Sea in southern Arabia from late 2nd -early 3rd century CE are reported (Munro-Hay 1991) while a hegemony of the maritime trade is attested by the 6th CE (Zazzaro 2013; Zazzaro *et al* 2014). The *Martyrium Sancti Arethae* (*Martyrium Sancti Arethae et sociorum in Civitate Negran Caput VII*) reports an important episode on the importance of Adulis and Aksum in the international and political developments of the Red Sea world in Late Antiquity. Aksumite alliance with the Byzantines in terms of trade network to India and a military intervention in South Arabia against the Jewish Himyarite ruler has been noted (Zazzaro *et al* 2014; Yule 2013; Massa and Giostra 2018). Archaeological evidence from Qani and Zafar in Yemen attest to Adulitan/Aksumite pottery types and coins, further highlighting Adulis and Aksum's period of major expansion in the Red Sea and beyond (Yule 2013). Glazed wares from southern Arabia have also been reported from excavations at Adulis. The port city of Adulis was, thus, a prominent port of trade for all its long history, spanning from the last centuries BCE to the 7th century CE. It also played a significant role in international policy in the Red Sea area, especially from the late 3rd to the 7th century CE.

The site has been identified for the first time by Henry Salt at the beginning of the 19th century in the Zula Bay (Peacock and Blue 2007). The first field-survey was conducted in 1840 by Vignaud and Petit, as part of the Theophile Lefebvre mission. The first excavation

was conducted in 1868 by Captain William West Goodfellow, under the auspices of the British Museum. Similarly, Theodore Bent produced a graphic documentation of the site at the end of the 19th century. In 1906 Richard Sundström, a team member of the Enno Littmann expedition, excavated a large building in the Northeastern sector of the site. After one year, in 1907 the Italian archaeologist Roberto Paribeni conducted a substantial excavation in different areas of the site (Peacock and Blue 2007; Zazzaro *et al* 2014). As a result, two Byzantine “Churches” and the early levels of occupation of the site were identified at the Southwest limit (Zazzaro *et al* 2014). Adulis was also excavated in the 1960s by Francis Anfray (Zazzaro 2013) to document residential areas in the central sector of the site (Peacock and Blue 2007; Zazzaro *et al* 2014). Moreover, survey works were conducted by the University of Southampton team in the early 2000s in collaboration with Eritrean institutions. The surveys highlighted the perimeters of the site, but no archaeological excavations were carried out (Peacock and Blue 2007).



Figure 6: Excavation Sectors at Adulis (Adulis Archaeological Project Reports, 2011-2018.)

At the present, excavation campaigns are conducted at Adulis in the framework of the joint Eritrean- Italian ventures which began in 2011. The aim has been to provide the first detailed chronological sequence of the occupation and development of the site and devise a conservation mechanism procedure for the exposed monuments. Archaeological finds, particularly ceramic and stone remains that presumably originated from central Italy, Northeast Africa, Eastern Mediterranean, South Arabia, the Gulf area, and from the territories

of the Nabataean Kingdom, the Byzantine and the Indian Empire of Gupta have been uncovered from the recent excavations at Adulis (Zazzaro 2013; Bortolotto *et al* 2013; Zazzaro *et al* 2014; Massa *et al* 2018). In this respect, imported Levantine and African ceramic assemblages have been brought to light.

Comparative analysis of architectural and ceramic typological sequences attest that the site was continuously inhabited from the 1st-2nd up to the 6th and early 7th c. CE and intensely occupied in the 5th- 6th c. CE (Zazzaro *et al* 2014). Late Roman and Byzantine transport and common wares that have been uncovered from excavations at Adulis are particularly of interest in terms of the scope of this archaeometric study, broadening our understanding of the extent of the trade exchanges that involved the ancient port city of Adulis. Future research is expected to explore in-depth these contacts in terms of socio-economic and cultural implications, particularly in the 1st millennium CE.

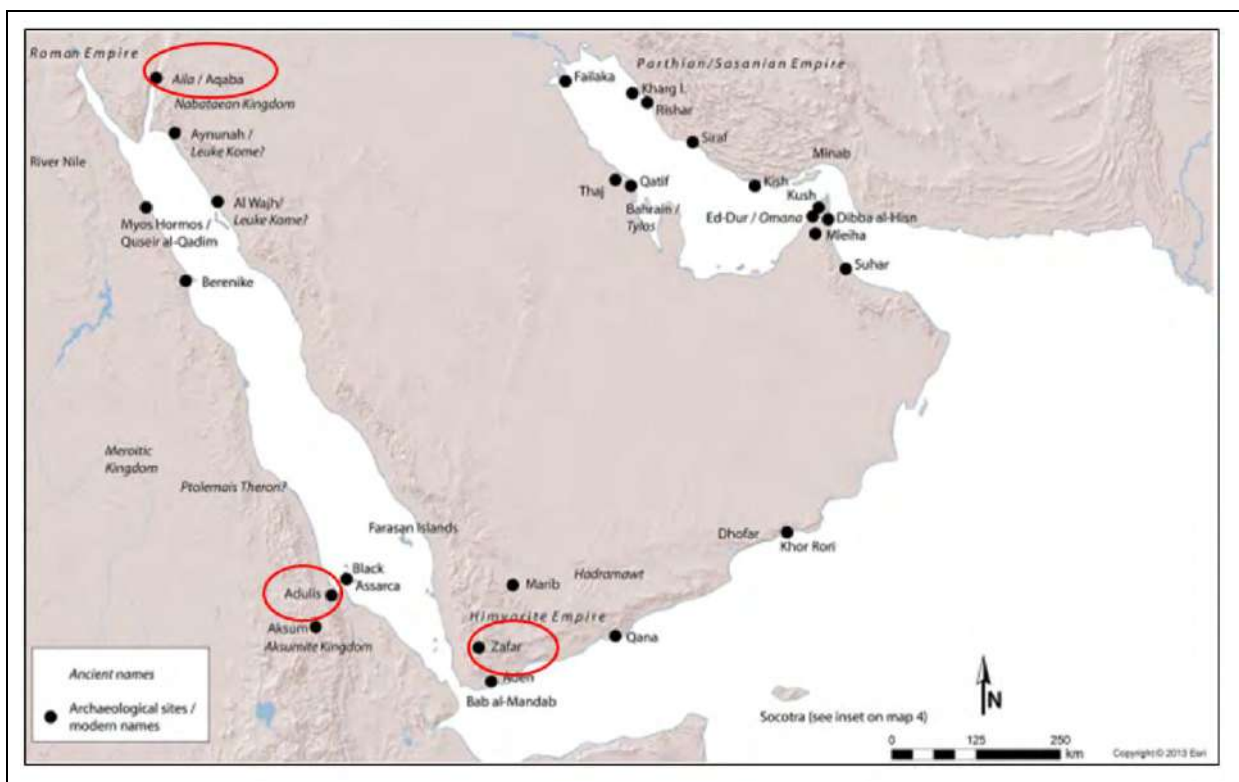


Figure 7: Map of archaeological sites mentioned (Seland 2014)

4.1.2. The Archaeological site of Zafar

Zafar was the capital of the Himyarites (110 BCE - 525 CE), which at its peak ruled most of the Arabian Peninsula. The settlement's beginnings are not well known from an archaeological perspective (Yule 2007 and 2013). Yet mentions of the site is provided in the

Periplus of the Erythraean Sea and Pliny's Natural History as well as in the Geographia of Claudius Ptolemaeus (Yule 2007; Periplus Maris Erythraei 23; Casson 1989).

It is mentioned that Himyar became the seat of power in South Arabia from the late 3rd century onwards (Yue 2013), while in the mid-4th century an early monotheism, Judaism, and subsequently Monophysite Christianity germinated in Arabia and particularly in Zafar, reaching the royal family in the later 4th century CE (Yule 2007 and 2013). During the 6th to 7th centuries CE competing religious and political interest groups made the Arabian Peninsula a hotbed of war and migration (Yule 2007). Himiyar's importance was significant as both the Sasanian and Byzantine empires tangled and manipulated it and its neighbours for their power struggle with an eye to strategic military advantage, Orthodox Byzantium and Monophysite north-east Africa successfully fostered Christian proselytism in Arabia (Yule 2007 and 2013; Bowersock 2013), hallmarking the contest for universal empire and religion. The naval expedition of the allied Byzantine and Aksumite fleet against the king of Himyar was gathered from Adulis to South Arabian territory in 525 A.D. (Massa and Goistra 2018) Consequently, the competition for trade and political advantage around Arabia between Persia, Aksum, and Byzantium culminated into the strategic importance of Zafar in the southern Red Sea during these epochs.

4.1.3. The Archaeological site of Ayla

Ayla/Aila (modern Aqaba) lies at the northern end of the Gulf of Aqaba in southern Jordan today. Ayla seems to have reached its height in late Roman times (Melkawi *et al* 1994; Whitcomb 2001). Excavations by North Carolina State University over six seasons between 1994 and 2002, and by the University of Chicago, revealed links between Ayla and other regions of the Red Sea (Parker 2002). Modern Aqaba has a long history as an international commercial center on the northern coast of the Red Sea. The history of the port city, also well linked with caravan routes, goes back to the Nabataean and Roman periods, to the 1st century BCE (Whitcomb 2001; Parker 2002). Contacts included some of the Egyptian Red Sea ports and, probably indirectly, as the finds of Aksumite/Adulis pottery and coins indicate, with the Kingdom of Aksum, via its main port of Adulis, and points in Southern Arabia. (Melkawi *et al* 1994). The archaeological evidence shows that the town also maintained its commercial and international role throughout the early Islamic period into the late 'Abbasid and Fatimid periods (Whitcomb 2001). The town had a significant, politically important, status in the Islamic period, as its control was essential for the Hajj route.

The archaeological evidence shows that the town also maintained its commercial and international role throughout the early Islamic period into the late Abbasid and Fatimid periods (Whitcomb 2001). The town had a relevant political role in the Islamic period, as its control was essential for the Hajj route.

The town is also of particular interest in terms of ceramic exchange, a specific type of transport vessel, the so-called Ayla-Aksum amphorae presumed to have been locally produced at Ayla kilns (Parker 2006; Melkawi *et al* 1994; Whitcomb 2001; Seland 2014). These amphorae were traded particularly in the Red Sea world and judging by their spread, contained a product highly appreciated in the past and maybe, from the beginning of the 4th century AD until the 7th century CE, arrived in some significant ports along the shorelines of the Red Sea and the Arabian Peninsula (Melkawi *et al* 1994; Pedersen 2008; Rath *et al* 2013; Harrower *et al* 2019). In addition to Egypt, the Ayla-Aksum amphorae were found in several sites along the eastern coast of Africa and in the southernmost part of Arabia.

4.2. Geological Context

Adulis lies north-northwest of the Danakil Depression, a continental rift which radiates north-northwest from a plate-tectonic triple junction within a complexly rifted and faulted basaltic lowland called the Afar triangle. The triangle is characterized by an active crustal spreading center and volcanism associated with basaltic centers of silicic volcanism (Clynne *et al* 2005). To the northwest of Adulis is Ghedem dome which exhumes a gentle arch of gneissose granitoids interleaved with thin layers of amphibolites, capped by thin, discontinuous, faulted panels of staurolite, kyanite, and garnet schists exposed in two young coast-parallel horsts (Talbot and Gebreab. 1997; Gebreab and Talbot, 2000). According to Gebreab and Talbot (2000), two tectono-stratigraphic units, orthogneisses and pelitic–semi-pelitic rocks, occur within the Ghedem Terrane. Many of the orthogneisses are garnet-bearing quartz–feldspar–amphibole–biotite, garnet-bearing quartz–feldspar–muscovite and feldspar–amphibole gneisses with conformable and locally slightly discordant thin amphibolites and actinolite–tremolite meta-igneous sheets (Gebreab and Talbot 2000). The Ghedem terrane also is characterized by a zone of mylonites, which occur where pale granitic gneisses are interleaved with dark amphibolites. Various generations and orientations of pegmatites also occur in aureoles around granitic plutons which intruded the orthogneisses and the pelitic–semi-pelitic rocks and are more concentrated in Mt Ghedem and its surroundings (Gebreab and Talbot 2000). Moreover, vesicular basalts crop out at the tract between E’ngua (vicinity

of Foro) and Kadra village as well as the Gumez and Galala hills. Recent Quaternary fluvial sediments cover the area, along the Red Sea shore, stretching North-South between the Mt. Ghedem and the Arfaile. This formation crops out within the western platform of the Foro-Wi'a region. The site of Adulis lies within a delta fan drained and deposited by the Alighede and Haddas rivers and numerous tributaries.

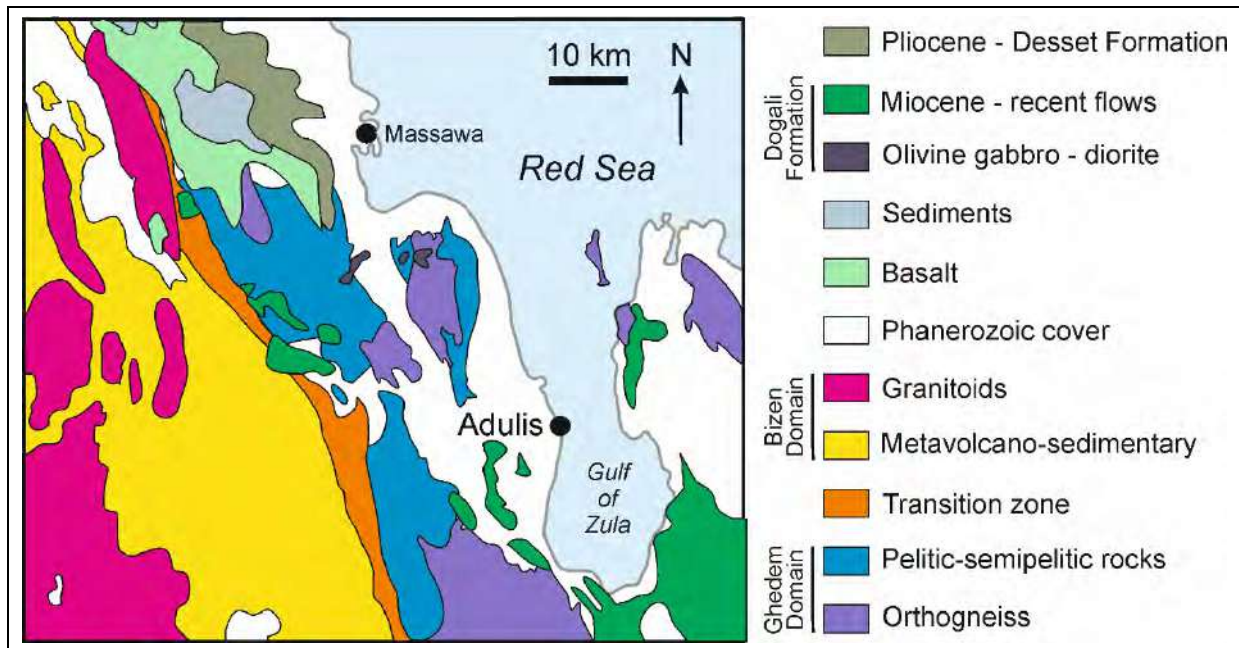


Figure 8: Geology of the area around Adulis (Gebreab and Talbot 2000)

As far as the geological frame of this study is concerned, it is also important to highlight the major geological features of the Aqaba area to make sense of the mineralogical and chemical characterization of the Ayal-Aksum amphorae. In this respect, the Wadi Arabah, Wadi Yutum and Wadi Shallala complexes are significant to understand the geology around Aqaba (Holmqvist 2019; Raith *et al* 2013). Geologically, the region within a 10km radius from Aqaba includes geological features from both sides of the Wadi ‘Arabah suite. The Negev side includes sedimentary units as well as more volcanic and metamorphic areas with granite and gneiss areas while to the southern Transjordan side the Wadi ‘Arabah is characterised predominantly by granite, gneiss and amphibolite (Holmqvist 2019). The Yutum and Shallala wadi systems which are the two southern wadis that culminate on Aqaba are also important to consider. The Neoproterozoic Yutum granitic suite immediate to the east of Aqaba and its proximity to the ceramic production centres has been discussed by Raith *et al* 2013. It has been indicated that the temper material for Ayla amphorae studied by Raith *et al* (2013) was taken from the unweathered and poorly sorted alluvial scree and fan deposits flanking the weathered monzogranitic rocks of the Imram complex. The wadi beds contain substantial

clay deposits which presumably were relatively easily accessible in antiquity as well (Raith *et al* 2013). On the other hand, Holmqvist (2019) in the study of Ayla amphorae from the Transjordan and Negev sites noted that the mineralogical inclusions of the Ayla amphorae studied included plagioclase, biotite, and garnet-group minerals, which can be related to the gneiss and granite areas, whereas augite and titanomagnetite inclusions have been attributed to the basaltic area on the Negev side.

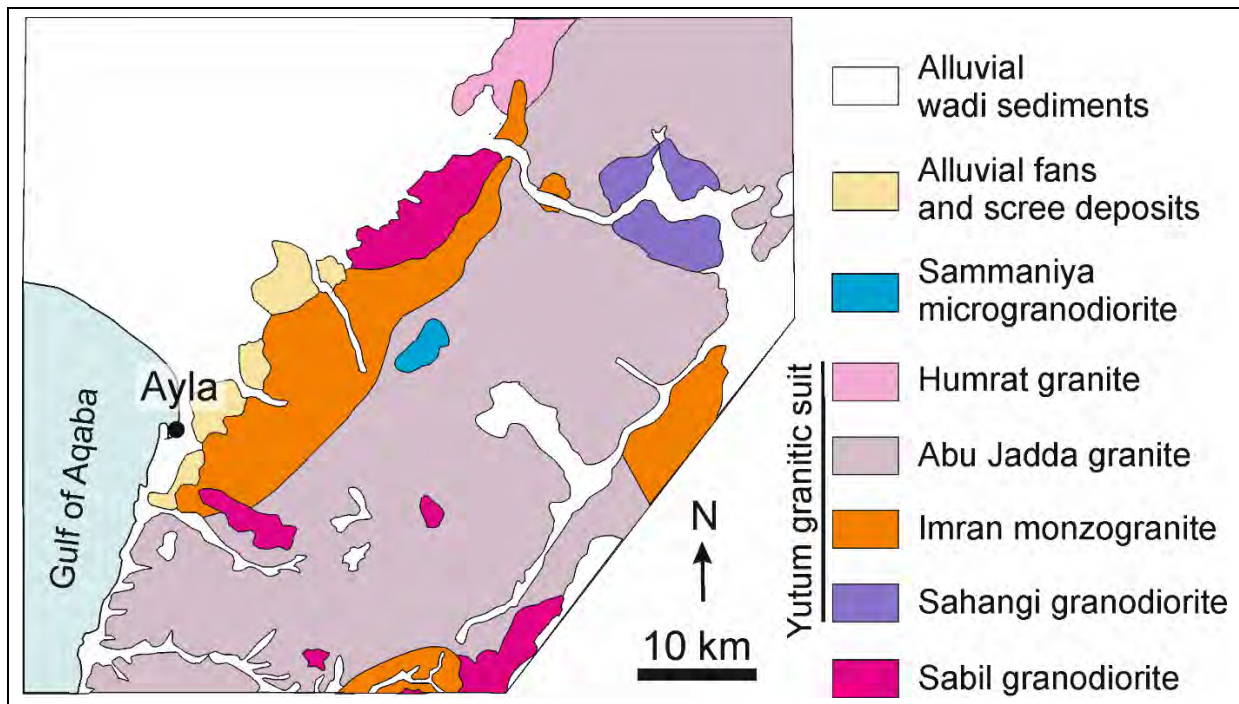


Figure 9: Map Showing the Geology around Aqaba (Raith *et al* 2013)

4.3. Bibliography

Acta Sanctorum 1869. Martyrium Sancti Arethae et sociorum in Civitate Negrans Caput VII. Acta Sanctorum, Octobris, Tomus Decimus. Paris et Romae.

Bortolotto S, Cattaneo N, Massa S. (2013). Adulis, una città-porto tra Mediterraneo e Oceano Indiano: archeologia e restauro, in Conservazione e valorizzazione dei siti archeologici: approcci scientifici e problemi di metodo, 29° Convegno Internazionale Scienza e Beni culturali, Bressanone 9-12 luglio 2013, Venezia, pp. 923-934.

Bowersock, G W. 2013. *The Throne of Adulis. Red Sea Wars on the Eve of Islam*. Oxford University Press. New York. ISBN 978-0-19-973932-5.

Castiglioni A, Castiglioni A, Gebreyesus Y, Giostra C, Massa S, Manzo A, Bortolotto S. (2018). Archaeological research at Adulis: the Eritrean-Italian joint project 2011-2015, in *International Conference on Eritrean Studies (20-22 July 2016), Proceedings, (Asmara, 20-22 July 2016)*, 895-915. Sabur Printing Services, Asmara.

Casson L. (ed. and tr.) 1989. *The Periplus Maris Erythraei. Text with Introduction, Translation and Commentary*. Princeton University Press, Princeton

Clyne M A, Weldell A D, Fournier R O, Woldegiorgis L, Janik C J, Kahsai G, Lowenstern J B, Teklemariam K, Smith J S, and Tesfai T. (2005). A Geological and Geochemical reconnaissance of The Alid Volcanic Center, Eritrea, east Africa. *Proceedings World Geothermal Congress 2005*: 1-8.

Fattovich R. (2019). From Community to State: The Development of the Aksumite Polity (Northern Ethiopia and Eritrea), c. 400 BC–AD 800. *Journal of Archaeological Research* 27:249–285. Springer. <https://doi.org/10.1007/s10814-018-9122-x>

Ghebreab W and Talbot C J. (2000). Red Sea extension influenced by Pan-African tectonic grain in eastern Eritrea, *Journal of Structural Geology* (22). No. 7, pp. 931-946. [https://doi.org/10.1016/S0191-8141\(00\)00022-5](https://doi.org/10.1016/S0191-8141(00)00022-5)

Harrower M J, Dumitru I A, Perlingieri C, Nathan S, Zerue K, Lamont J L, Bausi A, Swerida L, Bongers J L, Woldekiros HS, Poolman LA, Pohl C M, Brandt S A, Peterson E A (2019). Beta Samati: discovery and excavation of an Aksumite town. *Antiquity*, Volume 93, Issue 372:1534-155. <https://doi.org/10.15184/aqy.2019.84>.

Holmqvist E 2019. *Ceramics in Transition: Production and Exchange of Late Byzantine - Early Islamic Pottery in Southern Transjordan and the Negev*. Archaeopress Publishing Ltd. ISBN 978-1-78968-221-9(e-Pdf).

Melkawi A, Amr K, Whitcomb D. (1994) The excavation of two seventh century pottery Kilnsat Aqaba. *Annu Dept Antiquities Jordan* 38:447–467.

Manzo A. (2010). Adulis before Aksum? Possible 2nd and 1st millennium BC evidence from the site of the ancient port. In: Lusini, G. (ed.), *Current Trends in Eritrean Studies*. Annali Università degli Studi di Napoli “L’Orientale” 70. Arbor Sapientiae, Roma, pp. 29–42.

Massa S and Giostra C. (2018). The Christianisation of Adulis in light of the material evidence, In: Manzo, A. and Zazzaro, C.(eds) *Stories of Globalisation: The Red Sea and the Persian Gulf from Late Prehistory to Early Modernity*. Selected Papers of Red Sea Project VII. ISBN: 9789004362321. Brill.

Parker S T. 2002. ‘The Roman ‘Aqaba Project: The 2000 Campaign’, *Annual of the Department of Antiquities of Jordan* 46: 409-428.

Parker S T. (2006) Resources, routes, settlement patterns and interaction in the Wadi Arabah” In *Crossing the Rift*, Piotr Bienkowski, Katharina Galor, eds. (Oxford: Oxbow Books),223-230.

Peacock D. & Blue L. (eds.) 2007. *The Ancient Red Sea Port of Adulis, Eritrea Report of the Eritro-British Expedition, 2004–5*. Oxbow Books, Oxford.

Pedersen R K (2008). The Byzantine-Aksumite period shipwreck at Black Assarca Island, Eritrea. *Azania* 63, 77–94. <https://doi.org/10.1080/00672700809480460>.

Phillipson D W. 2000. *Archaeology at Aksum, Ethiopia, 1993–7*. Vol. 2. The Society of Antiquaries, London.

Raith M, Yule P and Damgaard, K. (2013). The view from Zafar: An archaeometric study of the Aqaba pottery complex and its distribution in the 1st millennium CE. *Zeitschrift für OrientArchäologie* 6: 318–348.

Schmidt P R, Curtis, M C. & Zelalem Teka. 2008. *The Archaeology of Ancient Eritrea*. Red Sea Press, Trenton, NJ.

Seland E H. (2014). Archaeology of Trade in the Western Indian Ocean,300 BC–AD 700. *Journal of Archaeological Research* 22:367–402. Springer. <https://doi.org/10.1007/s10814-014-9075-7>.

Talbot C J and Ghebreab W (1997). Red Sea detachment and basement core complexes in Eritrea. *Geology* 25, 655–658. [https://doi.org/10.1130/0091-7613\(1997\)025%3C0655:RSDABC%3E2.3.CO;2](https://doi.org/10.1130/0091-7613(1997)025%3C0655:RSDABC%3E2.3.CO;2)

Whitcomb D S. (2001). Ceramic production at Aqaba in the Early Islamic period. In Villeneuve, E., and Watson, P. M. (eds.), *La céramique Byzantine et proto-Islamique en Syrie-Jordanie (IVe-VIIIe siècles ap. J.-C.): Actes du colloque à Amman, 3–5 décembre 1994*, Institut Français d'Archéologie du Proche-Orient, Beirut, pp. 296–303

Yule P. 2007. *Himyar—Die Spätantike im Jemen /Late " Antiquity Yemen*. Aichwald: Linden Soft.

Yule P. (2013). A late antique Christian king from Zafar, southern Arabia. *Antiquity* 87: 1124–1135.

Zazzaro C. 2013. *The Ancient Red Sea Port of Adulis and the Eritrean Coastal Region. Previous Investigations and Museums Collections*. Cambridge Monographs in African Archaeology 85. BAR International Series 2569. Archaeopress, Oxford

Zazzaro C, Cocca E and Manzo A. (2014). Towards a chronology of the Eritrean Red Sea port of Adulis (1st – Early 7th Century AD). *Journal of African Archaeology* 12 (1), pp.43-73.

Ce.R.D.O. (ed.) unpublished A. Adulis Fieldwork Report 2011.

Ce.R.D.O. (ed.) unpublished B. Adulis Fieldwork Report 2012.

Ce.R.D.O. (ed.) unpublished C. Adulis Fieldwork Report 2013.

Ce.R.D.O. (ed.) unpublished C. Adulis Fieldwork Report 2014.

Ce.R.D.O. (ed.) unpublished C. Adulis Fieldwork Report 2015.

Ce.R.D.O. (ed.) unpublished C. Adulis Fieldwork Report 2017.

Ce.R.D.O. (ed.) unpublished C. Adulis Fieldwork Report 2018.

Ce.R.D.O. (ed.) unpublished C. Adulis Fieldwork Report 2019.

Ce.R.D.O. (ed.) unpublished C. Adulis Fieldwork Report 2020

5. Provenance

Abstract

This chapter discusses the results of analysis related to provenance. Information from petrography, SEM-EDX and ICP-OES are highlighted, focusing on the question of the provenance of Ayla-Aksum amphorae samples in relation to local pottery, Late Roman Amphora 1, dolia samples and the slipped ware.

5.1. Materials and Methods

5.1.1. Optical Microscopy (Petrography)

Thin sections were prepared from the selected pottery samples and studied following the protocol adopted by Whitbread to identify mineralogy, abundances and associations, pore/void distribution, surface treatments, grain-size distribution, shape of inclusions and the description of the groundmass/ matrix (Whitbread 1995). For the petrographic study of the raw clay samples, briquettes were prepared by clay modelling and firing at 600°C. The briquettes were then sliced to obtain thin sections. Thin sections were examined under a Polarizing Optical Microscopy (POM), using a Nikon Eclipse E660 microscope (Nikon Instruments Inc., New York, NY, USA) equipped with a CANON 650 digital camera and the Camera EOS digital microphotography system at IGG-CNR Padua (at the Department of Geosciences). Photomicrographs were obtained in plane and cross-polarized light at different magnifications for each sample.

5.1.2. Scanning Electron Microscopy with Energy Dispersive X-ray Analysis (SEM-EDX)

SEM-EDX was employed to examine the polished cross-sections of 22 samples representing the Ayla-Aksum amphorae, local pottery, LRA1, LRA 1(?) *dolia* samples, slipped ware and the fabrics whose typological classification is not well-defined (samples 2.4 and 2.9). Chemical data were obtained on 22 polished graphitized cross-sections by using a JEOL JSM-IT300LV SEM instrument coupled to an energy-dispersive X-ray spectrometer with a silicon drift detector (SDD; Oxford Instruments), available at the Dipartimento di Scienze della Terra of the University of Turin. An accelerating voltage of 15 kV, a counting time of 50 s and working distance of 10 mm were adopted for the elemental analysis. The

measurements were performed in high vacuum conditions, the SEM-EDS calibration was performed using the polished and carbon-coated 53 Minerals Standard (Structure Probe, Inc., West Chester, PA) and quantitation was performed using Oxford Instruments XPP correction. Oxford INCA Energy 300 Microanalysis suite was used for spectra recognition and data treatment. SEM-EDX as an analytical technique is suitable to provide chemical information on the ceramic bodies and their matrices to complement information from petrographic observations while the limitations to infer provenance postulate via the technique are also considered. As for the whole bulk, the EDX analyses were carried out by scanning five different areas on the polished and graphitized cross-sections at 50X magnification (around 5 mm²) and obtaining the mean composition. For the matrices, different magnifications from 100 to 250X were used depending on the sample characteristics; small frames were chosen from five different images avoiding the inclusions with dimensions > 0.2 µm and the mean composition was obtained from the five scanned areas. The results were expressed as the oxide weight % of the detected elements (Na₂O, MgO, Al₂O₃, SiO₂, K₂O, CaO, TiO₂, P₂O₅ and Fe₂O₃) whose sum was normalized to 100.

5.1.3. Inductively Coupled Plasma-Optical Emission Spectrometry (ICP-OES)

For the ICP-OES analysis, an aliquot (80 mg) from each powdered sample (25 archaeological fragments and 6 raw clays) was kept at 120°C in a furnace overnight in quartz crucibles. After having carefully determined the mass of the dry samples, the powder has been fused with a twofold amount of lithium metaborate at 1100°C in graphite crucibles. The melt was dissolved in 5% HNO₃ (50 ml) and diluted to 250 ml with UHQ water for elemental analysis. The obtained solutions were analysed by inductively coupled plasma optical emission spectroscopy by using a Varian Liberty Series II sequential instrument equipped with a quartz torch (1.8 mm inner diameter) and a GemTip Crossflow nebulizer mounted on a Scott spray chamber. The instrument was available at the Chemistry department of the University of Turin. The Loss of Ignition (L.O.I.) was calculated for each sample, by re-firing an aliquot from each powdered sample at 1000 °C for 2 hours. The final concentration of major, minor and trace elements was obtained considering the L.O.I. to obtain the initial mass of the sample. The ICP-OES instrument was calibrated using a blank solution and different multi-element standard solutions, each containing a set of the elements selected to fit at the best the detection limit and the linear range of the calibration curve. Precision and accuracy of the

method was tested using standard reference materials (SRM). The following set of elements was determined: Al, Fe, Ca, Mg, K, Na, Ti, Mn, Ba, Sr, Cr, Ni, Eu, Gd, V, Rb, La, Y, Yb, Zr, Sc and Cu. The concentrations of Eu, Gd and V were below the quantification values, while the values for Ni showed unacceptable bias from the certified values. Therefore, these elements were excluded from the element set for discussion. For data treatment, statistical tools such as Hierarchical clustering and PCA were used to observe patterns through different projections. Both Pirouette software (by Infometrix) and an in-house developed Python script were employed for calculations.

As for Principal Component Analysis, different approaches of data pre-treatment were used, such as autoscaling and centred log transformation procedures. The autoscaling method allows for each variable to be transformed to attain a zero mean and a variance equalling one and it is recommended when the variance of each variable affects the performance of a statistical method (Baxter 2001; Papageorgiou 2020). The method allows standardisation of all the data variables and thereby enabling all variances among the variables to be equal and thus can contribute to the analysis with the same weight. The centred log transformation is also commonly used logarithmic data transformation (to base 10) before principal component analysis. The method is based on the premise that within the raw materials of manufacture, elements tend to have a natural log-normal distribution and thus normality of the data is crucial (Baxter, 2001; Papageorgiou 2020). The variance of the variables is stabilized through the logarithmic transformation. A second reason is that all the variables will have an equal weight in an unstandardized principal component analysis. An extensive discussion on the use of each of the approaches is given in the literature (Papageorgiou,2020) and notwithstanding their limitations they were used to visualize patterns in the compositional data from this study. The first tests were obtained with the Pirouette software and were further elaborated using a Python script.⁵ The Pirouette is a complex chemometrics modelling software developed by Infometrix. The Python script, on the other hand, was prepared using Spyder scientific environment in Python language. After loading the dataset in csv format, it can perform PCA and plot the biplot with overlapping scores and loadings for the selected PCs.

⁵ The python script was adapted from Guidorzi, L. 2021, Physico-chemical characterization of diopside in lapis lazuli: a study from luminescence activators and quenchers to material provenance investigations, PhD thesis, Chemical and Materials Sciences, University of Turin

5. 2. Results and Discussion

5.2.1. Petrographic Observations

Petrographic analysis was conducted on samples from Adulis (belonging to different typological classes) to determine how, and to what degree the evolution of raw materials exploitation could shed light on provenance of particularly the Ayla-Aksum amphorae from Adulis in comparison with fabrics identified for the local pottery, Late Roman varieties, *dolia*, bricks samples and classes of imported coarse and common wares. The objective of the petrographic study was to establish information about the petrological variability observed in the different assemblages and was accomplished by characterizing the minerals, rock fragments, and other components identified in standard size petrographic thin sections. The presence of rock fragments such as granitic and basaltic rock fragments, sandstone, and clasts of metamorphic origin are quite informative to an extent where associations with the respective geology could be made. Unique observations in mineralogy and subtle differences in the abundance of the tempering materials or natural inclusions were considered to draw conclusions on attributions to a specific fabric and/or sub-fabrics. Textural and petrographic study under the optical microscope identified the main petrographic groups for the Ayla-Aksum amphorae, Late Roman Amphora 1, local pottery, *dolia* samples as well as red slipped wares based on and the nature of the inclusions in terms of their mineralogical and lithological composition, grain shape, size, roundness, and relative frequency. The petrographic information on fired clay samples is also included. Where typological classification posed uncertainties for some samples, the petrographic groups are included here to help further refinement of the ceramic sequence at Adulis. The details of petrographic information on the studied samples are summarised in appendix 3.

5.2.1.1. Ayla-Aksum amphorae

Petrographic observations show that Ayla-Aksum amphorae recovered from excavations at Adulis are homogenous in terms of composition of their inclusions (Fig.10 and 11). The ceramic bodies are characterised by sub-angular and sub-rounded to rounded small and medium to large-sized grains (20%). Two petro-fabrics, namely granite-and quartz-rich potsherds bearing volcanic rocks and granite-and feldspar-rich potsherds, are identified (Fig. 10 and 11). Comparisons with data from literature (Raith *et al* 2013; Holmqvist 2019) are in

agreement with petrographic observations in this study in coeval ceramics from Ayla (Jordan).

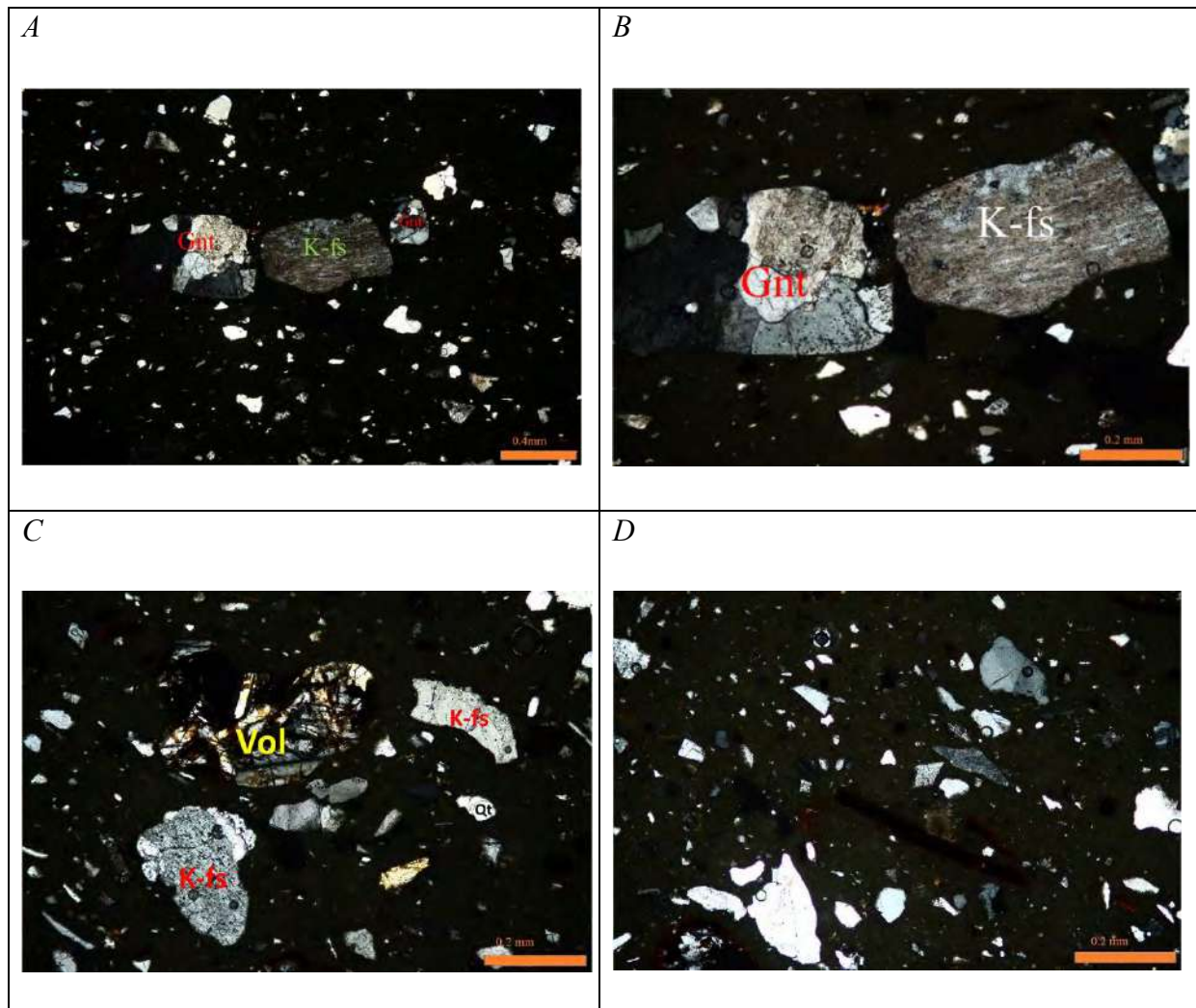


Figure 10: Photomicrographs in crossed-polarised light of Ayla-Aksum amphorae, granite and /quartz-rich potsherds, bearing volcanic rocks petro-fabric of Ayla-Aksum Amphora. Note the presence of granitic rocks (A and B), volcanic rocks(B) and strands of biotite (D in the center). Abbreviations. Gnt: granitic rocks; Vol: volcanic rocks; Qt: quartz and K-fs: K-feldspars.

Granite and /quartz-rich potsherds, bearing volcanic rocks: The fabric is characterized by the presence of dominant granitic rock fragments and common to few volcanic rock fragments (Fig. 10). Mineral inclusions are dominantly quartz, abundant feldspars, muscovites and biotites and rare clino-pyroxenes. The inclusions are mainly distinguished as angular to sub-angular and sub-rounded to rounded inclusions and generally well-sorted, comprising c. 20% of the field view. The fabric has an optically inactive matrix. The fabric seems to be more calcareous than petro-fabric 2.

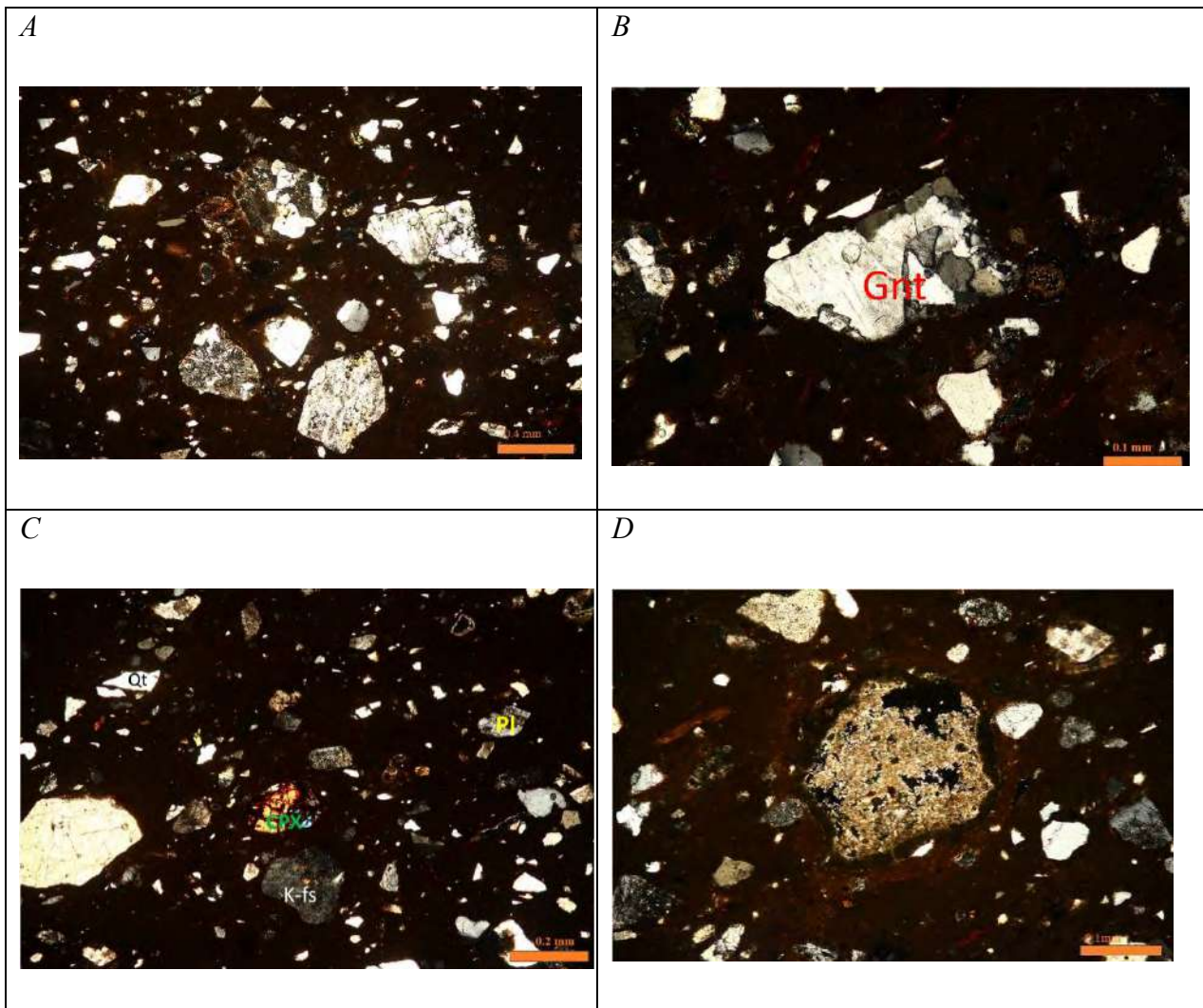


Figure 11: Photomicrographs in crossed-polarised light of Ayla-Aksum amphorae granite- and feldspar-rich potsherds. Note the granitic rock fragments (A and B) as well as pyroxene inclusions(C) shown. As well as the decomposition of carbonates(D). Abbreviations: K-fs: K-feldspars; Gnt; granite; Vol: volcanic Rocks; Pl: plagioclase; CPX: clinopyroxenes.

Granite- and feldspar-rich potsherds: This fabric is distinguished dominantly by granitic rock-fragments (Fig. 11). Abundant feldspars (plagioclase and perthitic feldspar) are characteristic of this fabric while common quartz, clino-pyroxenes and mica inclusions are present. The inclusions are angular to sub-angular and sub-rounded to rounded and well-sorted comprising c. 20% of the field view. Secondary infill and/or recrystallisation of the carbonates is discerned under microscopy (Fig. 11 D). An optically inactive calcareous matrix is noted for the Ayla-Aksum samples considered in the study, indicating that at least the fine-grained crystals of calcite underwent decomposition (Fig.11D) during firing (which exceeded 850°C). In some cases, carbonates recrystallisation is observed as a consequence of post-firing processes (Fabbri *et al* 2014).

5.2.1.2. Late Roman Amphora 1

The Late Roman Amphora 1 samples considered in this study are homogeneous and characterised by a petro-fabric rich in limestone and bio-clasts (Fig.12).

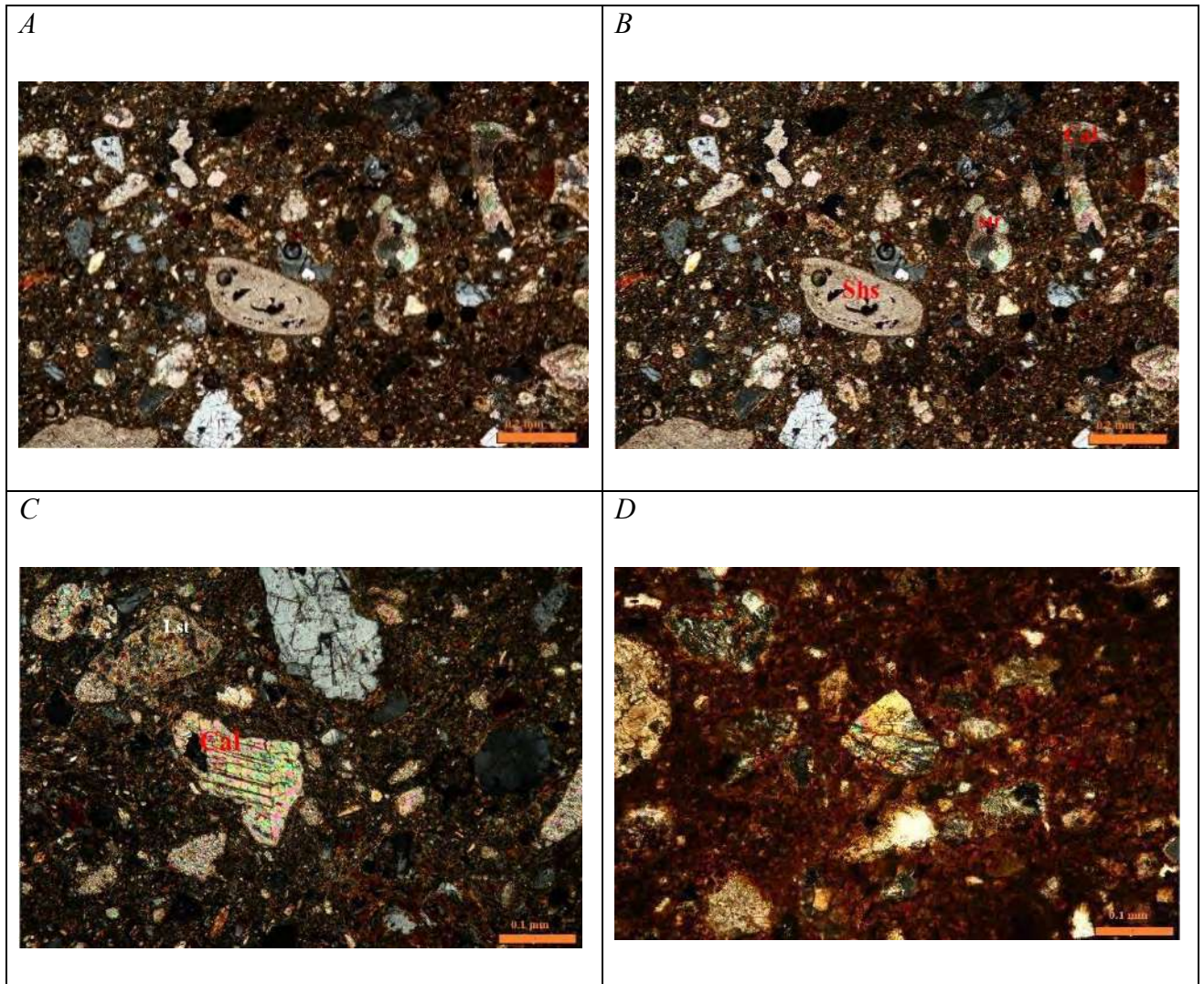


Figure 12: Photomicrographs in crossed-polarised light of Late Roman Amphora 1. Shells and microorganisms (A, B and D) and calcite inclusion (C) and foraminifera (D, in the center) noted. Abbreviations: Shs: shells; Mf; microorganisms; Cal: calcite; Lst; limestone.

It is represented dominantly by bio-clasts, where abundant micro-fossils (bivalve shells and foraminifera), calcite and limestone inclusions are noted (Fig.12). The samples representing the Late Roman Amphora 1 are characterised by a limestone-rich bodies with numerous medium and large-sized fragments of crypto-crystalline and fossiliferous limestone, shells, foraminifera, flecks of mica, a small number of quartz grains and a few of spathic calcite (Fig.12). Occasional presence of chert, feldspars as well as isolated grains of pyroxenes are noted. The micromass is mainly isotropic and optically active.

5.2.1.3. Late Roman Amphora 1(?)

The seven samples identified as LRA1(?) show a different petrographic composition, characterised by a calcareous matrix with inclusions of quartz, feldspars, chert, volcanic and metamorphic rocks (Fig.13 and 14). The description of the petro-fabrics is given below.

Limestone and volcanic rocks rich potsherds: The petro-fabric is characterized by a heterogenous composition where dominant limestone and few to common volcanic rocks are noted (Fig. 13). Mineral inclusions include common quartz, feldspars, pyroxenes and rare micas and amphiboles while contributions from chert are observed. The presence of opaque (ARFs) and clay mineral fragments is also common. Sub-angular to rounded and rarely angular inclusions characterize this petro-fabric, comprising 30 % of the field of view. An optically inactive calcareous matrix is observed, with indications of secondary infill and/or the recrystallisation of carbonates.

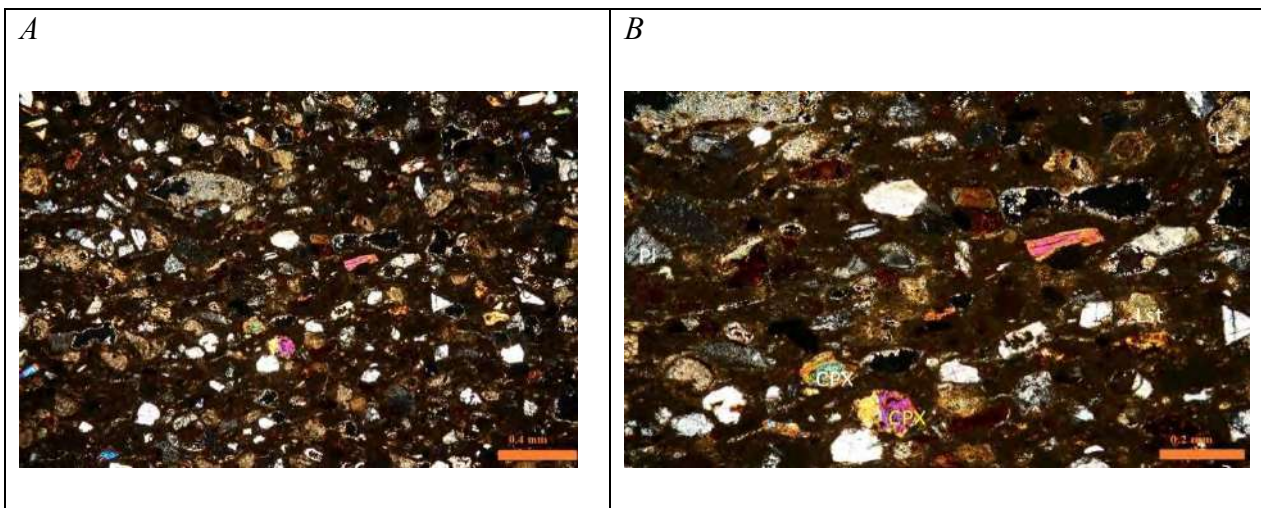


Figure 13: Photomicrographs in crossed-polarised light of LRA1(?), limestone and volcanic rocks rich potsherds petro-fabric. Note the common presence of limestone, clino-pyroxenes, and plagioclases(B). Abbreviations: Pl: plagioclase; Lst: limestone; CPX: clinopyroxenes.

Potsherds rich in volcanic rocks and bearing metamorphic rocks: The petro-fabric is characterized by inclusions of mainly igneous nature (dominantly basaltic rocks) and few to moderate metamorphic rocks (Fig. 14). Contributions from chert and rare sandstone are also noted. Common quartz, feldspars, and accessory minerals such as clino-pyroxenes and micas as well as rare amphiboles constitute the mineral inclusions. Inclusions are quite heterogeneous, comprising 30% of the field of view. An optically inactive calcareous matrix can be discerned under microscopy, where opaque (ARFs) and clay mineral fragments are

noted. Textural observations further pinpoint a secondary infill of carbonates and perhaps their recrystallisation.

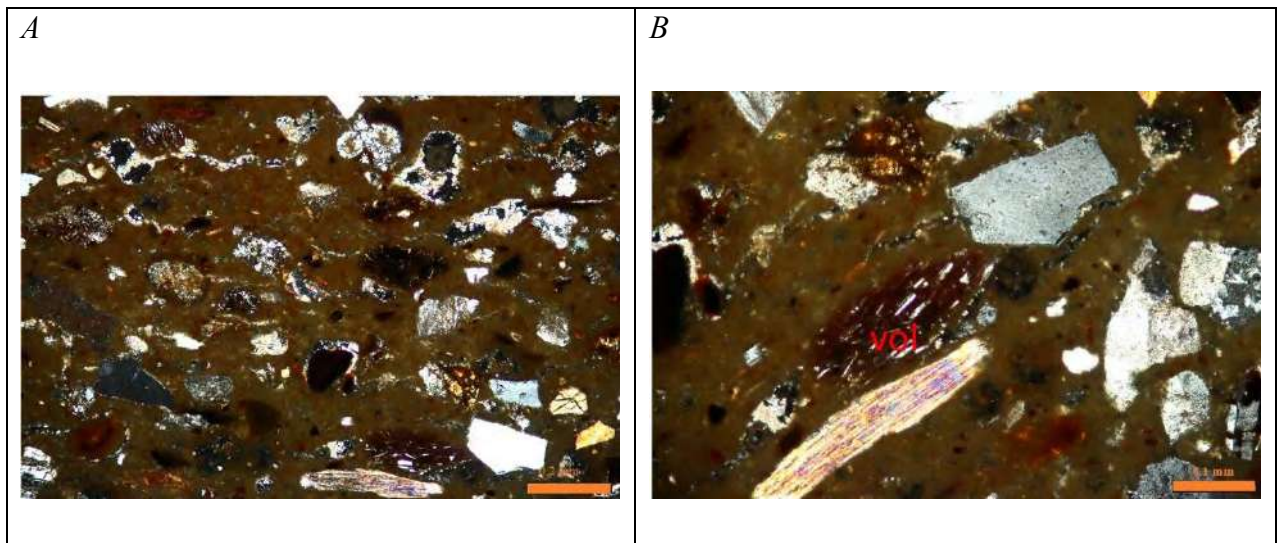


Figure 14: Photomicrographs in crossed-polarised light of LRA1(?), volcanic rocks and bearing metamorphic rocks petro-fabrics. Abbreviations: Vol; volcanic rocks.

The differences observed between these samples and those belonging to the well-known fabric of LRA1 mentioned above has prompted a detailed study of these fabrics to attribute them secure typological classification. In this respect, the study of the organic residues which are present in some of the samples (C02, C03, C06, C07, C08 and C09) together with petrographic observations has allowed to identify them as ‘Torpedo jars⁶’ from a bituminous lining of their interior (for a detailed discussion see chapter 7, where the details of the results of organic residue analysis are provided). The superficial resemblance of LRA1 and Torpedo jars, macroscopically, has been noted in several studies (Tomber *et al* 2020). The complexity of distinguishing LRA1 and Torpedo jars is attested well particularly when encountered with fragments, as in the case of this study. It should be noted here, therefore, that a distinction is made between LRA1, and Torpedo jars considering the microscopic observations and will be treated as per se in the essay.

⁶ The Torpedo jars represent a type of large handle-less amphora manufactured within the area of the Persian Gulf during the Late Antique and Early Islamic periods (c. 3rd – 9th century CE). No kilns have been identified for the production of these jars but a lining of a bituminous substance in their inner surfaces has often facilitated their identification (Tomber *et al* 2020; Lischi *et al* 2020).

5.2.1.4. Local Pottery and Clayey Materials

The petrographic observations in this study indicate that the local pottery considered are divided into different fabrics displaying differences in the nature and abundance of inclusions (Fig.15, 16 and 17).

Potsherds rich in fine-grained metamorphic rocks: The petro-fabric is characterized by mostly fine and medium-sized sand as well as inclusions of metamorphic nature (Fig. 15). Quartz, feldspars, and accessory minerals such as micas are present. Angular to sub-angular and sub-rounded fine and medium-sized well-sorted inclusions are noted. The petro-fabric is mainly represented by the presence of fine-grained metamorphic rocks (mainly phyllites and mica-schist) comprising c.15% of the field of view. A partially optically inactive matrix can be discerned under microscopy, where opaques are noted.

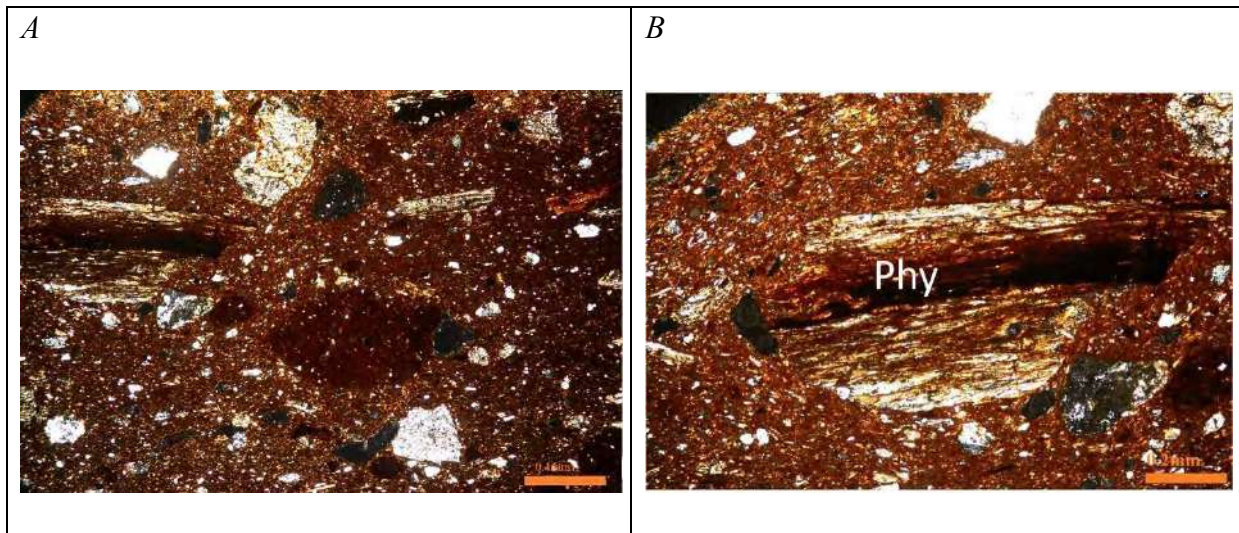


Figure 15: Photomicrographs in crossed-polarised light of local pottery, potsherds rich in fine-grained metamorphic rocks. Abbreviations: *Phy*; phyllites.

Granite-rich Petro-fabric: The petro-fabric is characterized by dominantly granitic rocks (Fig. 16). Mineral inclusions are dominantly quartz, feldspars, and micas. The petro-fabric is distinguished from the other petro-fabrics by granitic inclusions. Angular to sub-angular and sub-rounded fine and medium-sized inclusions dominate, comprising c.20 % of the field of view. A partially optically inactive matrix can be discerned under microscopy.

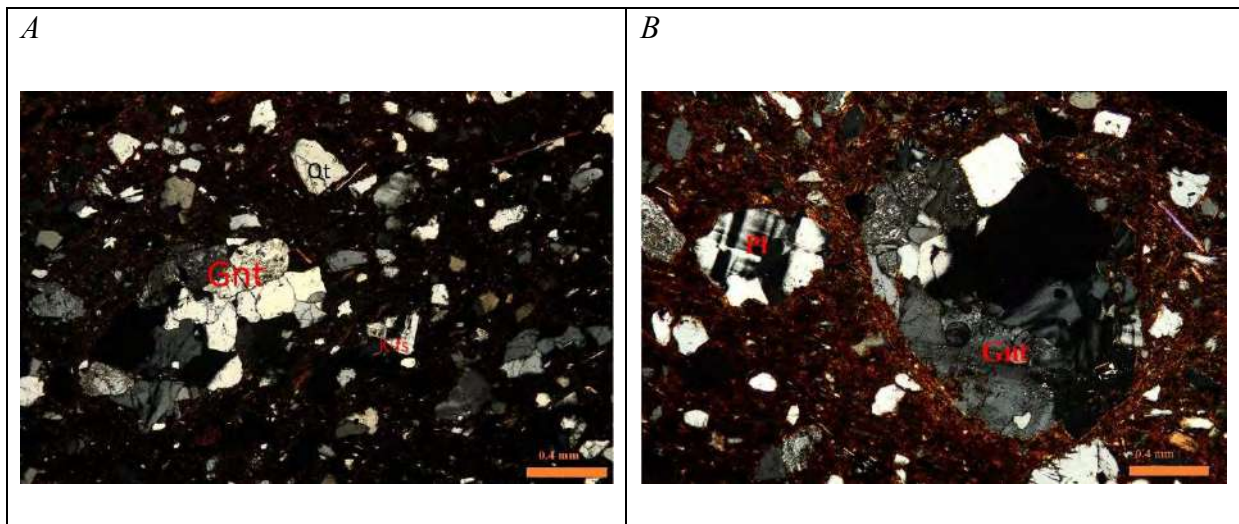


Figure 16: Photomicrographs in crossed-polarised light of local pottery, granite-rich petro-fabric petro-fabric. Abbreviations: Gnt: granitic rocks; Qt: quartz; K-fs: K-feldspars and Pl: plagioclases.

Potsherds rich in metamorphic rocks and sandstone: The petro-fabric is characterized by mostly fine and medium-sized sand as well as dominant metamorphic rocks (Fig.17). Rare to common occurrence of sandstone is also noted. Mineral inclusions are dominantly quartz, feldspars, and micas. The petro-fabric is represented by angular to sub-angular fine and medium-sized sand and ill-sorted inclusions are noted, comprising c. 20 % of the field of view. A partially optically inactive matrix can be discerned under microscopy (Fig.17).

The documentation of a wide range of materials and clasts that correspond to the geology around the area of Adulis can be attested in the production of the local pottery from petrographic observations. The contributions from metamorphic and granitic rocks, is therefore, related to the availability of these raw materials for pottery production. The Ghedem dome which is located to the northwest of Adulis is characterized by gneissose granitoids and garnet rich metamorphic clasts (Gebreab and Talbot 2000). The terrane is characterized by a zone of mylonites, which occur where pale granitic gneisses are interleaved with dark amphibolites (Gebreab and Talbot 2000). Various generations and orientations of pegmatites also occur in aureoles around granitic plutons which intruded the orthogneisses and the pelitic–semi-pelitic rocks and are more concentrated in Mt Ghedem and its surroundings (Talbot and Gebreab 1997; Gebreab and Talbot 2000).

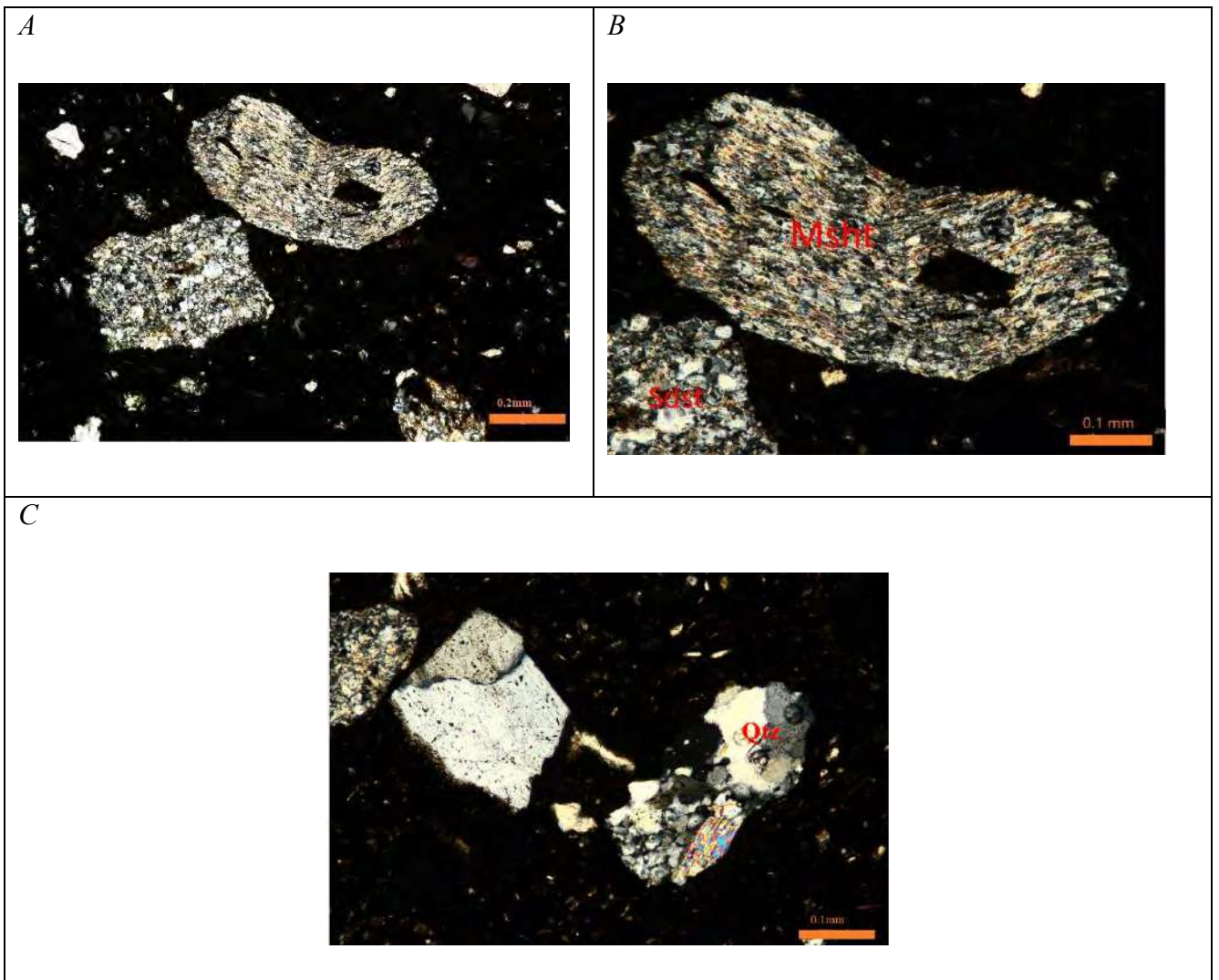


Figure 17: Photomicrographs in crossed-polarised light of local pottery, potsherds rich in metamorphic rocks and sandstone petro-fabric. Abbreviations: Msht: mica-schist; Qtz: quartzite Sdstn; sandstone.

As far as contribution of the local geology is considered, petrographic observations of two brick samples (presumably produced locally in the area) further show distinct petro-fabric with indications of mineralogy linked to the area around Adulis (Fig. 18). The petro-fabric is represented by fine and medium-sized sand and dominantly by metamorphic rocks. Rock inclusions include phyllites, mudstone, quartzite, mica-schist, and few to rare sandstone. Mineral inclusions are dominantly quartz, feldspars, micas as well as rare pyroxenes. The petro-fabric is represented by angular to sub-angular fine and medium-sized inclusions while ill-sorted inclusions are noted, comprising c. 20 % of the field of view. A partially optically inactive matrix can be discerned under microscopy.

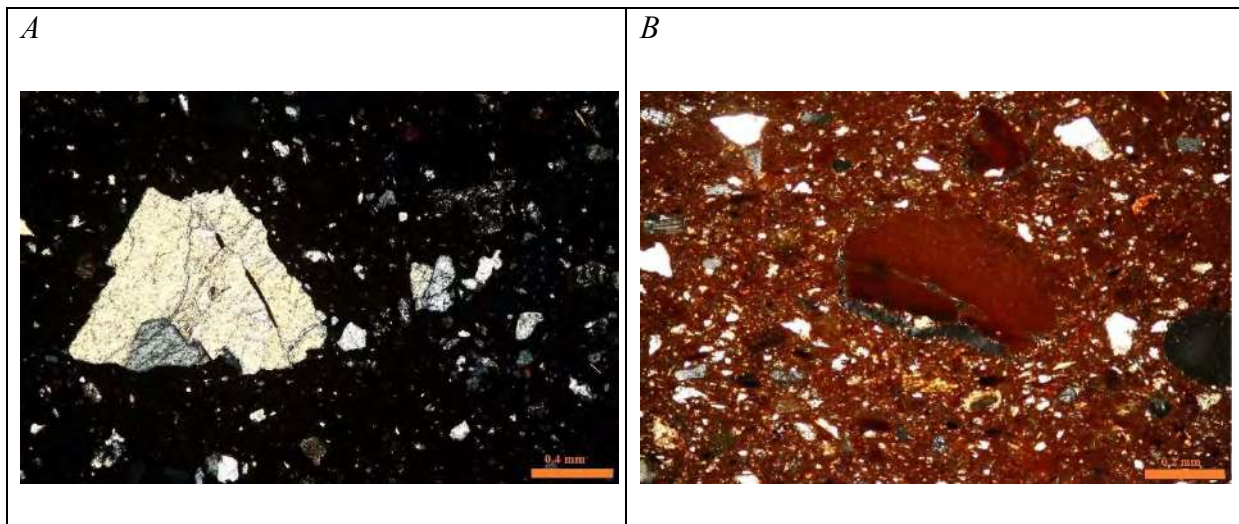


Figure 18: Photomicrographs in crossed-polarised light of brick samples, metamorphic dominated petro-fabric. Note the quartzite (A) and mudstone (B) clasts and that the brick samples are presumably of a local production.

Petrographic observations of the sections made on fired clay samples collected from the area of Adulis further provided the basis to correlate the petro-fabrics identified to potential raw material sources that might have been exploited to produce local pottery (Fig. 19). The description of the petrographic features of the clay samples is indicated in table 2.

Table 2: Petrographic features of fired raw clay samples

Sample	Petrographic Description
Petro-fabric 1	This fabric is characterized with dominantly quartz and feldspars as well as rare to common micas and pyroxenes. Clasts of sedimentary and metamorphic nature are noted. Carbonates are also noted as rare occurrences. Medium to large sized angular to sub -angular clasts are observed in as much as micritic inclusions. The petro-fabric represents raw clays F1 and F2(Fig. 19 A and B).
Petro-fabric 2	A fabric characterized by quartz, feldspars and micas. Fine grained metamorphic and sedimentary rocks dominate the fabric. The presence of carbonates is also noted with small to medium sized angular to sub-angular clasts representing the fabric. The petro-fabric represents raw clays M1 and M2(Fig. 19 C)
Petro-fabric 3	A fabric represented by dominant quartz, feldspar and pyroxene inclusions. Fine grained metamorphic rocks, sandstone as well as magmatic rocks are observed. Few to rare carbonates are also noted. Sub-angular to angular medium to large sized clasts characterize the fabric. The petro-fabric represents raw clays H1 and

	H2(Fig. 19 D)
--	---------------

While a wider range of raw materials and clayey sources could have been exploited for the local pottery production at Adulis, it can be said that the clay samples represented by F1 and F2 (Fig. 19 A and B) fabrics show close similarities to the fabrics identified for the majority of local pottery samples considered in this study. Fabric similarities and differences thus are the result of the exploitation of similar or different raw material sources as well as the use of analogous or different recipes. The arrangement and size of the inclusions visible from the fabrics identified for the local pottery and the raw clay samples pinpoint to short distances of transport and thus a raw material source close to the parent rocks.

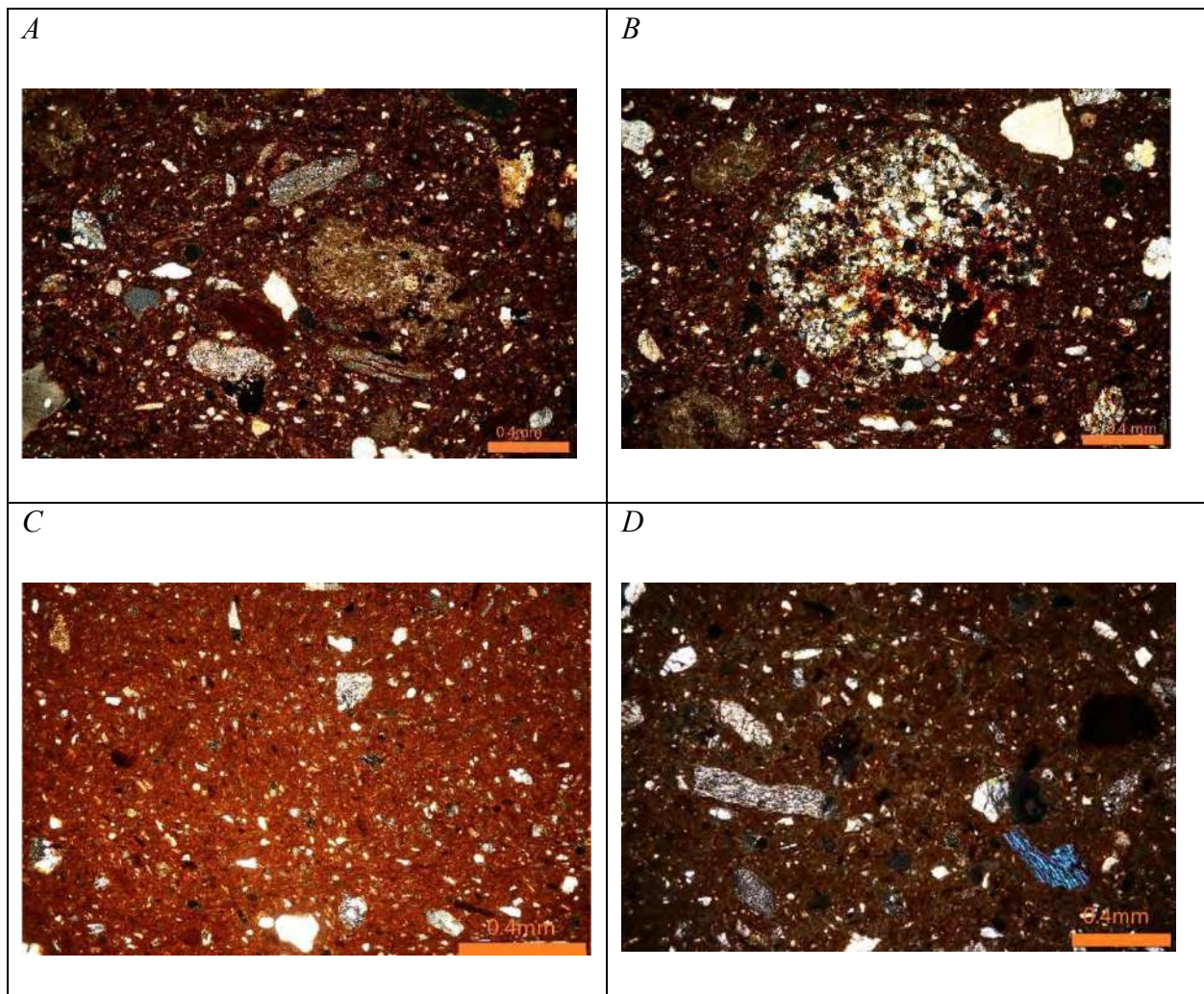


Figure 19: Photomicrographs in crossed-polarised light of fired raw clay samples. The photomicrographs of raw clay samples F1(A), F2(B), M2(C) and H1(D) are shown in crossed-polars.

5.2.1.5. *Dolia*

The *dolia* represent one of the classes of imported pottery at Adulis and have been least studied from typological and archaeometric point of view. With almost a little comparative petrological data available in the literature, it remains difficult to ascertain specific provenance from petrographic studies. Yet, petrographic observations in this study have indicated two different fabrics for this class (Fig. 20).

Argillaceous Rock Fragments (ARFs) Petro-fabric: The first fabric is dominantly characterised by Argillaceous Rock Fragments (ARFs) as can be seen from Fig. 20 A. Few quartz inclusions and decomposed carbonates are also noted for this fabric. The fabric is represented by subangular to sub-rounded and rounded medium to large sized grains (15%) with micritic sized limestones. Most of the samples identified as *dolia* (as can be seen in appendix 3) belong to this fabric. The petro-fabric has an optically inactive matrix.

Carbonates Petro-fabric: The second petro-fabric representing the *dolia* class is in contrast dominated by carbonates/ limestone. Abundant quartz, feldspars, and few flecks of micas as well as pyroxenes are noted as mineral inclusions (Fig. 20 B). Sub -angular to sub-rounded fine to medium sized grains dominate the fabric (15%). From textural perspectives, decomposed carbonates and their recrystallisation is noted in as much as an optically inactive matrix.

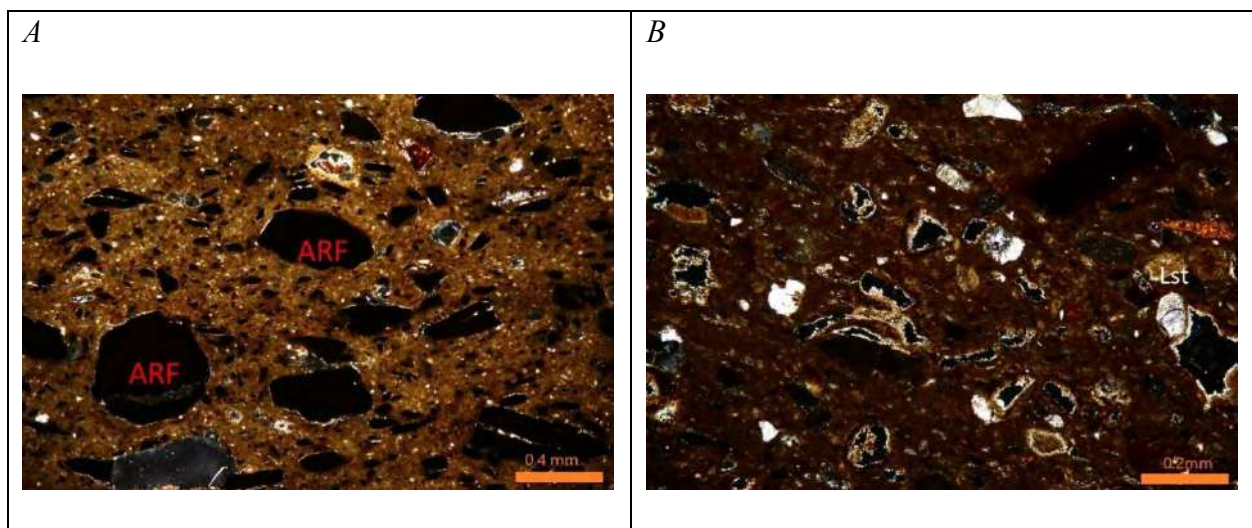


Figure 20: Photomicrographs in crossed-polarised light of *dolia* samples, Argillaceous Rock Fragments petro-fabric(A) and carbonates dominated petro-fabric(B) Note the ARFs(A) and limestone(B). Abbreviations: ARFs; Argillaceous Rock Fragments; Lst; limestone.

5.2.1.6. Red Slipped Ware

This class is represented by two samples in this study. The two samples are constituted in a single petro-fabric from microscopic observations. The fabric is characterized by dominant Argillaceous Rock Fragments (ARFs).

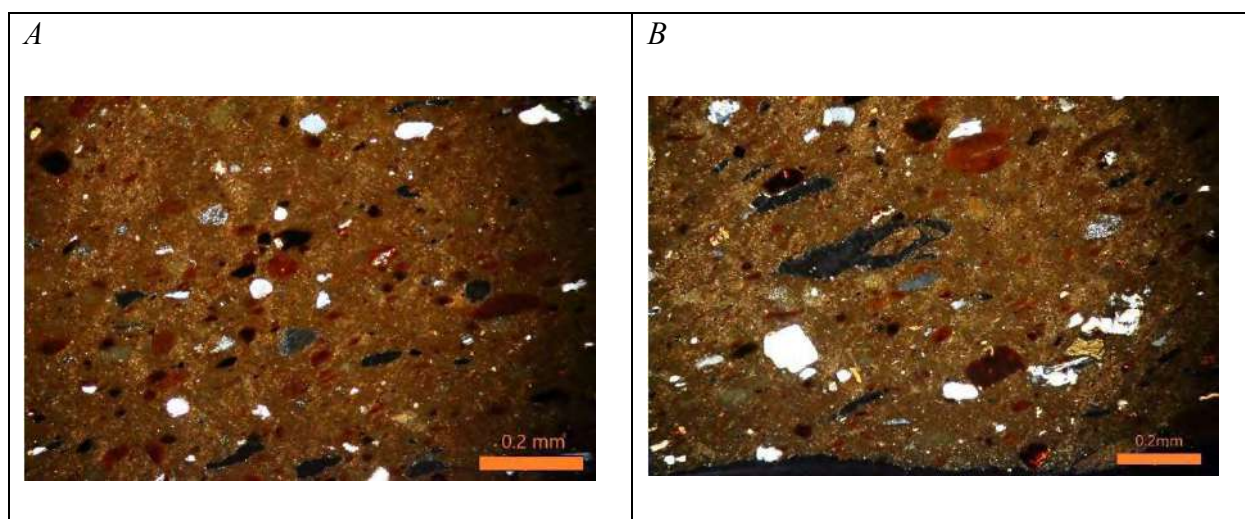


Figure 21: Photomicrographs in crossed-polarised light of red slip ware.

Rare basaltic rock fragments are also noted (Fig. 21). Quartz, feldspars, and few to rare accessory minerals including pyroxenes and amphiboles are observed. The presence of these accessory minerals and rock fragments pinpoint to input from volcanic rocks and may indicate a provenance to Eastern Mediterranean and/or Levant than North African sources. This hypothesis can be further examined in the future as conclusive remarks cannot be made presently. In these samples, an optically active matrix is noted.

5.2.1.7. Undetermined Class

While the above-mentioned classes of pottery can be linked to typological nomenclature with precision, some fabrics that were included in the study posed typological complexity due to insignificant diagnostic elements. Yet, the petrographic and textural details are provided here in order to lay the basis for future refinement of the ceramic sequence at Adulis (Fig. 22). Samples 2.9, 4.3 and 4.4 represent fabrics dominated by quartz and feldspars inclusions and few accessory minerals such as pyroxenes. The samples present a typological dilemma for which the attribution to specific class of pottery becomes difficult only based on petrographic observations. Sample 2.4 which represents a fabric dominantly characterized by limestone inclusions similarly poses a difficulty in ascribing specific class of imported pottery. Samples

2.9 and 2.4 were also included for SEM-EDX and ICP-OES studies to see correlations (if any) from chemical and geo-chemical point of view to the rest of the fabrics considered.

Quartz/ Felsic rocks Petro-fabric: This petro-fabric represents sample 2.9(22B). The sample is distinguished by dominant quartz and feldspars inclusions, while rare to common accessory minerals such as micas, pyroxenes and amphiboles are noted. Rare carbonates are also observed in as much as opaque minerals (ARFs). An optically inactive matrix is discerned from microscopic observations. Inclusions are ill-sorted ranging from sub-angular to sub-rounded fine to medium-sized sand, comprising c.15% of the field of view.

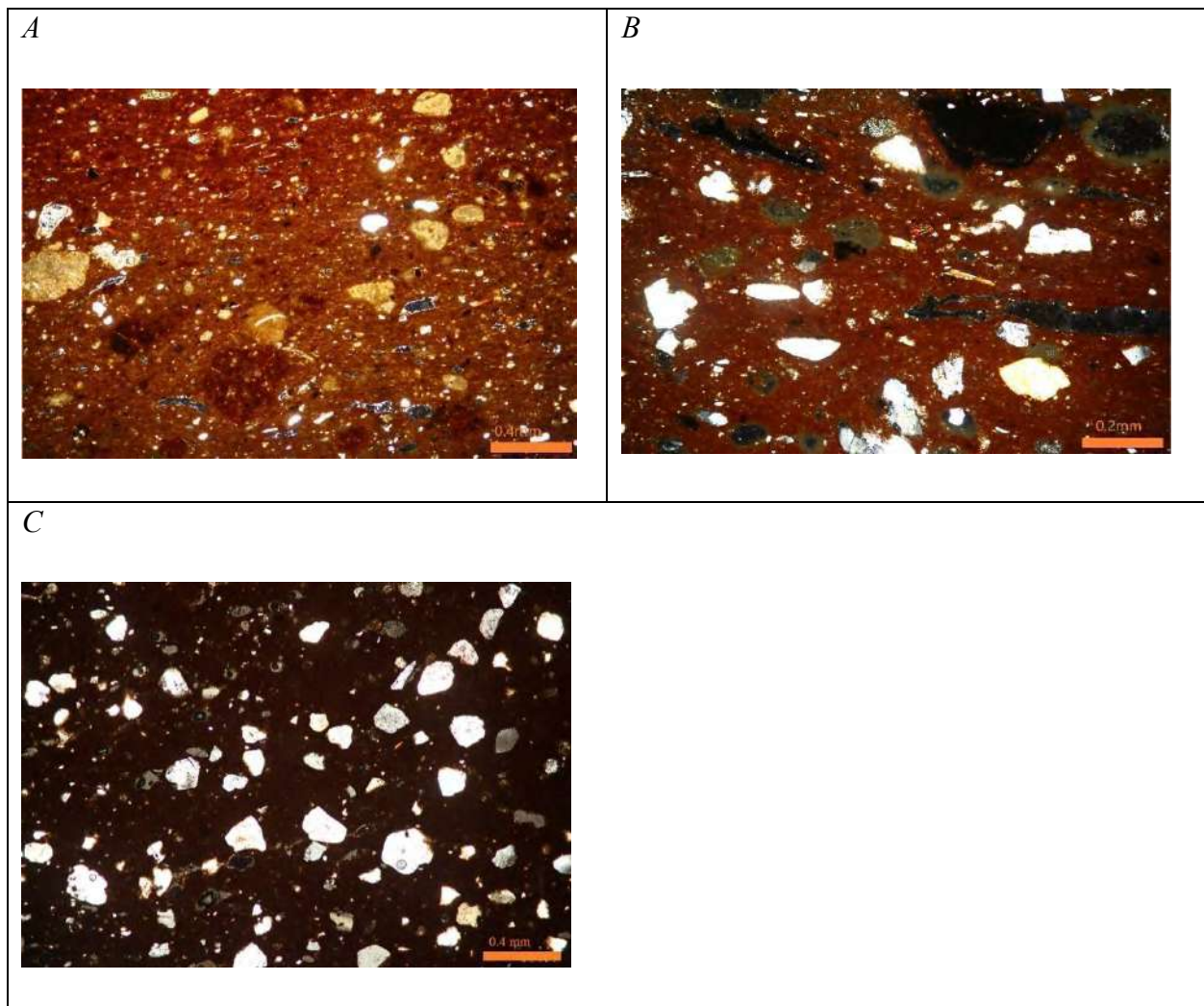


Figure 22: Photomicrographs in crossed-polarised light of fabrics with unknown typology. The fabrics represent samples 2.4 (A) Limestone dominated petro-fabric; 2.9(B) Quartz/ Felsic rocks petro-fabric dominated rocks and 4.3(C) Quartz/Feldspars- dominated fabrics.

Limestone dominated Petro-fabric: This petro-fabric represents samples 2.4 and 4.1(22A). The samples are distinguished by dominant limestone inclusions. Mineral inclusions are mainly quartz and clay mineral fragments. An optically inactive matrix is discerned from

microscopic observations. Inclusions are sub-rounded to rounded and silt to fine and medium-sized sand, comprise c.10% of the field of view.

Quartz/Feldspars dominated Petro-fabric: This petro-fabric represents samples 4.3 and 4.4(Fig.22 C). The samples are distinguished dominantly by quartz and feldspars. Common to rare limestones are observed. An optically inactive matrix is discerned from microscopic observations. Inclusions are sub-angular to sub- rounded and fine and medium-sized sand comprise c. 20% of the field of view.

5.2.2. Areal microchemical analysis of ceramic bodies by SEM-EDX

Bivariate plots of different oxides on the bulk and matrices show differences between the local and imported pottery samples considered in this study (Fig.23 and 24). The local pottery and bricks tend to show lower values of CaO in comparison to the classes of imported pottery as can be seen from the bivariate plots of CaO vs. MgO for both the bulk and matrices (Fig.23). These observations complement the petrographic information further indicating the non-calcareous nature of these samples. Moreover, the Ayla-Aksum amphorae, LRA1, Torpedo jars and *dolia* have generally higher CaO values ($> 10\%$), further collaborating petrographic information on the calcareous nature of these samples.

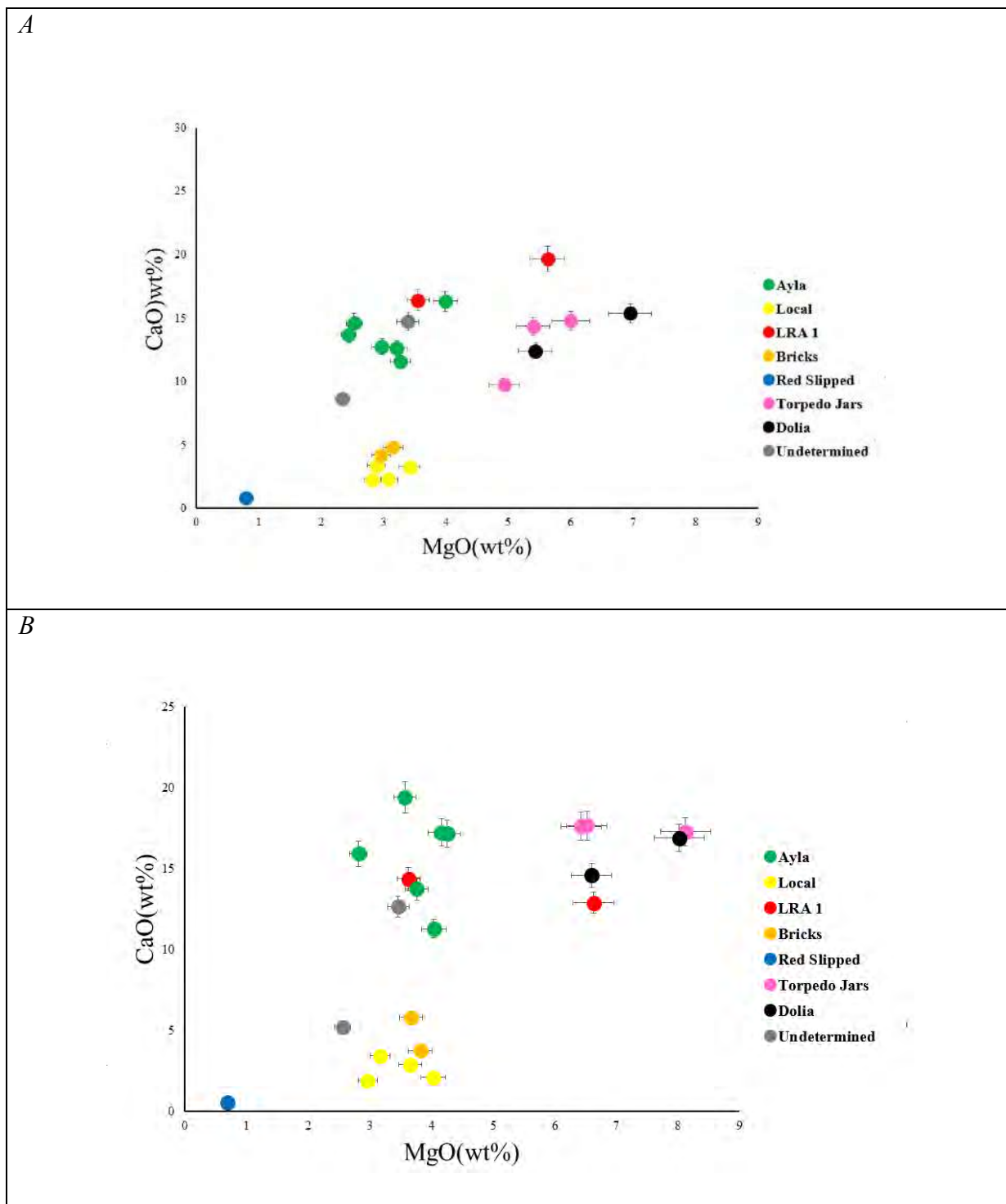


Figure 23: Bivariate plots of CaO vs. MgO obtained from SEM-EDX chemical composition data of the bulk(A) and the matrices(B). Error values are less than the size of the circles (appendix 10).

On the other hand, the bivariate plot of Al_2O_3 vs. Fe_2O_3 has been considered to see whether the values can indicate similarities/ difference in terms of the clay/s used to produce the different classes of pottery (Fig. 24).

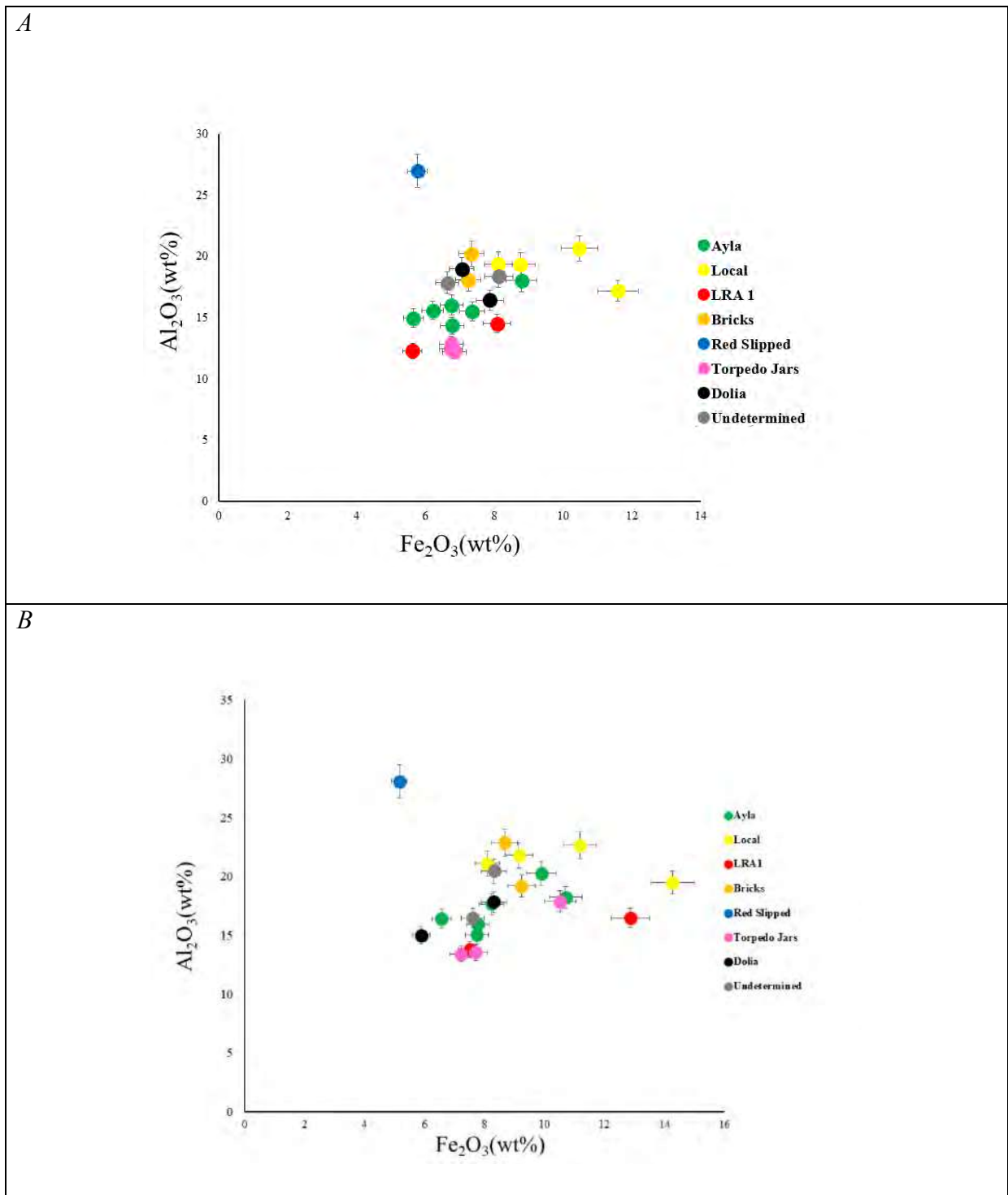


Figure 24: Bivariate plots of Al_2O_3 vs. Fe_2O_3 obtained from SEM-EDX chemical composition data of the bulk(A) and the matrices(B). Error values are less than the size of the circles (appendix 10).

In this respect, the red slipped ware sample is clearly isolated from all the others for the higher Al_2O_3 content which reflect the use of a clayey material richer in phyllosilicates and characterised by less aplastic inclusions, as also attested by the microscopic analysis. Among the other types of pottery, closer values of Al_2O_3 are shown for the LRA1 and Torpedo jars which tend to plot in the same area of the diagram, indicating the use of a clay/s similar in

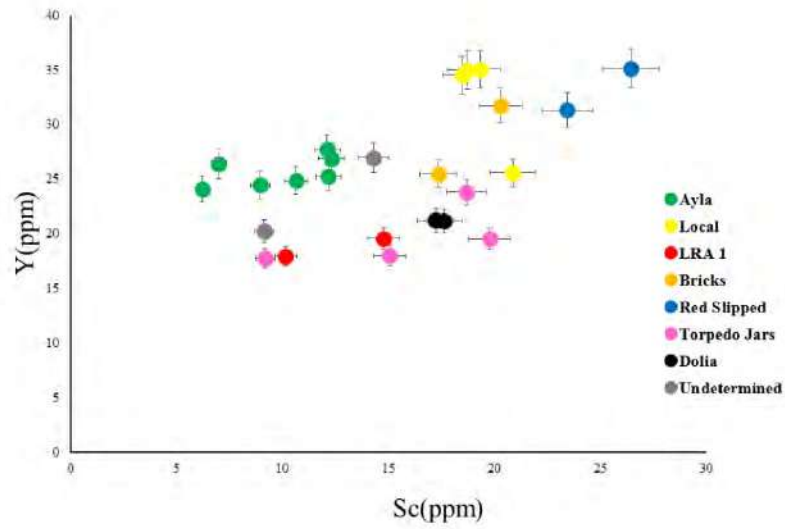
composition. The Ayla-Aksum amphorae, furthermore, have similar values when the plots of Al_2O_3 vs. Fe_2O_3 are considered in as much as the closer plotting of the values for the local pottery and the bricks (Fig. 24).

Generally similar trends are observed when the chemical composition of the bulk and the matrices are considered (Fig. 23 and 24), indicating that the dilution effect due to the large inclusions does not affect at least the relation between the selected chemical elements. While some differences are noted in the values between the local pottery samples and the imported classes, it can be said that no inferences can be made in terms of compositional groups based on the chemical data obtained by SEM-EDX. Therefore, apart from the fact that the high calcium and magnesium values seen in the Ayla-Aksum, LRA1, Torpedo jars and the *dolia* samples allowed to discriminate these classes from the local pottery, the chemical data of major oxides cannot discriminate clearly subtler compositional variability between the fabrics. In this respect, it was needed to further explore geo-chemical information including the trace elements, which can be quantified by ICP-OES chemical analysis. Such an approach provides further information on the petro-fabrics defined by petrography.

5.2.3. ICP-OES

Bivariate plots of chemical elements with different geochemical behaviours allowed to preliminarily explore trends from the geo-chemical data. Figures 25 and 26 illustrate the bivariate plots of La vs. Sc, Y vs. Sc, and Cr vs. Sr. The bivariate plots indicate that the Ayla-Aksum amphorae have higher values of La and Sr and lower values of Sc and generally Y in comparison to the local pottery and the brick samples (Fig. 25 and 26). The red slipped ware, on the other hand tend to show higher values of Sc and La in comparison to the rest of the pottery classes (Fig. 25) suggesting the use of a different clayey material (different in terms of provenance as well as preparation).

A



B

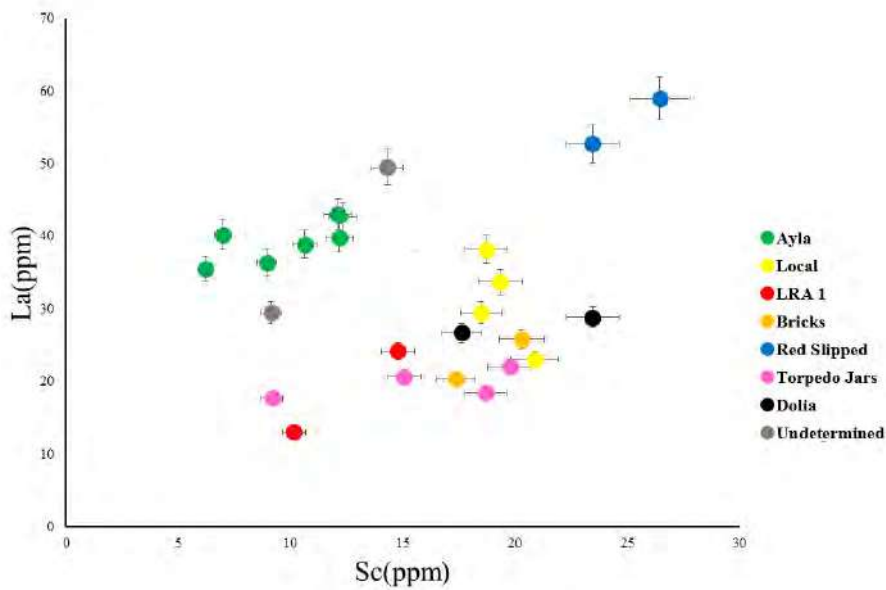


Figure 25: Bivariate plots of ICP-OES compositional data. Error values are less than the size of the circles (appendix 12).

The high Sr content of Ayla-Aksum amphorae, LRA1 and Torpedo jars (> 400 ppm) are related to different constituent of the ceramic body and in particular to the abundant inclusions of K-feldspars in the Ayla-Aksum amphorae, and of limestone in the LRA1 and Torpedo jars (Fig. 26). The latter are richer in Cr, as a consequence of their higher content of iron and magnesium. It can be said from the bivariate plots also that the LRA1, *dolia* samples

and Torpedo jars have lower values in Y and La in comparison to the other classes of pottery (Fig.26).

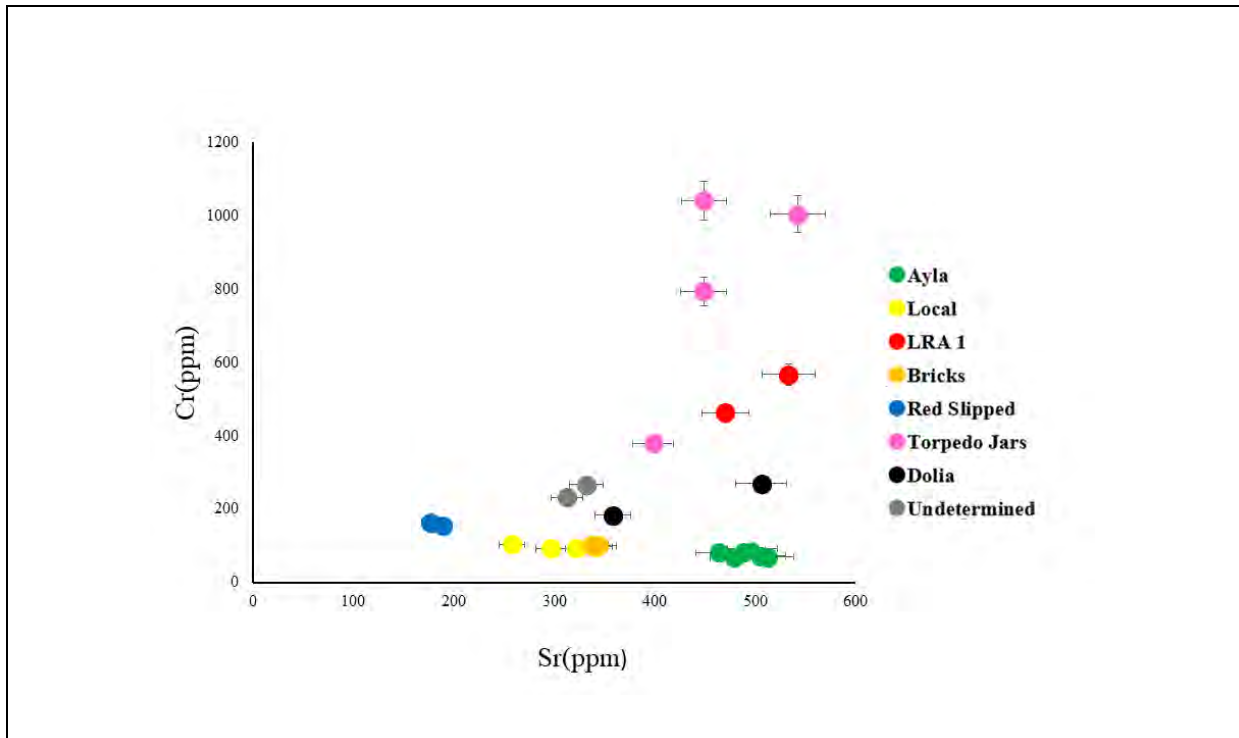
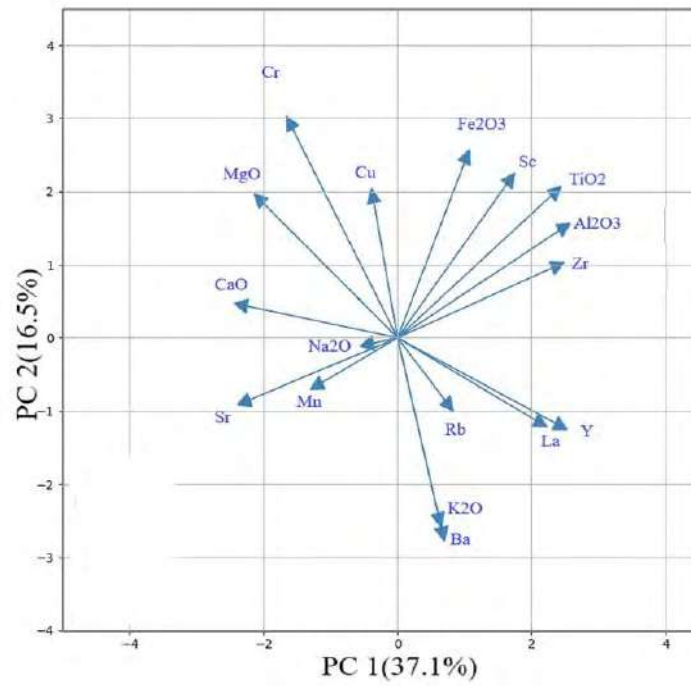


Figure 26: Bivariate plots of ICP-OES compositional data. Error values are less than the size of the circles (appendix 12).

This preliminary variation in the values of certain trace elements was further explored by multivariate analysis to see if inferences of compositional clusters can be established. PCA projections of data transformed by autoscaling, and log-transform ratio provided a comparative parallel to evaluate the different behaviours of the geo-chemical data.

Figure 27 illustrates the diagram for the first two principal components PC1 and PC2 (which are responsible for 53.6% of the total variance) of data-transformed by auto-scaling. The plots of the loading and scores are reported and in terms of the first principal component the plot displays positive loadings for Al, K, Fe, Rb, Sc, La, Zr, Ti, Ba and Y, while Sr, Mn, and Na, Cr, Mg, Ca, and Cu have negative values (Fig. 27). The second component clearly separates two sets of elements with large positive loadings, one including Cr, Ca, Mg and Cu in the second quadrant and the other, comprising K, Fe, Rb, Sc, La, Zr, Ti and Al in the first quadrant (Fig. 27).

A



B

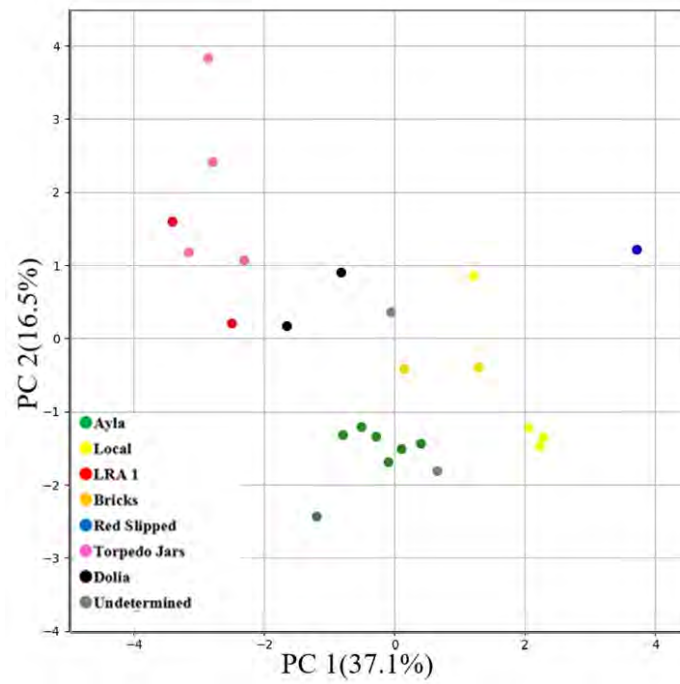


Figure 27: Score and loading plots of PC1 and PC2 obtained from the PCA considering ICP-OES auto scaled data.

When score and loading plots of PC1 and PC2 are taken into account the Ayla-Aksum amphorae cluster into one group distinctly from the local pottery and other classes of imported pottery. The biplots also indicate that the samples of the local pottery and bricks tend to cluster closely indicating similarities in composition while it is demonstrated that the LRA 1 and Torpedo jars tend to show similarities in composition.

PCA was also performed considering the log transformation ratio after Aitchison's approach and Buxeda's observations on compositional data.⁷ A logarithmic transformation was applied to compensate for the differences between absolute scales of major and trace elements and comparisons were performed using the ratios of logarithms obtained after dividing all the chemical components by a selected component. The component that introduces the lowest chemical variability to the entire set of specimens was taken as a divisor, Fe₂O₃ in this case (Fig. 28).

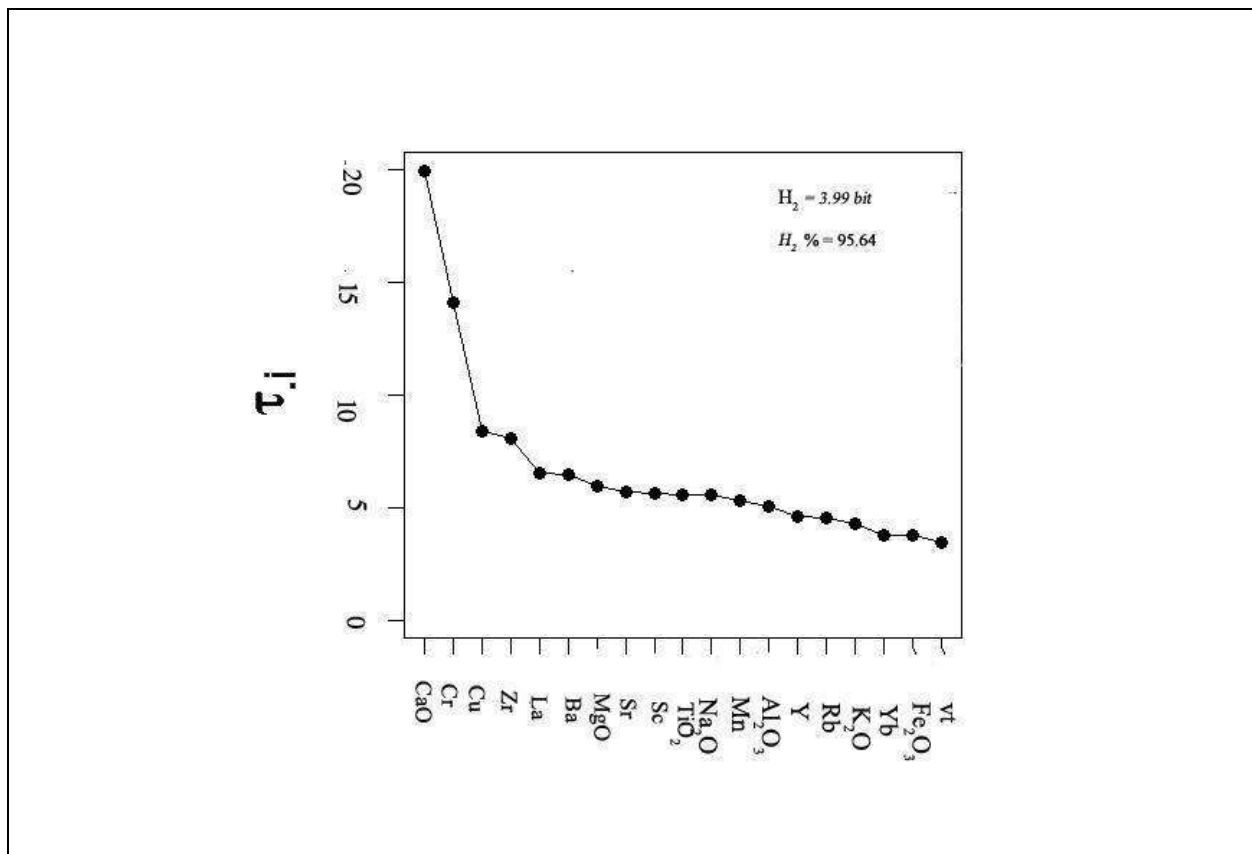


Figure 28: Graphical representation of the evenness of the compositional variability of analysed samples by ICP-OES; vt = total variability, H_2 = information entropy, $H_2\%$ = percentage of information entropy.

⁷ Aitchison, J. The statistical analysis of compositional data. J R Stat Soc Ser B Methodol. 1982;44(2):139–77, and Buxeda i Garrigós, J. Revisiting the compositional data. Some fundamental questions and new prospects in archaeometry and archaeology. 2008. In: Proc CODAWORK08 3rd Compos Data Anal Work Univ Girona Spain.

When score and loading plots of PC1 and PC2 (69.7% of the total variance) is considered, Sc, Al, Y, La and Ba, Zr and Ti contribute positively to PC1 while Ca, Sr, Mn, Na, Rb and K, Cr, Mg and Cu correspond to negative PC1 values (Fig. 29).

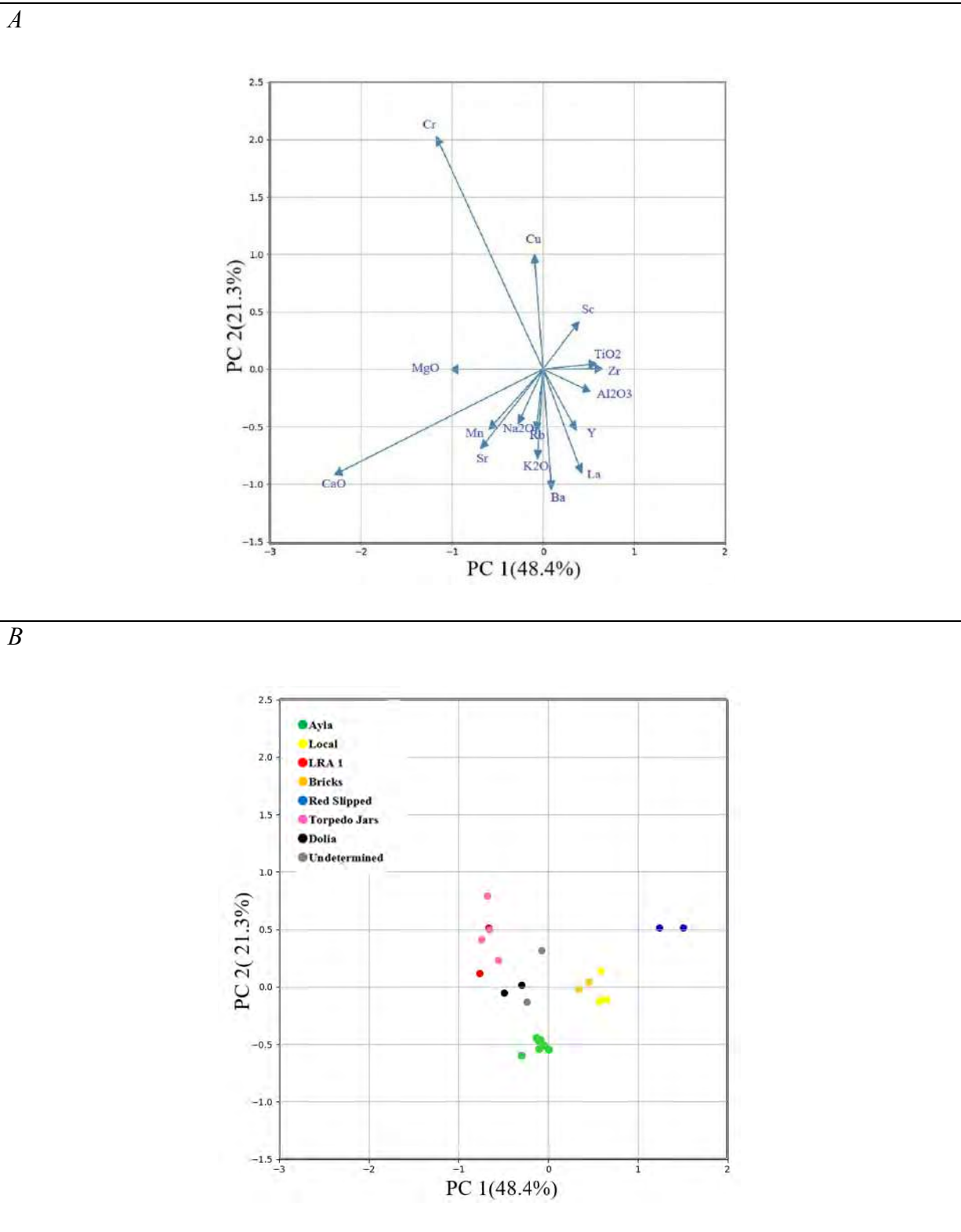


Figure 29: Score and loading plots of PC1 and PC2 obtained from the PCA considering ICP-OES log-ratio transformed data.

The second component separates Cr, Cu and Sc, Ti, Zr and Mg with positive values, from all the other variables. The obtained results follow a very similar pattern to that observed in the PCA plots of the data transformed through autoscaling, where the Ayla- Aksum amphorae are plotted together as a distinct group in as much as the observation of a separate compositional group from the local pottery in the biplot. It is also noted that the LRA1 and Torpedo jars show compositional affinities. Accordingly, when PC1-PC2 biplot (69.7% of the total variance) is considered, Sc, Al, Y, La and Ba, Zr and Ti contribute positively to PC1 while Ca, Sr, Mn, Na, Rb and K, Cr, Mg and Cu correspond to negative PC1 values (Fig. 29). On the other hand, the second component separates Cr, Cu and Sc, Ti, Zr and Mg with positive values, from all the other variables.

The score and loading plots of PC1 and PC2 clearly confirms the distinction between the Ayla-Aksum amphorae and the local pottery (Fig. 29). The loadings that mostly contribute to the distinction of the Ayla-Aksum amphorae into a single compositional group can be related to the suite of raw materials used to produce the pottery classes. The higher content of K_2O , Na_2O and Rb, Ba and Sr can be related to the presence of feldspars in granitic rocks while the contributions from REE (Rare Earth Elements) that indicate input from La and Y, may also attest to the use of raw materials from granite sources, accordingly with the petrographic observations on the Ayla-Aksum amphorae (rich in granitic rocks). On the geological map, the region within a 10 km radius from Aqaba includes geological features from both sides of the Wadi 'Arabah and the Negev side where sedimentary units as well as more volcanic and metamorphic areas with granite and gneiss areas prevail in contrast to the southern Transjordan side characterised predominantly by granite, gneiss, and amphibolite (Holmqvist 2019).

Moreover, the LRA1, and Torpedo jars show similarities in composition (Fig. 29). The higher Cr, MgO, Na_2O , Sr and mainly CaO content is responsible for the differentiation of these samples from the rest of the classes of pottery along with the relatively lower concentrations of Al_2O_3 , K_2O , Rb, Zr and TiO_2 , which are related to the use of a calcareous clay raw material. The petrographic observations on the LRA1 fabrics particularly pinpoint to probable addition of moderately to well sorted sandy tempers highlighting an abundant calcareous contribution while rare contributions from pyroxenes are noted. Samples C02, C03, C06 and C07 display petrographically both an abundant calcareous component and many inclusions derived from an ophiolitic source which could be related to the high content of Cr, MgO, as well as to heavy metals like Cu as discerned from the PCA (Fig. 29). Notwithstanding the

low number of samples and the internal variability observed petrographically and chemically, it can be said the consistency observed in the similarities of particularly composition further pinpoints to address the question of the provenance of the Torpedo jars considering known production centres for the well-known LRA1.

The plotting of the local pottery in a single compositional group is, on the other hand, the first indication of a geochemical signature for pottery that was produced in the area around Adulis. Variations observed in the PCA biplot (Fig. 29) reflect the relatively diverse fabrics inherent to the local production at Adulis. It can be, thus, attested from this study that different fabrics of local pottery were produced using similar clay sources and yet the differences in fabrics could be related rather to different recipes than compositional variations of the base clays.

Furthermore, samples 2.9 and 2.4 which remain unidentified from a typological point of view are plotted together closer to the *dolia* and the Ayla-Aksum amphorae, respectively. Yet, the data is inadequate to make inferences as regards their provenance. The red slipped wares represented by two samples, on the other hand, plot isolated from all the others.

Data transformed through autoscaling was considered for Hierarchical Cluster Analysis, where the Average Linkage method and Euclidean distance function were adopted (Fig.30 and 31). When the projections of the compositional data of all the pottery classes are considered, the dendrogram clearly shows that the Ayla-Aksum amphorae represent a distinct cluster which include samples 3.6, C04, 1.7.2, 1.5, 1.4.2 and 1.7.1) with respect to the local pottery and the rest of the pottery classes (Fig. 30). Samples 2.4 and 2.9 are shown in the same cluster with the Ayla-Aksum amphorae but tend to show differences in comparison to the rest of the Ayla-Aksum samples. Moreover, the local pottery which shows a grouping in cluster 1 indicate a distinct production at Adulis further enhancing trends observed from PCA biplots (Fig. 27 and 29) and petrographic, as well as SEM-EDX observations.

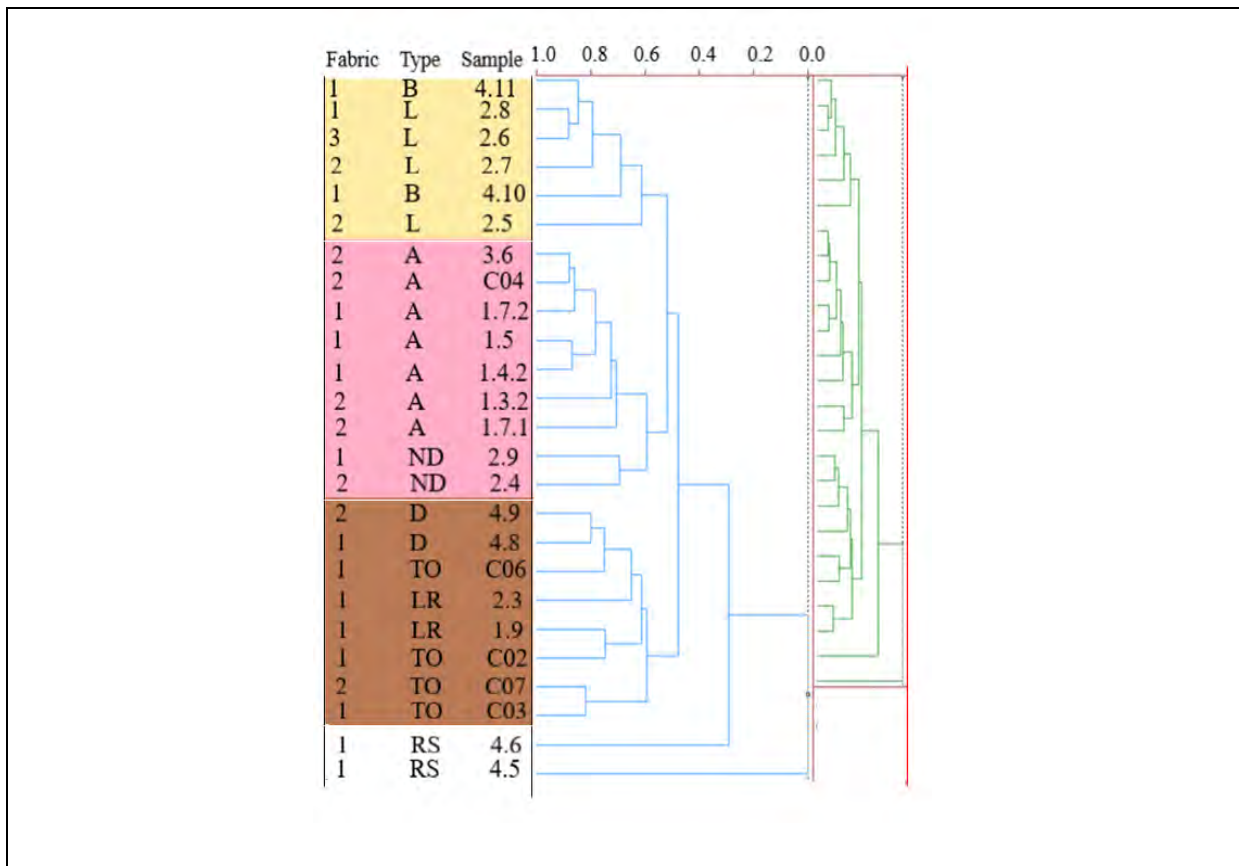


Figure 30: Dendrograms of Euclidean squared distances using average linkage algorithm. Data transformed by auto scaling for all the archaeological samples considered. Association to petro-fabrics is given based on observation under optical microscopy. Abbreviations: A= Ayla-Aksum, Fabric 1(granite- and /quartz-rich potsherds, bearing volcanic rocks), Fabric 2(granite- and feldspar-rich potsherds); L= Local pottery. Fabric 1(potsherds rich in fine-grained metamorphic rocks), Fabric 2(granite-rich Petro-fabric), Fabric 3(potsherds rich in metamorphic rocks and sandstone); B= Bricks, Fabric 1(metamorphic rocks rich Petro-fabric); LR= Late Roman Amphora 1, Fabric 1(petro-fabric rich in limestone and bio-clasts); TO= Torpedo jars, Fabric 1(limestone and volcanic rocks rich potsherds), Fabric 2(potsherds rich in volcanic rocks and bearing metamorphic rocks); D= dolia, Fabric 1(Argillaceous Rock Fragments (ARFs) Petro-fabric), Fabric 2(carbonates Petro-fabric); RS=red slipped ware; ND= Undetermined, Fabric 1(quartz/ felsic rocks Petro-fabric), Fabric 2(limestone dominated Petro-fabric) and Fabric 3(quartz and feldspars-dominated fabric).

The LRA1, Torpedo jars and *dolia* samples are grouped together and particularly the closer similarities in composition between the LRA1 and Torpedo jars is intriguing and can be perhaps related to the use of similar clay raw materials as has been suggested in the literature (Tomber *et al* 2020). The patterns seen in the dendrograms further enhance SEM-EDX observations and PCA plots. The red slipped wares are plotted as outliers in comparison to the rest. Cluster analysis was also performed excluding the red slipped wares (Fig. 31). Similar observations are noted regarding the local pottery which are shown in a distinct cluster in as much as affinities are shown between the Torpedo jars and LRA1 together with

the *dolia*. The samples representing the Ayla-Aksum amphorae are grouped together as a single cluster, further enhancing the observations made in petrography and the patterns noted by the PCA treatment of the geo-chemical data from ICP-OES to suggest a unique production.

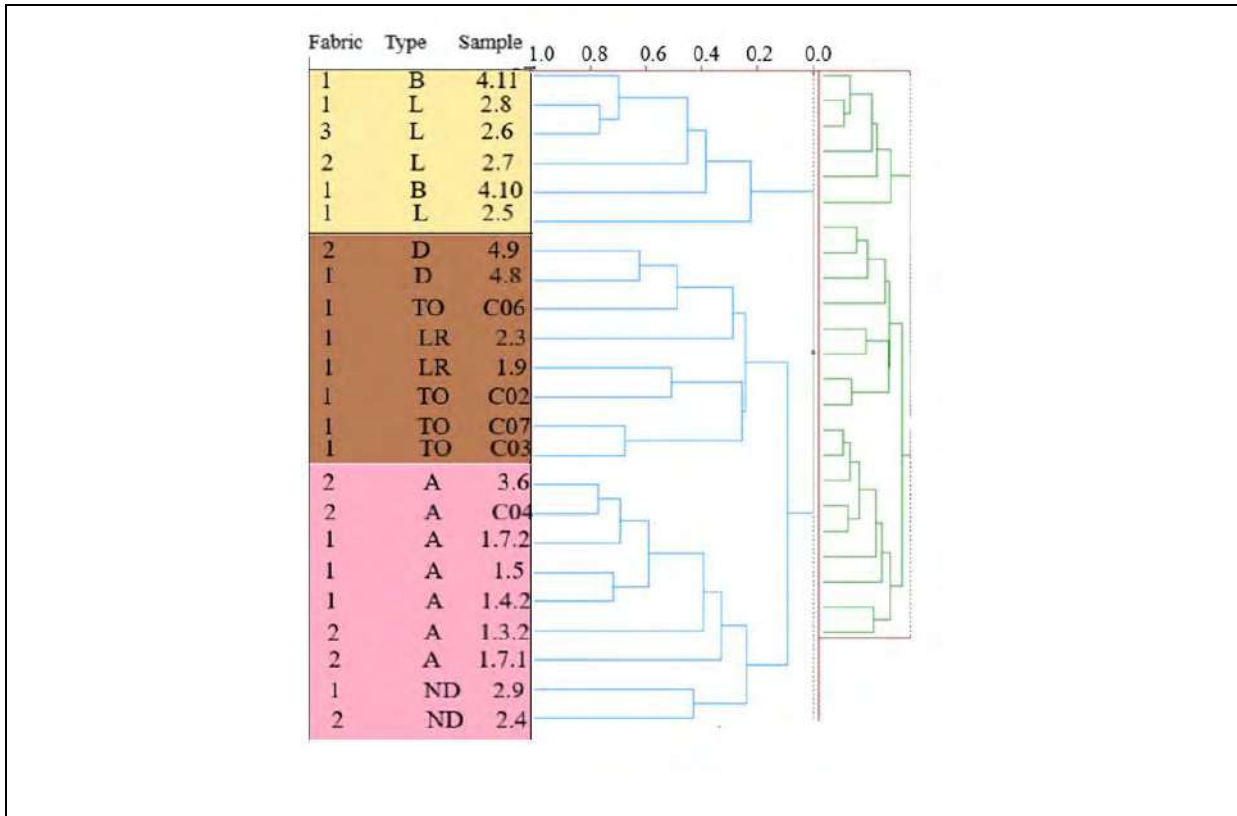


Figure 31: Dendrograms of Euclidean squared distances using average linkage algorithm. Data transformed by auto scaling considering all the samples, except the red slipped ware. Association to Petro-fabrics is given based on observation under optical microscopy. Abbreviations: A= Ayla-Aksum, Fabric 1(granite- and /quartz-rich potsherds, bearing volcanic rocks), Fabric 2(granite- and feldspar-rich potsherds); L= Local pottery. Fabric 1(potsherds rich in fine-grained metamorphic rocks), Fabric 2(Granite-rich petro-fabric), Fabric 3(potsherds rich in metamorphic rocks and sandstone); B= Bricks, Fabric 1(metamorphic rocks rich petro-fabric); LR= Late Roman Amphora 1, Fabric 1(petro-fabric rich in limestone and bio-clasts); TO= Torpedo jars, Fabric 1(limestone and volcanic rocks rich potsherds), Fabric 2(potsherds rich in volcanic rocks and bearing metamorphic rocks); D= *dolia*, Fabric 1(Argillaceous Rock Fragments (ARFs) petro-fabric), Fabric 2(carbonates petro-fabric); RS=red slipped ware; ND= Undetermined, Fabric 1(quartz/ felsic rocks Petro-fabric), Fabric 2(limestone dominated petro-fabric) and Fabric 3(quartz and feldspars-dominated fabric)

Moreover, the obtained results on pottery samples have been compared with the data from local clays to verify the possible identification of raw materials used in the production processes. Data transformed through autoscaling, and log ratio have been considered for these purposes. The plot based on log-ratio transformation includes all the pottery classes (Fig. 32 A) while the red slipped wares are excluded in the diagram based on data transformation by

auto scaling as they tend to show outlier values (Fig. 32B). PCA biplots highlight that the local pottery samples show compositional similarities with the raw clay samples, further suggesting that the local pottery samples might have been produced by using such raw materials, eventually after mixing different clays.

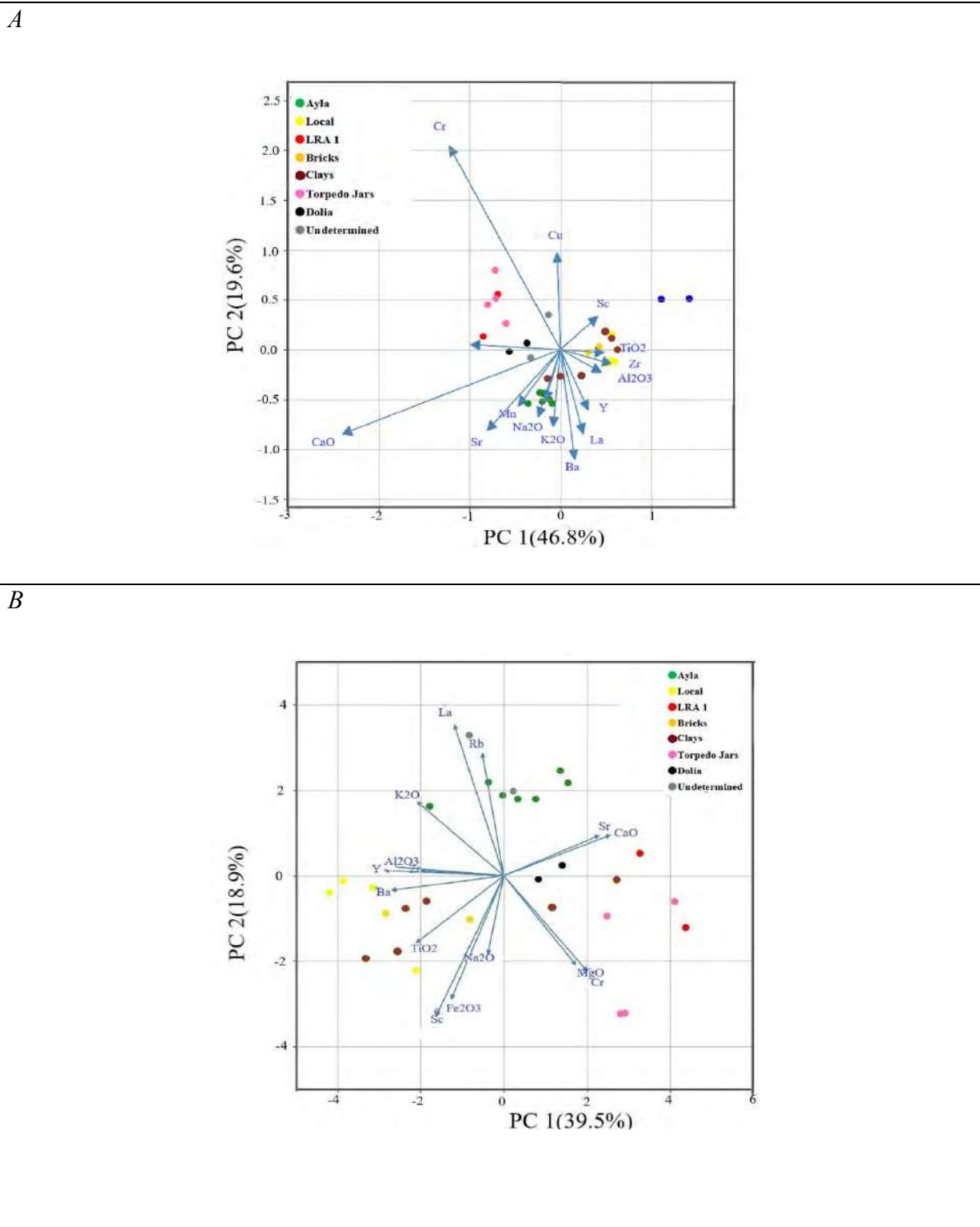
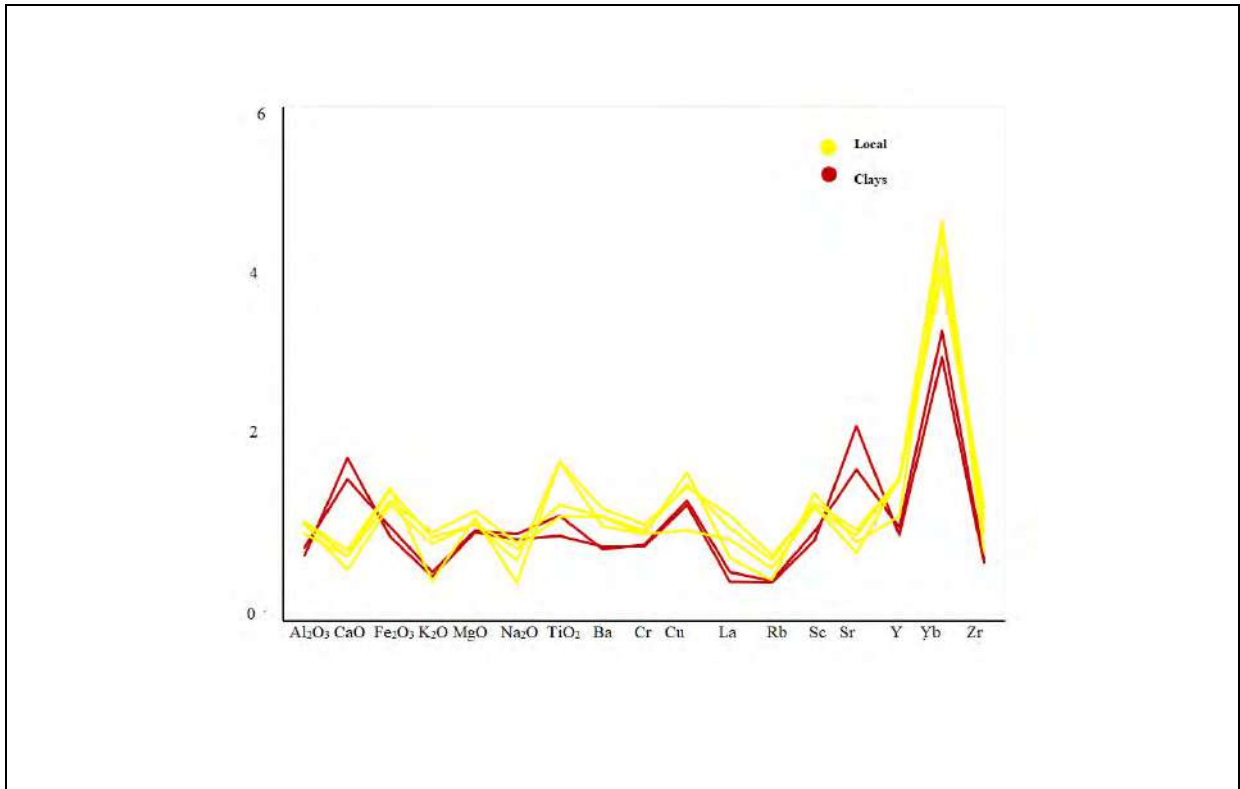


Figure 32: PCA biplots including raw clay samples. Projections based on data transformed by log ratio (A) and autoscaling (B).

Different recipes of clays and raw materials around the area of Adulis could, therefore, have been exploited and the observations collaborate the petro-mineralogical information obtained in this study. Yet, raw clay samples H1 and H2, which show relatively higher values of Ca and Sr are plotted closer to the Ayla-Aksum in the projections made from data transformed through log-ratio (Fig. 32 A) on one hand and closer the *dolia*, torpedo jars and LRA1 considering the projections made on data transformed by auto-scaling (Fig. 32 B). Such anomalies should not suggest similarities in production with Ayla-Aksum amphorae and/or the rest of the imported classes of pottery and further show that direct comparisons of the chemical composition of archaeological samples and untreated raw clays on a one-to-one basis should be considered very cautiously.

The anomalous nature of the raw clay samples is further discerned from the multi-element diagrams in Figure 33, where the element abundances of the archaeological samples and the raw clays are normalized to the average values of the crust. The effect of the dilution on the composition of specific chemical species due to added tempering materials is a well-known phenomenon as the manipulation of the clays by firing, mixing, homogenisation, decantation and levigation can bring compositional variations/similarities.

While the local clays H1 and H2 represent a possible source of clay materials for production of the local pottery in a basin drained by Haddas and Alighede rivers around Adulis, it should be noted that the petrographic observations of the briquettes produced from these raw clays indicates differences with the fabrics of Ayla-Aksum amphorae (Fig. 19 D). The petro-mineralogical information, as has been noted, refutes any postulation of the production of Ayla-Aksum amphorae at Adulis in as much as the patterns visible from the geo-chemical information on the Ayla-Aksum, local pottery, and raw clay samples.



B

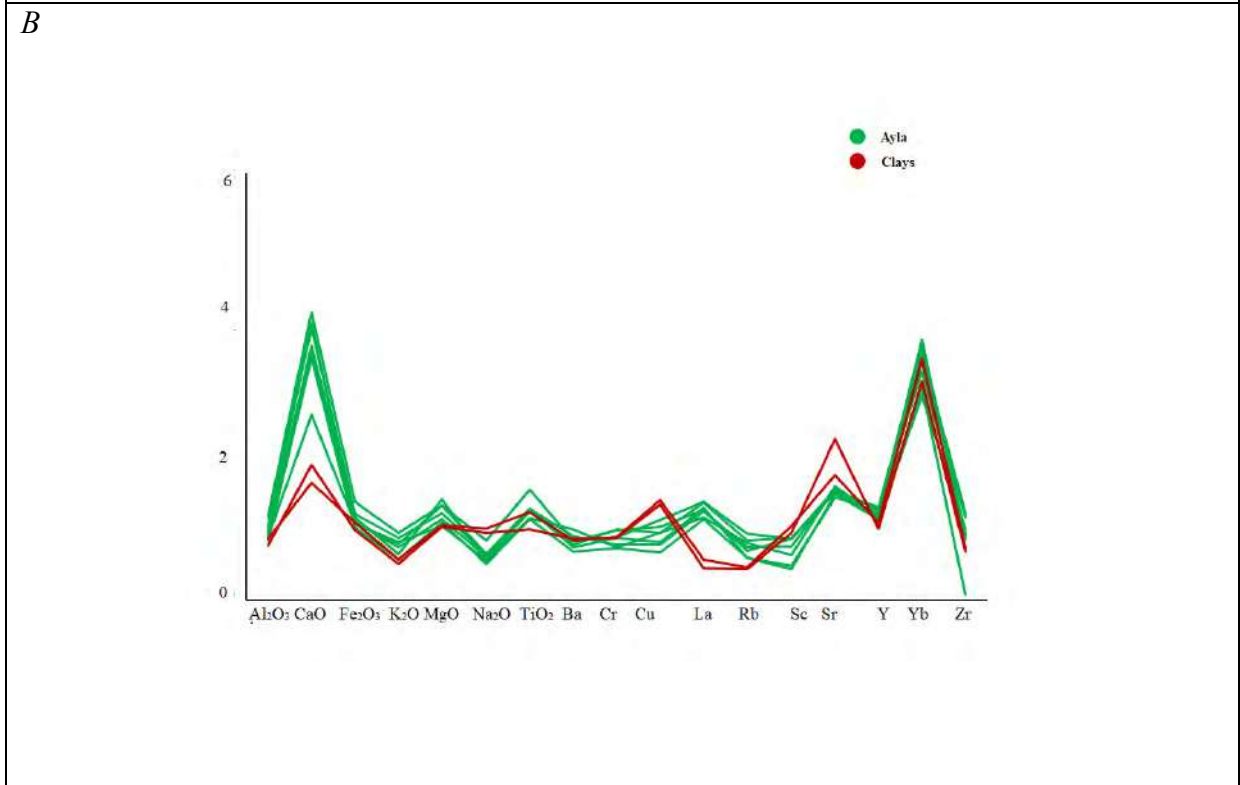


Figure 33: Multi-element diagrams showing element abundances of local pottery and raw clays(A) and element abundances of Ayla-Aksum and raw clays H1 and H2(B) normalised to the average values of the crust.

5.3. Archaeological Implications

The archaeometric study on the Ayla-Aksum amphorae recovered from Adulis to solve their provenance issue has established a strong link with the Ayla products attested in production areas (kilns, therefore, representing local reference materials) and further highlighted similarities to the results of previous archaeometric works from Zafar and Ayla (Raith *et al*, 2013). The distribution of these amphorae into Adulis and further into sites of the hinterland of the Horn of Africa as evinced from the sites of Matara and Aksum reinforces the direct links of the Red Sea port of Ayla to Adulis from the 4th century CE, and particularly at the end of 5th -early 6th CE. The role of Adulis is, moreover, attested in the articulation of the Roman, Aksumite and Byzantine commerce in Late Antiquity.

Moreover, the prevalent discussion on imported versus local production in archaeological studies at Adulis prompted to provide archaeometric information on local pottery. This study has outlined petrographic, mineralogical, and geo-chemical information on what has been classified as local (Adulitan) pottery by establishing different fabrics related to the local production. The extent of pottery production at Adulis has also been further elaborated by integrating the study of raw clay samples. This study has for the first time enabled to correlate the production of pottery to raw clay materials at Adulis. Adulitan pottery, represent a source of evidence for investigating the relationship between the port city to centres further in the hinterland in the northern Horn of Africa. The identification of petro-mineralogical and geo-chemical signatures of Adulitan pottery provide, on one hand, a key source of tangible archaeological evidence for the evolving connection and interplay between the Coast and the highlands in central Eritrea and northern Ethiopia in Late antiquity. The distinction of local pottery at Adulis, furthermore, allows one to understand the extent of distribution and exchange of imported pottery at Adulis.

The archaeometric work also established the petrographic and geo-chemical information on other imported transport and common wares, dominantly represented by Levantine forms (LRA1 and *dolia*) as well as the slipped ware. The petro-mineralogical information obtained from this study enabled to establish a fabric for the LRA1 (produced primarily between 4th to mid-7th centuries CE), that shows similarities to a type manufactured at numerous workshops in eastern Turkey and Cyprus (Peacock and Williams 1986).

An intriguing result has been the study of a set of samples which have been initially attributed to LRA 1(?) from macroscopic observation and yet from a multi-analytical approach encompassing petrography, ICP-OES and organic residue analysis (discussed in subsequent chapters) yielded an attribution to what is referred to as the ‘Torpedo jars. The petrographic observations coupled with the organic residue analysis in this study has provided information on Torpedo jars’ fabrics from Adulis for the first time, further broadening the scope of their distribution to the shores of the northern Horn of Africa in Late antiquity. Interestingly, similarities observed in geo-chemical composition between LRA1, and the Torpedo jars further enhance the complexities in distinguishing between fabrics as has been indicated from recent studies on Torpedo jars from elsewhere (Tomber *et al* 2020). High contents of Cr, MgO, as well as contributions to heavy metals like Cu as discerned from patterns the geo-chemical data of the LRA1 and Torpedo jars may pinpoint to clays related to ophiolitic terrains as contributions from ultra-basic rocks can be suggested. Production sites for LRA1 in eastern Turkey and Cyprus were located on geological deposits where an ophiolite-rich clay was exploited in as much as the production of Torpedo jars in Mesopotamia using similar raw materials. Tomber *et al* (2020) suggested two main geological features where Torpedo jars are most likely to originate, namely the Tigris-Euphrates basin of Iraq (Mesopotamia) and the continuous mountain range stretching from Troodos, Cyprus to Semail, Oman.

The fact that there are no known kilns to produce the Torpedo jars and that their fabrics are characterized by a matrix rich in mafic minerals, thus, broadens the scope of potential production centres and the similarities in composition with the LRA1 as demonstrated in this study enhance the need for a systematic comparison of the vessels from different sites to LRA1 production. The results from this study, therefore, contribute to the on-going discussions on the provenance of Torpedo jars considering comparisons of regional pottery assemblages. The distinction between the fabrics belonging to LRA1 and Torpedo jars is further investigated to understand micro-structural features and the technology of production discussed in the next chapter.

It has also to be noted that the petro-mineralogical and chemical characterization in this study allowed to establish fabrics for the red slipped ware and *dolia* samples and yet conclusions cannot be drawn on their provenance due to the limited number of samples. Future archaeometric works, thus, need to draw from inclusion of similar samples from sites in the Levant and East Mediterranean to have comparative parallels. The question of fabrics

belonging to undetermined typology similarly posed difficulties to infer on their provenance, further leaving the subject to be systematically approached in the future by identifying complete forms.

In conclusion, the petrographic observations coupled with SEM-EDX, and ICP-OES provided information on different fabrics belonging to the different classes of pottery considered and lay the basis for building ceramic sequence at Adulis. The information on fabric attribution and provenance highlighted in this chapter are further broadened by the comprehension of micro-structural features and technology of production discussed in chapter 6.

5.4. Bibliography

Baxter MJ. (2001) Statistical modelling of artefact compositional data. *Archaeometry* 43(1):131–147. <https://doi.org/10.1111/1475-4754.00008>.

Fabbri B, Gualtieri S, Shoal S (2014) The presence of calcite in Archeological ceramics. *J Eur Ceram Soc* 34(7):1899–1911. <https://doi.org/10.1016/j.jeurceramsoc.2014.01.007>.

Ghebreab W and Talbot, C. J. (2000). Red Sea extension influenced by Pan-African tectonic grain in eastern Eritrea, *Journal of Structural Geology* (22). No. 7, pp. 931-946. [https://doi.org/10.1016/S0191-8141\(00\)00022-5](https://doi.org/10.1016/S0191-8141(00)00022-5).

Holmqvist-Sipilä E. 2019. *Ceramics in Transition: Production and Exchange of Late Byzantine-Early Islamic Pottery in Southern Transjordan and the Negev*. Archaeopress. ISBN 978-1-78969-225-9 (e-Pdf).

Papageorgiou I. (2020) Ceramic investigation. How to perform statistical analyses. *Archaeol Anthropol Sci.*12, 210. <https://doi.org/10.1007/s12520-020-01142-x>.

Peacock D P S and Williams, D F (1986) *Amphorae and the Roman Economy*. London: Longman

Raith M, Yule P, and Damgaard K. (2013). The view from Zafar: An archaeometric study of the Aqaba pottery complex and its distribution in the 1st millennium CE. *Zeitschrift für Orient Archäologie* 6: 318–348.

Tomber R, Spataro M, Priestman S. (2020). Early Islamic Torpedo Jars from Siraf: Scientific Analyses of the Clay Fabric and Source of Indian Ocean Transport Containers, Iran, <https://doi.org/10.1080/05786967.2020.1792797>.

6. Technology of Production

Abstract

This chapter deals with the characterization of samples belonging to the different classes of pottery considered in the study from the microstructural, morphological, and mineralogical point of view, in order to assess the technologies of production and – mainly – the estimated firing temperatures from these proxies. SEM-EDX examination of polished thin-sections and fresh fractures allowed to provide a comparison based on the detailed microstructural assessment and understanding of the vitrification stages, in reference to calcareous and non-calcareous ceramic classes. Information on the mineralogy and/or firing phases of all studied samples from XRPD is also included, to complement the reliability of the firing temperatures estimates determined by microstructural analysis. The existence of different stages of vitrification, confirmed by the observed microstructures, and the assessment of the thermal stability of different crystalline phases have been discussed and compared to parallel situations, available in the extensive literature. The information obtained through complementary analytical techniques, namely SEM-EDX and XRPD, are thus jointly incorporated to infer specific information on the technological choice/s related to specific pottery classes.

6.1. Materials and Methods

6.1.1. Sampling

The sampling procedure followed a protocol for the selection of representative samples, based on the fabric variability as established by optical microscopy. In this respect, representative samples that include the Ayla-Aksum amphorae, local pottery, Late Roman Amphorae 1, Torpedo jars, *dolia* samples and red slipped ware were selected, also for a comparative purpose. A great deal of the fragments considered for this study come from contexts dated to 5th -7th CE. The observations of the micro-structural and morphological features, as well as the comprehension of the diffraction patterns, enabled to make inferences in light of the specific classes considered. The study of briquettes of raw clay samples was also considered for XRPD.

6.1.2. Analytical Methods

6.1.2.1. X-ray Powder Diffraction (XRPD)

X-ray Powder Diffraction (XRPD) data were collected on 50 pottery samples, by using a Rigaku Miniflex 600 diffractometer (working voltage and current of 40kV and 15mA, respectively) in Bragg-Brentano geometry with Theta/Theta setup, flat sample-holder and Cu-K α radiation. Diffractograms were collected in the 3-70 2 θ range, by using a step size of 0.010° and a step-time of 1.000 s.

XRPD data were also collected on raw clay samples belonging to the area of Adulis, in order to study the mineralogy of the precursor clay materials that could have been used to produce the local pottery. For each sample, the clay was dispersed in H₂O and pipettes were used to isolate the < 2 μ m dimensional fraction. For each sample, two glass slides were prepared with oriented clay particles – smeared and air-dried. Glycolation and heat treatments (at 350 °C and 500 °C) were applied in order to thoroughly characterize the constituent clay mineral/s by XRPD. Each slide was scanned in the 2-30° 2 θ range, with a 0.005° step size and 1.0 s step-time. For all samples, data interpretation was performed with the EVA-Diffrac Plus evaluation program, by Bruker.

6.1.2.2. Scanning Electron Microscopy (SEM)

Micro-structural and morphological evaluation of the ceramic bodies was performed on polished thin-sections and on fresh fractures, respectively, using two different instrumentations. Backscattered electron (BSE) images were obtained on graphitized polished thin sections of archaeological pottery and fired clay samples using a CamScan MX 2500 SEM (Department of Geosciences, University of Padua, Italy) equipped with a LaB₆ crystal and an energy-dispersive X-ray spectrometer (EDS), working at 25 kV accelerating voltage and 40 nA current.

The observation of the degree of sintering and/or vitrification allowed us to make hypotheses on the technology adopted during the firing step, also supported by the evaluation of the chemical composition of newly formed phases by using EDS data.

Secondary Electron images, on the other hand, were obtained on 22 fractures(gold-coated) of archaeological samples using a Zeiss EVO60 microscope (Centro Conservazione e Restauro

dei Beni Culturali La Venaria Reale), working at 20kV accelerating voltage. Magnifications at 2000x and 3000x were obtained to evaluate presence or absence of vitrification structures.

6.2. Results and Discussion

6.2.1. SEM Micro-structural Features

For microstructural SEM analyses, observations made on polished thin sections and fresh fractures are combined to provide information on technology of production, namely the firing regimes. In this respect, detailed insights are provided by referring to the specific pottery classes considered in this study.

Samples belonging to the Ayla-Aksum amphorae are produced using a relatively high calcareous clay, where the average concentration of calcium oxide in the matrices of these samples is around 15% (as obtained from SEM-EDX analyses). The observations of microstructures of the Ayla-Aksum amphorae generally reveal similar regimes of firing; few exceptions are noted, however, and could be attributed to slight variations intrinsic to the firing procedure, such as the duration of the whole firing step or the residence time at a certain temperature and eventually the atmosphere in the furnace (Fig. 34- 39).

The observation of shrinkage rims around aplastic inclusions, and the intensive bridges (Fig. 34A) coupled with the decomposition of phyllosilicates (Fig. 34B), which result in the diffusion of potassium in the amorphous phase and the hematite growth are observed on sample 3.6, where the indication of an continuous vitrification structure is evenly distributed in the matrix and the sample perhaps might have been fired at a relatively higher temperature between 850-900 °C (Tite and Maniatis 1981; Chatfield 2010; Montesana *et al* 2019; Xanthopoulou *et al* 2021). The decomposition of carbonates present in the original clay and the eventual growth of clino-pyroxenes is an indication where a framework of calcium alumina-silicates formed by the concentration of calcium oxide are noted (Fig. 34C).

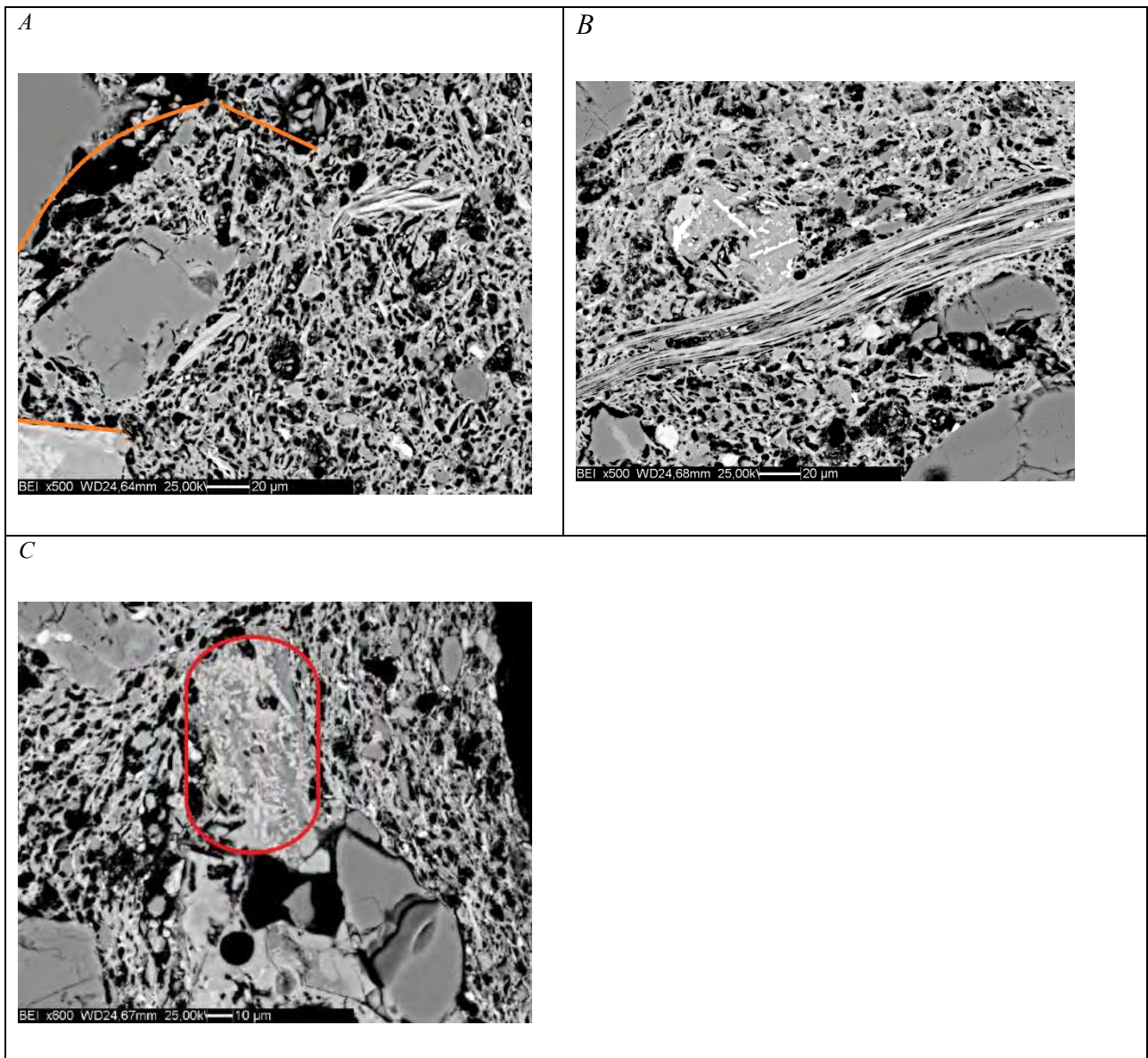


Figure 34: SEM-BSE images of polished thin sections for sample 3.6; reaction rims (A); decomposition of phyllosilicates (B); formation of new phases (C)

A Ca-rich micromass (as revealed from SEM-EDX data), as well as the distribution and small calcite crystals affected the vitrification structure (Fig. 35A). The calcite crystals in the raw material were probably very fine, thus helping to form evenly distributed initial vitrification structures in the samples. The observation of the bloating pores (vesicles) under SEM s of the fractures also pinpoints to the development of continuous vitrification structures in the sample (Fig. 35B). As far as the development of continuous vitrification structures in calcareous ceramics is concerned, it has been demonstrated in the literature that a firing temperature in the range of 850- 900 °C can be established (Chatfield 2010; Montesana *et al* 2019; Pérez-Monserrat *et al* forthcoming).

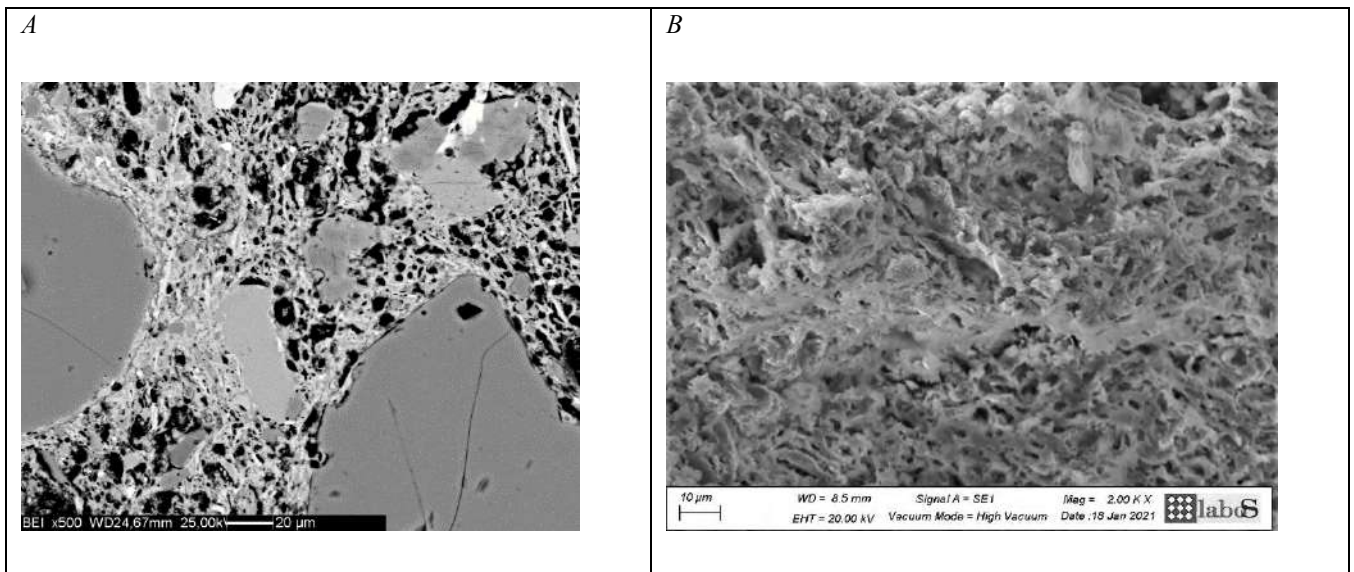


Figure 35: SEM images of continuous vitrification structure for sample 3.6, BSE image on the polished section (A) and SE image on a fresh fracture(B)

The onset of initial vitrification structures is also observed in samples 1.3.2, 1.4.2, 1.5 and 1.7.2 (Fig. 36), in which the vitrification structures are unevenly distributed in contrast to sample 3.6 (Fig. 34 and 35). This could be related to differences in the pristine mineralogical composition in the various parts of the ceramic matrices. In these samples, the vitrification structures are associated with neo-formation of clinopyroxenes, as confirmed by compositional mapping by SEM-EDX. According to literature data (Tite and Maniatis 1981; Chatfield 2010; Montesana *et al* 2019; Xanthopoulou *et al* 2021), a firing temperature interval of 800-850 °C can be suggested for the onset of initial vitrification and the fact that the structures are distributed unevenly pinpoint to a slightly lower temperature equivalent in comparison to sample 3.6.

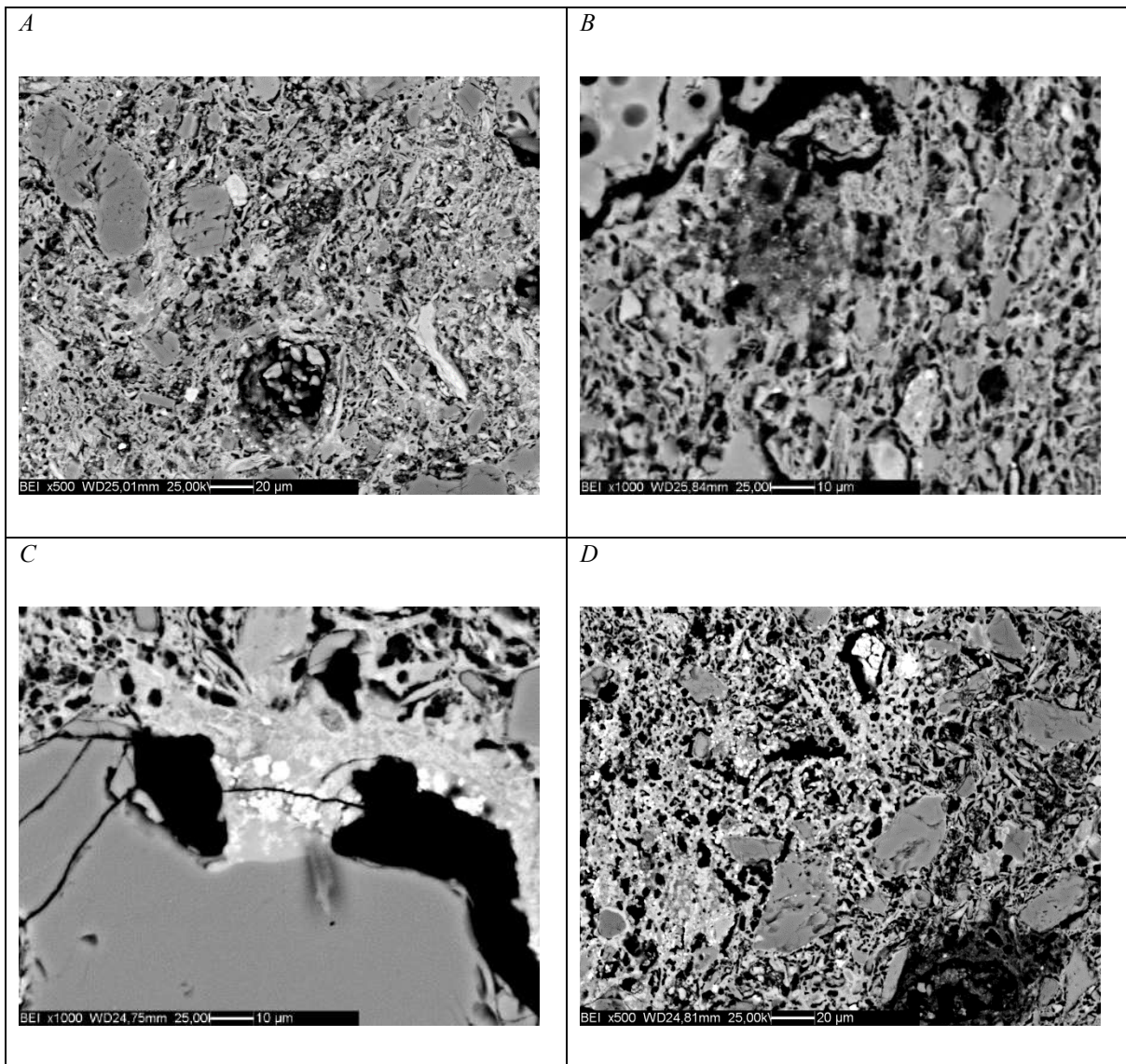


Figure 36: SEM -BSE images of initial vitrification in samples 1.3.2(A), 1.4.2(B), 1.5(C) and 1.7.2(D).

The observations of the fractures also revealed similar phenomena to pinpoint the development of initial vitrification structures in these samples (Fig. 37)

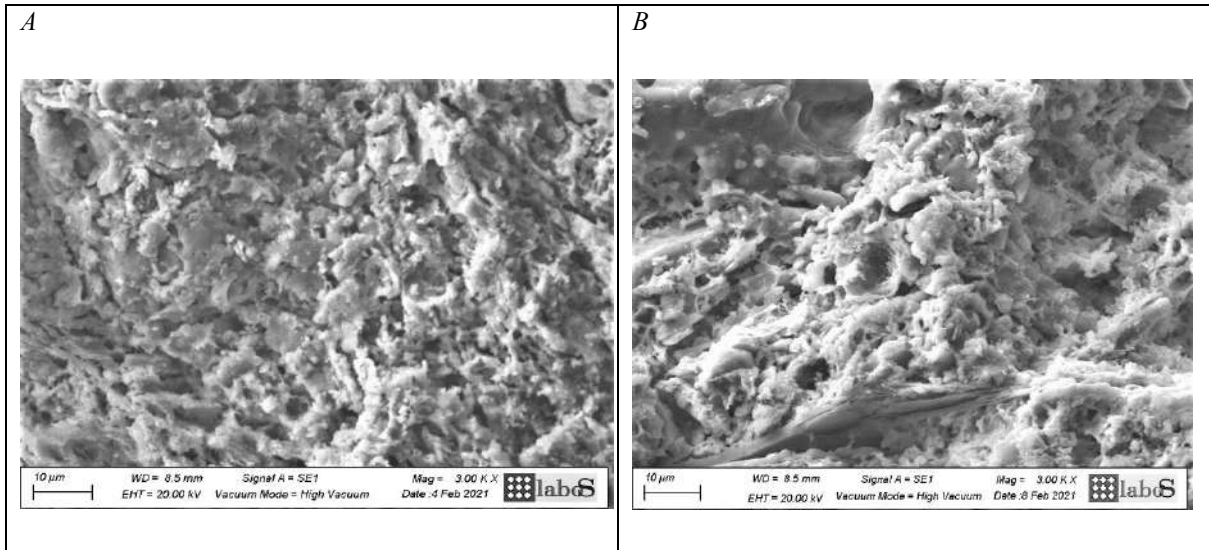


Figure 37: SEM-SE images of the fractures of samples 1.4.2 (A) and 1.7.2(B)

Conversely, for sample 1.7.1 indication of vitrification structures is lacking as illustrated in Fig. 38, where a partially sintered matrix can be observed, indicating that the temperatures reached were not sufficient to decompose calcite, thus implying a temperature around 750-800 °C. The presence of phyllosilicates (Fig. 38A) is noted, as well as of secondary calcite (Fig. 38B).

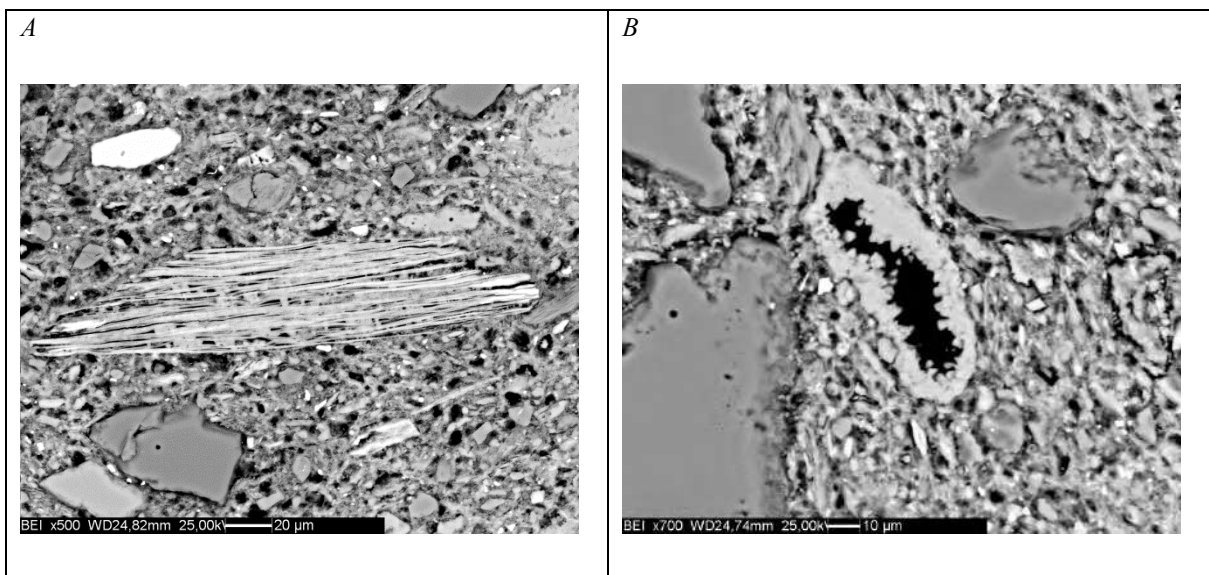


Figure 38: SEM-BSE images of sample 1.7.1: sintered matrix(A) and recrystallisation of calcite(B)

The observations of the fresh fracture of this sample, furthermore, indicate the presence of flakes of phyllosilicates and the clay materials to pinpoint lower temperatures (Fig. 39). Data from literature support this hypothesis where the presence of non-vitrified structures in a calcareous rich matrix account for a temperature equivalent of 800 °C (Tite and Maniatis 1981; Montesana *et al* 2019).

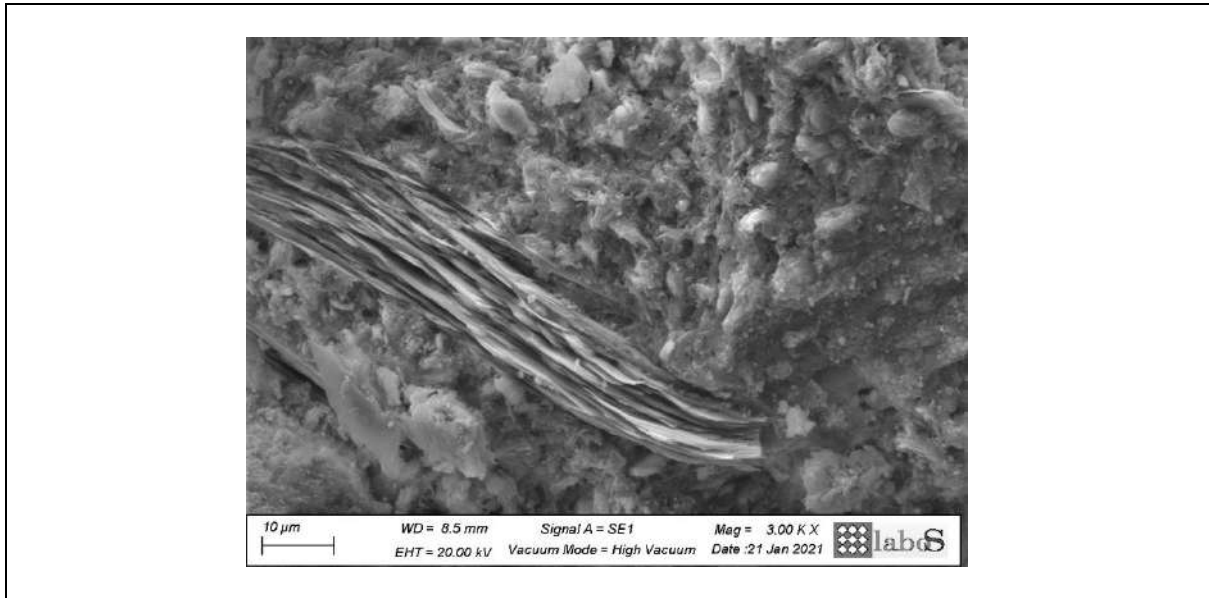


Figure 39: SEM-SE images of sample 1.7.1(fracture)

The samples belonging to the Late Roman Amphora 1 class show the presence of intact microfossils, mollusc shells, foraminifera, bryozoa, spathic calcite and limestone (Fig. 40). The presence of carbonates, microfossils and limestone rich in shells is clearly indicative of a highly calcareous clay material. The microstructural feature of mollusc shells can be used to constrain the thermal interval reached during firing (Maritan *et al* 2007). A partially recrystallized limestone rich in shells and bryozoan, and the formation of pores as well as transverse fractures (Fig. 40 A-D) as seen from the SEM observations of the polished thin sections of samples 1.9 and 2.3, reveal the fading of the growth of internal layers of the bivalves. Experimental works on the assessment of firing changes visible in mollusc-shell rich pottery have indicated the observation of such phenomenon is consistent with firing temperature around 700-750 °C (Maritan *et al* 2007).

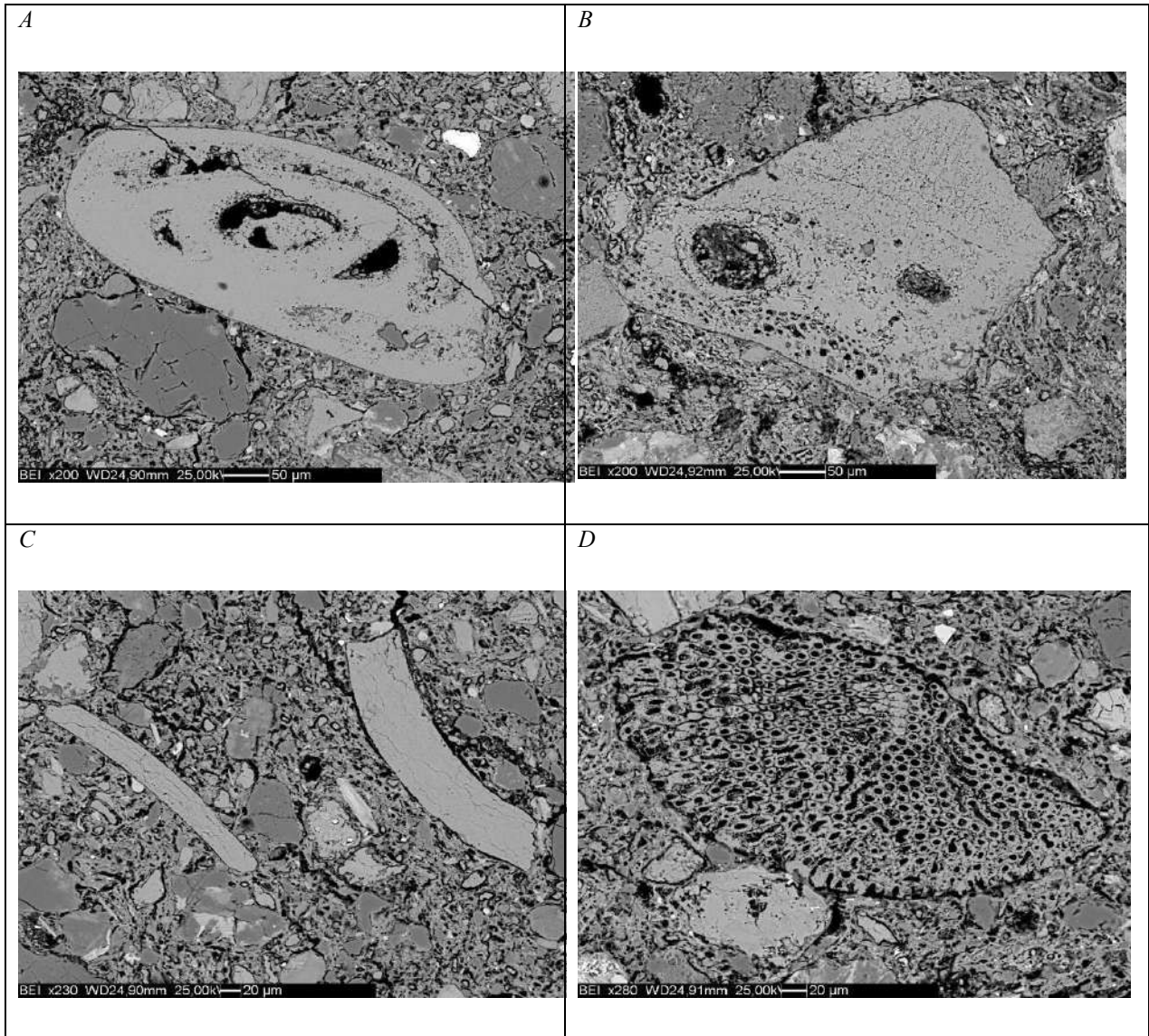


Figure 40: SEM-BSE images of LRA 1. note the presence of mollusc and bryozoan shells in sample 1.9 (A-D).

The observation of the fractures of these samples under SEM also indicate absence of bloating pores, further highlighting temperatures below the decomposition of carbonates and below the onset of initial and/or extensive vitrification (Fig. 41). Such an indication of non-vitrified structures in a calcareous rich ceramic paste (> 15%) can be related to firing temperatures not exceeding 800 °C (Tite and Maniatis 1981; Montesana *et al* 2019). In this respect, the postulation of firing temperatures based on the observation of the structures of the mollusc shells fits within the temperature interval.

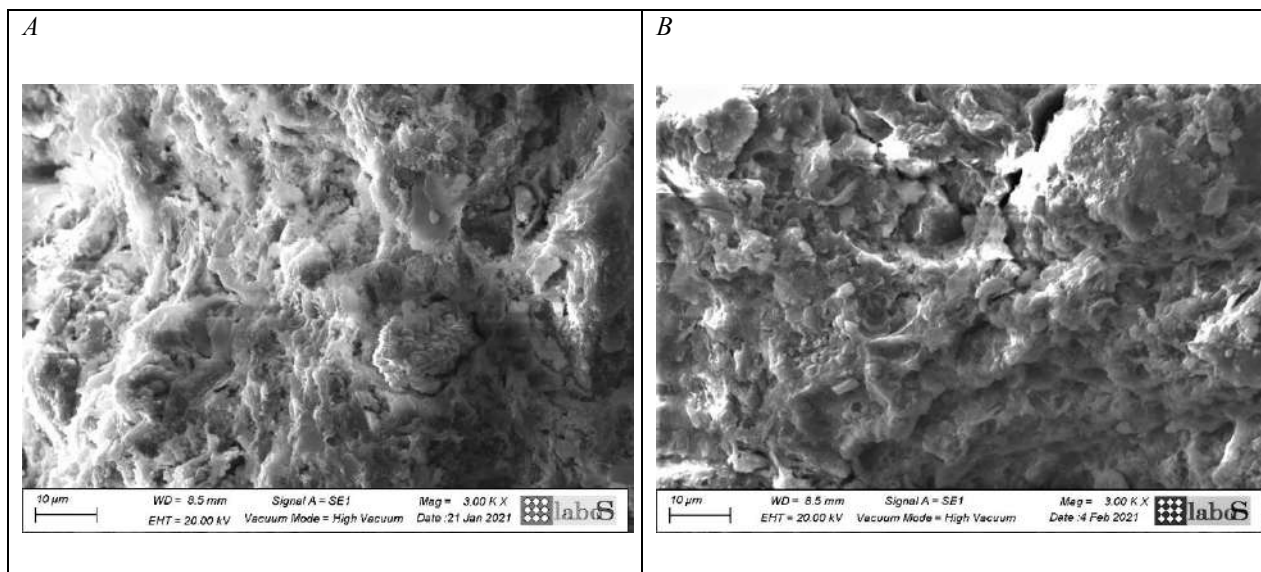


Figure 41: SEM-SE images of the fresh fractures of LRA 1, sample 1.9 (A) and sample 2.3 (B)

SEM microscopic examination of samples, which have been initially classified as LRA1(?) and were later securely identified as Torpedo jars from the coupling of petrographic observations and the study of organic residues (see chapters 5 and 7 respectively), in contrast attest to the development of initial vitrification structures in a calcareous matrix (> 10%), further complementing the differentiation between the LRA1 and the Torpedo jars (Fig.42). The SEM observations in the latter suggest the initial stages of vitrification, indicating temperatures in the range of 800- 850°C based on comparisons with available literature (Tite and Maniatis 1981; Chatfield 2010; Montesana *et al* 2019). The decomposition of the carbonates through firing is discerned from SEM-BSE images and the subsequent neo-formation of high temperature phase (please, list them), as a result of the interaction of calcium oxides with quartz, feldspars and other minerals (Fig. 42 A and B). Moreover, bloating pores observed from SEM-SE images on the fresh fractures of these samples, illustrated in Figure 42 C and D, equally suggest initial vitrification structures to substantiate a postulation of an estimated firing regime reaching 800-850 °C (Tie and Maniatis, 1981; Montesana *et al* 2019).

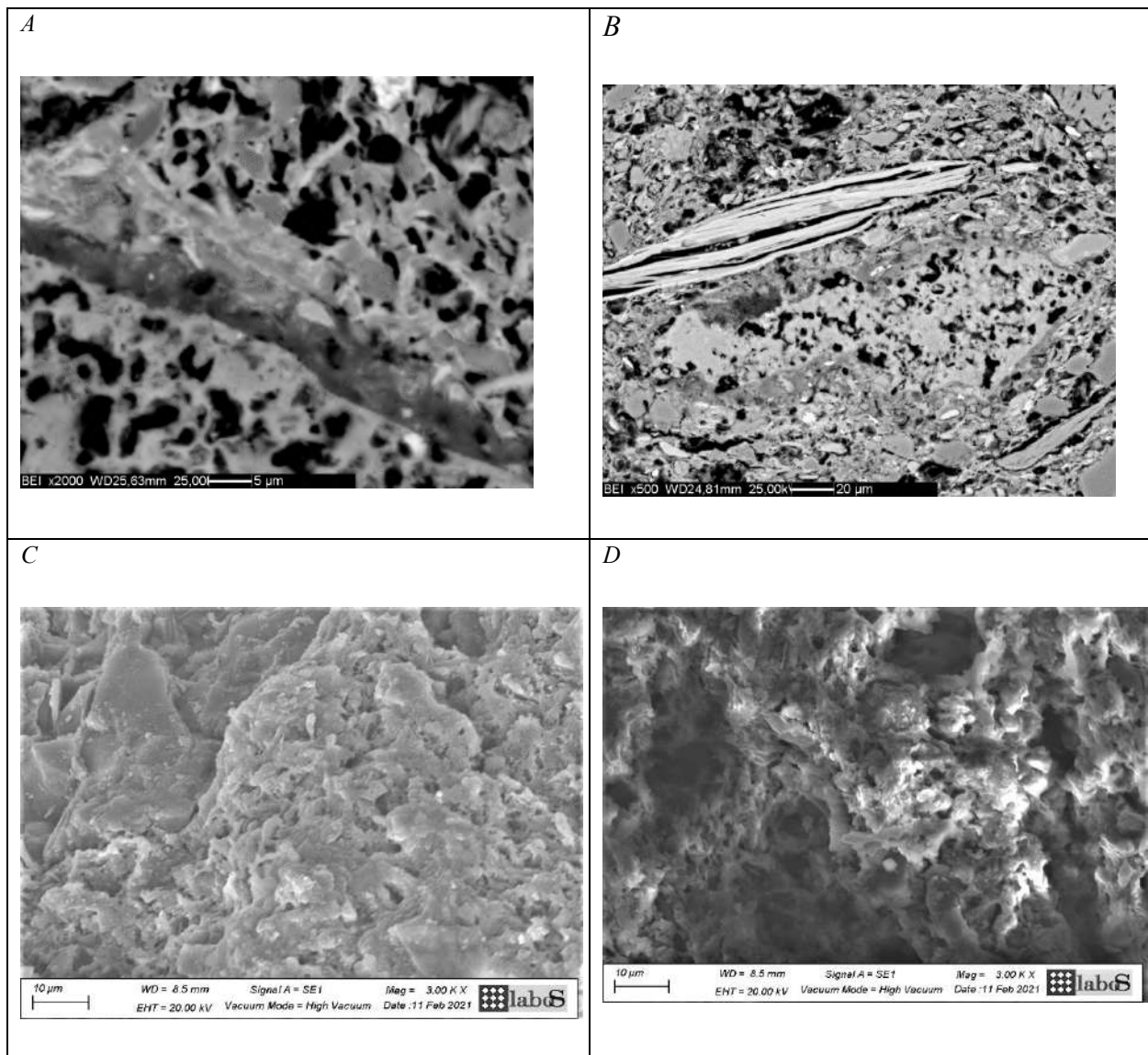


Figure 42: SEM-BSE images of micromass of samples C02(A) and C06(B). SEM-SE images of their fresh fractures also shown (C and D)

The samples which belong to the local pottery represent, on the other hand, a unique production in terms of micro-structural and morphological features in as much as the attribution of these phenomena to a specific production choice/s in comparison to the rest of the imported classes of pottery.

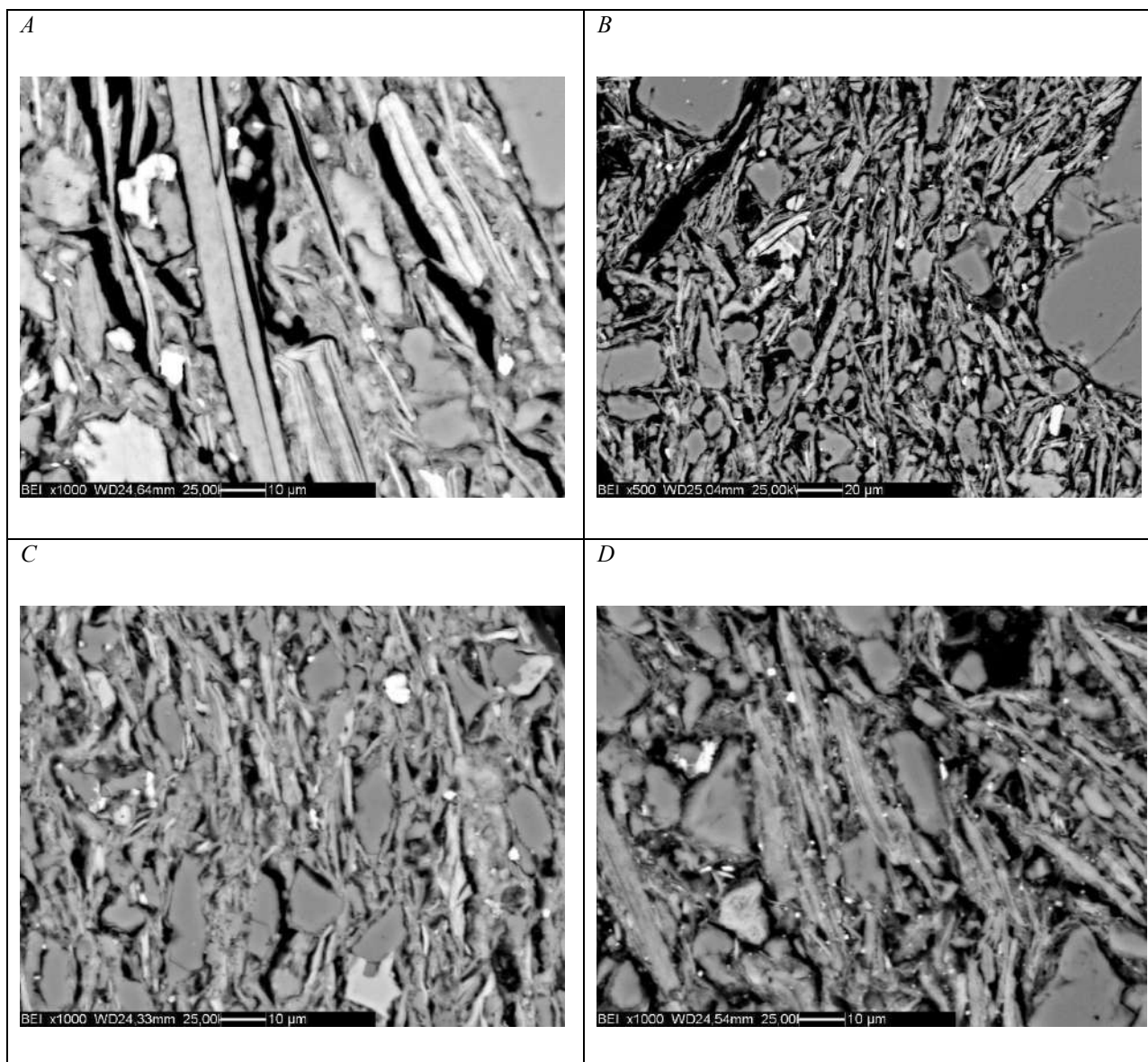


Figure 43: Micro-structural features visible from local pottery: SEM-BSE images of samples 2.5(A), 2.6(B), 2.7(C) and 2.8(D).

SEM-BSE images from the study of the polished thin sections (Fig. 43) reveal a non-calcareous matrix for the local pottery (< 6%) and the micro-structures observed pinpoint to a lower firing temperature based on comparisons from the literature not exceeding 800 °C (Tite and Maniatis 1981). From a morphological and micro-structural point of view, the BSE images indicate intact phyllosilicates' structures unaltered by firing in as much as revealing a little or no interactions of individual grains and/or clasts with the matrices and the lack of neo-formation phases. The presence of phyllosilicates in these samples has been also confirmed by petrographic observations where an optically active matrix noted in the samples can also attest to unaltered phyllosilicates due firing temperatures below their

dihydroxylation. These features are pronounced in samples 2.5, 2.6, 2.7 and 2.8 (Fig. 10) in as much as the non-sintered and not vitrified matrices (Fig. 43). The SEM observations of the fractures of these samples also attest to absence of bloating pores indicative of vitrification structures and the presence of flakes of the clay minerals and/or phyllosilicates is markedly observed in these samples (Fig. 44). Non-vitrified structures inherent in non-calcareous ceramics have been linked to temperatures not exceeding 800° C as has been indicated in the literature (Tite and Maniatis 1981) and such information can be linked to observed micro-structures in the local pottery considered in this study.

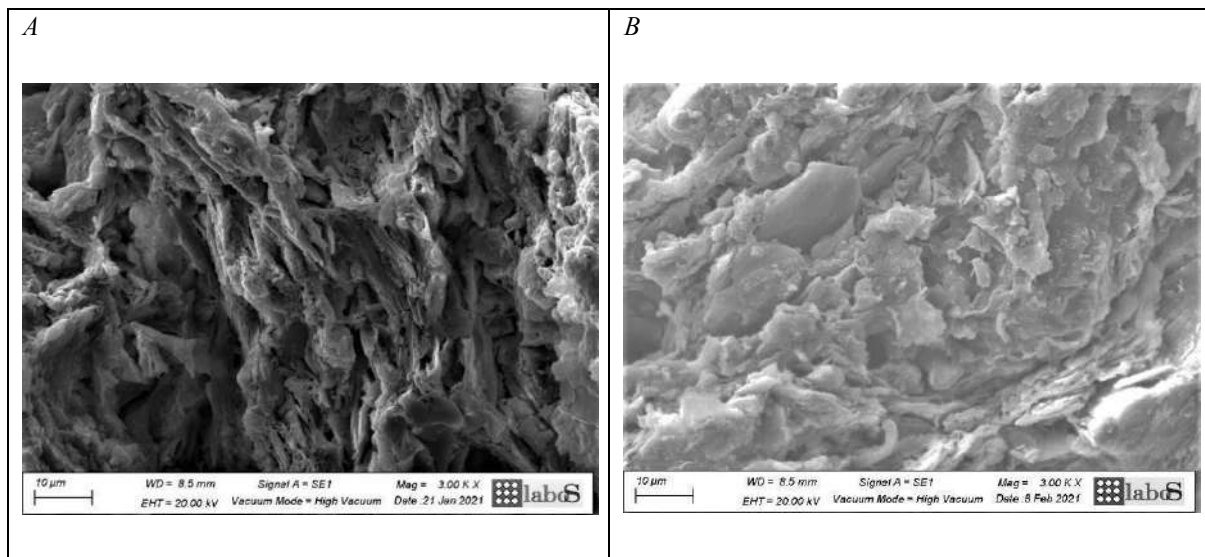


Figure 44: SEM-SE images of the fractures of samples 2.6 (A) and 2.8(B).

On the other hand, the brick samples (4.10 and 4.11), which are considered of local production, show typical microstructures formed during sintering as illustrated in Fig. 45 while the on-set of vitrification structures remain absent.

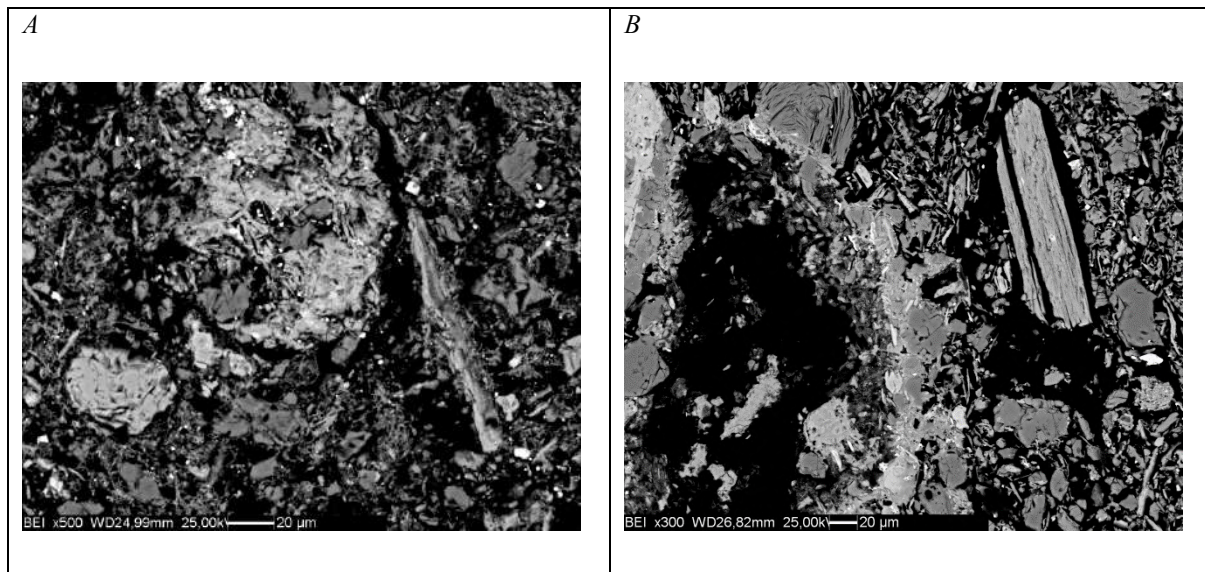


Figure 45: SEM-BSE Images of Samples 4.10(A) and 4.11(B)

The brick samples represent non-calcareous matrices from SEM-EDX data (< 6%) and the formation of shrinkage rims and bridging visible due to the interaction of quartz, feldspars and perhaps calcite with the phyllosilicates (Fig. 45 A and B) and the decomposition of the phyllosilicates (Fig. 45 B) can be attested from the SEM BSE images. Where sintering and non-vitrified structures are noted for non-calcareous ceramics, a temperature not exceeding 800 °C can be postulated (Tite and Maniatis 1981; Montesana *et al* 2019).

From a morphological and micro-structural point of view, observations were also made on the selected samples representing the *dolia* samples and the red slipped ware (Fig. 46 and 47 respectively). The *dolia* samples reveal similarities in the observed microstructures, namely in samples 4.8 and 4.9 as illustrated in figure 46 A and B. The *dolia* samples are characterized by a calcareous matrix (>10%). The decomposition of the carbonates and the interaction of quartz with mainly ARFs and other inclusions induced the onset of initial vitrification structures in sample 4.8 and 4.9(Fig. 46 A and C).

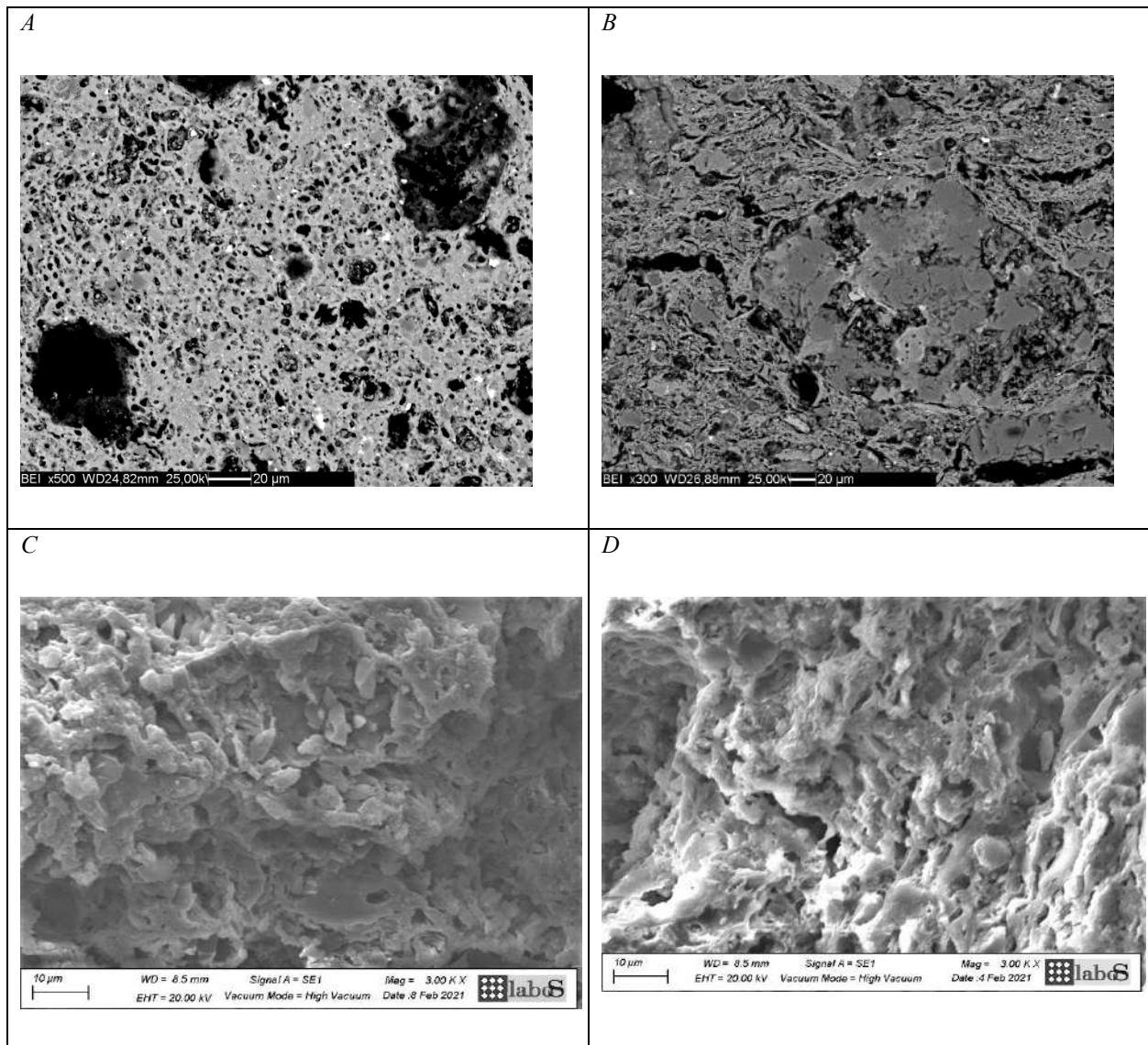


Figure 46: BSE images of samples 4.8 (A) and 4.9 (B). The SEM Images of their Fractures seen also seen (C and D respectively)

The observation of the fresh fractures of these samples demonstrates bloating pores indicative of initial vitrification structures in samples 4.8 and 4.9 as illustrated in Fig. 46 C and D respectively. Based on the comparative parallels of the development of initial vitrification structures (Tite and Maniatis 1981; Mentessana *et al* 2019), it can be said that a temperature gradient of 800-850 °C can be suggested for samples 4.8 and 4.9.

Furthermore, the red slipped ware considered in this study represent another class of pottery where lower firing temperatures can be postulated from the observations of the polished thin sections and fresh fractures (Fig. 47). The slip layer is barely visible under SEM observation perhaps due to its complete degradation and the study of the morphological and micro-

structural features of the ceramic body indicated the absence of vitrification structures and/or sintering (Fig. 47 A and B). The red slipped ware sample considered in the study represent a non-calcareous matrix and the absence of vitrification or sintering indications pinpoint a temperature lower than 800 ° C based on comparisons from literature (Tite and Maniatis 1981; Mentessana *et al* 2019; Xanthopoulou *et al* 2021).

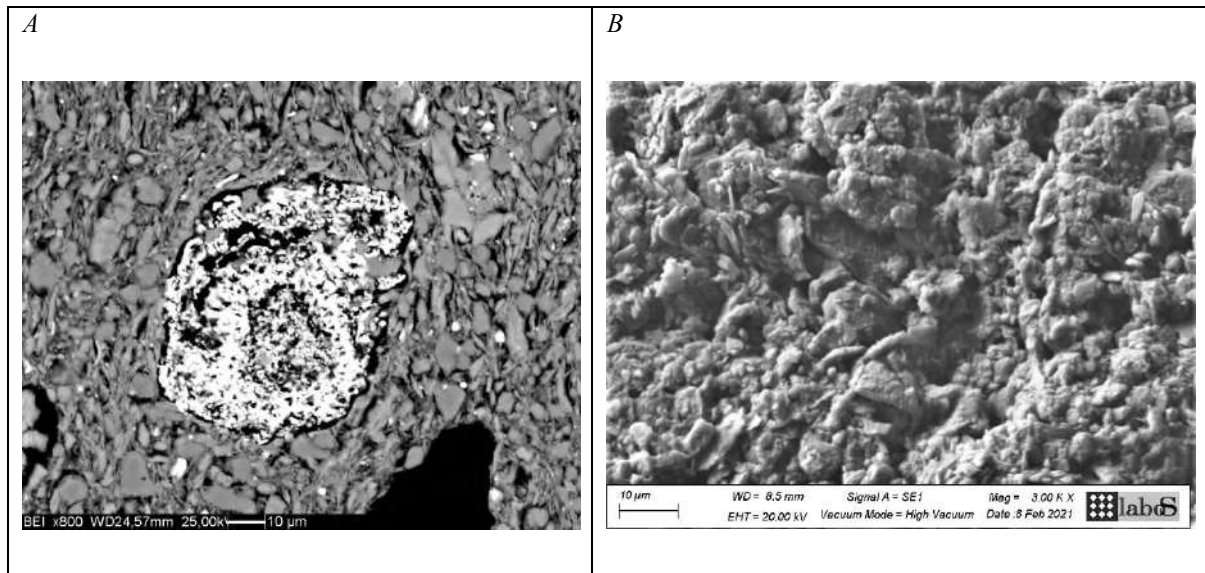


Figure 47: SEM- BSE images of samples 4.6(A) and SEM-SE images of its fresh fracture(B).

Finally, SEM observations of samples 2.9 and 2.4, which remain securely unidentified from typological point of view, revealed varying degrees of the presence of vitrification structures as can be seen from Figure 48. Both the samples are calcareous (> 6%). SEM-BSE images show the development of initial vitrification structures in sample 2.4 (Fig. 48 A and C), where interaction of calcite with other inclusions has resulted in the formation of new phases in a limestone-rich matrix. The vitrification structures are unevenly distributed in the matrix, attesting perhaps compositional variations and differences in the exposure to firing temperatures. The presence of carbonates is noted together with the presence of new phases in areas where vitrification structures developed (Fig. 48 A). On the other hand, BSE images of sample 2.9 pinpoint to an even distribution of the onset of continuous vitrification structures as seen in Figure 48 B and D, thus indicating a higher temperature in comparison to sample 2.4. The evenly distributed vitrification structures are also noted from visible fine bloating pores understood from the observation of the fresh fracture of the sample (Fig. 48 D).

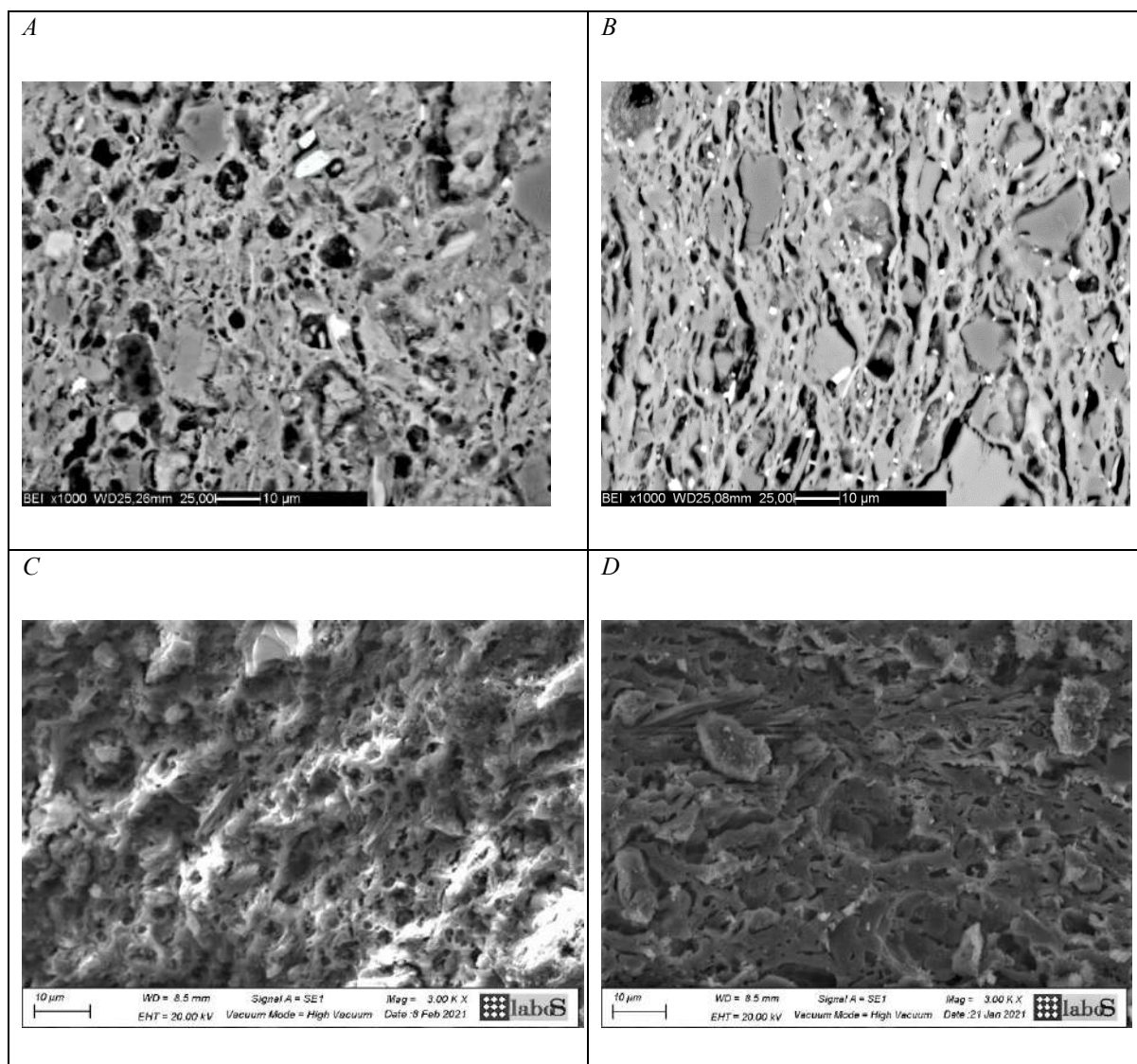


Figure 48: SEM images of polished thin sections and fractures of samples 2.4(A and C) and 2.9 (B and D).

A summary of the micro-structural features observed in the samples studied is provided in table 3.

Table 3: Summary of SEM- micro-structural features of the analysed samples. Reference made to matrix micro-structure; NV- Non-Vitrified, IV- Initial Vitrification and CV- Continuous Vitrification. Also note composition where; Low Calcareous (< 6%), Calcareous (> 6%) and High Calcareous (> 10%)

Pottery Class	Sample/Fabric	Matrix microstructure	Body Composition	Estimated Firing Temp
Ayla	1.3.2./2	IV	High Calc.	800- 850 °C
	1.4.2/1	IV	High. Calc.	800-850 °C
	1.5/1	IV	High Calc.	800-850° C
	1.7.1/2	NV/Sintering	High. Calc.	800°C

	1.7.2/1 3.6/2	IV CV	High Calc. High. Calc.	800-850 °C 850- 900° C
LRA1	1.9 2.3	NV NV	High. Calc. High Calc.	700-750 °C 700-750° C
Local	2.5 2.6 2.7 2.8 4.10 4.11	NV NV NV NV NV NV	Low Calc. Low Calc. Low Calc. Low Calc. Low Calc. Low Calc.	650-700 °C 650-700° C 650-700 °C 650-700 °C 800° C 800 °C
Torpedo	C02 C03 C06 C08	IV IV IV IV	High Calc. High Calc. High Calc. High Calc.	800-850° C 800-850 °C 800-850 °C 800-850 °C
<i>Dolia</i>	4.8 4.9	IV IV	High Calc. High Calc.	800-850 °C 800 -850°C
Red Slipped	4.6	NV	Low Calc.	600-750 °C
ND	2.9 2.4	CV IV	Calcareous High Calc.	850- 900° C 800-850°C

6.2.2. XRPD Phase Analysis

The interpretation of XRPD data of the samples belonging to Ayla-Aksum fabrics shows that the major phases present include quartz, K-feldspars, plagioclases, and clino-pyroxenes (Fig. 49). The presence of the diffraction peaks of muscovite/illite is also evident in some samples belonging to these fabrics in as much as the presence of calcite peaks in some samples. The information of mineralogy provided by XRPD is consistent with petrographic observations and SEM-EDX analysis.

The presence of the peaks of clino-pyroxenes, particularly begs a further discussion as to their nature and formation. The presence of clino-pyroxenes in the Ayla-Aksum amphorae as raw materials was observed from both petrography and SEM, since it is related to the occurrences of granitic rock suites and basaltic fragments in the raw materials. On the other hand, clino-pyroxenes are also formed during the firing process through reactions involving calcite and clay minerals. A reference can be made in these regards in light of the thermal stability of calcite and the framework of the formation of new phases (calcium-silico-alluminates). The absence of calcite reflections in the diffraction patterns of these amphorae classes suggests its intervened decomposition, while the presence of clino-pyroxenes peaks

suggests that these phases might also have formed at higher firing temperatures (i.e., 800-950 °C).

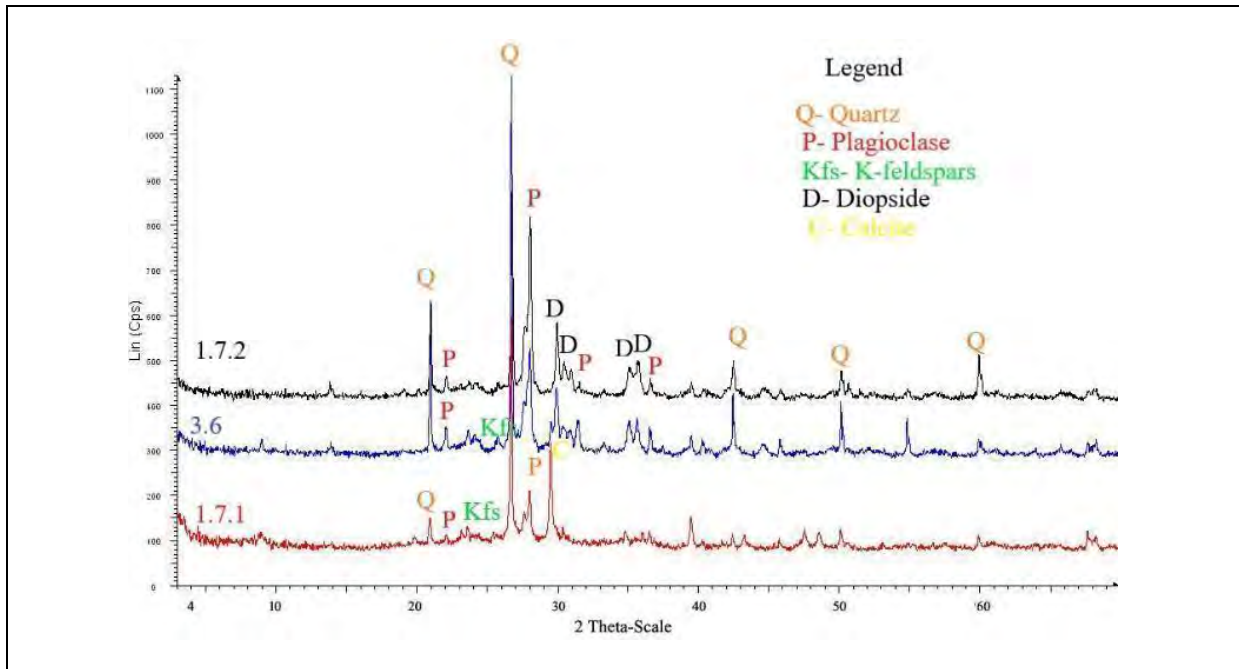


Figure 49: XRPD patterns of representative Ayla-Aksum amphorae.

However, some specimens (see, for example, Fig. 49, sample 1.7.1) show calcite as well as clino-pyroxenes reflections in their diffraction patterns: in these cases, petrographic observations revealed that the latter appear as inclusions in the raw materials, rather than neo-formations during firing. This trend is confirmed by SEM micro-structural observations, which show no indication of vitrification

The XRPD data information for the Late Roman Amphora 1 samples, on the other hand, indicate that the dominant calcite peaks distinguish these samples from the rest of the pottery classes considered in this study in addition to the peaks of quartz, K-feldspars and plagioclase (Fig. 50). In this respect, the calcite peaks complement the petrographic and SEM information that shell-rich tempers and spathic calcite dominate the fabrics. The presence of the peaks of calcite in the diffraction patterns of the LRA1 thus can be attributed to temperatures below the decomposition of calcite in the range between 600-800 °C. The trend can also be linked to the micro-structural and morphological features observed from SEM analysis.

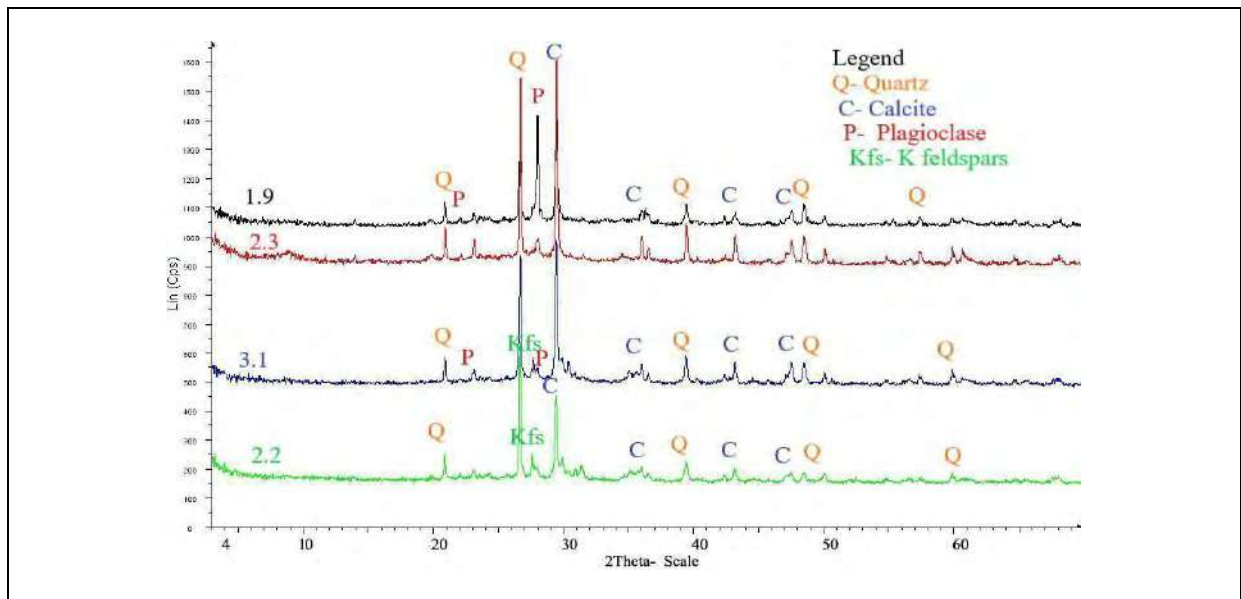


Figure 50: XRPD patterns of representative Late Roman Amphora 1.

The LRA1 assemblage, as explained in the literature (Reynolds 2014), represents wider production centres and the peculiarities observed in the diffraction patterns may suggest differences in the technology of production and or/raw material recipes. By considering the scarce XRPD studies so far performed on LRA1, the obtained outcomes add important information to the phase identification of this fabric.

Moreover, samples which were initially attributed to LRA1(?) and later securely identified as Torpedo jars (see chapters 5 and 7), show differences in the diffraction patterns in comparison to the LRA1 samples (Fig.51). The presence of phases such as diopside (a clino-pyroxene) together with calcite in these samples are indicative of a production at a relatively higher temperature compared to the LRA1 (Fig. 51). Petrographic information on the Torpedo jars shows contributions from basic to ultra-basic rocks and the presence of clino-pyroxenes as part of the clay raw materials and/or the coarser grain-size fraction is observed. Yet, the presence of diopside peaks in the diffraction patterns of these samples also pinpoint to new formations related to the eventual firing of the matrix. In this respect, clino-pyroxenes are present as inclusions and firing phases in these samples.

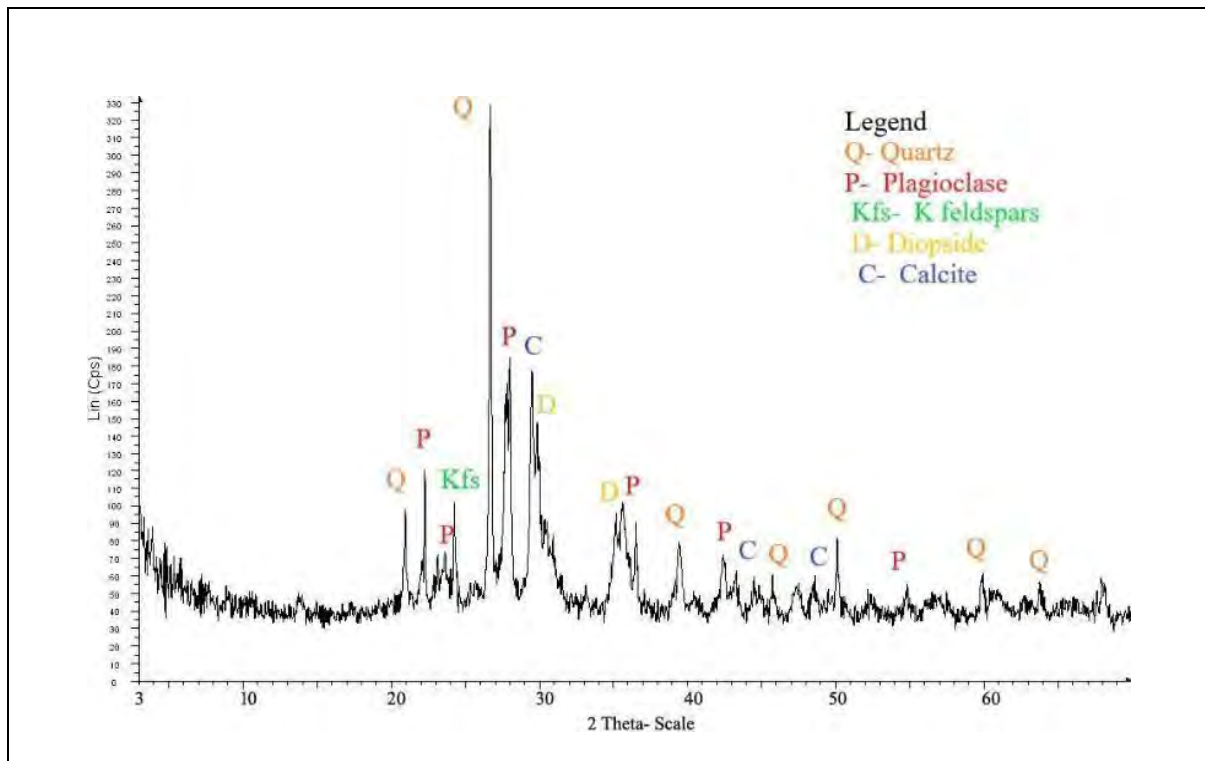


Figure 51: XRPD patterns of representative Torpedo jar Sample.

The presence of calcite peaks with clino-pyroxenes (diopside) in the diffraction patterns can be situated within the decomposition of calcite and formation of diopside in the range of 750-850/900 °C as explained in the literature (Gliozzo 2020). These phases thus can be attributed to onset of initial vitrification noted from the microstructures of the Torpedo jars observed under SEM.

Furthermore, the local pottery samples show distinct diffraction patterns in contrast to the rest of the pottery classes considered for XRD analysis. Quartz, K-feldspars and sodic to intermediate plagioclases constitute the major phases in these samples (Fig. 52). More importantly, the presence of systematic pronounced illite/muscovite peaks distinguish the diffraction patterns of the local pottery from the other classes. More importantly, the systematic presence of pronounced illite/muscovite peaks is typical of this class. All these features, coupled to the absence of high-temperature firing phases pinpoint to the adoption of rather lower firing temperatures for the local pottery class – namely in the 650-800 °C range (Gliozzo 2020).

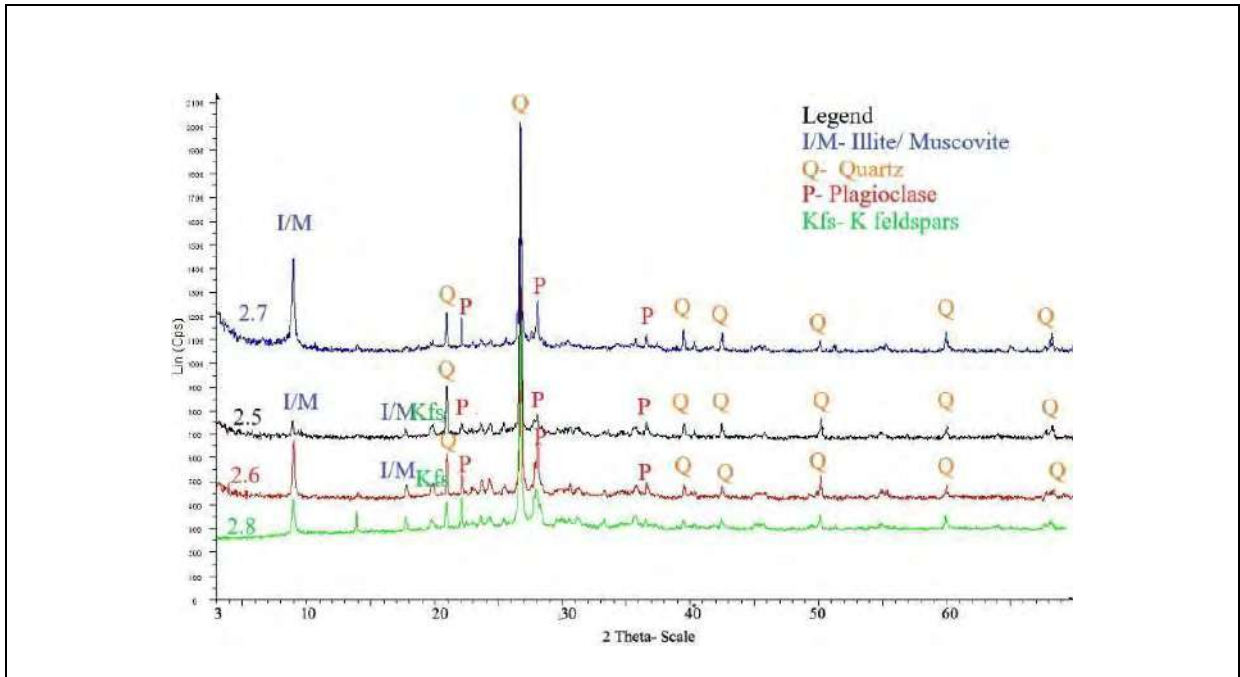


Figure 52: XRPD patterns of representative local pottery.

The XRPD analysis of 6 raw clay samples, potentially used to produce the local pottery, was also performed in order to possibly obtain information about the mineralogy of the precursor crystalline phases.

In this respect, the diffraction patterns of the oriented, glycolated and heat-treated (at 350°C and 500°C respectively) samples show that a mixture of chlorite and smectite clay minerals, together with a subordinate fraction of kaolinite, appear in the raw clay samples collected at Adulis (Fig. 53).

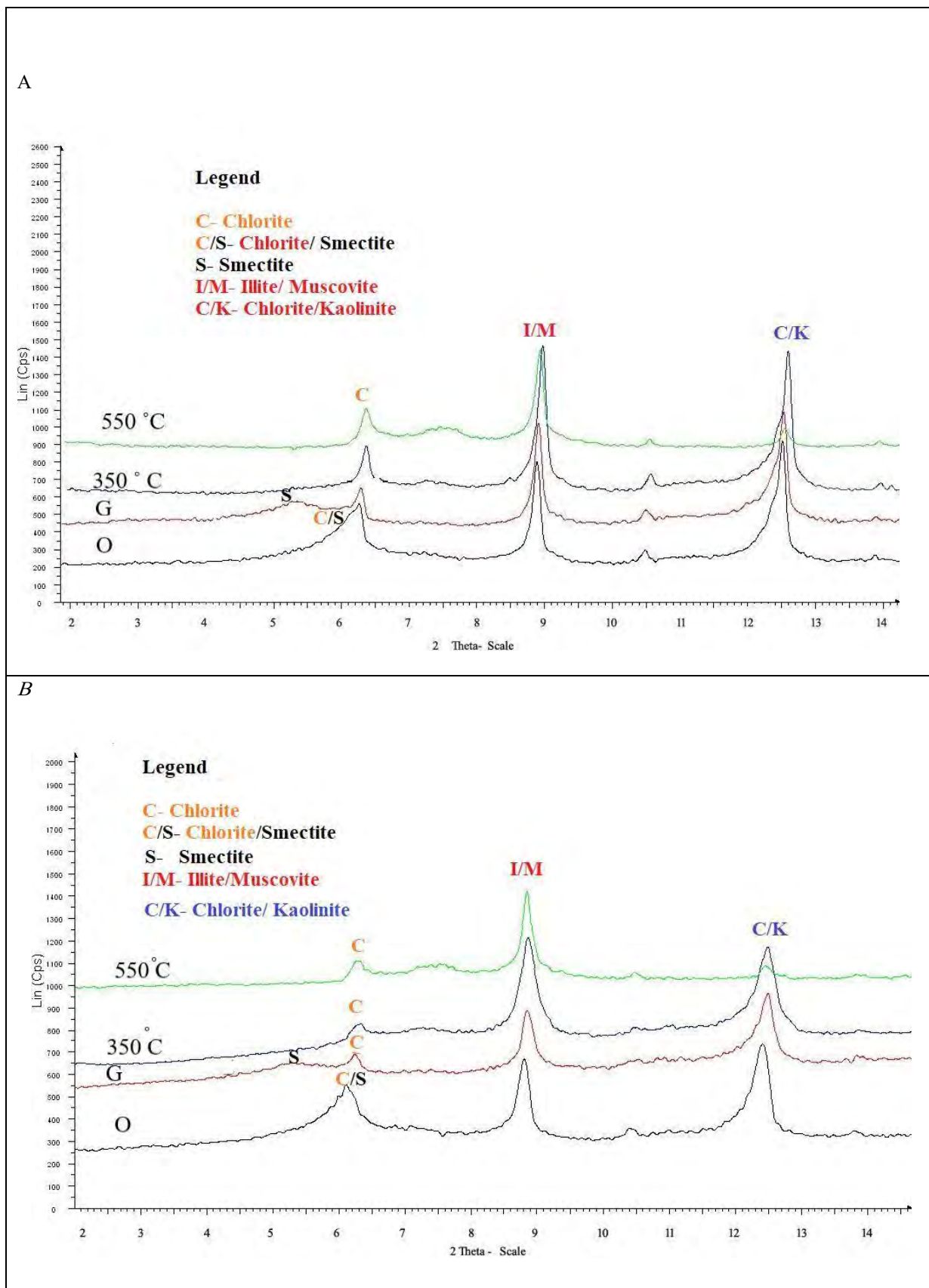


Figure 53: Diffraction patterns of representative clay samples.: note that the acquisition was stopped at 15° 2Theta, since it focused on the study of the clay mineral fraction. Abbreviations: O= oriented; G= glycolated.

In particular, the visible swelling (from H 6.3 to H 5.4 2θ degrees) that is evident in the diffraction patterns of the glycolated samples, indicate presence of a smectite group clay together with chlorite. Besides, the (only) incomplete disappearance of the peak at H 12.5 2θ degrees when heated at 550 °C indicates that this reflection can be related to kaolinite, and a minor contribution of chlorite. Moreover, the reflections of illite and/or muscovite are also visible. These XRPD outcomes, coupled with the petrographic and SEM micro-structural information, suggest that this kind of clays might have been used to produce the local pottery at Adulis.

The swelling pattern visible from the diffraction patterns of glycolated samples indicate the presence of a smectite group clays in the raw clay samples. Furthermore, a composite peak is an indication of a contribution from chlorite and a fraction of kaolinite clays. The peaks of illite/muscovite are also visible. The information from XRPD observations together with the petrographic and SEM micro-structural observations suggest that these clays could have been utilized to produce local pottery at Adulis. The different minerals or phases present in the samples considered for XRPD are summarized in table 4.

Table 4: List of main minerals/phases identified by XRPD. The estimated firing temperature is also provided based on literature (Gliozzo 2020; Xanthopoulou et al 2021). Abbreviations: K-fels= k-feldspars, pcls= plagioclases, cpx= clino-pyroxenes.

Class	Sample	Quartz	K-fels	pcls	Calcite	Cpx	Muscovite/biotite	Iron-oxide	EFT
Ayla	1.1	x	x	x		x			800-900°C
	1.2	x	x	x		x			800-900°C
	1.3.1	x	x	x		x			800-900°C
	1.3.2	x	x	x		x		x	800-900°C
	1.4.1	x	x	x		x		x	800-900°C
	1.4.2	x	x	x		x			800-900°C
	1.5	x	x	x		x			800-900°C
	1.6	x	x	x		x	x	x	800-900°C
	1.7.1	x	x	x	x	x		x	700-850°C
	1.7.2	x		x		x			800-900°C
	1.8	x	x	x		x		x	800-900°C
	2.0	x	x	x		x		x	800-900°C
	3.3	x	x	x		x			800-900°C
	3.4	x	x	x		x			800-900°C
	3.5	x	x	x		x		x	800-900°C
	3.6	x	x	x		x		x	800-900°C
	3.7	x	x	x		x			800-900°C

Class	Sample	Quartz	K-fels	pcls	Calcite	Cpx	Muscovite/biotite	Iron-oxide	EFT
	3.8	x	x	x		x		x	800-900°C
	3.8	x	x	x		x		x	800-900°C
	C01	x	x	x	x	x			700-850°C
	C04	x	x	x		x			800-900°C
	C05	x	x	x		x			800-900°C
LRA 1	1.9	x		x	x				700-850°C
	2.1	x		x	x				700-850°C
	2.2	x		x	x				700-850°C
	2.3	x		x	x				700-850°C
	3.0	x		x	x				700-850°C
	3.1	x		x	x	x			700-850°C
	3.2	x		x	x				700-850°C
LRA1 (?)	3.9	x	x	x	x	x			800-900°C
	C02	x		x	x	x			800-900°C
	C03	x		x	x	x			800-900°C
	C06	x		x	x	x			800-900°C
	C07	x	x	x	x	x			800-900°C
Local	2.5	x	x	x			x		650-800°C
	2.6	x	x	x			x		650-800°C
	2.7	x	x	x			x		650-800°C
	2.8	x	x	x			x		650-800°C
Bricks	4.10	x	x	x			x		650-800°C
	4.11	x	x	x			x		650-800°C
<i>Dolia</i>	1.0	x	x	x	x			x	700-850°C
	4.0	x	x	x	x			x	700-850°C
	4.8	x	x	x	x	x		x	800-900°C
	4.9	x	x	x	x			x	700-850°C
Red Slip	4.5	x	x	x			x	x	650-800°C
	4.6	x	x	x			x	x	650-800°C
ND	2.4	x	x	x	x	x	x	x	700-850°C
	2.9	x	x	x		x		x	800-950°C
	4.1	x	x	x		x			800-900°C
	4.3	x	x	x		x		x	800-900°C
	4.4	x	x	x	x	x			700-850°C

Moreover, cluster analysis of X-ray powder diffraction (XRPD) data was tested on datasets of the different classes of pottery, to explore the possibility of using this method for an automatic comparison of all the diffraction patterns. The interpretation and comparison of all collected diffraction patterns, in fact, allows the feasible comparison of the related scans, sorting them into potential classes of similarity. The application of this method to XRPD analysis of pottery is based upon the fact that mineralogical affinities between different samples might depend on many factors, mainly the raw materials used (mineralogical and

textural composition of the clay and any added temper) and the firing conditions (maximum firing temperature, firing atmosphere), if secondary phases are not formed after burial (Maritan *et al* 2015). The clustering is based on the position of the peaks in the diffraction patterns of all samples considered. The presence and absence of one or more phases as well as peaks of one or more minerals, therefore, can allow clustering. In this respect, the different fabrics identified in this study for all classes of pottery based on petrographic evaluation are suitable to see comparisons and are included in the information illustrated in the dendrogram (Fig. 54).

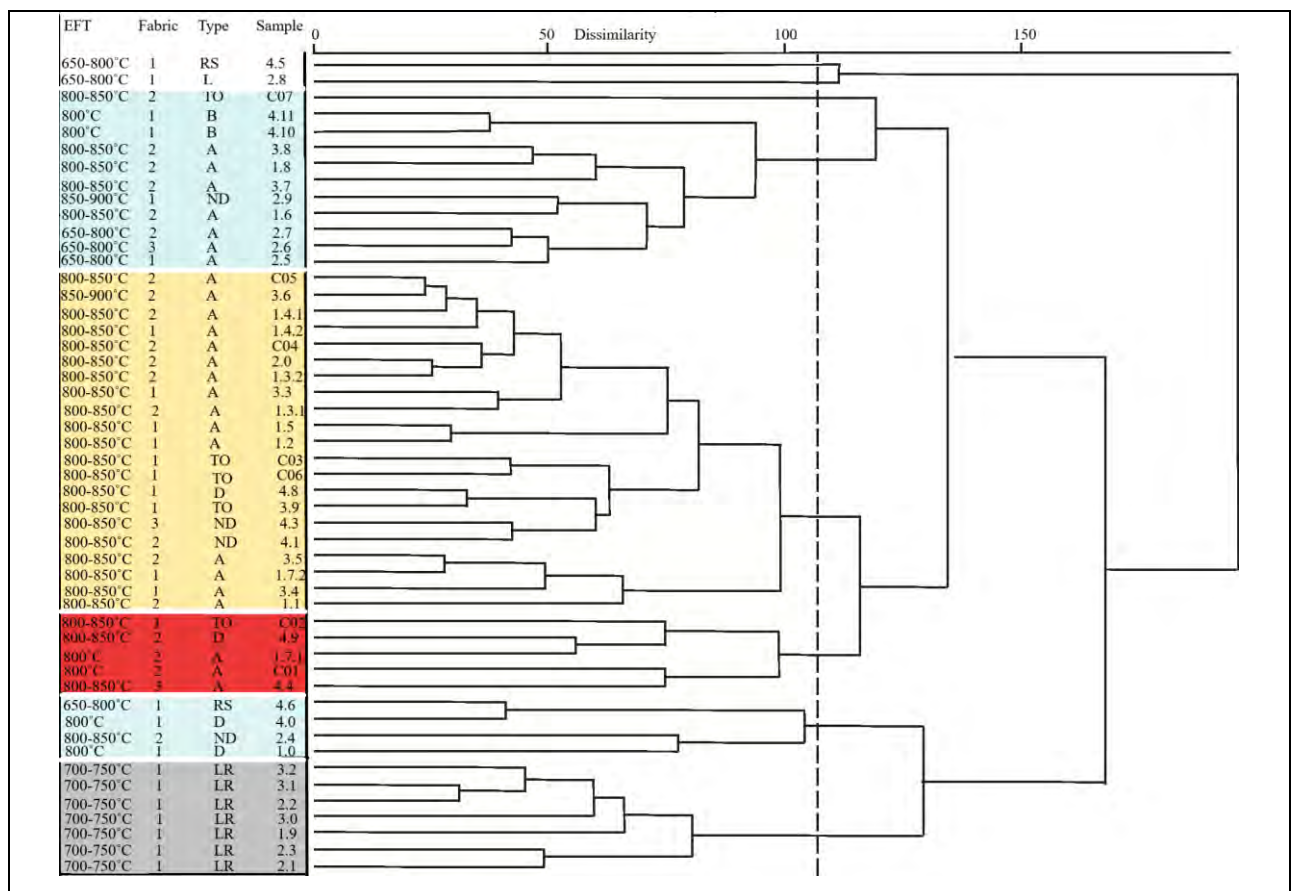


Figure 54: Dendrogram from cluster analysis of XRPD patterns according to Euclidean distance and average linkage method on position of peaks. Association to petro-fabrics is given based on observation under optical microscopy. Abbreviations: A= Ayla-Aksum, Fabric 1(granite- and /quartz-rich potsherds, bearing volcanic rocks), Fabric 2(granite- and feldspar-rich potsherds); L= Local pottery. Fabric 1(potsherds rich in fine-grained metamorphic rocks), Fabric 2(Granite-rich Petro-fabric), Fabric 3(potsherds rich in metamorphic rocks and sandstone); B= Bricks, Fabric 1(metamorphic rocks rich Petro-fabric); LR= Late Roman Amphora 1, Fabric 1(petro-fabric rich in limestone and bio-clasts); TO= Torpedo jars, Fabric 1(limestone and volcanic rocks rich potsherds), Fabric 2(potsherds rich in volcanic rocks and bearing metamorphic rocks); D= dolia, Fabric 1(Argillaceous Rock Fragments (ARFs) petro-fabric), Fabric 2(carbonates petro-fabric); RS=red slipped ware; ND= Undetermined, Fabric 1(quartz/ felsic rocks petro-fabric), Fabric 2(limestone dominated Petro-fabric) and Fabric 3(quartz and feldspars-dominated fabric).

Similarly, the Estimated Firing Temperatures (EFT) is provided in the dendrograms considering the information from the diffraction patterns of all samples studied and the SEM observations of the micro-structural and morphological features of representative samples for all the fabrics. The dendrogram in Fig. 54 shows that the LRA1 samples which belong to a single petro-fabric rich in limestone and bioclasts, are grouped in a single cluster mainly due to the presence of dominant calcite peaks from XRPD analysis. It can be said from these observations and the information provided from SEM evaluation of their non-vitrified matrices as well as the changes seen in the morphology of mollusc shells, that the EFT for the LRA 1 can be established in the range of 700-750 °C, highlighting similarities in the raw materials used and the firing regimes employed.

On the other hand, the samples which were initially identified as LRA1(?) from macroscopic observations but later ascribed to the Torpedo jars (see chapters 5 and 7) show variations in clustering mainly due to absence / presence of one or more crystalline phases present and owing to variations in fabrics (limestone/volcanic rocks petro-fabric and volcanic/metamorphic rocks dominated petro-fabric respectively) rather than implying different regimes of firing. Moreover, they show differences in their diffraction patterns in comparison to the well-defined LRA1 fabrics. Observations of polished thin-sections and fractures have revealed presence of microstructures that suggest the onset of vitrification structures. This evidence coupled to the diffraction patterns that reveal the contextual presence of calcite and diopside, suggest temperatures in the 800-850° C range. It should also be noted that the clustering of these samples with fabrics belonging to the Ayla-Aksum amphora and *dolia* samples pinpoint to the onset of the phases of clino-pyroxenes as result of firing temperatures high enough to attain vitrification structures in all these classes.

Similarly, the samples of the Ayla- Aksum amphorae group into clusters owing to certain variability in the petro-fabrics as well as the presence/absence of selected minerals in the XRPD patterns. All the samples that belong to the granitic/volcanic rock petro-fabric 1 of the Ayla -Aksum amphorae (Fig. 54) are clustered together with most of those belonging to the granitic dominated petro-fabric 2. However, some samples belonging to the latter fabric tend to plot in different clusters, thus highlighting fabric variability on one hand and absence/presence of some mineral XRPD reflections. SEM observations prove that differences exist in micro-structures and morphological features. In this respect, indications of new formations which result from the interaction of calcium oxides with quartz, feldspars, and accessory minerals coupled with the development of initial vitrification phases are noted for most of the

studied Ayla- Aksum samples under SEM. It can be said, thus, a temperature gradient It can be said, thus, a temperature gradient of $\approx 800-900$ °C can be suggested for the Ayla-Aksum samples that reveal the presence of clino-pyroxenes(diopside) as firing phases and the onset of initial and continuous vitrification structures observed from SEM observations. The variations in light of the microstructures seen in sample 3.6 in contrast to samples 1.3.2, 1.4.2, 1.5 and 1.7.2 demonstrate the slight variations in firing temperatures despite the grouping in similar clusters. However, in those samples where visible indications of vitrification are lacking (e.g., sample 1.7.1), the estimation of temperature gradient can be narrowed to ≤ 800 °C. In summary, the XRD patterns of the Ayla-Aksum amphorae samples attest for the mineralogical composition observed by optical microscopy in as much as SEM-EDX comprehension of the reaction phases and micro-structural features formed through original firing.

The local pottery which represents a different production in comparison to the rest of the imported classes, show variability in terms of petro-fabrics as demonstrated from optical microscopy owing to the use of different recipes of raw materials from the same basin/s and yet their diffraction patterns demonstrate similarities particularly and are clustered together due to the presence of prominent peaks of illite/muscovite and the indication of similar minerals present. This observation together with the SEM studies suggest an Equivalent Firing Temperature in the range of 650-800 °C.

The XRPD patterns for the *dolia* samples are also in agreement with variations seen in the fabrics (ARFs dominated petro-fabric and carbonates-dominated petro-fabric respectively). The attribution of the firing temperatures for the *dolia* samples, similarly confirms an estimated temperature of 800-850° C can be established for the samples. On the other hand, the indications of the diffraction patterns and micro-structural features of the Red slipped wares attest to a rather lower firing temperature in the range of 650-800 °C.

Finally, the information inferred by the diffraction patterns and micro-structural features of those samples belonging to undetermined typology are consistent with the related variability observed in the petro-fabrics and thus their consequent grouping in different clusters.

6.3. Archaeological Implications

In conclusion, micro-structural and mineralogical studies by SEM-EDX and XRPD performed on the different classes of pottery recovered from Adulis show differences in

production technology in terms of micro-structural features and mineralogical (both original and firing) phases. These differences further corroborate the information from the petrographic and chemical analyses described and commented in the previous chapter.

From an archaeological point of view, the differences in the technology of production between Ayla-Aksum amphorae and local pottery are particularly important to further refute any hypothesis of local production of Ayla-Aksum amphorae at Adulis. The observation complements the information on the provenance of the amphorae.

For the local pottery, for which no kilns have been identified yet, the information obtained from the present study can provide a comparative parallel for future studies. A detailed study of the evolution of local production at Adulis across the different phases of occupation, however, needs to be tackled in a more systematic approach in the future. The study, in general, has enabled to broaden the knowledge of local production and imported pottery at Adulis, where inter-regional trade exchanges became elaborated by the 5th-7th CE, as discerned from excavated contexts in the site.

The differences in the technology of production visible between the Late Roman Amphora 1 and those which were initially identified as LRA1(?) due to superficial similarities is equally important to establish secure typological classification. The latter classes have been securely attributed to Torpedo jars, thanks to the coupling of petrographic, chemical studies and organic residues analysis. The organic residue analysis particularly allowed the characterization of the resinous lining present in these samples and the next chapter discusses the data obtained from the analysis to complement the argument on the provenance and technology of production of these specific vessels.

6.4. Bibliography

Chatfield M. (2010). Tracing firing technology through clay properties in Cuzco, Peru, *Journal of Archaeological Science*, Volume 37, Issue 4, <https://doi.org/10.1016/j.jas.2009.11.003>.

Gliozzo E. (2020). Ceramic technology. How to reconstruct the firing process. *Archaeol Anthropol Sci* 12, 260. <https://doi.org/10.1007/s12520-020-01133-y>

Maritan L, Mazzoli C, Freestone I C. (2007) Modelling changes in mollusc shell internal micro-structure during firing: implication for temperature estimate in shell-bearing pottery. *Archaeometry* 49:529–541. <https://doi.org/10.1111/j.1475-4754.2007.00318.x>.

Maritan L, Holakooei P, Mazzoli C. (2015). Cluster analysis of XRPD data in ancient ceramics: What for? *Applied Clay Science*, Volume 114, pp. 540-549. <https://doi.org/10.1016/j.clay.2015.07.016>.

Mentesana R, Kilikoglou V, Todaro, S V, & Day, P M. (2019). Reconstructing change in firing technology during the Final Neolithic–Early Bronze Age transition in Phaistos, Crete. Just the tip of the iceberg? *Archaeological and Anthropological Sciences*, 11, 871-894. <https://doi.org/10.1007/s12520-017-0572-8>.

Pérez-Monserrat EM, Maritan L, Cultrone G. (forthcoming) Firing and post-firing dynamics of Mg- and Ca-rich bricks shaping the built heritage of Padua (North-eastern Italy). *European Journal of Mineralogy*, forthcoming.

Tite MS, Maniatis Y. (1981) Technological examination of Neolithic-Bronze Age pottery from central and southeast Europe and from the Near East, *Journal of Archaeological Science*, Volume 8, Issue 1. pp. 59-76. <https://doi.org/10.1038/257122a0>.

Xanthopoulou V, Iliopoulos I, Liritzis I. (2021) Mineralogical and Microstructure Analysis for Characterization and Provenance of Ceramic Artifacts from Late Helladic Kastrouli Settlement, Delphi (Central Greece). *Geosciences*, 11,36. <https://doi.org/10.3390/geosciences11010036>

7· Organic Residue Analysis

Abstract




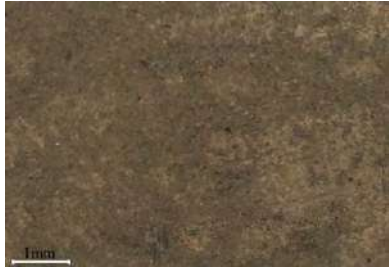
Transport vessels were coated by resinous and/or bituminous materials in antiquity to make them suitable to transport different liquids and/or food. In this respect, the characterisation of coating materials on ceramics has allowed to shed light on the function of different classes of transport vessels found from sites in the Indian ocean and Red Sea worlds. The characterisation of the organic residues on a set of samples identified from macroscopic examination as LRA1(?) by FT-IR and GC-MS is discussed in this chapter. The characterisation of the residues has allowed to securely establish the typological classification of these samples within the wider class of the so-called ‘Torpedo jars, posing complexity in terms of provenance attribution. The study, therefore, allowed to broaden the scope of the distribution of the Torpedo jars to Adulis beyond solving the question of typological complexity posed from a macroscopic point of view.




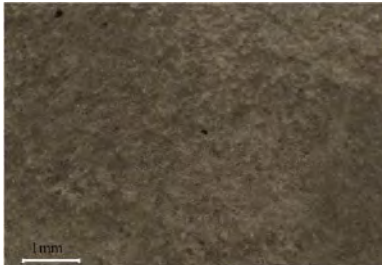



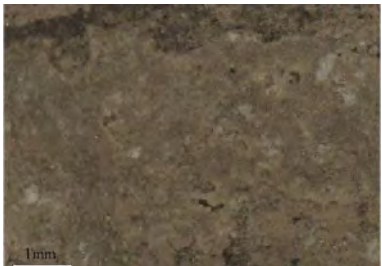
7.1. Materials and Methods

7.1.1. Sampling

The analyzed samples are listed in table 5.

Table 5: List of the analysed archaeological samples

ID Code	Year (of sampling)	Image of Fragments	Stereo-Microscopy Images
C02	2019		
C03	2019		

C06	2019		
C07	2020		
C08	2020		
C09	2020		

7.1.2. Analytical Methods

In order to have a preliminary view on the chemical composition of these residues, FTIR was employed on extracts obtained with solvents of various polarities. Then a GC-MS insight was performed, to shed more light on the composition.

7.1.2. 1. Fourier Transform-InfraRed (FT-IR)

Powdered samples were collected from the ceramic fragments and subdivided into three subsamples of 0.1 mg each. Each subsample was extracted with 2 mL of one the following

solvents: acetone, methanol, and dichloromethane, to leach specific classes of substances. The supernatant was transferred and left to dry in a fume hood. The resulting deposits were collected, set in a diamond anvil cell and analysed in transmission mode using a Vertex 70 FT-IR benchtop spectrometer by Bruker, equipped with an Hyperion3000 Microscope. Spectra were collected in the range from 4000 cm^{-1} to 400 cm^{-1} , with a resolution of 4 cm^{-1} and 64 scan acquisitions. The instrument was available by the Centro di Conservazione e restauro “la Venaria Reale”.

7.1.2.2. Gas Chromatography-Mass Spectrometry (GC-MS)

About 10 mg of each sample were treated with 1 mL of n-hexane, dichloromethane, and methanol (80:15:5) in MLS-1200 MEGA microwave extractor by Milestone FKV (Soriso, Italy) for 5 minutes at 500 W and 60°C . The extract was centrifuged at 2000 rpm for 5 minutes and the supernatant was dried under a nitrogen flow. $300\ \mu\text{L}$ of n-hexane were added and the solution was sonicated for 10 minutes at 40°C ; the extraction with n-hexane was repeated 3 times and the supernatant from each of the three steps was collected in a vial and subjected to GC-MS with a 6809N-Network GC gas-chromatographic system with a PTV injector and coupled with a 5975 Agilent Technologies (Palo Alto, CA) single quadrupole mass spectrometer. The PTV injector was used in splitless mode at 280°C . The chromatographic separation was performed on a HP-5MS (5% Diphenyl / 95% Dimethylpolysiloxane, Inner Diameter: 0.25mm, Length: 30m, Film: 0.25m, J&W Scientific Agilent Technologies, Palo Alto, CA) capillary column, coupled with a deactivated fused silica guard column (Inner Diameter: 0.32 mm, Length: 2 m, J&W Scientific Agilent Technologies, Palo Alto, CA). The chromatographic oven was set with the following temperature program: initial temperature 80°C for 2 minutes, a first ramp rate of $20^{\circ}\text{C}/\text{min}$ up to 200°C , 200°C for 1 minute, a second ramp rate of $4^{\circ}\text{C}/\text{min}$ up to 300°C , 300°C for 60 minutes. The mass spectrometer ionization source was set at 230°C , the quadrupole was kept at 150°C . The mass spectrometer was used in the EI mode (70 eV), acquiring in the range 50-700 m/z (Nardella *et al* 2020).

After conditioning the column with 1 mL of n-hexane, the sample was loaded in the column and then it was eluted with 3 mL of a n-hexane-dichloromethane mixture (1:1 in volume). The collected hydrocarbon fraction was dried under a nitrogen flow and then added with $50\ \mu\text{L}$ of isooctane (Nardella *et al* 2020). The GC-MS investigation was performed by the SCIENCE for Cultural Heritage (SCICH) team at the University of Pisa.

7.2. Results and Discussion

7.2.1. FT-IR Analysis

Analysis of all the extracts from the samples showed clear evidence of the presence of resins in the pottery fragments. The analysis showed bands in the FT-IR spectra that clearly arise from organic components (Fig.53). The acquired spectra for extracts from samples C08 and C09 exhibit absorptions at 2925 and 2854 cm^{-1} , respectively due to asymmetric CH_3/CH_2 and symmetric CH_3 stretching, and at 1702/1705/1713 cm^{-1} , due to the $\text{C}=\text{O}$ stretching of the resinous acids, suggesting the presence of a natural resin. Further characteristic sharp, moderately strong peaks are produced by the CH bending vibrations at 1455 cm^{-1} (CH_3/CH_2 groups) and 1380 cm^{-1} (CH_3 group). On the other hand, the spectra of samples C03, C06 and C07 show absorptions at 2926 and 2856/2855/2856 cm^{-1} (asymmetric CH_3/CH_2 and symmetric CH_3 stretching) and 1459/1457/1453 cm^{-1} (C-H bending of methyl and methylene groups). Some of the sample spectra exhibited the presence of the signals associated with natural resins, as reported in table 6. A distinction between partially degraded natural resins and heavily deteriorated ones is discerned from the FT-IR analysis. Spectra corresponding to heavily deteriorated resins are recorded for the extracts from samples C03, C06 and C07(Fig. 55) while the FT-IR spectra recorded for the extracts from samples C08 and C09 presumably relate to aged natural resins.

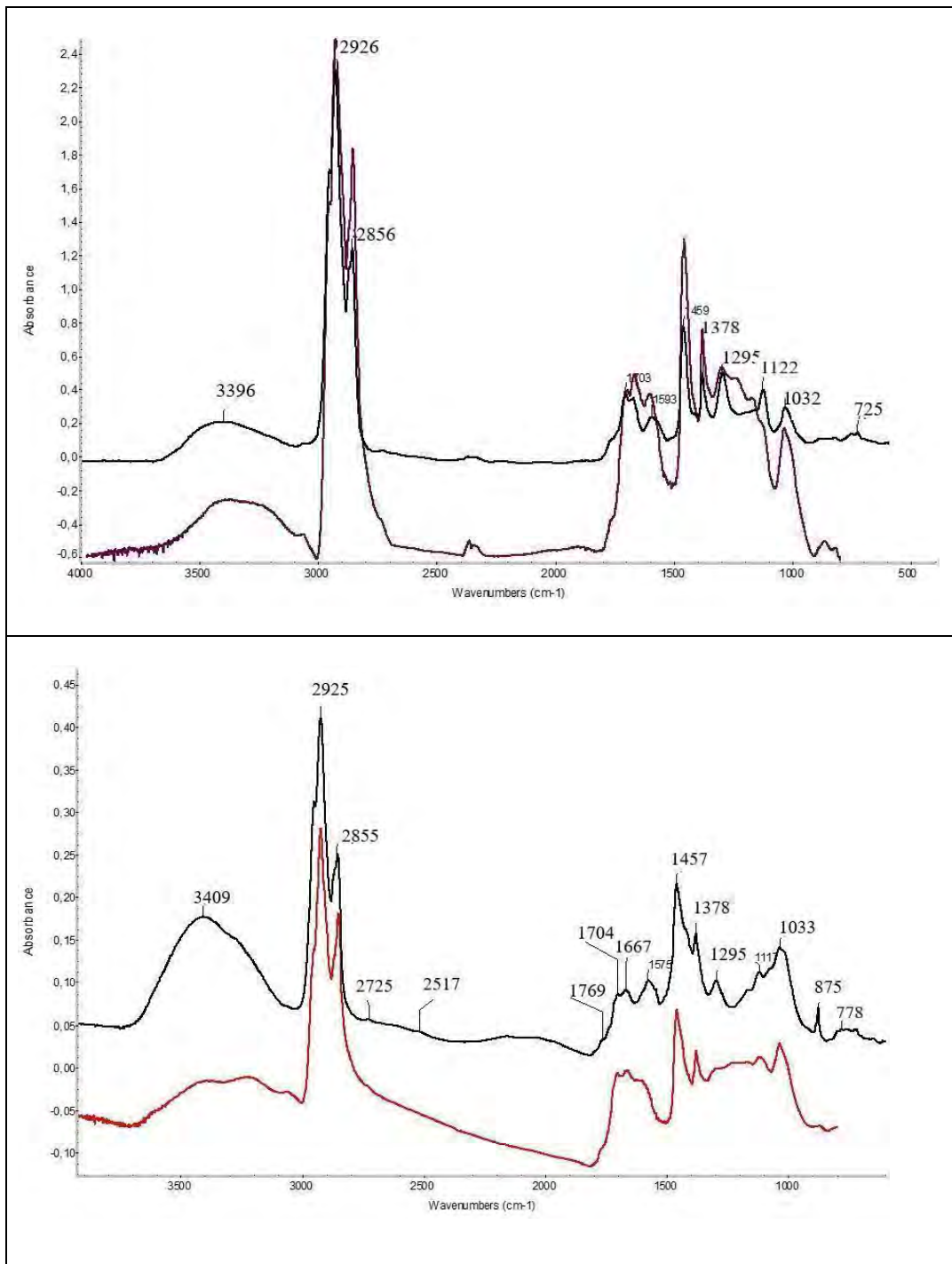


Figure 55: FT-IR Spectra of resinous materials: heavily deteriorated resins; C03 extract in methanol, in black the spectrum of the extract and in violet the spectrum of the reference resin material (top); C07 extract in methanol, in black the spectrum of the extract and in red is the spectrum of the reference material(bottom)

The presence of natural resins is, therefore, highlighted further pinpointing the information from FT-IR needs to be complemented by GC-MS for the proper identification of the resinous materials.

Table 6: Summary of FT-IR spectra for resinous materials

Sample No.	Extracts from	Bands	Origin of bands
C03	Methanol	2926 2856 1459 1378 1032	Asymmetric Stretching of CH ₃ /CH ₂ Symmetric stretching of CH ₃ C-H bending of CH ₂ , organic Bending of C, stretching of H of CH ₃ Stretching of C=O
C06	Methanol	2925 2854 1602 1454	Asymmetric Stretching of CH ₃ /CH ₂ Symmetric stretching of CH ₃ Stretching of C=C C-H bending of CH ₂ , organic
C07	Acetone	2925 2855 1598 1455	Asymmetric Stretching of CH ₃ /CH ₂ Symmetric stretching of CH ₃ Stretching of C=C C-H bending of CH ₂ , organic
C07	Methanol	2925 2855 1573 1457 1033	Asymmetric Stretching of CH ₃ /CH ₂ Symmetric stretching of CH ₃ C-H bending of CH ₂ , organic Bending of C, stretching of H of CH ₃ Stretching of C=O
C07	Dichloromethane	2925 2855 1573 1457 1023	Asymmetric Stretching of CH ₃ /CH ₂ Symmetric stretching of CH ₃ C-H bending of CH ₂ , organic Bending of C, stretching of H of CH ₃ Stretching of C=O
C08	Acetone	2925 2854 1702 1458 1374	Asymmetric Stretching of CH ₃ /CH ₂ Symmetric stretching of CH ₃ Stretching of C=O C-H bending of methyl and methylene groups C-H bending of methyl groups
C08	Dichloromethane	2925 2855 1667 1456 1378	Asymmetric Stretching of CH ₃ /CH ₂ Symmetric stretching of CH ₃ Stretching vibration of C=C C-H bending of methyl and methylene groups C-H bending of methyl groups
C09	Acetone	2925 2854 1704 1668 1453 1375 1032	Asymmetric Stretching of CH ₃ /CH ₂ Symmetric stretching of CH ₃ Stretching of C=O Stretching vibration of C=C C-H bending of methyl and methylene groups C-H bending of methyl groups C-O vibrations

Sample No.	Extracts from	Bands	Origin of bands
C09	Methanol	2925 2854 1598 1455	Symmetric Stretching of CH ₃ Symmetric stretching of CH ₃ Stretching of C=C C-H bending of CH ₂ , organic
C09	Dichloromethane	2925 2854 1713 1455 1378	Asymmetric Stretching of CH ₃ /CH ₂ Symmetric stretching of CH ₃ Stretching of C=O C-H bending of methyl and methylene groups C-H bending of methyl groups

7.2.2. GC-MS

The chromatographic profile obtained from the analysis of all the archaeological samples is typical of a bituminous material (Fig. 56), attested from the presence of the terpane compounds including the hopane and homo-hopane series (H28-H35). The most abundant peaks, identified in the extracted ion *m/z* 191 chromatograms by the examination of their mass spectra (Nardella *et al* 2019; Lischi *et al* 2020; Armonius *et al* 2020) are ascribable to H29 (17 α (H),21 β (H)-30-norhopane) and to H30 (17 α (H),21 β (H)-30-hopane), both belonging to the hopane class. In sample C06 a tricyclic terpane (TR23), a tetracyclic terpane (TET24) and the unsaturated forms of many homo-hopanes (H32-H35) were detected as minor components.

Table 7: List of the detected compounds in the bitumen samples

Identified compound		
<i>Tricyclic terpanes</i>		
1	TR23	tricyclic terpane C 23
<i>Tetracyclic terpanes</i>		
2	TET24	tetracyclic terpane C24
<i>Trisnorhopanes</i>		
3	Ts	18 α (H),21 β (H)-22,29,30-Trisnorhopane
4	Tm	17 α (H),18 α (H),21 β (H)-22,29,30-Trisnorhopane
<i>Bisnorhopanes</i>		
5	H28	17 α (H),18 α (H),21 β (H)-28,30-Bisnorhopane
<i>Norhopanes</i>		
6	H29	17 α (H),21 β (H)-30-Norhopane
7	M29	17 β (H),21 α (H)-30-Norhopane

<i>Hopanes</i>		
8	H30	17 α (H),21 β (H)-Hopane
9	M30	17 β (H),21 α (H)-Hopane
<i>Homohopanes</i>		
10	H31S	22S-30-Homohopane
11	H31R	22R-30-Homohopane
<i>Gammacerane</i>		
12	GAM	Gammacerane
<i>Bishomohopanes</i>		
13	H32S	22S-30,31-Bishomohopane
14	H32R	22R-30,31-Bishomohopane
<i>Trishomohopanes</i>		
15	H33S	22S-17 α (H),21 β (H)-30,31,32-Trishomohopane
16	H33R	22R-17 α (H),21 β (H)-30,31,32-Trishomohopane
<i>Tetrakishomohopanes</i>		
17	H34S	22S-17 α (H),21 β (H)-30,31,32,33-Tetrakishomohopane
18	H34R	22R-17 α (H),21 β (H)-30,31,32,33-Tetrakishomohopane
<i>Pentakishomohopanes</i>		
19	H35S	22S-17 α (H),21 β (H)-30,31,32,33,34-Pentakishomohopane
20	H35R	22R-17 α (H),21 β (H)-30,31,32,33,34-Pentakishomohopane

Only in sample C02 gammacerane (GAM) was not identified. Steranes (m/z 253, 217, 231) are absent in all the samples. The relative percent distribution of the detected compounds is illustrated in Figure 57 while the detected compounds are listed in table 7. The identification of a bituminous substance in all the samples studied allows us to significantly identify the samples which were initially attributed to LRA 1(?) as torpedo jars. The typological complexity posed due to superficial similarities with the LRA1 is, thus, resolved by the coupling of the information from organic residue analysis to petro-mineralogical and chemical data. The identification of bituminous materials in these samples in contrast to pitch, which is often found as a coating material in Late Roman Amphora thus, reinforces the attribution to Torpedo jars for samples C02, C03, C06, C07, C08 and C09.

Comparisons of the chromatographic profile obtained for the samples from Adulis to other similar studies on Torpedo jars (from Shaghab, Siniz, Mahroyan, Siraf, Rig Port along the coast of Iran, Sir Bani Yas in Abu Dhabi, UAE, Anuradhapura in Sri Lanka, Alagankulam in southern India, Al Hamr al-Sharqiya in Oman as well as from the shipwreck of Phanom-

Surin in Thailand) show similarities to a greater extent to indicate similar bituminous material present in torpedo jars production (Fig.56).

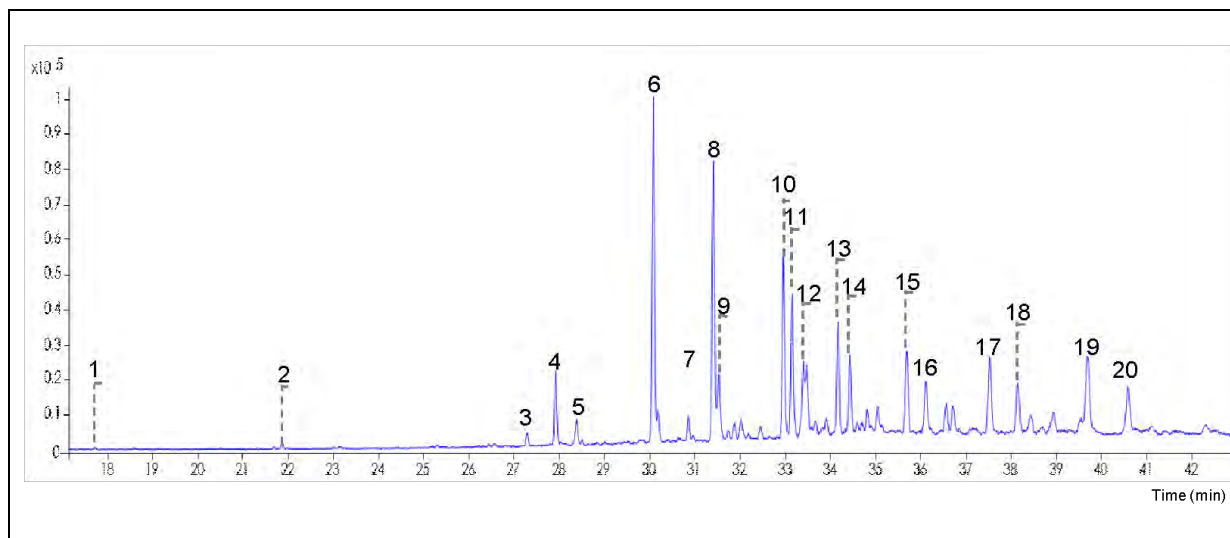


Figure 56: Sample C06 extracted ion (m/z 191) chromatogram.

Yet, the absence of steranes in the samples from Adulis can be marked as the difference in comparison to the chromatographic profiles obtained by the studies from elsewhere. On the other hand, recent archaeometric research on torpedo jars have attempted to correlate GC-MS profiles of archaeological samples to reference bitumen from Judea and Babylonia areas as well as those from the Dead Sea and Hit Abu Jir in Iraq (Fig. 58). It is well-known that bitumen was used from the Palaeolithic or early Neolithic periods for several purposes. Long distance commercial networks were eventually established to provide different settlements with bitumen, where the bitumen trade expanded in the Middle- Bronze Age and continued until the Early Islamic period and beyond (Connan 1999; Van del Velde 2015). The presumed production of the Torpedo jars in Mesopotamia from the characterisation of the bitumen, falls within the later periods of the elaboration of trade in bitumen in antiquity.

Bitumen sources from Mesopotamia, Iran and the Dead Sea have been widely discussed in the literature, where different sites across the Persian Gulf, Indian Ocean and the Mediterranean were included in the long-distance trade of the material. It is known that settlements under Mesopotamian influence used exclusively bitumen from Hit in Iraq while bitumen sources in northern Iraq and Iran supplied other settlements (Van del Velde 2015; Lischi *et al* 2020). Moreover, it is mentioned that bitumen from Iran played a bigger role in the Gulf from starting from the second half of the first millennium BCE, as is attested from settlements in Southeast Arabia, the Oman coast and as far as across the Indian Ocean at Anuradhapura in Sri Lanka (Stern *et al* 2008). While bitumen from Mesopotamia and Iran

were widespread across the Near East, many sites in the Eastern Mediterranean were provided with bitumen from the Dead Sea (Spiro *et al* 1983; Van del Velde 2015). Therefore, the reconstruction of bitumen trade in antiquity is framed within the framework of comparing the biomarkers (GC-MS profiles, chemical compositions, source of the bitumen rocks) of these known sources.

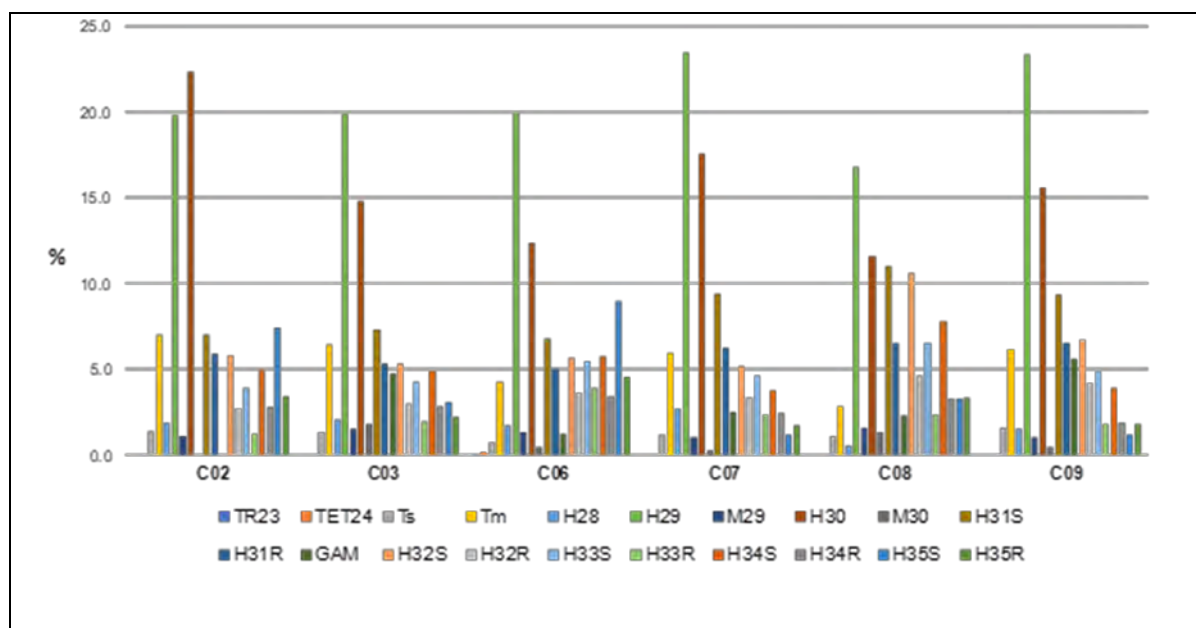


Figure 57: Relative percent distribution of the detected compounds in the samples analyzed by GC/MS

Archaeometric work on torpedo jar samples from the third to the ninth century levels at Anuradhapura (Sri Lanka) indicated that the source of most of the bitumen could be in the region within the vicinity of Dehluran and Susa in southern Ilam or northeast Khuzestan in Iran (Stern *et al* 2008). Similarly, a recent publication by Connan *et al* (2020) on fabric belonging to TORP-S and TORP-C fragments from Phanom-Surin wreck has attributed the source of the bitumen from a set of deposits near Dehluran and Khuzestan (Connan *et al* 2020). Furthermore, the analysis of two sets of torpedo jars from Alagankulam in southern India and the site of Al Hamr al-Sharqiya1 in Oman by Lischi *et al* (2020) has attested to sources in Iraq. The comparison of the profiles obtained for the torpedo jars recovered from Adulis to reported reference material highlighted similarities with bitumen sources from the Babylonia area to perhaps indicate source in Mesopotamia (Fig. 58d). It should be noted, however, that it remains unclear whether torpedo jars were manufactured in the same location in which the bitumen was obtained, or if the vessels were later lined after being fired with a bituminous material imported from elsewhere (Tomber *et al* 2020). Such a phenomena leaves

open the comparison of the archaeometric study of the clay paste and the source of the bitumen for approaching the provenance of the vessels. Similarities in composition between the LRA1 and the samples identified as torpedo jars (from the characterization of residues) are attested from geo-chemical data in this study, further indicating perhaps production areas exploiting materials from similar geological basins that extend wider geographical areas from Eastern Mediterranean to Mesopotamia. In fact, it has been argued that two main geological features namely, the Tigris-Euphrates basin of Iraq (Mesopotamia) and the continuous mountain range stretching from Troodos, Cyprus to Semail, Oman dominate the area where Torpedo jars are most likely to originate (Tomber *et al* 2020). It is, therefore, plausible that similarities in geo-chemical patterns can be linked to these explanations. On the other hand, the possibilities of the transport of solid bitumen to production centres elsewhere from Mesopotamia cannot be ruled out, to pinpoint multiple production for the vessels.

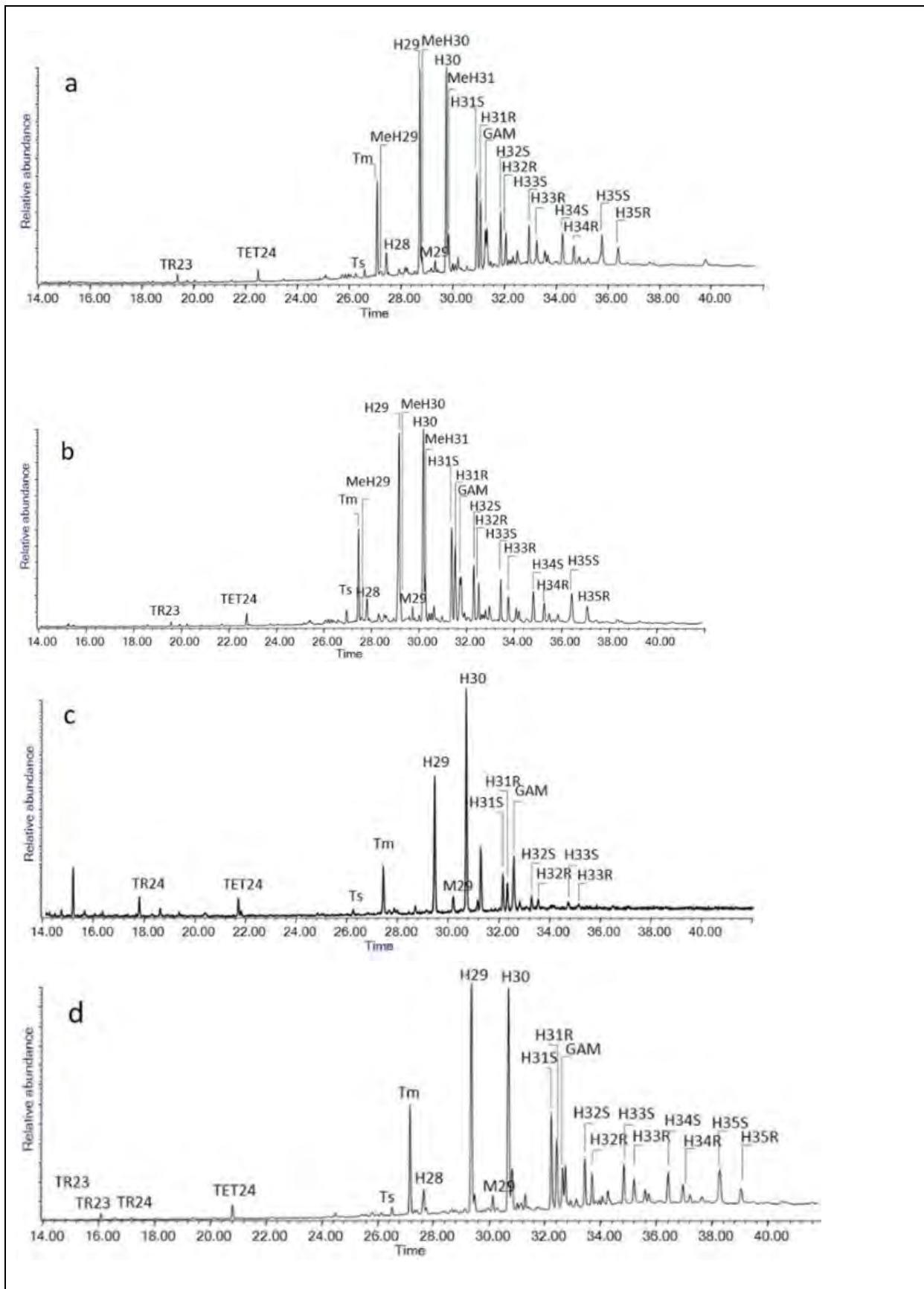


Figure 58: Extracted ion chromatograms (m/z 191) of the sample extracts (Lischi et al 2020). Examples show AGM11 from India(a), Oman (b), Judea(c) and Babylonia(d).

7.3. Archaeological Implications

The study of the organic residues found on samples which were initially attributed to LRA 1(?) from macroscopic observations, represents the first evidence that situates Adulis within the framework of the distribution of transport vessels to the African shores of the Red Sea. The characterization of organic residues and the confirmation of bituminous substance in this study, significantly allowed to securely attribute the samples to the Torpedo jars. The results of the FT-IR and GC-MS studies, therefore, have broadened the themes revolving around the distribution of the Torpedo jars on the wider Indian Ocean and Red Sea Worlds.

The archaeometric results indicate that the trade connections in the Indian Ocean involved a very large area, including the Red Sea, East Africa, the Persian Gulf, Southern Arabia, and India. The scope of regional exchanges involving the Mediterranean, Red Sea and Indian Ocean Worlds encompassed multiple routes (Lischi *et al* 2020) and the western route going from Oman to the Red Sea, in the direction of the Mediterranean Sea could have contributed to the distribution of transport vessels from the Indian Ocean the Eritrean Coast. The extent of these contacts is further attested by the expansion of the Sassanian trade into the Red Sea by late antiquity. By the chemical characterization of the coating found in the pottery fragments, the already well attested role played by Adulis in the trading in aromatics, textiles, spices, precious stones, and a range of other commodities can be further enhanced in a new perspective of commercial interactions within the wider Indian Ocean.

The analysis undertaken in this study presents a starting point from a small number of samples from excavated contexts at Adulis. As far as the provenance and technology of production of the torpedo jars is considered, the study of the bitumen lining and the fabric using archaeometric approaches proves to be useful as has been suggested also by similar works from elsewhere. The results from this study indicate that the bitumen could be related to sources in Mesopotamia while a detailed petro-mineralogical and geo-chemical analysis is required to further shed light into production centres for the vessels. The current study places Adulis within the growing archaeometric discussion on the production, distribution, and use of the Torpedo jars. The information from Adulis enhances the fact that the jars provide a direct proxy for trade and exchange throughout the Indian Ocean. It should be noted also that the closer examination of the clay fabric, form and bitumen lining of the torpedo jars needs to be systematically approached in the future by including samples obtained from different sites

in the Red Sea and Indian Ocean world for a complete typo-chronological framework and provenance.

7.4. Bibliography

Connan J. (1999). Use and trade of bitumen in antiquity and prehistory: Molecular archaeology reveals secrets of past civilizations. *Philosophical Transactions of the Royal Society B: Biological Sciences*. 354, 33-50. <https://doi.org/10.1098/rstb.1999.0358>.

Connan J, Zumberge J, Imbus K, Moghaddam A. (2008). The bituminous mixtures of Tall-e Abu Chizan: a Vth millennium BC settlement in southwestern Iran. *Org.Geochem*. 39, 1772-1789. <https://doi.org/10.1016/j.orggeochem.2008.07.004>.

Connan J, Priestman S, Vosmer T, Komoot A, Tofighian H, Ghorbani B, Engel M, Zumberge A and Van Velde T. (2020). Geochemical Analysis of Bitumen from West Asian Torpedo Jars from the c. 8th Century Phanom Surin Shipwreck in Thailand. *Journal of Archaeological Sci*. 117. <https://doi.org/10.1016/j.jas.2020.105111>.

Lischi S, Odelli E, Perumal, J L, Lucejko, J J, Ribechini E, Mariotti Lippi M, Selvaraj T, Colombini M P, Raneri, S. (2020). Indian Ocean trade connections: characterization and commercial routes of torpedo jars. *Herit Sci* 8, 76. <https://doi.org/10.1186/s40494-020-00425-9>.

Nardella F, Landi, N, Degano I, Colombo M, Serradimigni M, Tozzi C and Ribechini E. (2019) Analytical Methods Chemical investigations of bitumen from Neolithic archaeological excavations in Italy by GC/MS combined with principal component analysis. *Anal. Methods* 11, 1449–1459. <https://doi.org/10.1039/C8AY02429D>.

Stern B, Connan, J, Blakelock E, Jackman R, Coningham R A E, Heron C. (2008). From Susa to Anuradhapura: reconstructing aspects of trade and exchange in bitumen coated ceramic vessels between Iran and Sri Lanka from the third to the ninth centuries AD. *Archaeometry* 50, 409–428. <https://doi.org/10.1111/j.1475-4754.2007.00347.x>.

Spiro B, Welte D H, Rullkötter J, Schaefer R G. (1983). Asphalts, Oils, and Bituminous Rocks from the Dead Sea Area—A Geochemical Correlation Study. AAPG Bulletin 67 (7): 1163–1175. <https://doi.org/10.1306/03B5B71D-16D1-11D7-8645000102C1865D>.

Tomber R, Spataro M, Priestman S. (2020). Early Islamic Torpedo Jars from Siraf: Scientific Analyses of the Clay Fabric and Source of Indian Ocean Transport Containers, Iran, <https://doi.org/10.1080/05786967.2020.1792797>

Velde T. (2015). Black magic bitumen: an archaeometrical approach to 5000 years of bitumen imports in the Persian Gulf.

8. Conclusions

The archaeometric characterization of a group of Ayla-Aksum amphorae recovered from excavations in the archaeological site of Adulis has been performed together with pottery samples representing local pottery, Late Roman Amphora 1, *dolia* and Red Slipped ware. The chemical and mineralogical information as well as the characterization of residues of the organic lining enabled the first comprehensive distinction of local versus imported pottery at Adulis by combining morpho-stylistic classification and archaeometric data.

A major gap existed in terms of building a complete ceramic sequence at Adulis, previously, as much of the work dwelled upon typological studies of local pottery and imported transport and common wares from the Levant, north Africa, Arabian Peninsula, and the Indian Ocean world. The investigation of provenance of the Ayla-Aksum amphorae from archaeometric perspectives, was central to the realisation of this study, which was further extended to incorporate information on different classes of pottery found at Adulis to provide comparative parallels. Similarly, it has been envisaged in this study to draw correlations with existing geo-chemical and mineralogical data on different classes of pottery from elsewhere in the Red Sea world, Levant, and Indian Ocean to fully understand patterns of production, distribution and use of pottery assemblages that were uncovered from on-going excavations at Adulis. In this respect, a multi-analytical approach which includes the study of mineralogical composition through Optical microscopy (petrography) and Powder XRD as well as chemical composition via ICP-OES and SEM-EDX has been integrated for purposes of this study. Moreover, analytical techniques which comprised FT-IR and GC-MS also allowed the characterization of organic residues present in some fragments to corroborate information on provenance and technology of production.

Petrographic studies allowed to establish distinct fabrics for the local pottery and Ayla-Aksum amphorae to suggest any hypothesis for the production of the latter classes of pottery elsewhere from Ayla is refuted. The petrographic information on the Ayla-Aksum amphorae from Adulis, moreover, parallels petrographic studies on Ayla amphorae from sites in the Trans-Jordan and Negev as well as Zafar in Yemen, which established production in the Ayla kilns. Inter-fabric variability is observed in the samples representing the Ayla-Aksum based on some fabric attributes while a mineralogical homogeneity can be established to pinpoint a unique production over centuries. The results from petrographic studies on Ayla-Aksum

amphorae from Adulis are further corroborated by chemical and geo-chemical data from SEM-EDX and ICP-OES respectively in as much as the information from XRPD.

On the other hand, different fabrics have been established for the local pottery at Adulis, where petrographic studies indicated the use of raw materials available within the basin/s and geological outcrops around Adulis. The information has been further substantiated by petrographic observations on briquettes of local clay samples. In general, the local pottery samples show a wide variability in terms of fabrics attesting to the use of different recipes from the basins around Adulis and the study of the local pottery together with briquettes obtained from firing local clay samples has allowed to establish for the first-time fabrics unique to Adulitan pottery. Furthermore, information on technology of production from Scanning Electron Microscopy (SEM) and Powder X-ray Diffraction (XRPD) indicated differences in production between Ayla- Aksum amphorae and the local pottery to support the information from petrographic and geo-chemical studies and thus establish distinct provenance for these classes of pottery. It has been also discerned that the geo-chemical signatures of the local pottery and the raw clay samples share affinities to suggest a production from the basins fed by the Alighede and Haddas rivers in the area of Adulis and the available raw materials within the geological scope of the area adjacent to the Gulf of Zula on the Red Sea coast of Eritrea.

The wider fabric variability within the local pottery perhaps pinpoint to dynamics in exploitation of clay raw materials and the establishment of fabrics for the local pottery at Adulis will help from archaeological point of view to study in- depth regional ceramic forms from highlands of Eritrea and northern Ethiopia as well as the coastal peripheries that may share similarities in morpho-stylistic attributes. It should be noted here that there has not been a systematic approach to study local pottery at Adulis in light of what has been often discussed as regional ceramic tradition to pinpoint production at coeval sites in the highlands of Eritrea and northern Ethiopia. The diffusion of morpho-stylistic attributes at a regional scale (northern Horn of Africa) is discerned from pottery found across sites in the northern Horn of Africa (Zazzaro *et al* 2014) and thus, a systematic archaeometric approach is significant to discriminate compositional groups and production centres in the region or else assess whether a standardized production can be attested. In this respect, future research should focus on distinguishing the regional forms considering the established fabrics of local pottery at Adulis.

The archaeometric work also has highlighted distinction of fabrics between Late Roman Amphora 1, torpedo jars and *dolia*. The fabric for Late Roman Amphora 1 show uniformity in terms of mineral clasts present as well as the fabric attributes and comparisons with existing databases suggest that the fabric dominated by micro-fossils and shells could be related to production in Cyprus and southern Turkey, where kilns prominent for the LRA1 are present.

In a similar vein, the study has established fabrics for the samples belonging to torpedo jars (which were initially attributed to LRA1? on the basis of macroscopic observations). A major difficulty in terms of securely identifying the fabrics is primarily the result of the macroscopically superficial resemblance of LRA1 and torpedo jars whose contemporaneous production with the Roman amphora has been attested in the Indian Ocean world. Thanks to the coupling of petrographic observations and the organic residue studies, however, it was possible to securely recognize the samples as fragments of torpedo jars. Petrographic observations revealed two fabrics that could be related to the Torp-S class of these vessels, where production is attested between 3rd -8th CE (Tomber *et al* 2020). The identification of the torpedo jars has been to a great deal based on the study of the bitumen lining of their internal surfaces, presumably originating from Mesopotamia, a case which also has been indicated by FT-IR and GC-MS analyses in this study. It should be noted, therefore, that where typological classification based on macroscopic attributes yield complexities and/or deficiencies, the archaeometric approach becomes quite useful to complete a secure attribution as demonstrated in this case. What is, however, intriguing is the fact that the treatment of the geo-chemical data showed similarities in composition between the LRA1 and Torpedo jars, a subject that needs to be further tackled systematically in the future. Current scholarship has indicated that the study of the Torpedo jars with the LRA1 perhaps might indicate information on provenance of the torpedo jars, where at present no kilns have been identified for their production.

The use of ophiolitic clays have been suggested for the production of Torpedo jars in recent studies and the fact that the production of the LRA 1 exploited raw materials rich in ophiolites in Cyprus and southern Turkey partly explains the similarities in composition and the superficial resemblance of fabrics as has been suggested previously. The Tigris-Euphrates basin of Iraq (Mesopotamia) and the continuous mountain range stretching from Troodos, Cyprus to Semail, Oman were recently suggested by Tomber *et al* (2020) as the two main geological features where torpedo jars are most likely to originate. It can be said, therefore,













that the bitumen characterization showed affinities to sources in Mesopotamia, and yet similarities in chemical composition with the LRA1 stimulate a careful examination of the clay by incorporating larger number of samples from sites in the Red Sea world and the coasts of the Indian Ocean. While broader generalizations remain unwarranted, the results pose a question whether bitumen was transported and/or traded over long distances in areas which are known to be linked with LRA1 production. In this respect, Adulis becomes a significant archaeological site to understand the distribution of the Torpedo jars in as much as of the LRA1 while the results contribute to on-going discussions on the provenance of the Torpedo jars.

Furthermore, fabrics have been identified for the *dolia* and the red slipped ware samples and yet conclusions cannot be drawn as to their provenance due to limited number of samples and absence of reference materials. Similarly, few samples whose fabrics are characterized by ARFs, and carbonates posed difficulties to establish typologies due to poor diagnostic attributes and lack of comparative parallels. The problem is further evinced from the absence of complete databases adequate to discriminate different pottery classes that were produced by exploiting similar raw materials as explained above. This gap has been indicated in this study and the attribution of fabrics will dwell upon the progress of the work elsewhere in the Levant and the study of comparative materials with securely established typologies. This should be considered the existing gap considering the need to build a complete sequence at Adulis as far as the specific classes of imported transport and common wares are concerned.

In conclusion, the study of Ayla-Aksum amphorae, local pottery, Late Roman Amphora 1, Torpedo jars, *dolia* and red slipped ware allowed to correlate the archaeometric data to existing classifications while shedding light into the gaps that exist in terms of establishing secure typological classes. A great deal of the samples was recovered from contexts dated to 5th- 7th CE, which coincides with intensive occupation phases at Adulis. The attribution of provenance to Eastern Mediterranean, Levant, and Indian Ocean World of the different classes of imported transport and common wares supports the notion of connections with the Byzantine in light of trade networks to India and military alliances to control maritime supremacy in the Red Sea world in Late antiquity. Late Roman and Byzantine transport and common wares that have been uncovered from excavations at Adulis are, thus, particularly of interest in terms of the scope of this archaeometric study, broadening our understanding of the extent of the trade exchanges that involved the ancient port city of Adulis. The establishment of fabrics for the local pottery, are also equally important to tackle the least

understood regional ceramic exchanges in the northern Horn of Africa from mineralogical and chemical studies. This study, therefore, enabled to lay the basis for building a complete ceramic sequence at Adulis from the current archaeometric data encompassing typological classification, petro-mineralogical information, geo-chemical signatures, and organic residue analysis while charting the path for future research aimed at filling the gaps identified.

Appendix 1: Photos of Samples Considered in the Study

 <p>Sample 1.1</p>	 <p>Sample 1.2</p>	 <p>Sample 1.3.1</p>	 <p>Sample 1.3.2</p>
 <p>Sample 1.4.2</p>	 <p>Sample 1.6</p>	 <p>Sample 1.7.2</p>	 <p>Sample 1.8</p>
 <p>Sample 2.0</p>	 <p>Sample 3.3</p>	 <p>Sample 3.4</p>	 <p>Sample 3.5</p>



Sample 3.6



Sample 3.8



Sample C04



Sample C05



Sample 2.5



Sample 2.6



Sample 2.7



Sample 2.8



Sample CW 07



Sample CW 08



Sample CW 11



Sample CW 16



Sample 1.9



Sample 2.3



Sample 3.0



Sample 3.1



Sample 3.2



Sample C02



Sample C03



Sample C06



Sample C07



Sample C08



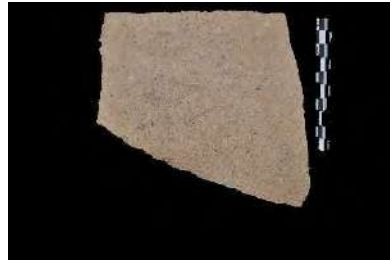
Sample C09



Sample 1.0



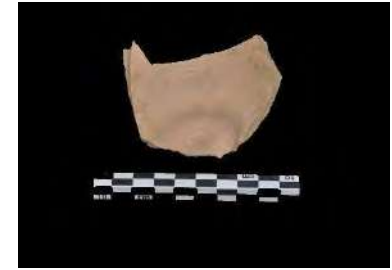
Sample 4.0



Sample 4.8



Sample 4.9



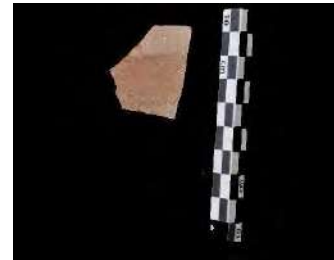
Sample 4.5



Sample 4.6



Sample 4.11


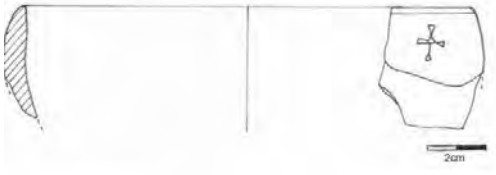
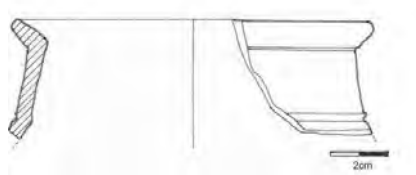


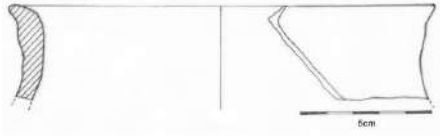
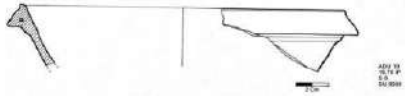
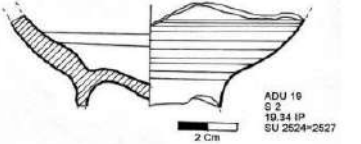
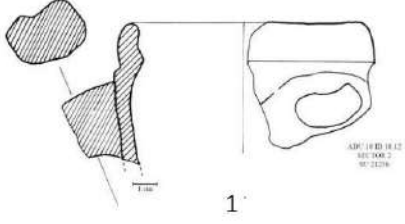
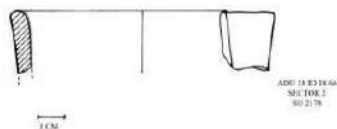
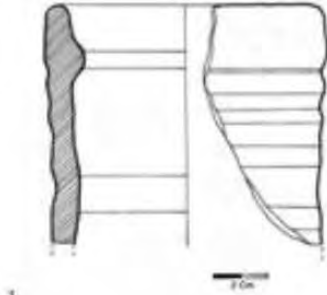
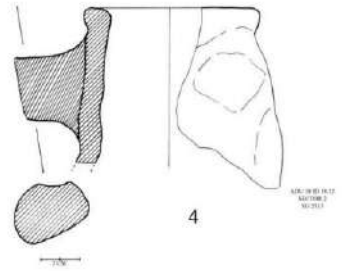


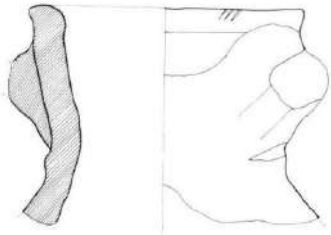
Sample 2.9



Sample 4.1

Appendix 2: Drawings of Representative Samples

 <p>Sample CW 07</p>	 <p>Sample CW 08</p>	 <p>Sample CW 11</p>	 <p>Sample CW 16</p>
 <p>Sample CW 18</p>	 <p>Sample CW 21</p>	 <p>Sample 4.5</p>	 <p>Sample 4.6</p>
 <p>Sample 1.6</p>	 <p>Sample 1.4.1</p>	 <p>Sample 1.8</p>	 <p>Sample 1.9</p>



1234

1234
1234
1234

Sample 2.3

Appendix 3: List of Samples and Analytical Methods Applied

Class	Sample	OM	SEM-EDX	SEM/Fracture	SEM/Polished thin sections	XRPD	FT-IR	ICP-OES	GC-MS
Ayla	1.1	x				x			
	1.2	x				x			
	1.3.1	x				x			
	1.3.2	x	x	x	x	x		x	
	1.4.1	x				x			
	1.4.2	x	x	x	x	x		x	
	1.5	x	x	x	x			x	
	1.6	x				x			
	1.7.1	x	x	x	x	x		x	
	1.7.2	x	x	x	x	x		x	
	1.8	x				x			
	2.0	x				x			
	3.3	x				x			
	3.4	x				x			
	3.5	x				x			
	3.6	x				x		x	
	3.7	x				x			
	3.8	x				x			
	C01	x				x			
	C04	x				x		x	
C05	x				x				

Class	Sample	OM	SEM-EDX	SEM/Fracture	SEM/Polished thin sections	XRPD	FT-IR	ICP-OES	GC-MS
Local	2.5	x	x	x	x	x		x	
	2.6	x	x	x	x	x		x	
	2.7	x	x	x	x	x		x	
	2.8	x	x	x	x	x		x	
	CW01	x							
	CW02	x			x				
	CW03	x							
	CW05	x							
	CW07	x			x				
	CW08	x							
	CW09	x			x				
	CW11	x							
	CW16	x			x				
	CW18	x							
	CW19	x							
	CW20	x			x				
CW21	x								
Bricks	4.10	x	x	x	x	x		x	
	4.11	x	x	x	x	x		x	
Raw Clay	H1	x			X	x		x	
	H2	x			X	x		x	
	F1	x			X	x		x	
	F2	x			X	x		x	
	M1	x			X	x		x	
	M2	x			X	x		x	

Class	Sample	OM	SEM-EDX	SEM/Fracture	SEM/Polished thin sections	XRPD	FT-IR	ICP-OES	GC-MS
LRA1	1.9	x	x	x	X	x		x	
	2.1	x				x			
	2.2	x				x			
	2.3	x	x	x	x	x		x	
	3.0	x				x			
	3.1	x				x			
	3.2	x				x			
LRA1 (?)	C02	x	x	x	x	x	x	x	x
	C03	x	x	x	x	x	x	x	x
	C06	x	x	x	x	x	x	x	x
	C07	x		x	x	x	x	x	x
	C08	x			x	x	x		x
	C09	x				x	x		x
	3.9	x				x			
<i>Dolia</i>	1.0	x				x			
	4.0	x				x			
	4.8	x	x	x	x	x		x	
	4.9	x	x	x	x	x		x	
Red Slipped	4.5	x				x		x	
	4.6	x	x	x	x	x		x	
ND	2.9	x	x	x	x	x		x	
	2.4	x	x	x	x	x		x	
	4.1	x				x			
	4.3	x				x			
	4.4	x				x			

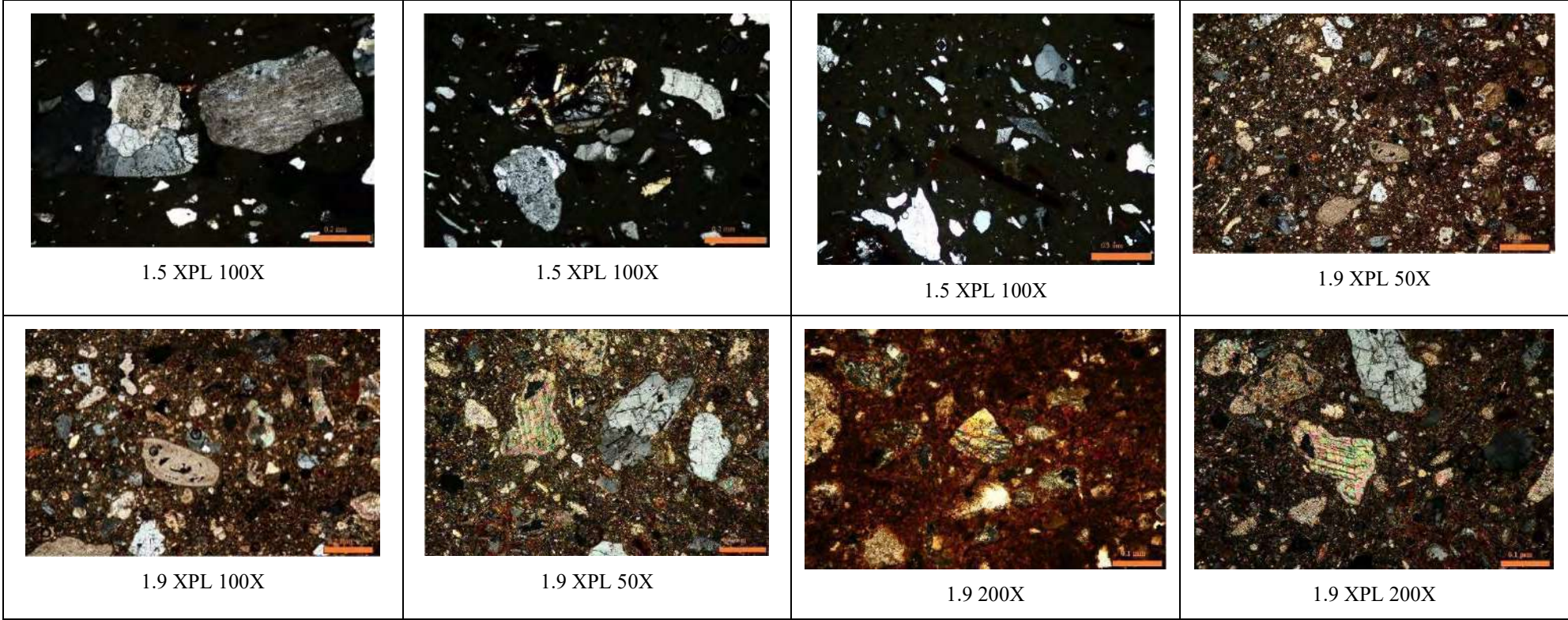
Appendix 4: The Petrographic Information of studied potsherds and briquettes. Qt, Quartz; K-fs, K-feldspars; Pl, Plagioclase; Ms, Muscovite; Bt; biotite; Ca, Calcite; ARF, argillaceous rock fragments; Lstn, Limestone; Py, Pyroxenes; Am, amphibole; Cht, Chert; Irox, Iron oxides; Gt, Granite; Bast, Basalt; Phy, Phyllite; Quatz, Quartzite; Sandn, Sandstone; Msht, Mica-Schist, Msn, Mudstone. +++, abundant; ++, common to few; +, few to rare.

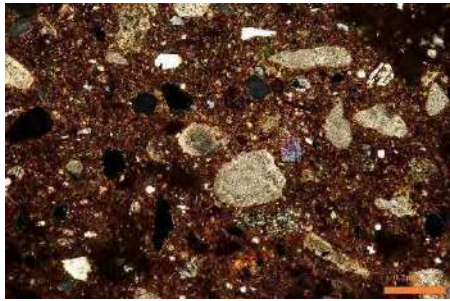
Class	Name	Qt	K-fs	Pl	Ms	Bt	Ca	ARF	Lstn	Py	Am	Cht	Irox	Shells	Gt	Bast	Phy	Quatz	Sandn	Msht	Msn	Fabric
Ayla	1.1	++	+++	++	++					++					++							2
	1.2	+++	++	++						+					+							1
	1.3.1	++	+++	++						++					++							2
	1.3.2	++	+++	++		++				++					++							2
	1.4.1	++	+++	++		+				+					++							2
	1.4.2	+++	++	++		+				++						+						1
	1.5	+++	++	++		++				++					++	+			+			1
	1.6	++	+++	++		++				++					++							2
	1.7.1	++	+++	++		+				+			+		++	+						2
	1.7.2	+++	++	++		+				+			+		++							1
	1.8	++	+++	++											++							2
	2.0	++	+++	++			+				+				++							2
	3.3	+++	++	++							++				++							1
	3.4	+++	++	++							+				++							1
	3.5	++	+++	++		++					++				++	+						2
	3.6	++	+++	++		++					++				++	+						2
	3.7	++	+++	++							++				++							2
	3.8	++	+++	++							++						++	+				2
	C01	++	+++	++		++					+			+		++						2
	C04	++	+++	++		++					+			+		++						2
C05	++	+++	++		++					+			+		+	+			+		2	

Class	Name	Qt	K-fs	Pl	Ms	Bt	Ca	ARF	Lstn	Py	Am	Cht	Irox	Shells	Gt	Bast	Phy	Quartz	Sandn	Msht	Msn	Fabric	
Local	2.5	+++	++	+	++	++				+							+++		+++			1	
	2.6	+++	++	+	++	++												+++	+++			3	
	2.7	+++	++	+	++	++									+++				+++			2	
	2.8	+++	++	+	++	++											+++		+++			1	
	CW01	+++	++	+	++	++										++			++	++			2
	CW02	+++	++	+	++	++										++			++	++			2
	CW03	+++	++	+	++	++										++			+++	++			2
	CW05	+++	++	+	++	++					+								++	++			3
	CW07	+++	++	+	++	++													++	++			3
	CW08	+++	++	+	++	++												++		++			1
	CW09	+++	++	+	++	++						+							++	++			3
	CW11	+++	++	+	++	++										++			++	++			2
	CW16	+++	++	+	++	++										++			++	++			2
	CW18	+++	++	+	+	+												++		++			1
	CW19	+++	++	+	+	+													++	++			3
CW20	+++	++	+	+	+										++			++	++		+	2	
CW21	+++	++	++	+	+					+						+		++	++			3	
Bricks	4.10	++	++	+	+	+				+			+					++	+			1	
	4.11	+++	++	+	+	+			+	+			+				++				++	1	
Raw Clay	H1	++	++	+	+				+	+						+	+					3	
	H2	++	++	+	+				+							+	+					3	
	F1	++	++	+	++	++			+							+	+		+			1	
	F2	++	++	+	++	++			+							+	+		+			1	
	M1	++	++	+	++	++										+			+			2	
	M2	++	++	+	++	++										+			+			2	

Class	Name	Qt	K-fs	Pl	Ms	Bt	Ca	ARF	Lstn	Py	Am	Cht	Irox	Shells	Gt	Bast	Phy	Quartz	Sandn	Msht	Msn	Fabric
LRA1	1.9	++	++				+++		+++	+	+	++		+++								1
	2.1	++	++				+++		+++	+	+	++		+++								1
	2.2	++	++				+++		+++	+	+	++		+++								1
	2.3	++	++				+++		+++	+	+	++		+++								1
	3.0	++	++				+++		+++	+	+	++		+++								1
	3.1	++	++	+			+++		+++	+	+	++		+++								1
	3.2	++	++	+			+++		+++	+	+	++		+++								1
LRA1(?)	C02	++	++	++	++	++			+++	++	+	++	+			++			++	+		1
	C03	++	++	++	++	++			+++	++		++	+			++			++	+		1
	C06	++	++	++	++	++			+++	++	+	++	+			++			++	+		1
	C07	++	++	++	+	+			+++	++	+	++	+			++			++	+		2
	C08	++	++	++	++	++			+++	++	+	++	+			++			++	+		2
	C09	++	++	++	++	++			+++	++	+	++	+			++			++	+		2
	3.9	++	++	++	++	++			+++	++	+	++				++						1
<i>Dolia</i>	1.0	++	+	+				+++	+													1
	4.0	++	+	+				+++		+												1
	4.8	++	+	+				+++	+													1
	4.9	++	++	+	+			+	+++													2
Red Slipped	4.5	+++	++	+				++	+	+	+		+			+						1
	4.6	+++	++	+				++	+	+	+		+			+						1
ND	2.9	+++	+++	++	+	+			++	+	+											1
	2.4	+++	+	+		+			+++													2
	4.1	+++	+	+					+++													2
	4.3	+++	++	++																		3
	4.4	+++	++	++																		3

Appendix 5: Photomicrographs from Petrographic Observations of Representative Samples

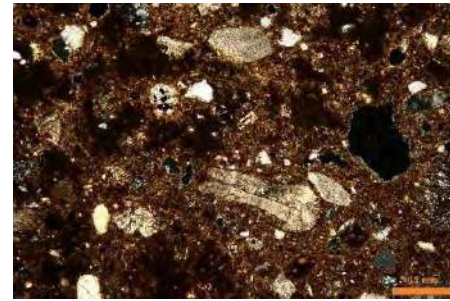




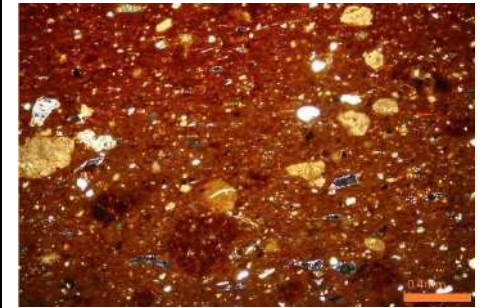
2.3 PPL 100X



2.3 XPL 50X



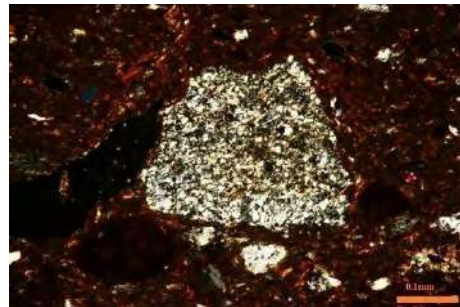
2.3 XPL 100X



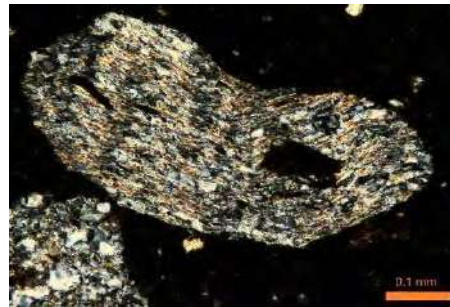
2.4 XPL 50X



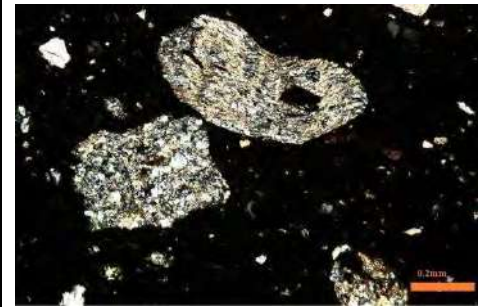
2.5 XPL 100X



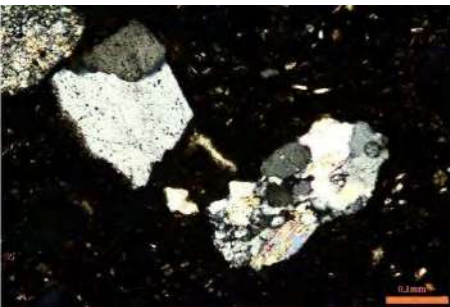
2.5 XPL 200X



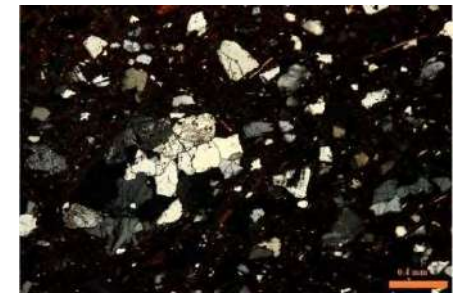
2.6 XPL 200X



2.6 XPL 50X



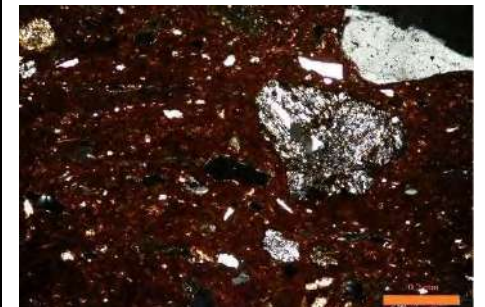
2.6 XPL 200X



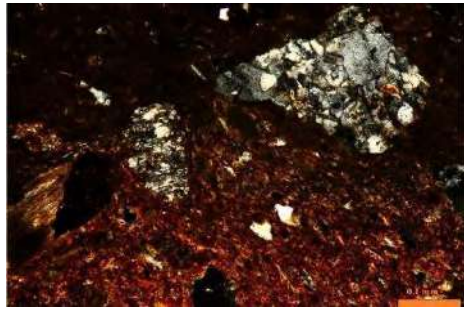
2.7 XPL 50X



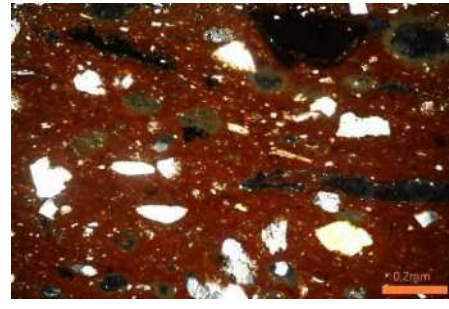
2.7 XPL 100X



2.8 XPL 100X



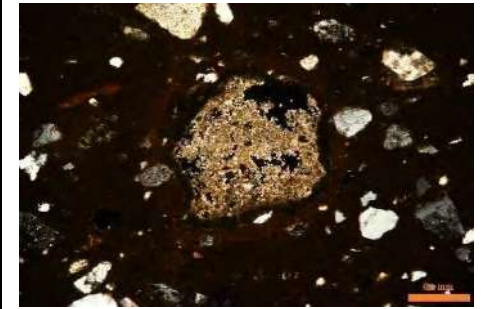
2.8 XPL 200X



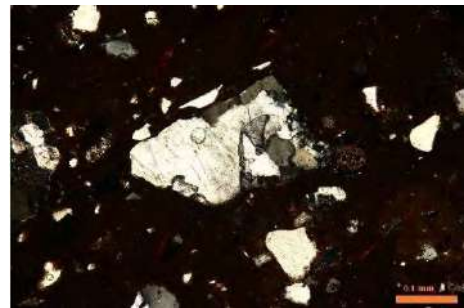
2.9 XPL 100X



3.6 XPL 50X



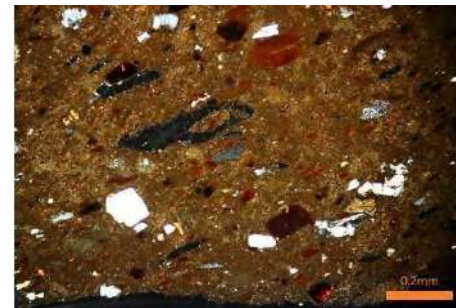
3.6 XPL 200X



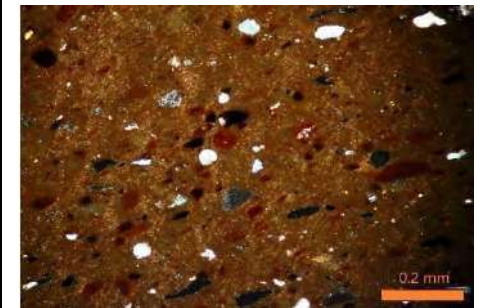
3.6 XPL 200X



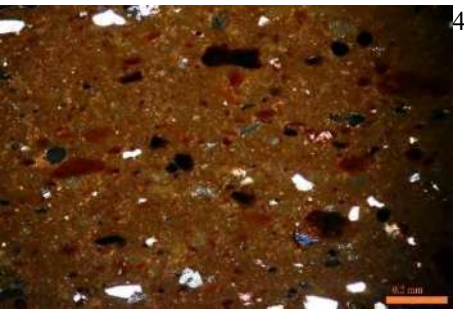
3.6 XPL 100X



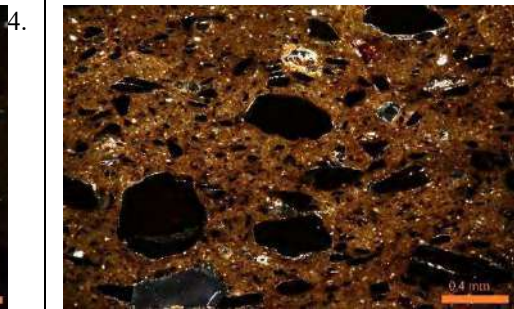
4.6 XPL 100X



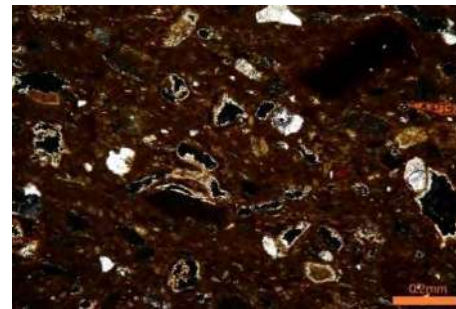
4.6 XPL 100X



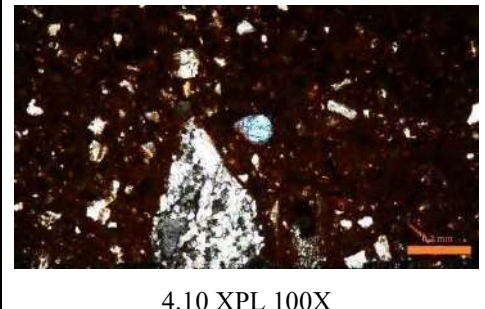
6 XPL 100X



4.8 XPL 100X



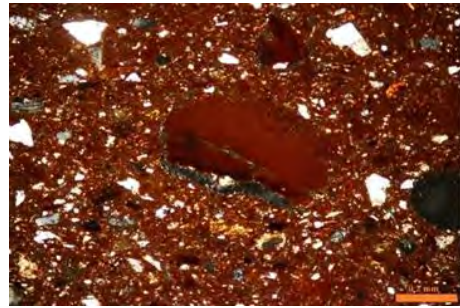
4.9 XPL 100X



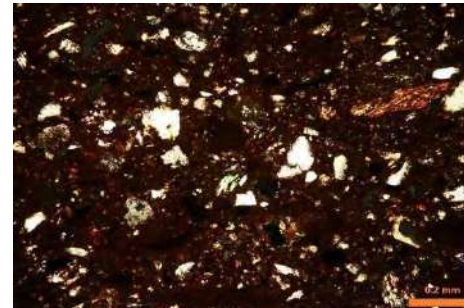
4.10 XPL 100X



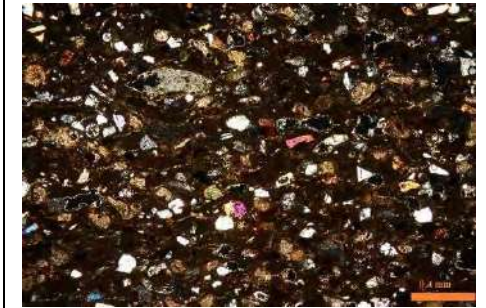
4.10 XPL 50X



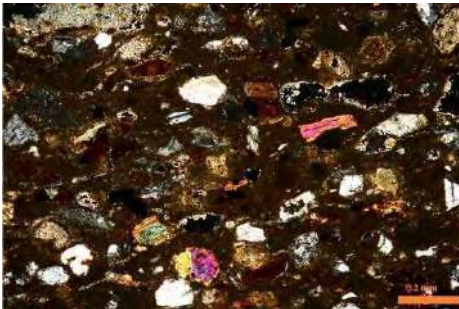
4.11 XPL 100X



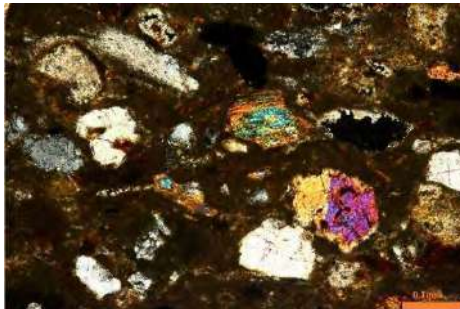
4.11 XPL 100X



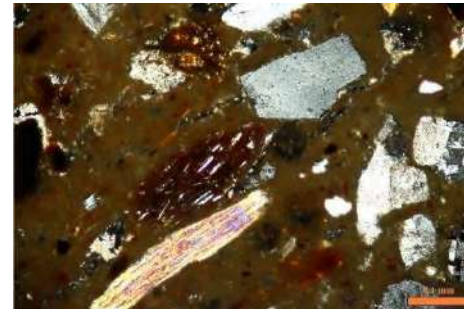
C03 XPL 50X



C03 XPL 100X



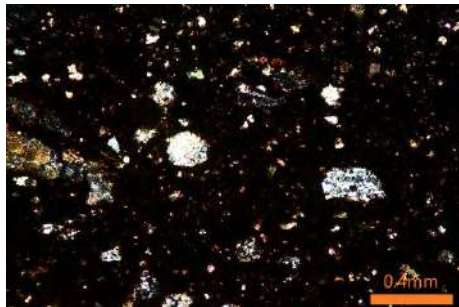
C03 XPL 200X



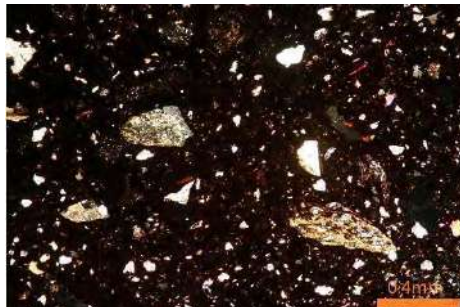
C08 XPL 200X



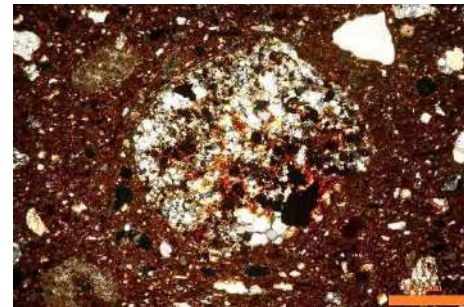
CW 19 XPL 50X



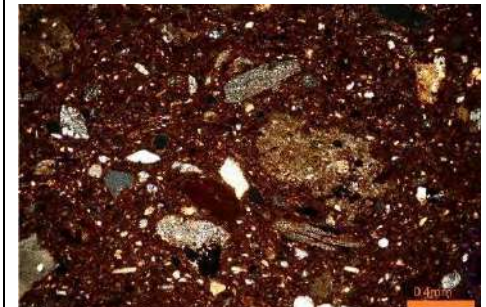
CW 09 XPL 50X



CW 20 XPL 50X



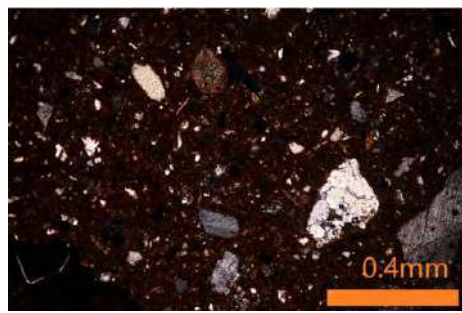
F1 XPL 50X



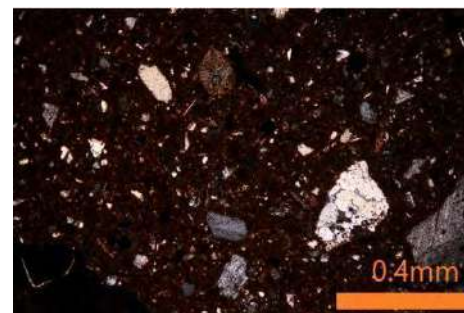
F1 XPL 50X



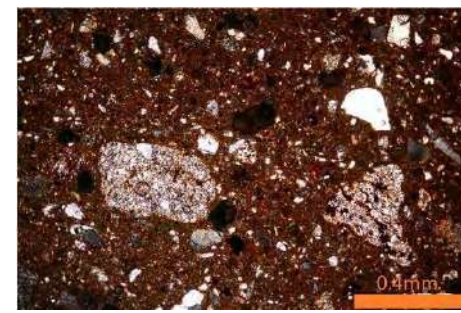
F2 XPL 50X



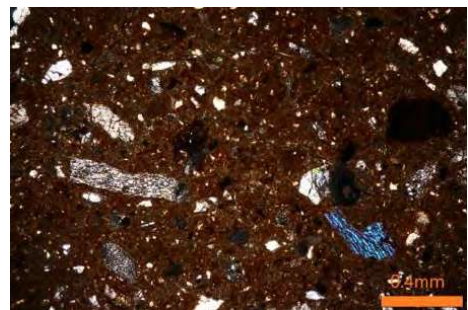
H1 XPL 50X



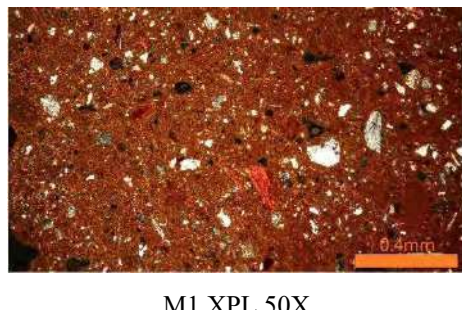
H1 XPL 50X



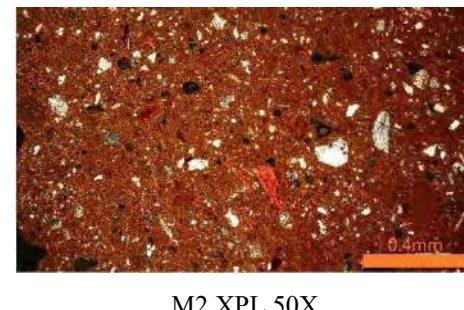
H2 XPL 50X



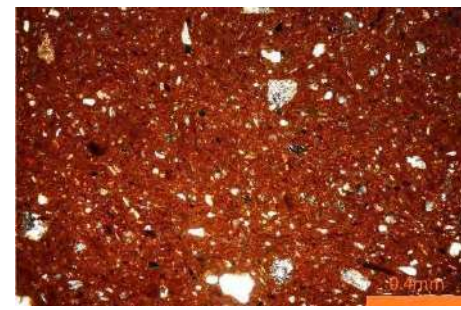
H2 XPL 50X



M1 XPL 50X

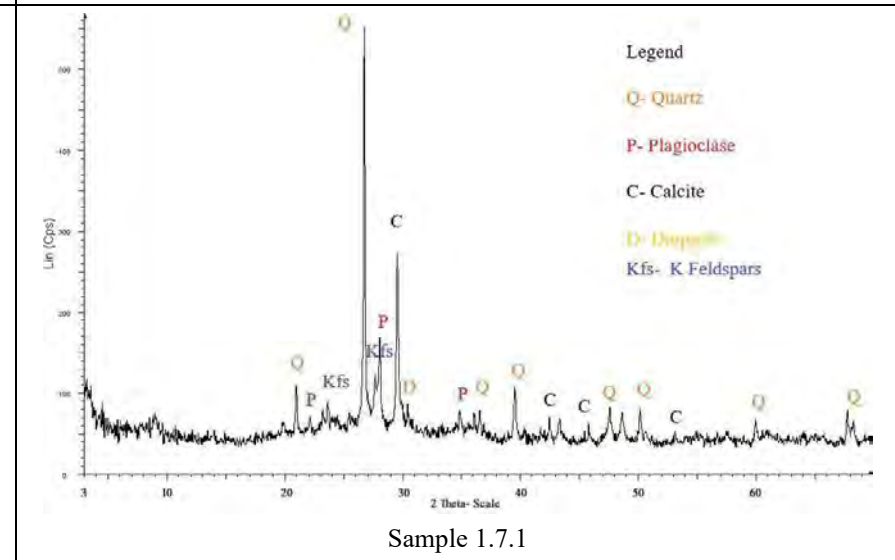
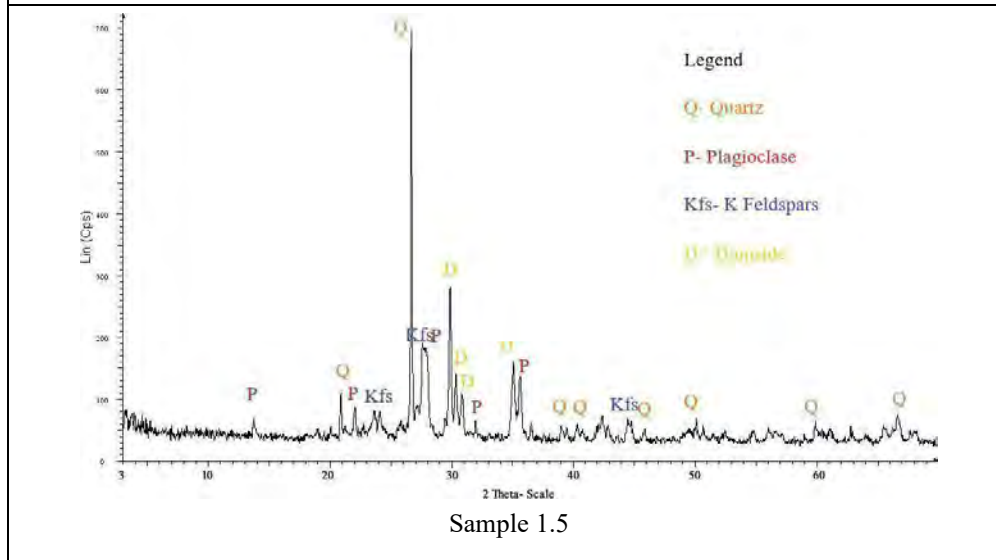
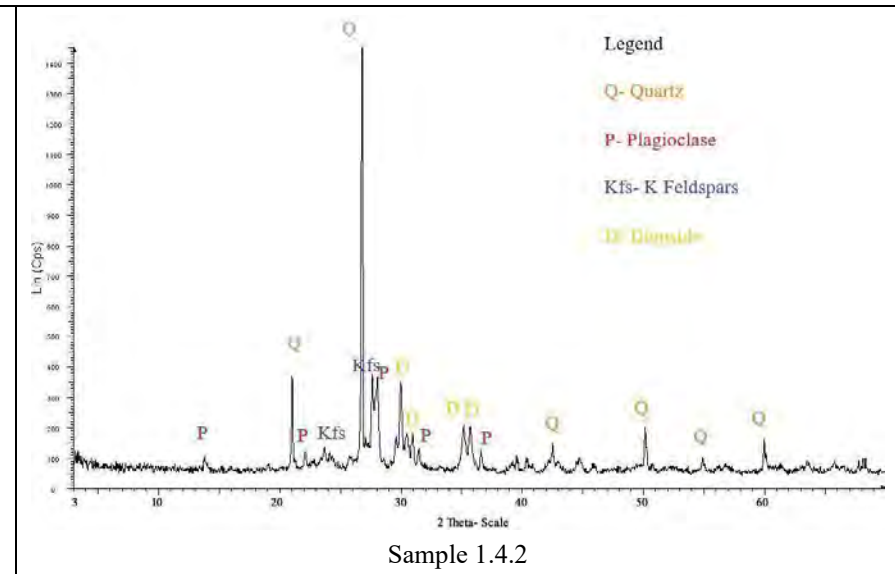
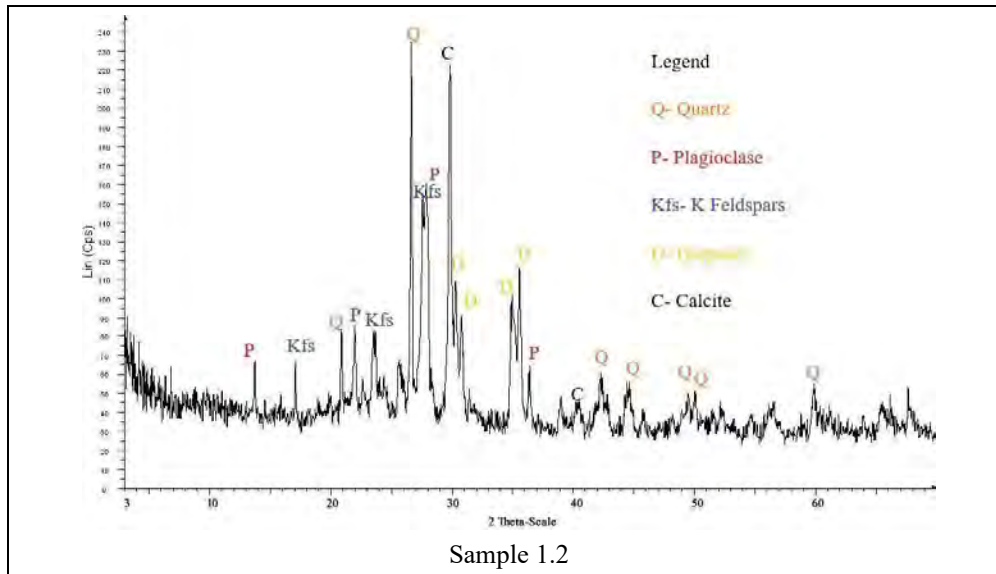


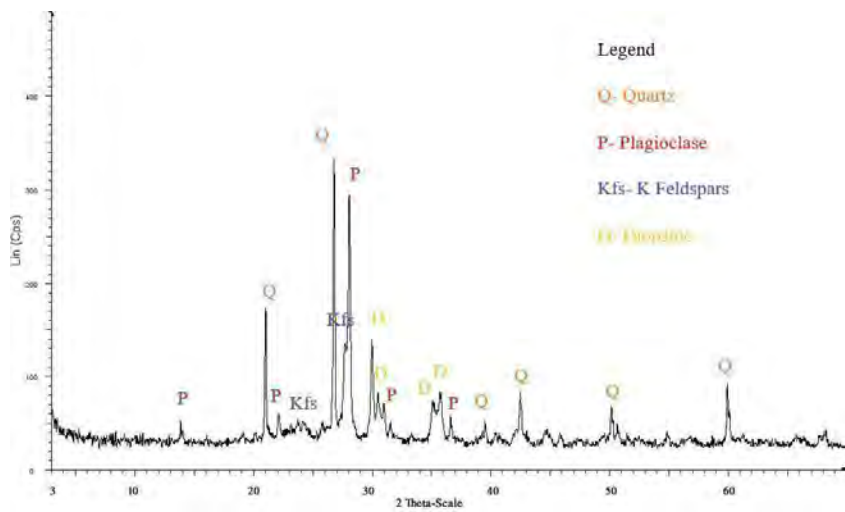
M2 XPL 50X



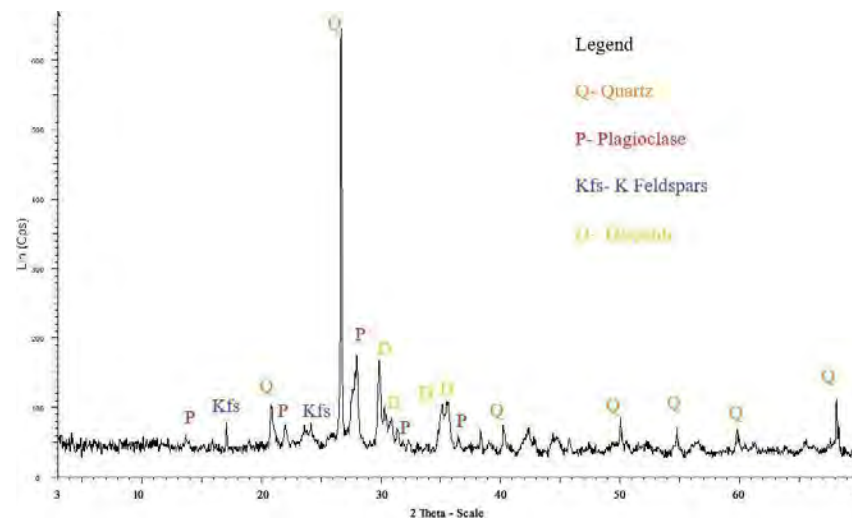
M2 XPL 50X

Appendix 6: XPRD Data of Representative Samples

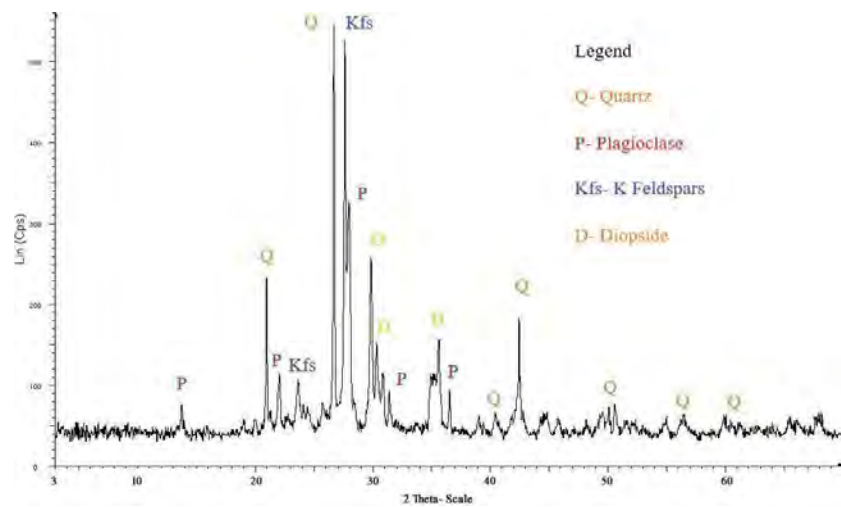




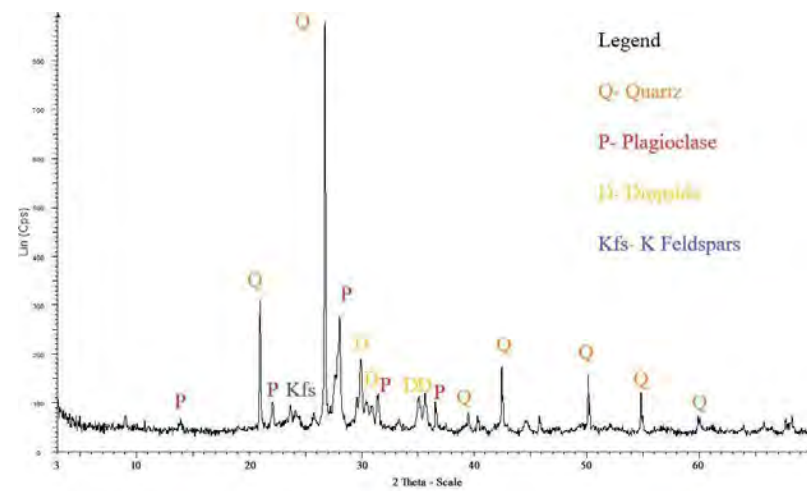
Sample 1.7.2



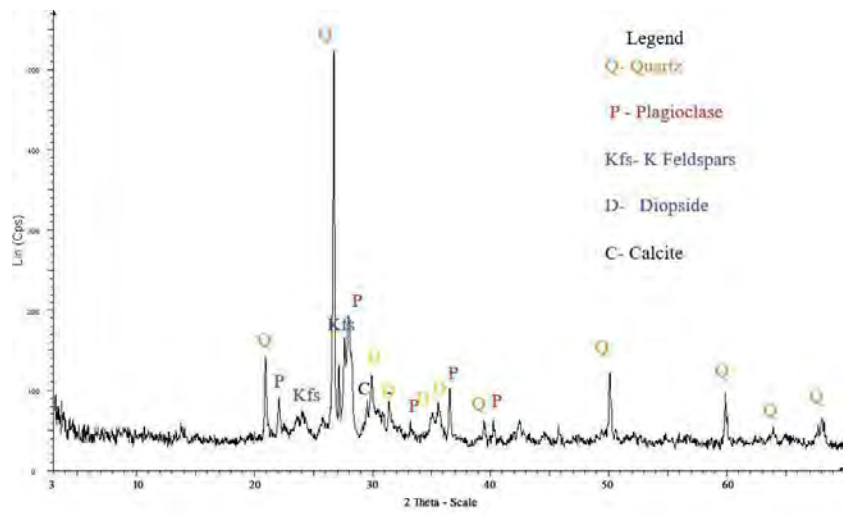
Sample 3.3



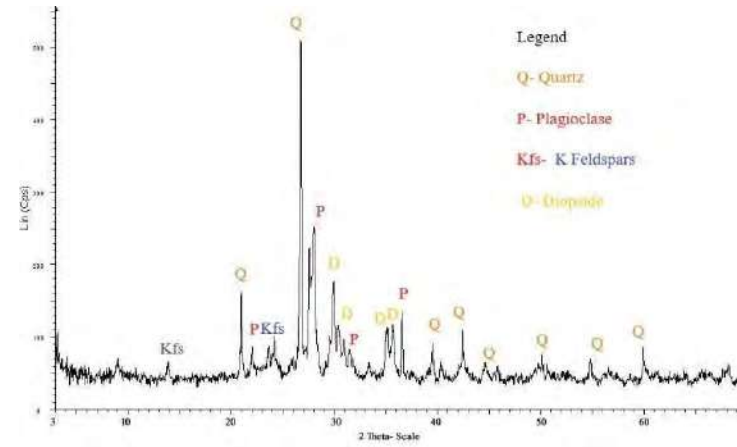
Sample 3.4



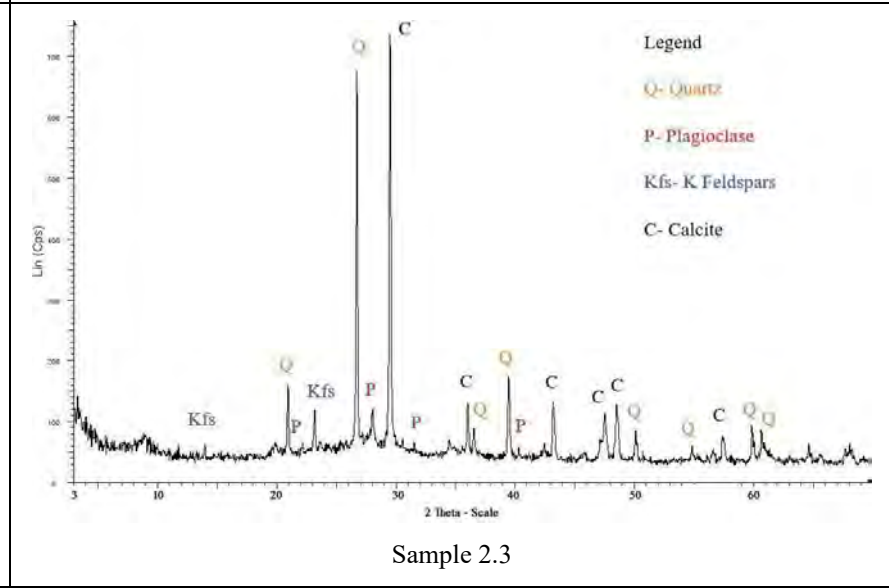
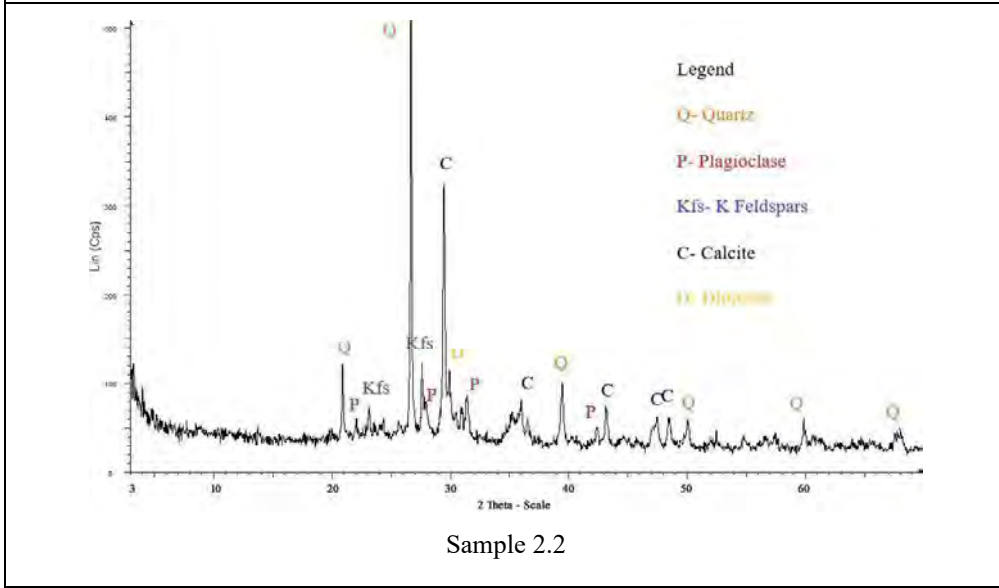
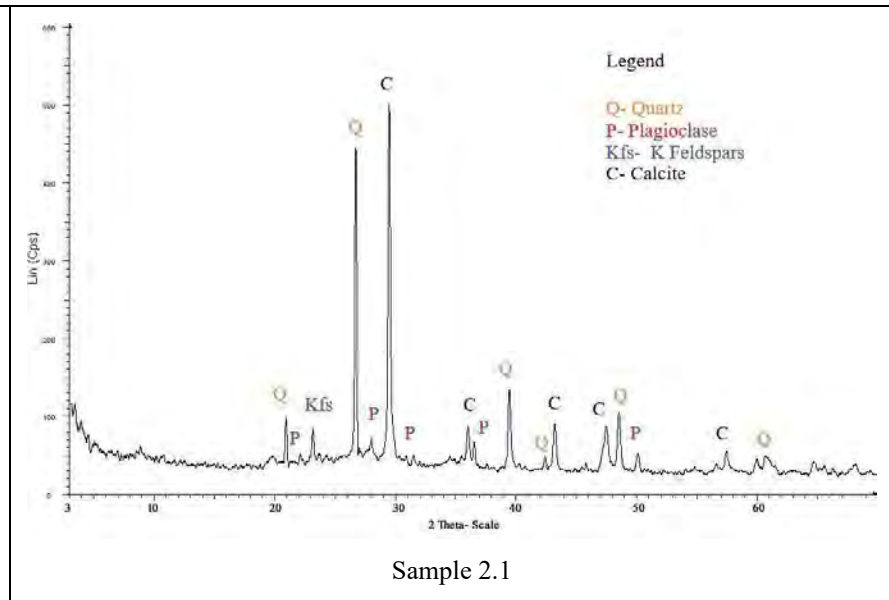
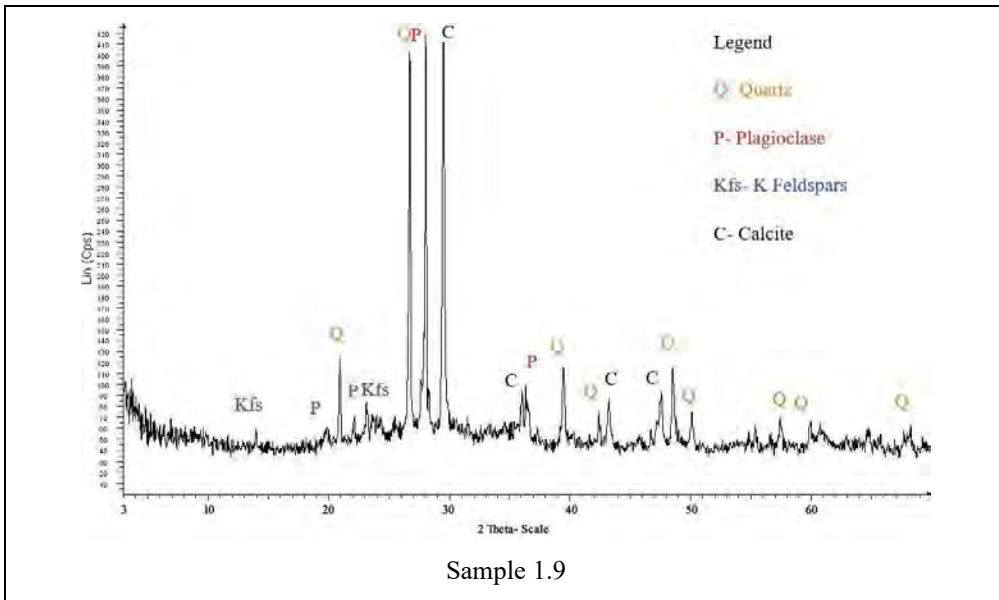
Sample 3.6

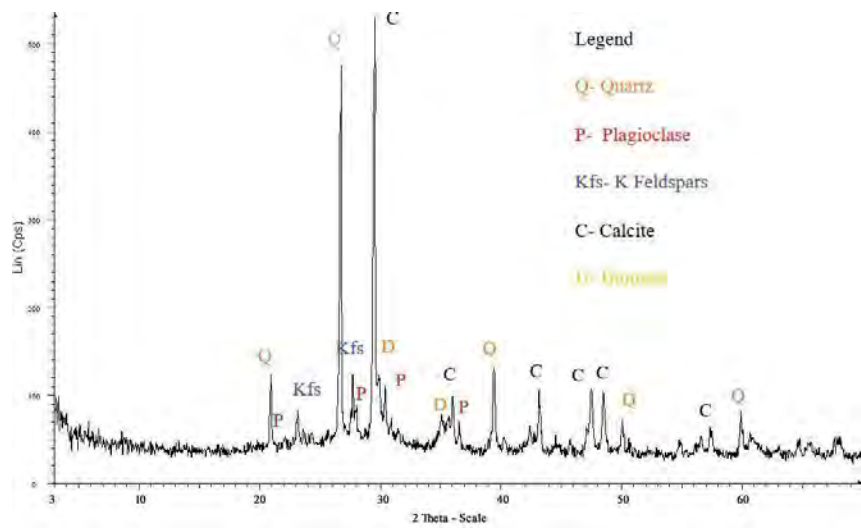


Sample C01

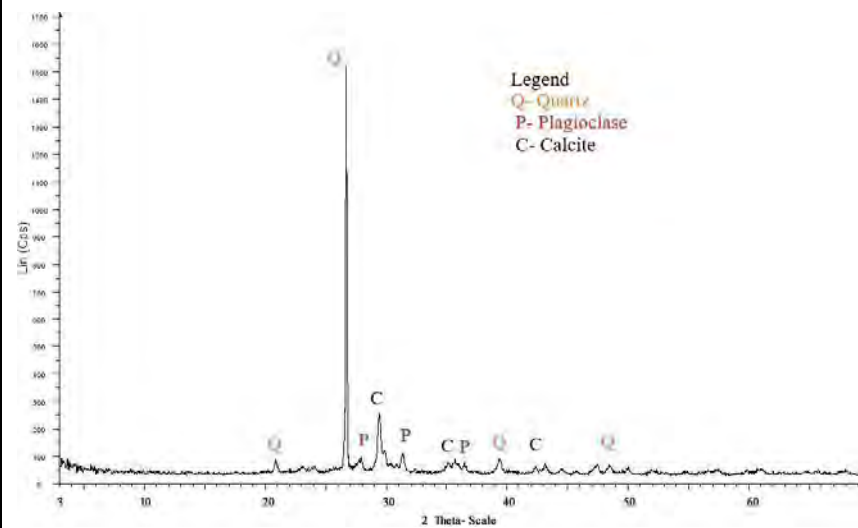


Sample C05

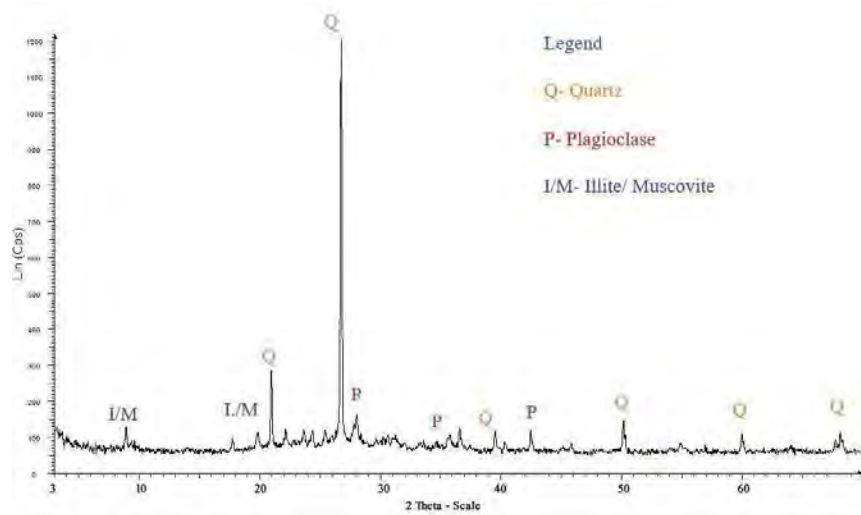




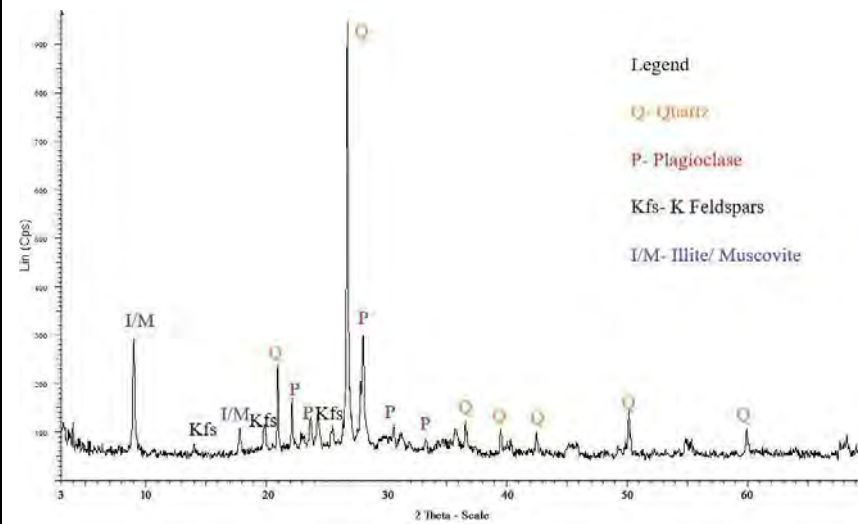
Sample 3.1



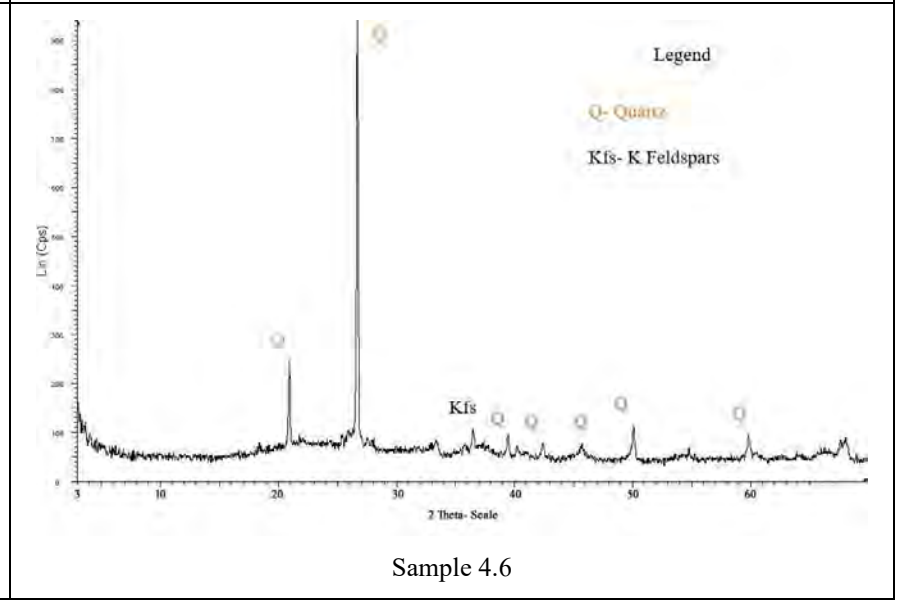
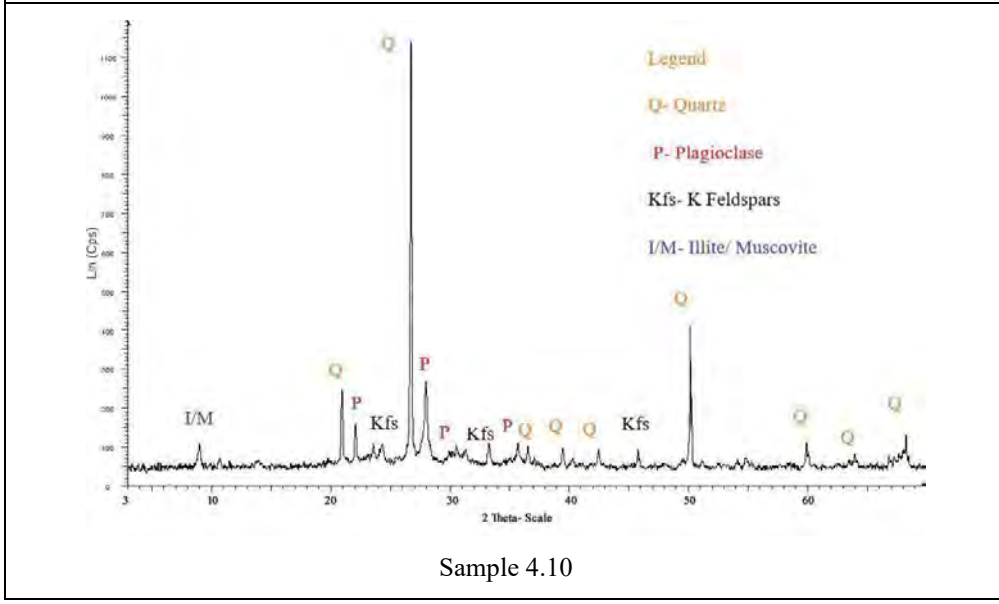
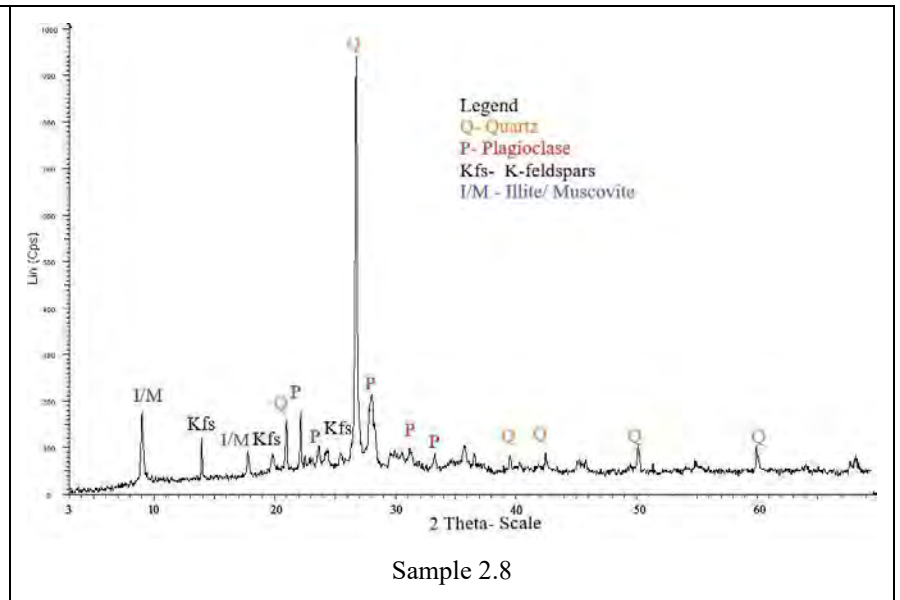
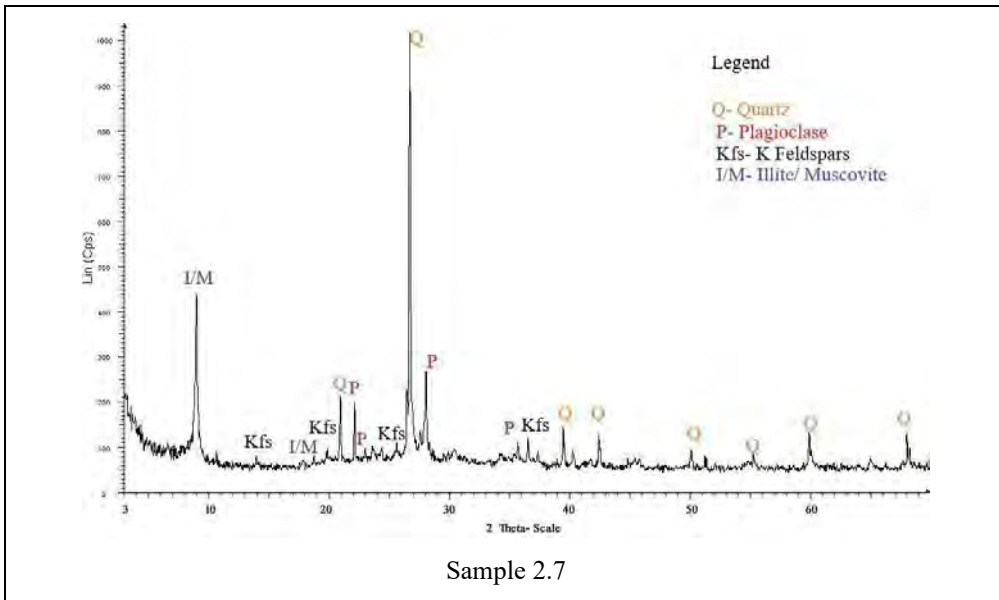
Sample 3.2

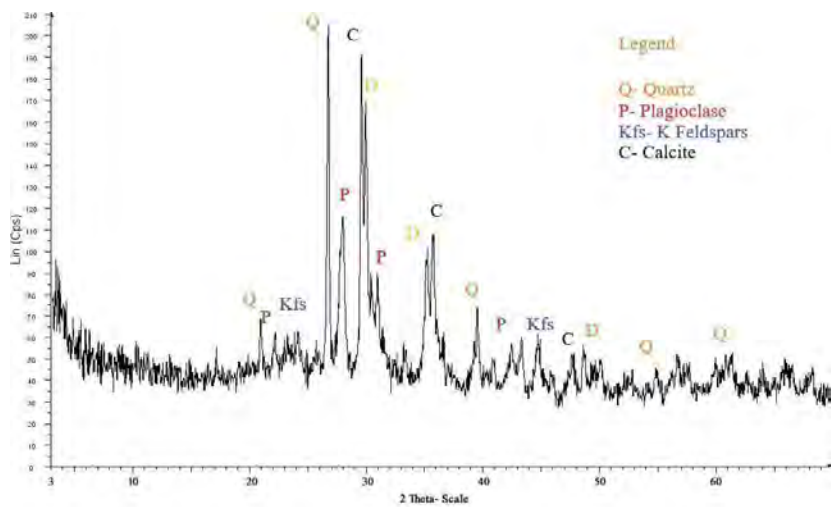


Sample 2.5

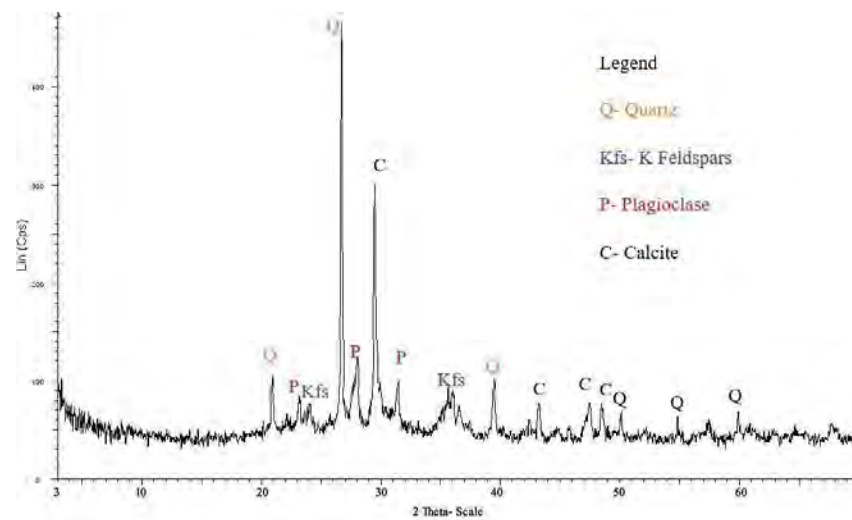


Sample 2.6

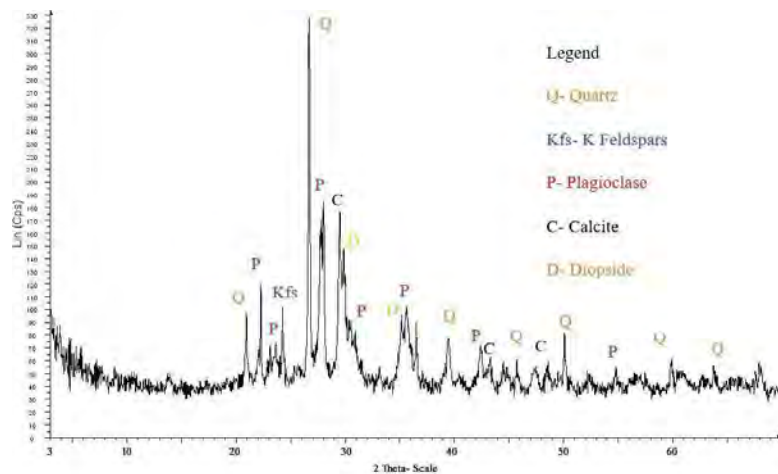




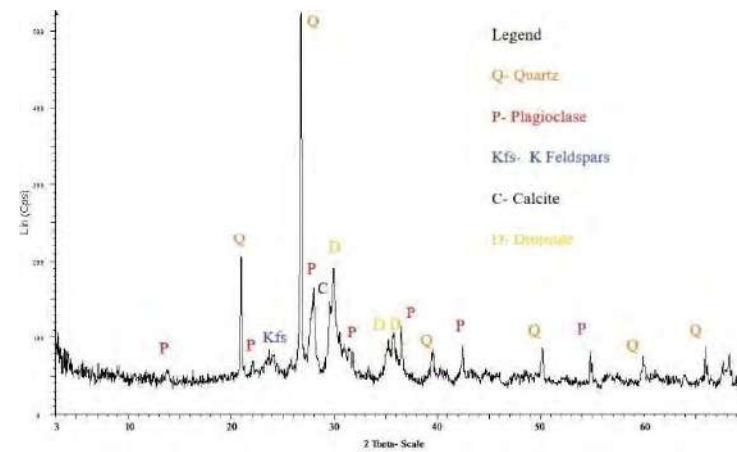
Sample 4.8



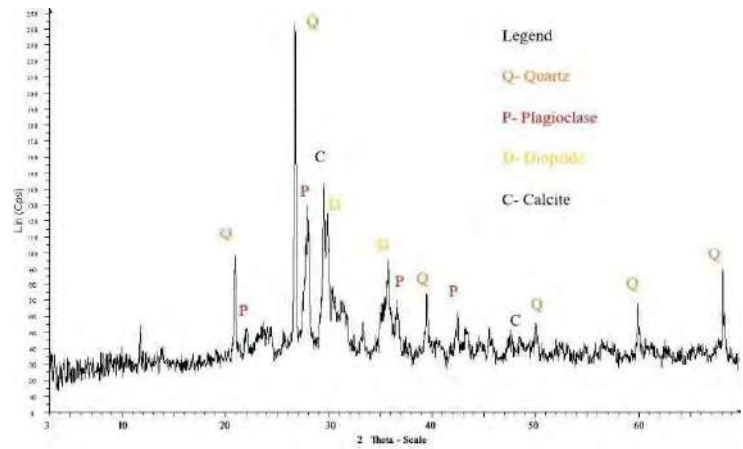
Sample 4.9



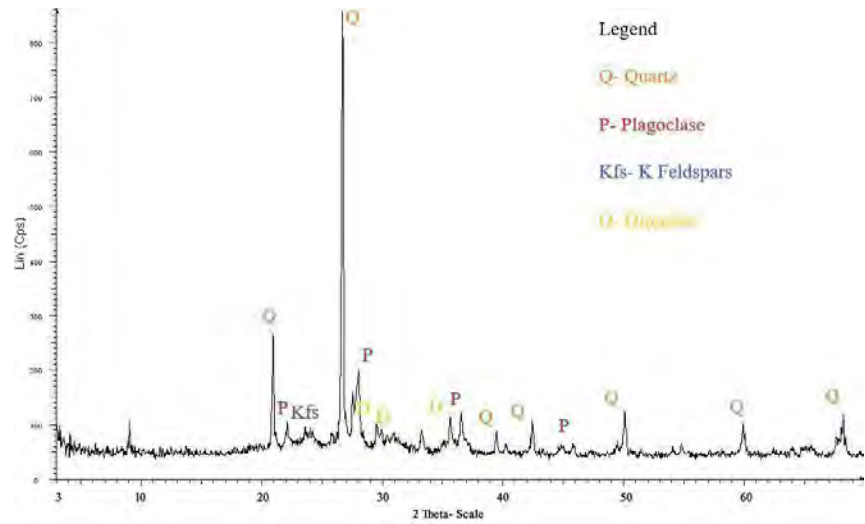
Sample C03



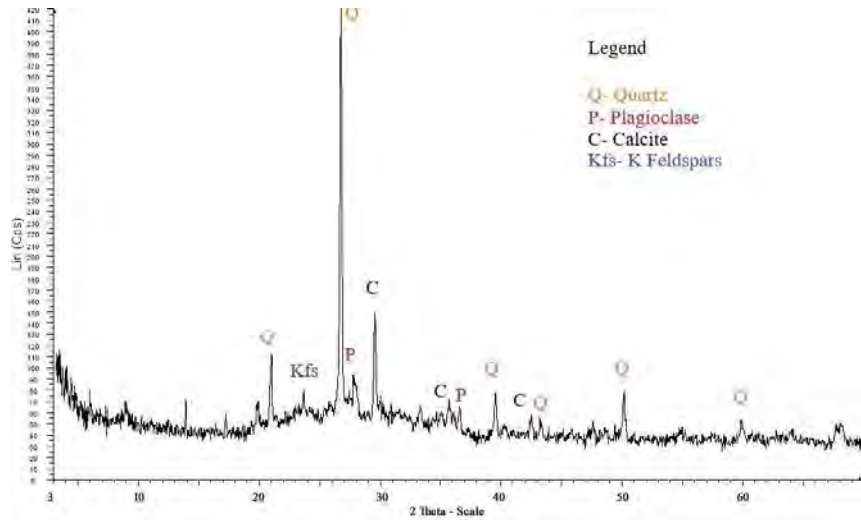
Sample C06



Sample C07

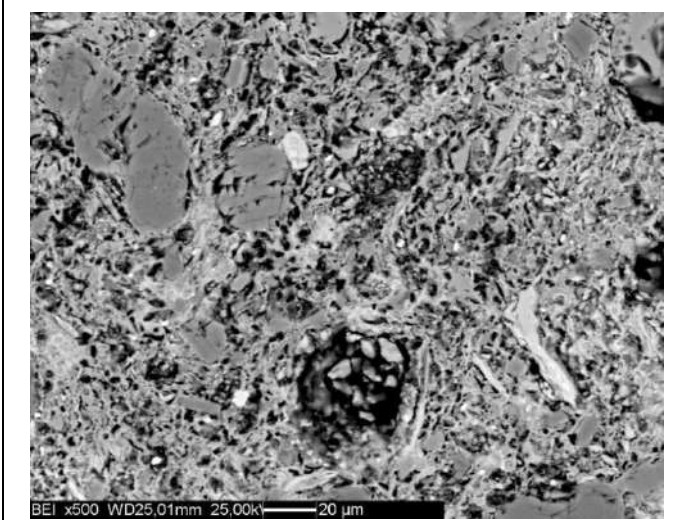


Sample 2.9

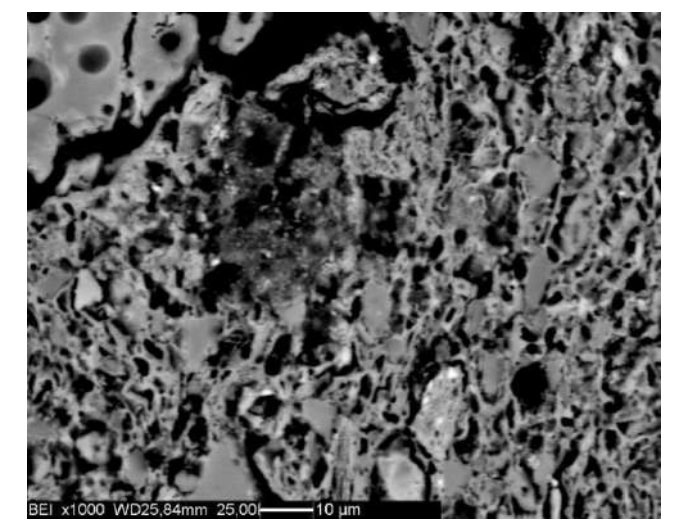


Sample 2.4

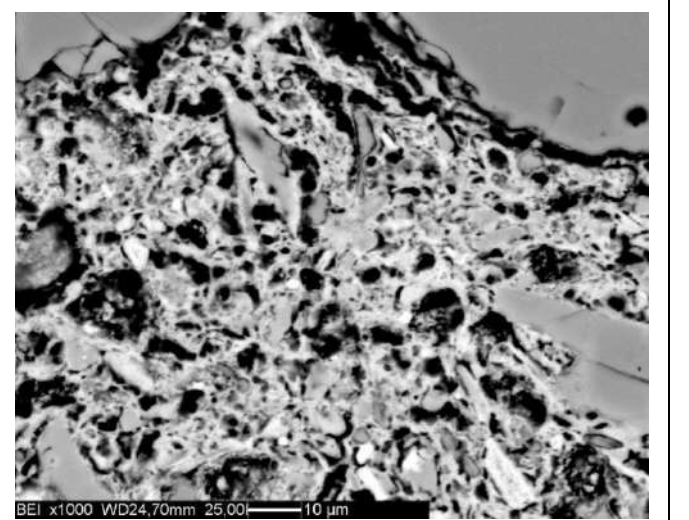
Appendix 7: BSE SEM Images of Polished Thin Sections



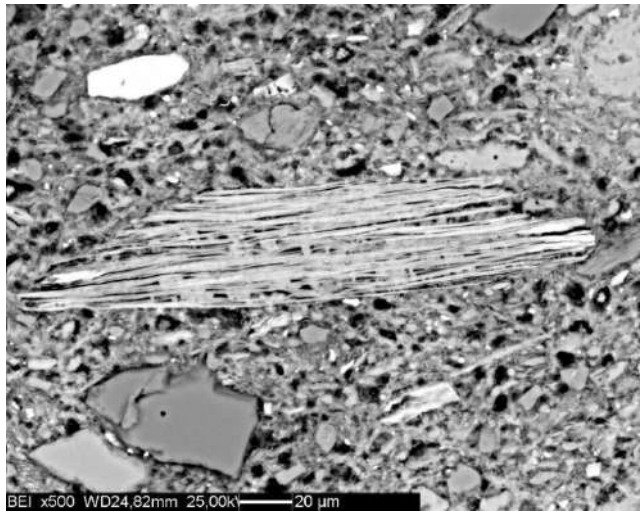
Sample 1.3.2



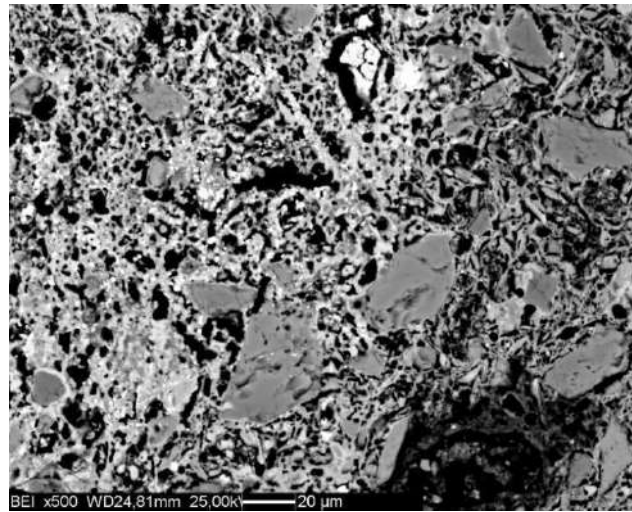
Sample 1.4.2



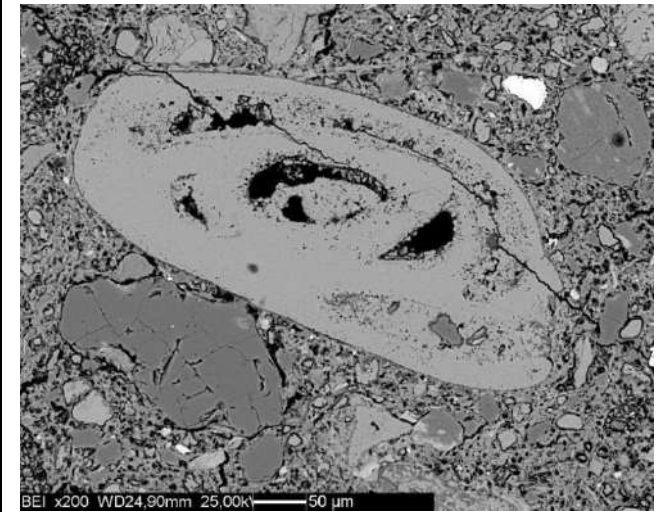
Sample 1.5



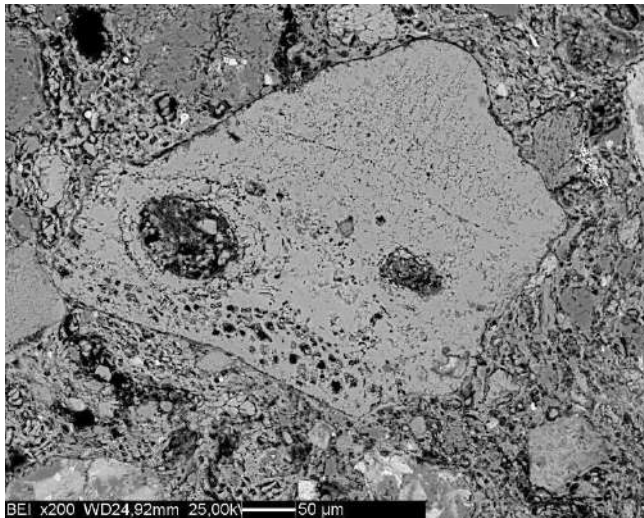
Sample 1.7.1



Sample 1.7.2



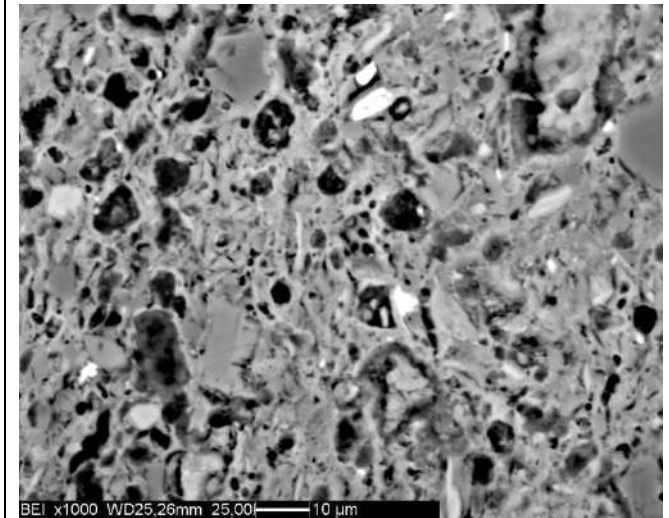
Sample 1.9



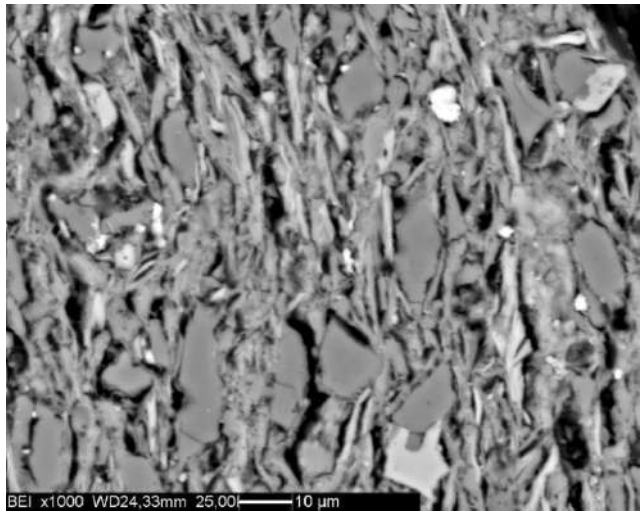
Sample 1.9



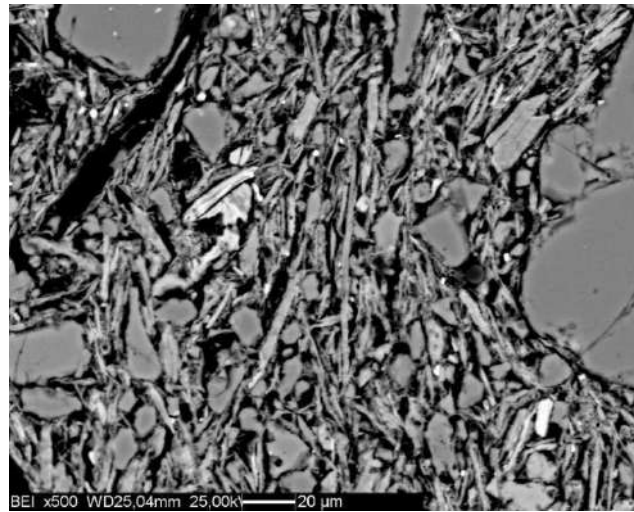
Sample 1.9



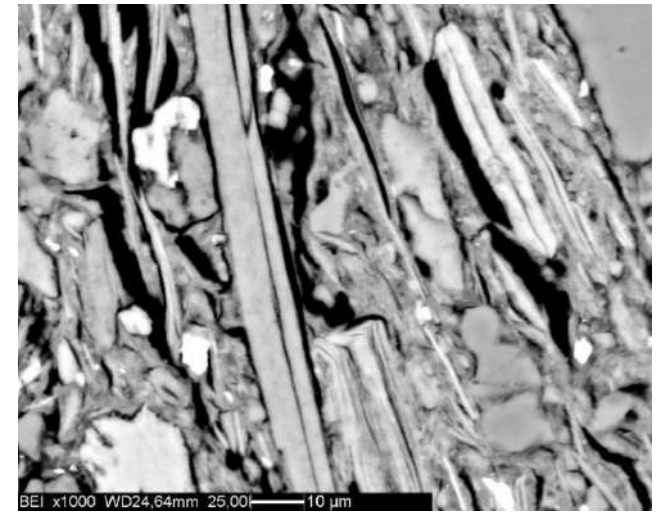
Sample 2.4



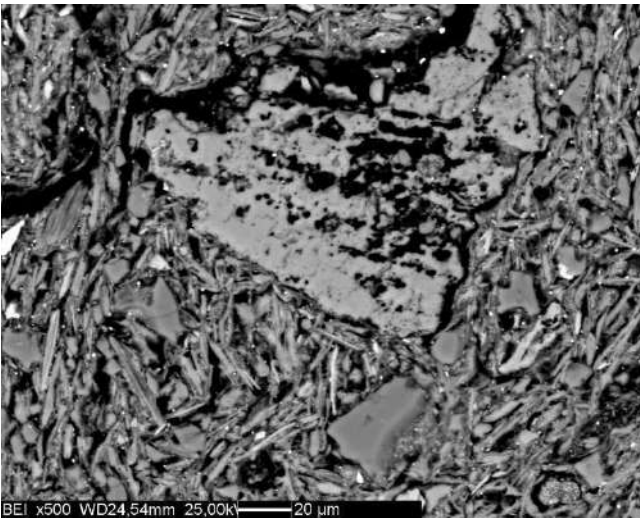
Sample 2.5



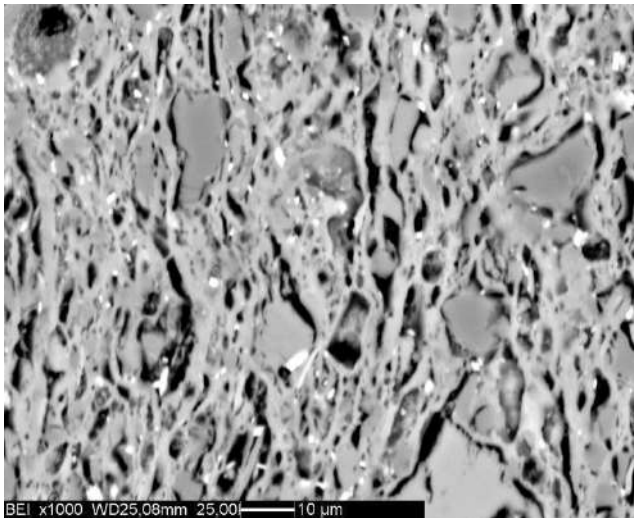
Sample 2.6



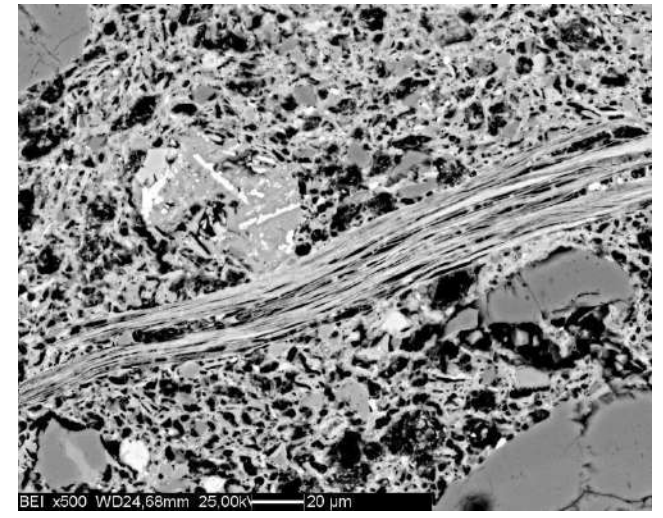
Sample 2.7



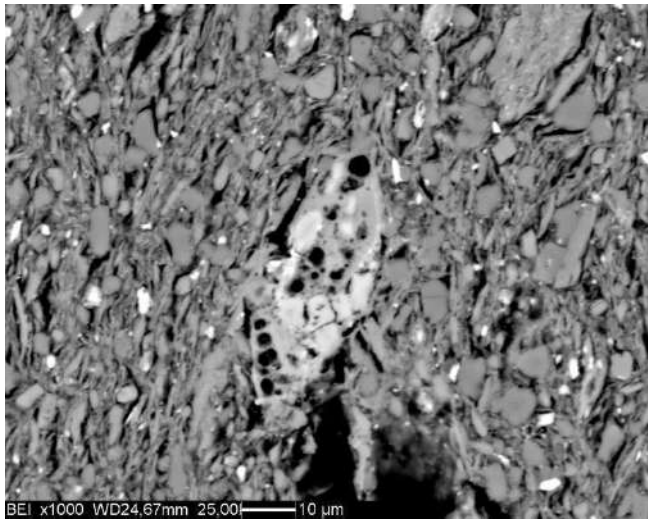
Sample 2.8



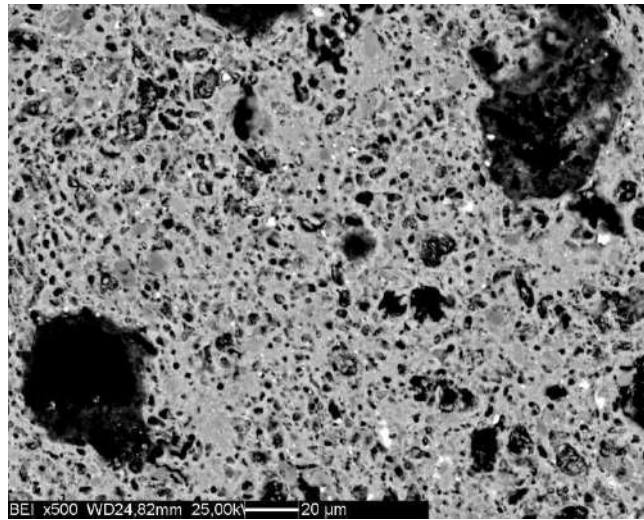
Sample 2.9



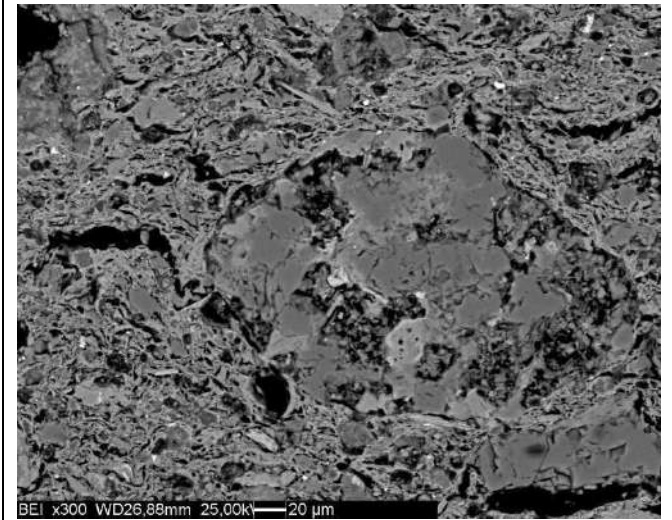
Sample 3.6



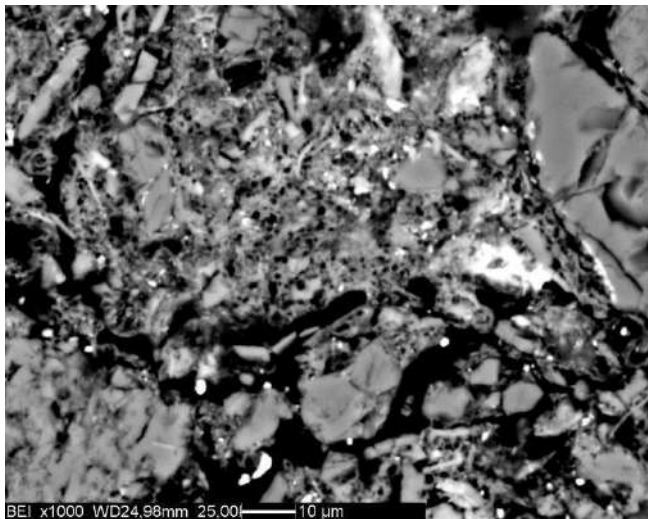
Sample 4.6



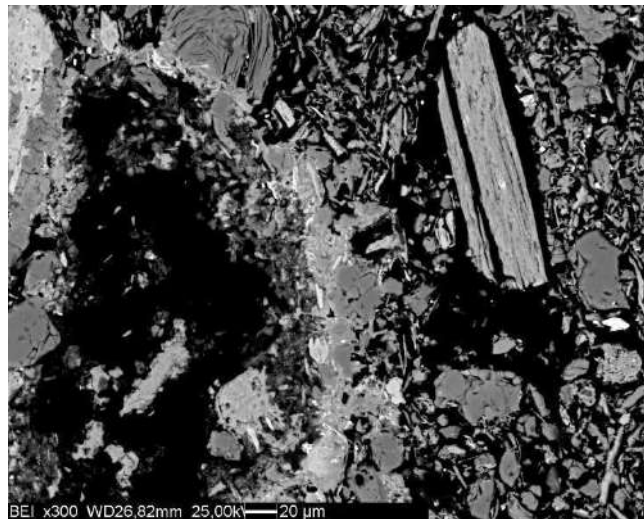
Sample 4.8



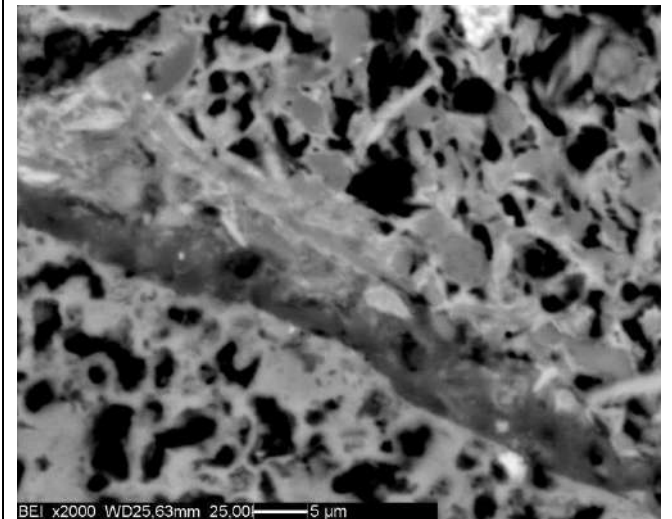
Sample 4.9



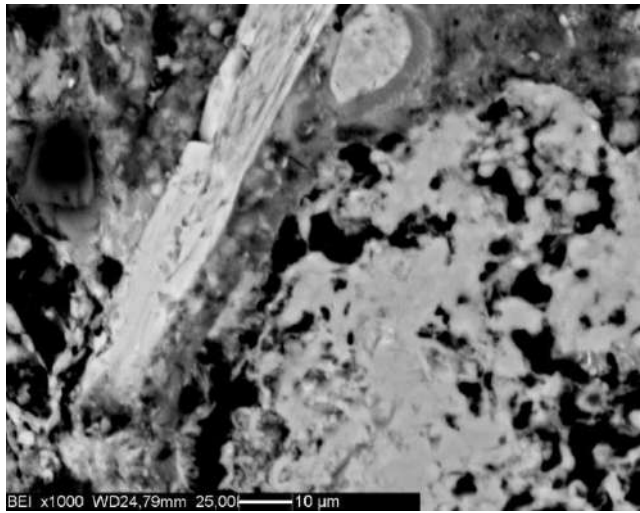
Sample 4.10



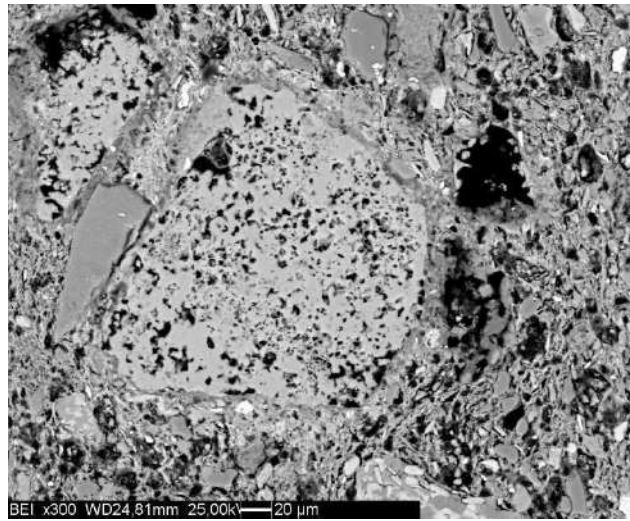
Sample 4.11



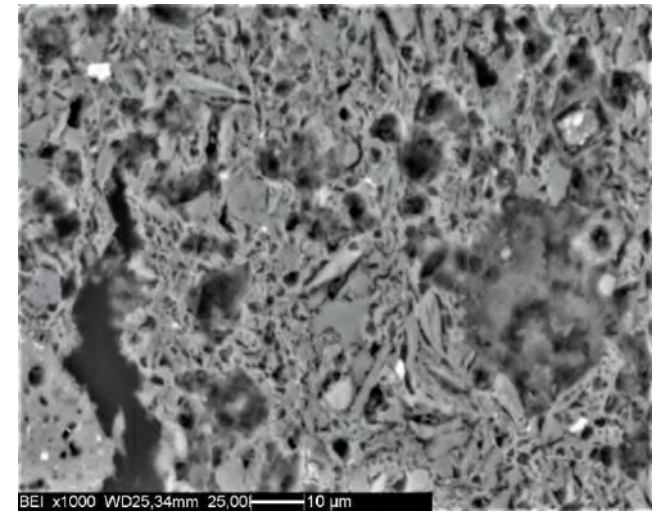
Sample C02



Sample C03

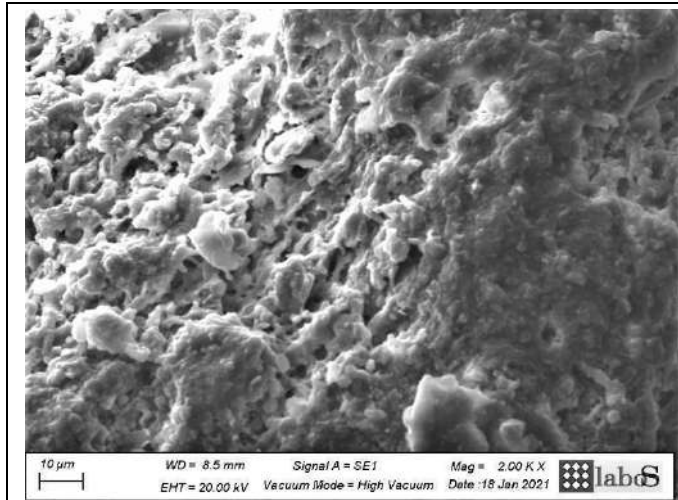


Sample C06

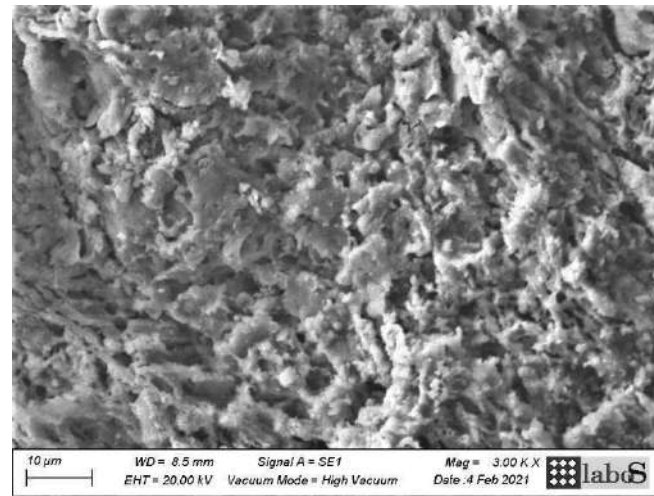


Sample C08

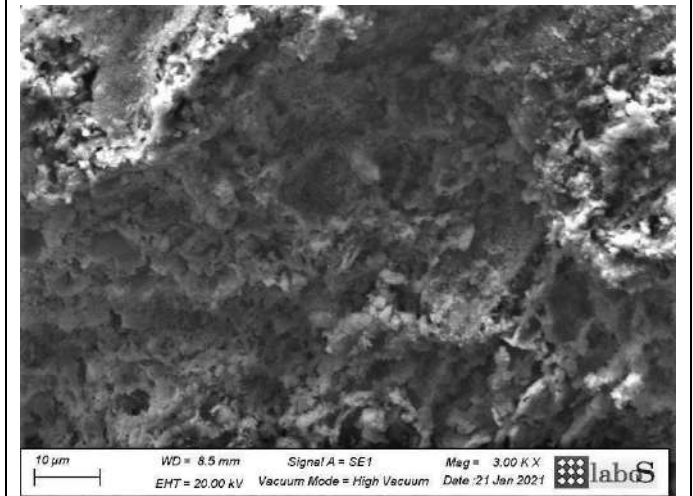
Appendix 8: SEM SE Images of Fractures



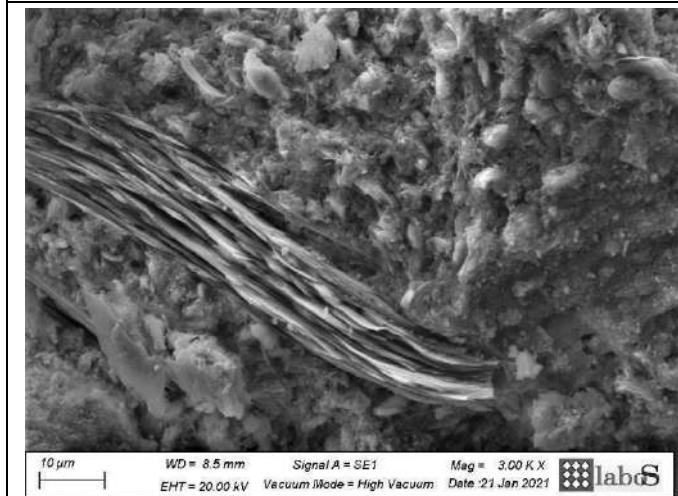
Sample 1.3.2



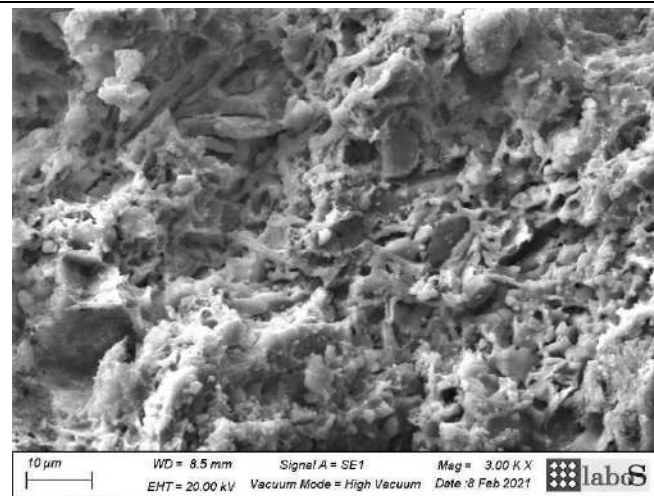
Sample 1.4.2



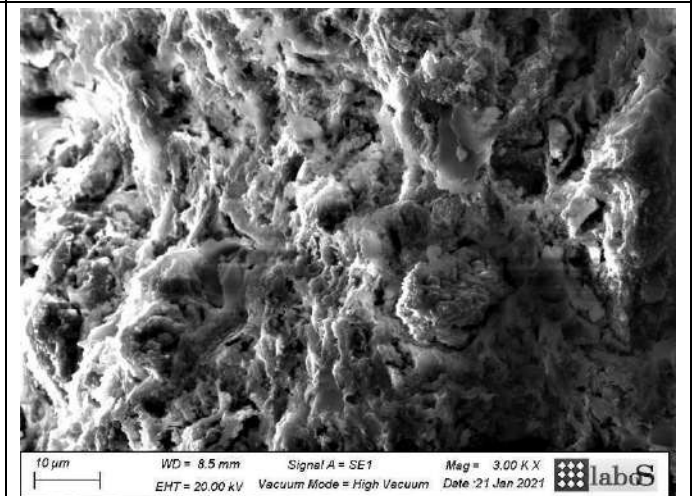
Sample 1.5



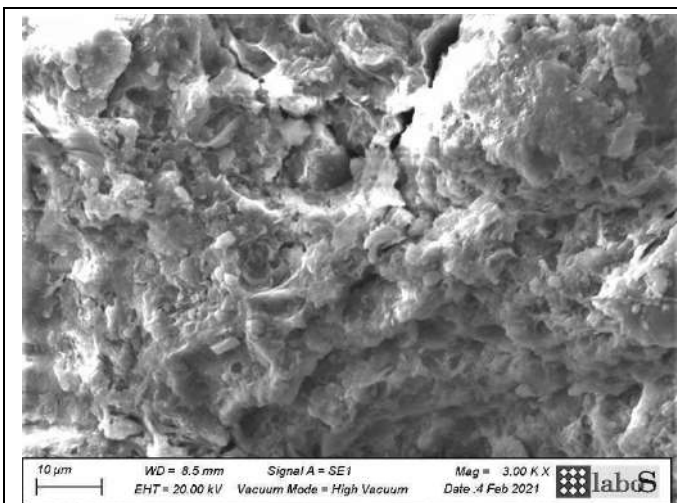
Sample 1.7.1



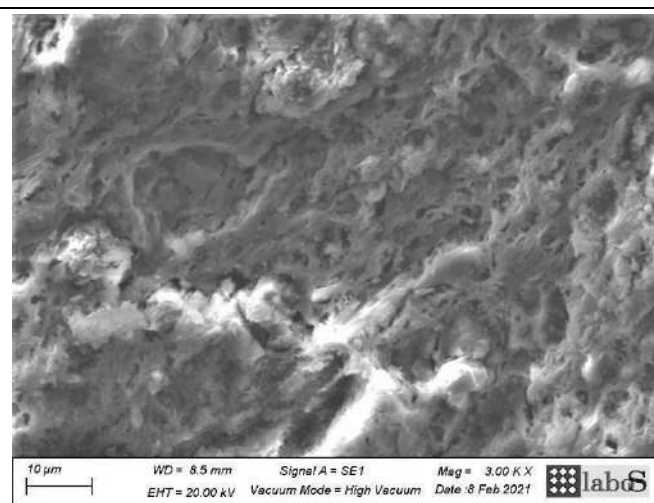
Sample 1.7.2



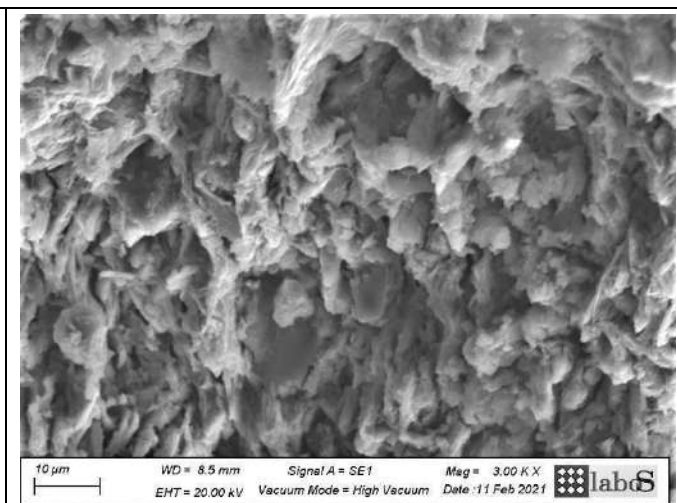
Sample 1.9



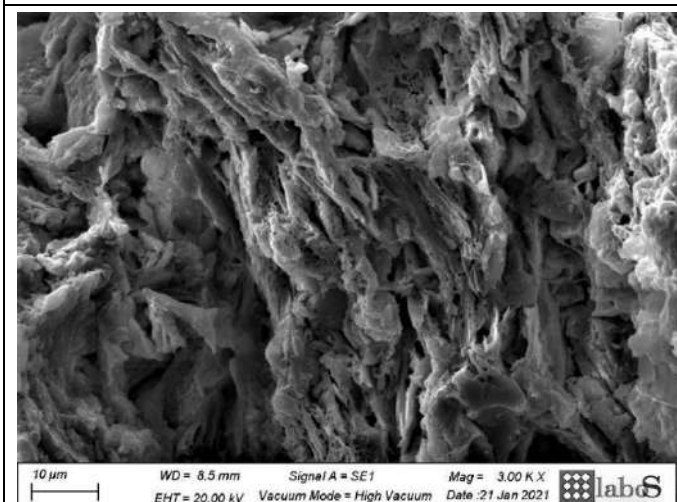
Sample 2.3



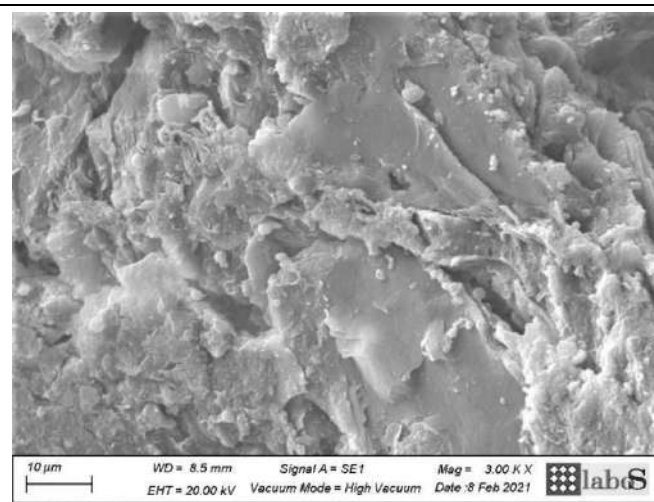
Sample 2.4



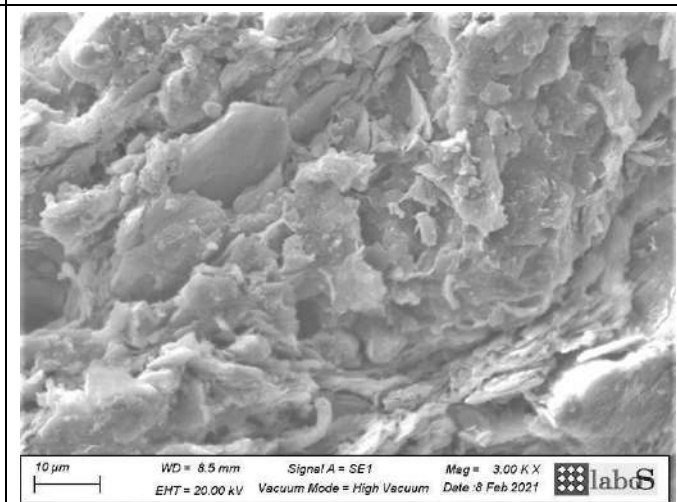
Sample 2.5



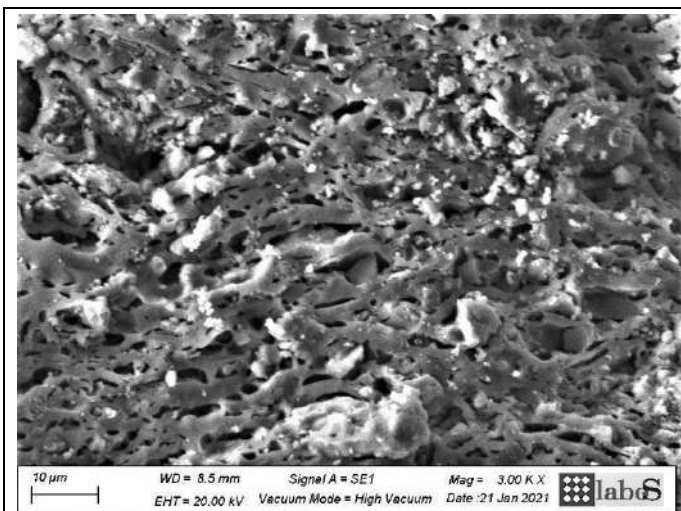
Sample 2.6



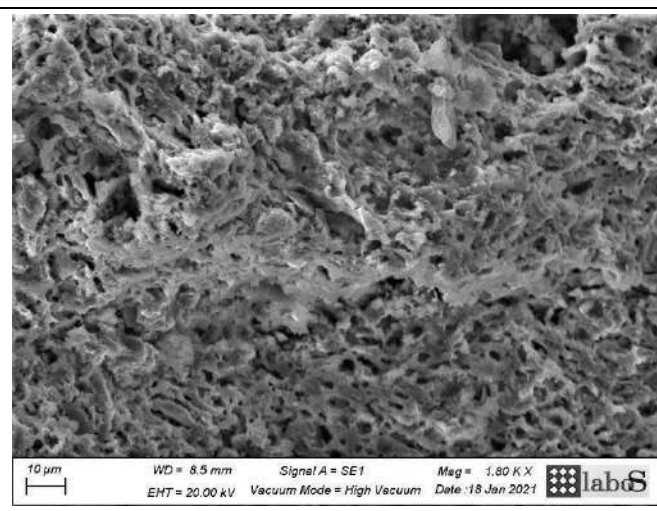
Sample 2.7



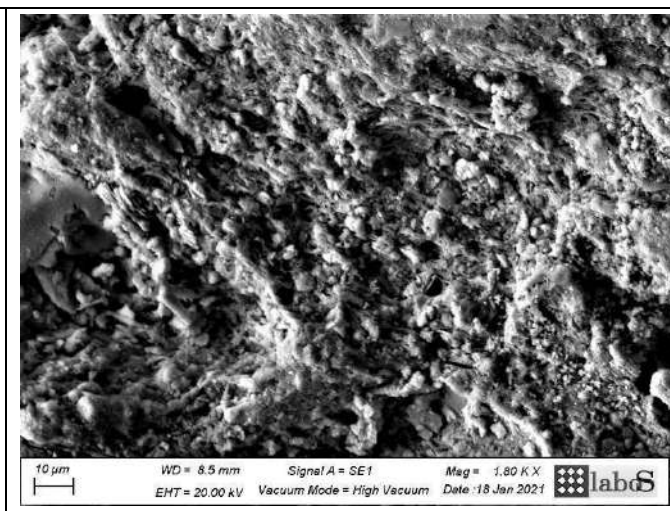
Sample 2.8



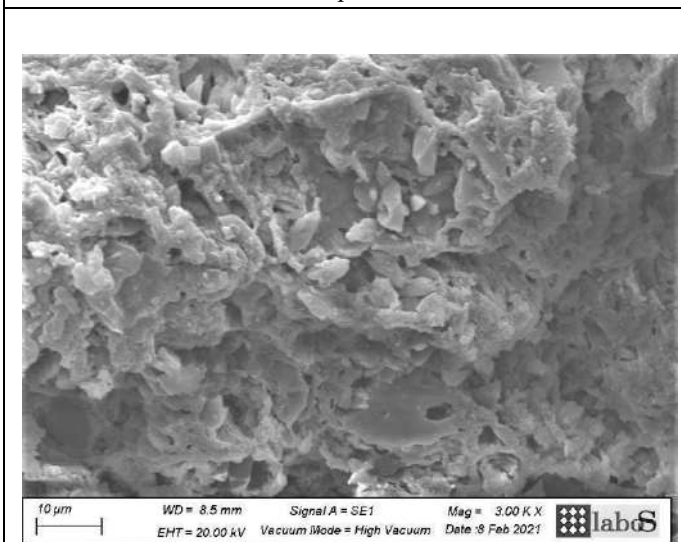
Sample 2.9



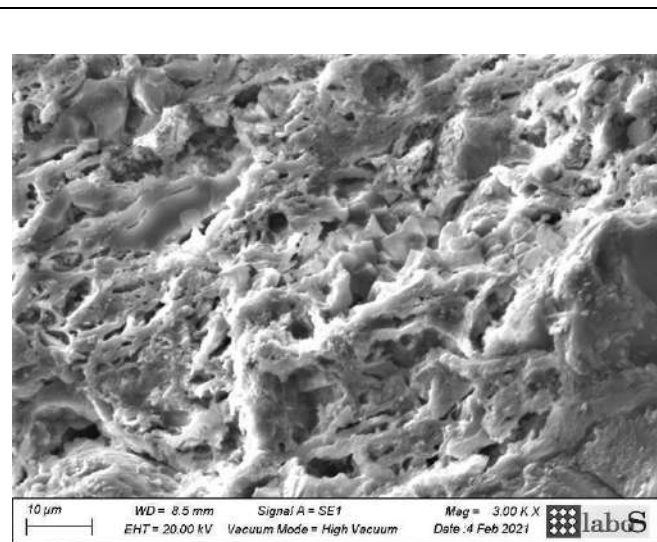
Sample 3.6



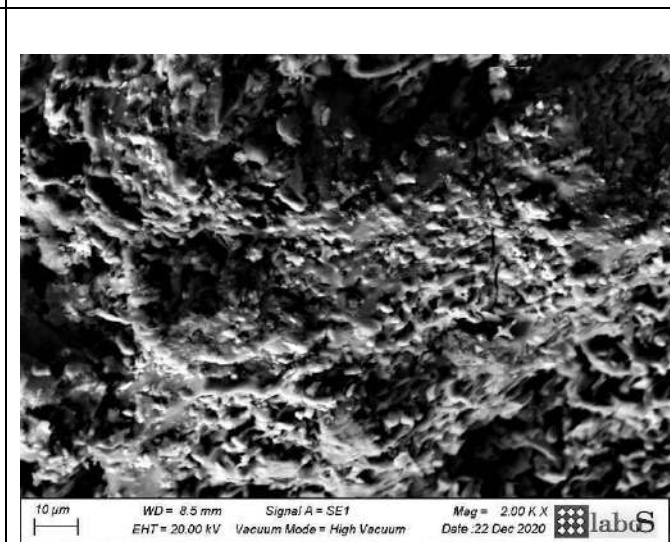
Sample 4.6



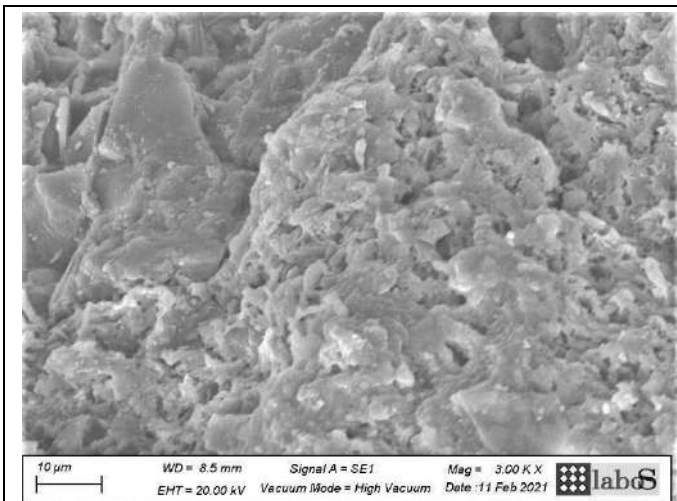
Sample 4.8



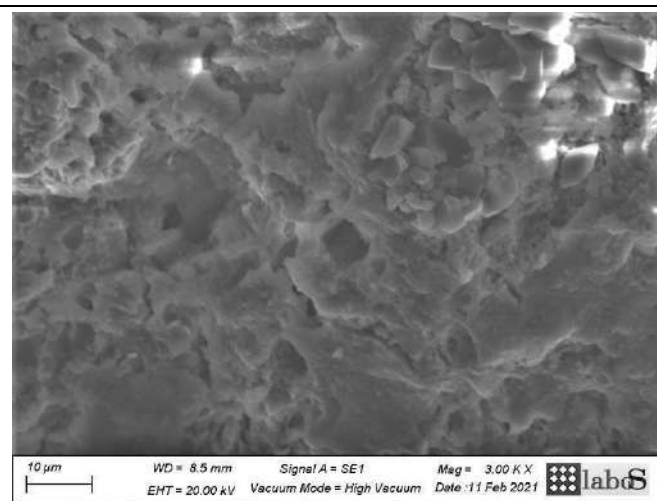
Sample 4.9



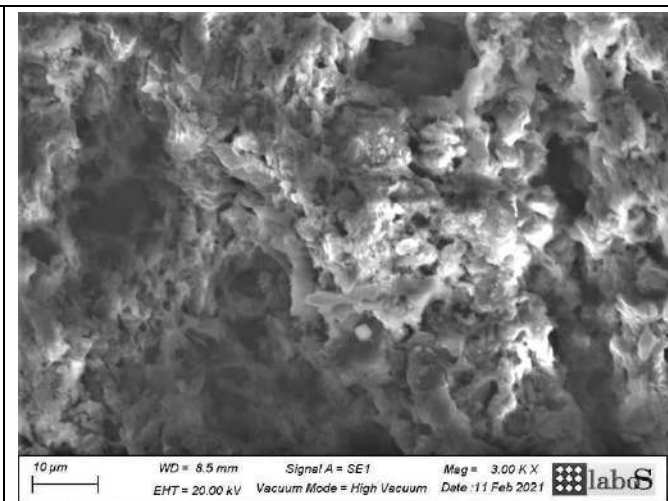
Sample 4.10



Sample C02

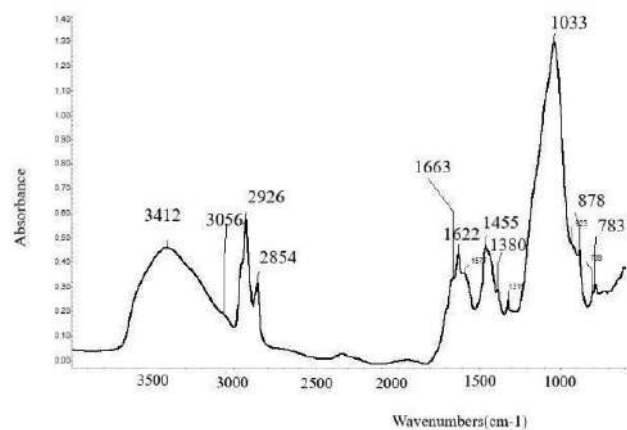


Sample C03

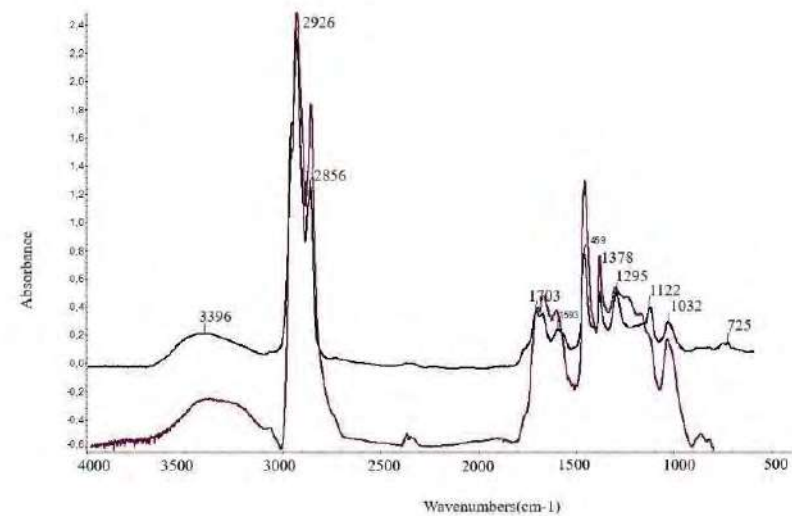


Sample C06

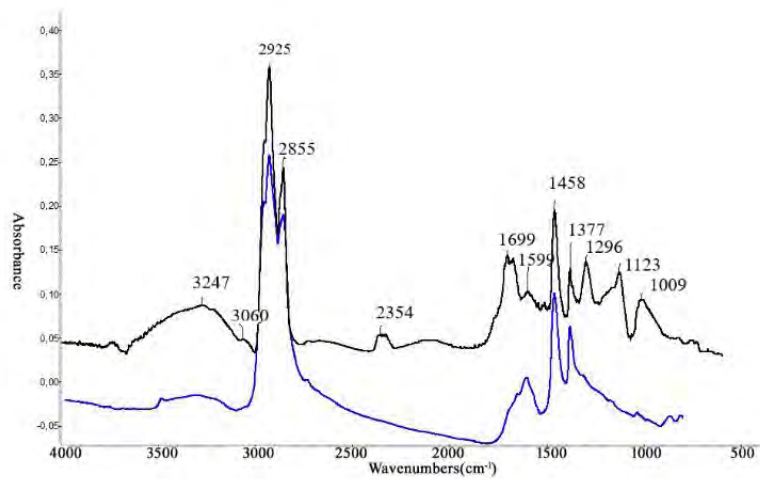
Appendix 9: FT-IR Spectra of Extracts



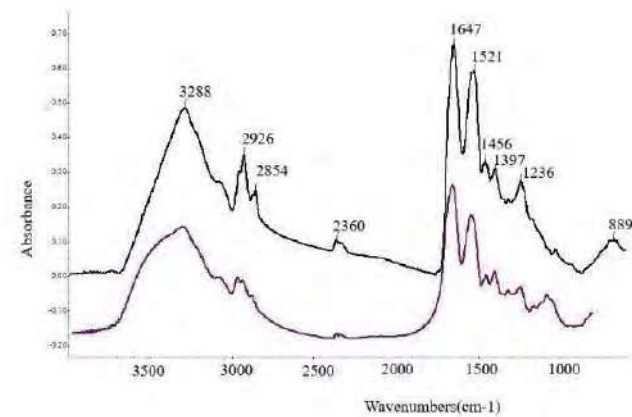
C03, spectrum of the extract in dichloromethane



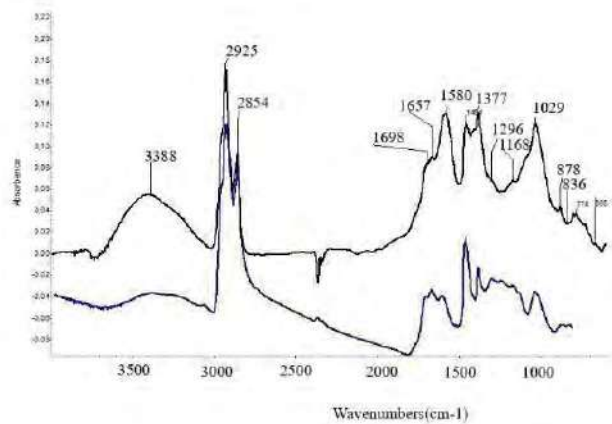
C03, in black is the spectrum of the extract in methanol and in violet is the spectrum of bitumen from database.



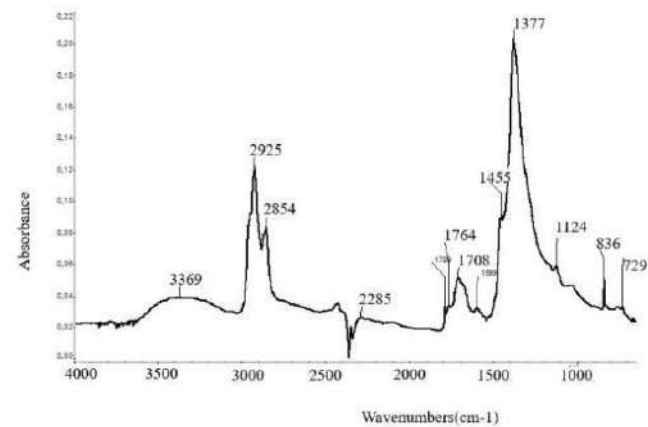
CO3, in black is the spectrum of the extract in acetone and in blue is the spectrum of bitumen from database.



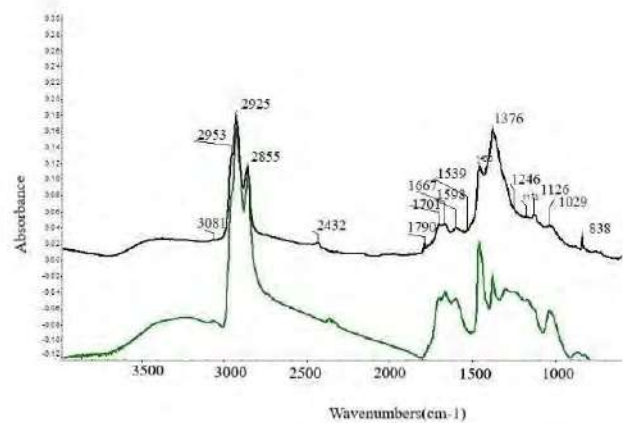
CO6, in black is the spectrum of the extract in dichloromethane and in violet is the spectrum of a Proteinaceous substance.



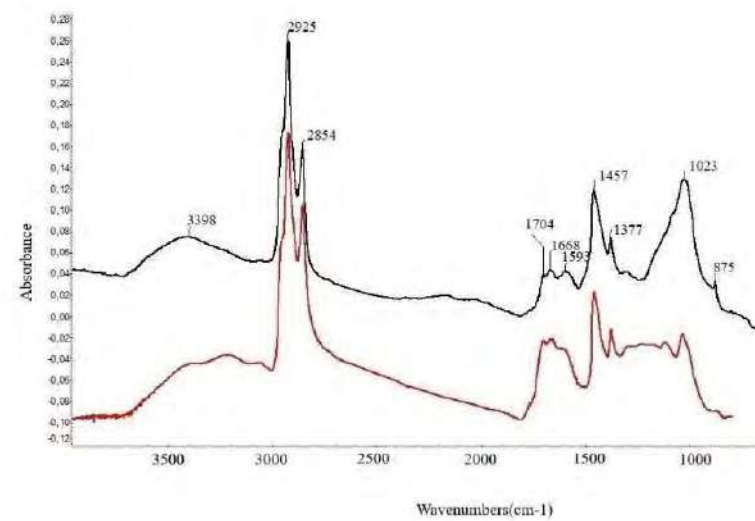
C06, in black is the spectrum of the extract in methanol and in blue the spectrum of bitumen from database.



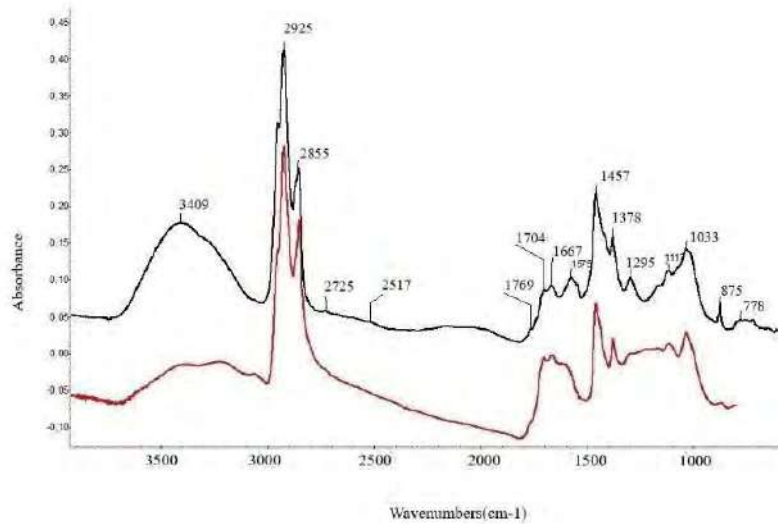
C06, spectrum of extract in acetone.



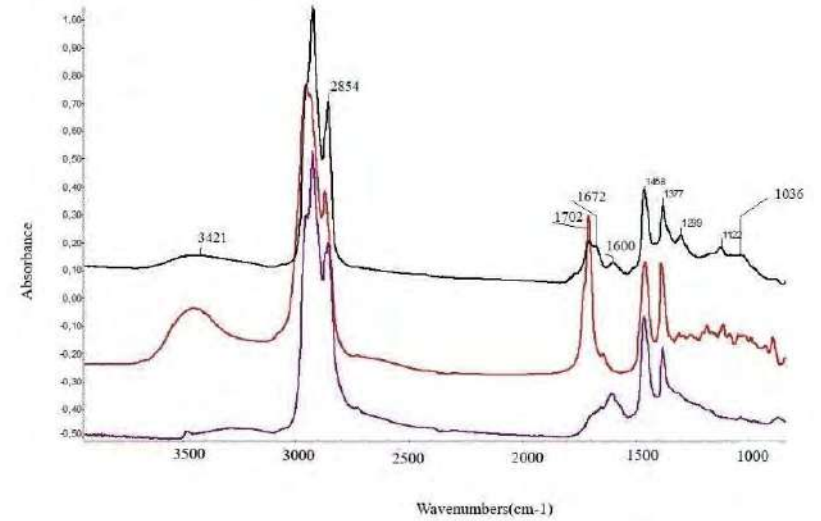
C07, in black is the spectrum of the extract in acetone and in green is the spectrum of bitumen from database



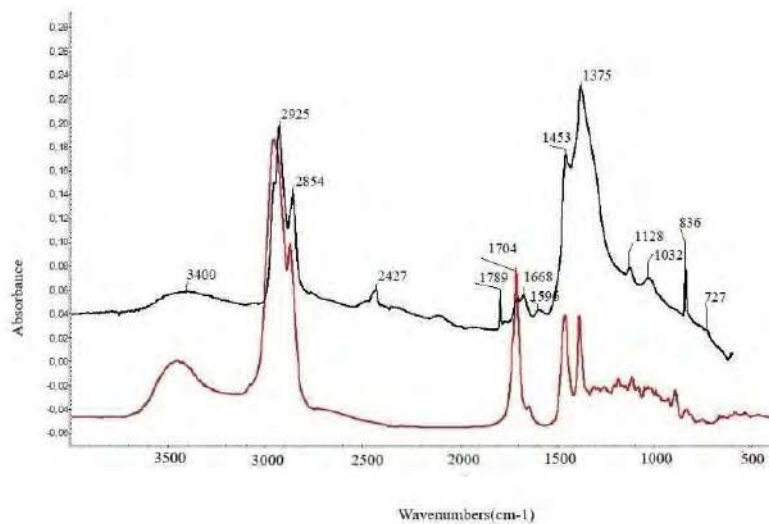
C07, in black is the spectrum of the extract in dichloromethane and in red is the spectrum of bitumen from database.



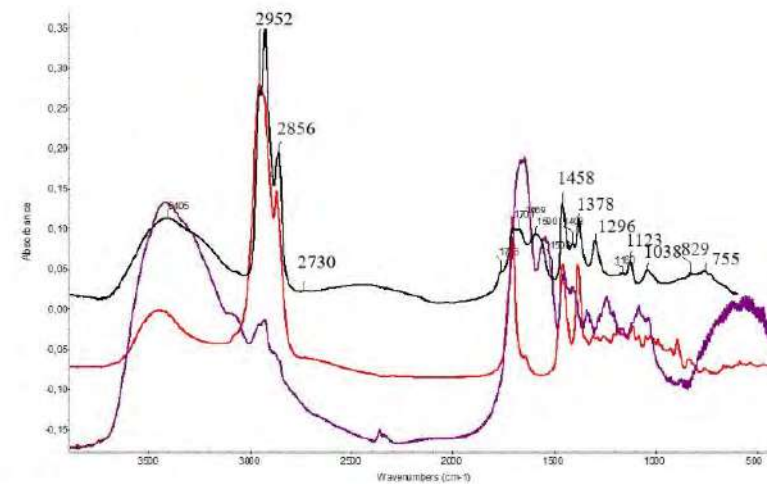
C07, in black is the spectrum of the extract in methanol and in red is the spectrum of bitumen from database.



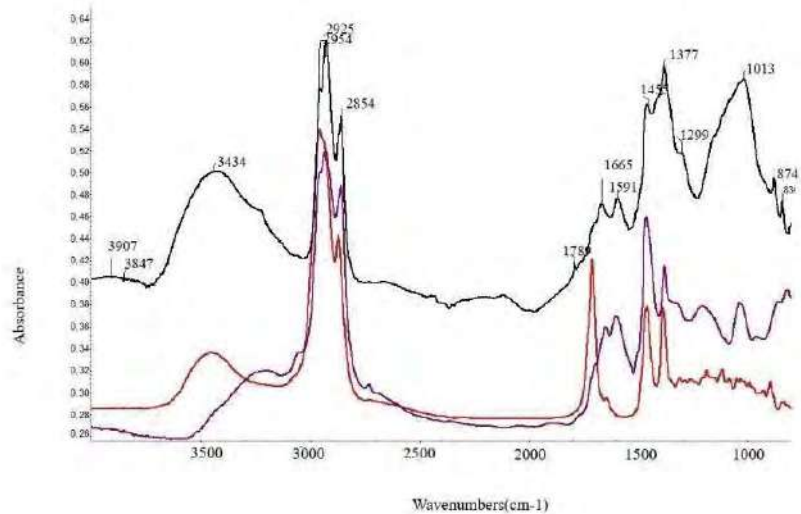
C08, in black the spectrum of the extract in acetone, in dark violet is the spectrum of a bitumen reference material and in red is the spectrum of dammar resin from database.



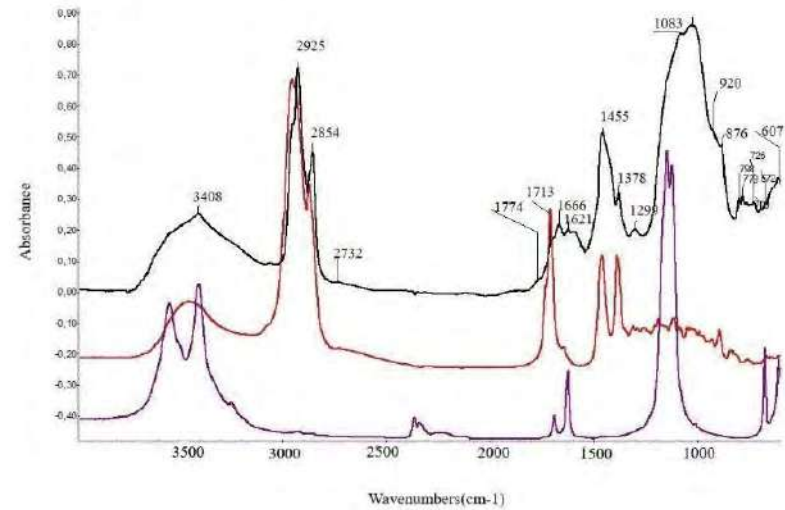
C09, in black is the spectrum of an extract in acetone, in red a reference spectrum of dammar resin, as an example of natural resin. Moreover, the signals of carbonates and silicates are present.



C08, in black the spectrum of the extract in methanol, in dark violet is the spectrum of animal glue as an example of proteinaceous material and in red is the spectrum of dammar resin from database.



C09, In black the spectrum of the extract in methanol, in dark violet a reference spectrum of a bitumen, as an example of natural resin and in red a reference spectrum of dammar resin. Moreover, the signals of carbonates and silicates are present.



C09, in black is the spectrum of the extract in dichloromethane, in dark violet a reference spectrum of gypsum and in red a reference spectrum of dammar resin, as an example of natural resin. Moreover, the signals of carbonates and silicates are present.

Appendix 10: SEM-EDX Data on the Bulk

Name	Class	Na ₂ O(wt %)	MgO(wt%)	Al ₂ O ₃ (wt%)	SiO ₂ (wt%)	SO ₃ (wt%)	P ₂ O ₅ (wt%)	K ₂ O(wt%)	CaO(wt%)	TiO ₂ (wt%)	Fe ₂ O ₃ (wt%)	
1.3(2)	Ayla	2.9±0.1	2.4±0.1	15.0±0.1	53.8±0.1	0.7±0.03	2.1±0.1	2.1±0.1	13.7±0.1	0.8±0.1	5.7±0.1	
1.4(2)	Ayla	2.4±0.1	3.0±0.1	16.1±0.2	65.1±0.4	0.5±0.04	0.36±0.02	2.1±0.2	12.8±0.3	0.82±0.03	6.8±1.0	
1.5	Ayla	2.3±0.1	4.0 ±0.1	15.5±0.1	50.7±0.1	0.8±0.1	0.47±0.04	1.5±0.1	16.3±0.1	0.8±0.1	7.4±0.2	
1.7(1)	Ayla	1.6±0.1	3.2±0.1	18.0±0.2	60.6±0.4	0.9±0.1	0.62±0.03	3.0±0.2	12.6±0.3	0.63±0.04	8.9±1.0	
1.7(2)	Ayla	1.9±0.1	3.3±0.1	14.4±0.1	58.1±0.2	0.59±0.03	0.48±0.03	2.1±0.1	11.6±0.1	1.0±0.1	6.8±0.2	
3.6	Ayla	2.3±0.1	2.53±0.04	15.6±0.1	55.2±0.1	0.32±0.04	0.58±0.03	2.1±0.1	14.6±0.1	0.82±0.1	6.3±0.1	
2.5	Local	1.3 ±0.1	2.9±0.1	20.67±0.1	57.7±0.1	0.20±0.04	0.88±0.02	1.3±0.2	3.38 ±0.0	1.53±0.03	10.6±0.2	
2.6	Local	2.74±0.04	2.82±0.04	19.4±0.1	59.0±0.1	1.02±0.03	0.77±0.03	3.1±0.1	2.3±0.1	0.97±0.04	8.2±0.1	
2.7	Local	2.18±0.04	3.07±0.03	17.2±0.1	59.0±0.1	0.50±0.03	0.68±0.03	3.0±0.1	2.3±0.1	1.2±0.1	11.7±0.8	
2.8	Local	2.6±0.1	3.4±0.1	19.4±0.1	57.0±0.1	0.59±0.03	0.85±0.04	3.7±0.1	3.3±0.1	0.9±0.1	8.8±0.1	
2.9	ND	1.4±0.1	2.3±0.1	17.9±0.1	58.2±0.1	0.62±0.03	0.7±0.1	2.8±0.1	8.7±0.1	0.8±0.1	6.7±0.1	
1.9	LRA1	2.2±0.1	5.6±0.1	14.5±0.2	59.0±0.4	0.68±0.04	0.34±0.03	2.4±0.2	19.7±0.4	0.66±0.04	9.0±1.1	
2.3	LRA1	2.7±0.1	3.6±0.1	12.3±0.1	53.8±0.2	0.46±0.03	0.18±0.02	3.2±0.1	16.4±0.1	0.6±0.1	6.3±0.2	
2.4	ND	1.1±0.1	3.4±0.1	18.4±0.2	56.3±0.4	0.3±0.1	1.40±0.03	3.0±0.2	14.7±0.3	0.67±0.04	8.2±1.0	
C02	LRA1(?)	2.0±0.1	4.9±0.1	12.9±0.2	66.4±0.4	1.5±0.1	2.4±0.1	2.1±0.2	9.8±0.3	1.29±0.04	6.8±1.0	
C03	LRA1(?)	2.2±0.1	6.0±0.1	12.5±0.1	53.9±0.1		0.65±0.04	1.6±0.1	14.8±0.1	0.8±0.1	6.81±0.2	
C06	LRA1(?)	1.9±0.1	5.40±0.04	12.2±0.1	54.7±0.1	1.06±0.04	0.60±0.03	0.63±0.03	2.0±0.1	14.4±0.1	0.7±0.1	6.9±0.1
4.8	<i>Dolia</i>	1.5±0.1	5.4± 0.1	19.0±0.1	48.8±0.1		0.74±0.04	2.7±0.1	12.4±0.1	1.1±0.1	7.1±0.1	
4.9	<i>Dolia</i>	1.33±0.04	6.95±0.04	16.4±0.1	48.1±0.1	0.80±0.04	0.53±0.02	0.60±0.03	2.4±0.1	15.4±0.1	0.99±0.04	8.0±0.1
4.10	Brick	3.7±0.1	3.0±0.1	18.1±0.2	70.5±0.4	0.55±0.02	0.37±0.03	3.0±0.1	4.2±0.2	0.91±0.03	7.3±0.8	
4.11	Brick	3.2±0.1	3.2±0.1	20.2±0.2	67.2±0.5	1.22±0.03	0.7±0.02	3.1±0.2	4.8±0.2	0.85±0.03	7.4±1.1	
4.6	Red Slip	1.22±0.03	0.79±0.03	27.0±0.1	60.1±0.1	0.33±0.03	0.64±0.03	1.09±0.03	0.87±0.03	2.14±0.04	5.8±0.1	

Appendix 11: SEM-EDX Data on the Matrices

Name	Class	Na ₂ O(wt %)	MgO(wt%)	Al ₂ O ₃ (wt%)	SiO ₂ (wt%)	SO ₃ (wt%)	P ₂ O ₅ (wt%)	K ₂ O(wt%)	CaO(wt%)	TiO ₂ (wt%)	Fe ₂ O ₃ (wt%)
1.3(2)	Ayla	2.6±0.1	2.8±0.1	16.4±0.1	49.5±0.1	0.78±0.03	2.0±0.1	2.1±0.1	15.9±0.1	0.9±0.1	6.6±0.1
1.4(2)	Ayla	1.6± 0.1	4.2±0.1	18.2±0.2	54.4±0.4	0.40±0.03	0.61±0.02	1.3±0.2	17.3±0.3	0.99±0.0	10.8±1.0
1.5	Ayla	1.9±0.1	4.3±0.1	15.9±0.1	49.8±0.1	0.8±0.1	0.52±0.04	1.1±0.1	17.2±0.1	0.9±0.1	7.9±0.2
1.7(1)	Ayla	1.3±0.1	4.0±0.1	20.3±0.2	58.3±0.4	0.5±0.1	0.56±0.03	3.2±0.2	11.3±0.3	1.00±0.0	10.0±1.0
1.7(2)	Ayla	2.0±0.1	3.8±0.1	15.0±0.1	53.8±0.2	0.68±0.03	0.67±0.03	1.9±0.1	13.8±0.1	0.9±0.1	7.8±0.2
3.6	Ayla	1.7±0.1	3.57±0.04	17.7±0.1	46.5±0.1	0.31±0.04	0.65±0.03	1.5±0.1	19.4±0.3	1.06±0.4	8.3±0.1
2.5	Local	1.1±0.1	3.2±0.1	22.7±0.1	55.1±0.1	0.18±0.04	0.92±0.02	1.6±0.2	3.4±0.1	1.33±0.03	11.3±0.2
2.6	Local	3.07±0.04	2.97±0.03	21.1±0.1	58.1±0.1	0.65±0.03	0.66±0.03	3.1±0.1	1.9±0.1	0.76±0.04	8.2±0.1
2.7	Local	1.68±0.04	4.03±0.04	19.5±0.1	53.2±0.1	0.26±0.03	0.68±0.03	4.0±0.1	2.1±0.1	1.3±0.1	14.4±0.8
2.8	Local	2.8±0.1	3.7±0.1	21.8±0.1	54.4±0.1	0.45±0.03	0.77±0.04	4.0±0.1	2.9±0.1	0.6±0.1	9.2±0.1
2.9	ND	1.7±0.1	2.6±0.1	20.8±0.1	57.4±0.2	0.52±0.03	0.3±0.1	3.4±0.1	5.2±0.1	0.9±0.1	7.7±0.1
1.9	LRA1	1.9±0.1	6.6±0.1	16.5±0.2	57.5±0.4	0.81±0.04	0.50±0.03	2.9±0.2	12.9±0.4	0.97±0.04	13.0±1.1
2.3	LRA1	2.9±0.1	3.6±0.1	13.8±0.1	52.6±0.2	0.51±0.03	0.1±0.02	3.4±0.1	14.4±0.1	0.66±0.0	7.6±0.2
2.4	ND	1.0±0.1	3.5±0.1	20.5±0.2	58.7±0.4	0.34±0.1	0.59±0.03	3.4±0.2	12.7±0.3	0.7±0.1	8.4±0.5
C02	LRA1(?)	1.3±0.1	8.1±0.1	17.9±0.2	63.1±0.4	4.06±0.1	2.04±0.1	2.6±0.2	17.3±0.3	2.33±0.04	10.6±1.0
C03	LRA1(?)	1.4±0.1	6.5±0.1	13.4±0.1	46.9±0.1	4.46±0.04	0.62±0.04	1.4±0.1	17.7±0.1	0.7±0.1	7.3±0.2
C06	LRA1(?)	1.7±0.1	6.43±0.0	13.5±0.1	48.4±0.1	0.62±0.1	0.69±0.03	1.8±0.1	17.6±0.1	0.9±0.1	7.8±0.1
4.8	Dolia	1.3±0.1	8.0±0.1	15.0±0.1	48.9±0.1	0.70±0.04	0.85±0.03	1.5±0.1	16.9±0.1	0.9±0.1	6.0±0.1
4.9	Dolia	1.30±0.04	6.60±0.04	17.8±0.1	47.1±0.1	0.46±0.02	0.68±0.03	2.6±0.1	14.6±0.1	1.05±0.03	8.4±0.1
4.10	Brick	3.2±0.1	3.8±0.1	19.2±0.2	67.6±0.4	0.40±0.02	0.67±0.02	3.2±0.2	3.8±0.2	0.68±0.0	9.3±0.1
4.11	Brick	2.8±0.1	3.7±0.1	22.9±0.2	63.7±0.5	1.28±0.03	0.59±0.02	3.6±0.2	5.8±0.2	0.78±0.03	8.8±1.1
4.6	Red Slip	1.26±0.03	0.69±0.03	28.1±0.1	60.0±0.1	0.36±0.03	0.65±0.03	1.1±0.1	0.5±0.1	2.07±0.04	5.2±0.1

Appendix 12: ICP-OES Data of Major, Minor and Trace Elements

Class	Name	Al ₂ O ₃ (wt%)	CaO(wt%)	Fe ₂ O ₃ (wt%)	K ₂ O(wt%)	MgO(wt%)	Na ₂ O(wt%)	Ba(ppm)	Cr(ppm)
Ayla	1.3(2)	18.3±0.1	14.54±0.03	7.0±0.1	2.67±0.02	3.34±0.01	2.77±0.02	532.34±0.02	82.11±0.02
	1.4 (2)	13.1±0.1	12.22±0.04	5.2±0.1	1.61±0.02	2.73±0.01	1.70±0.04	434.77±0.02	67.80±0.02
	1.5	14.6±0.1	12.81±0.04	5.9±0.1	1.84±0.02	3.53±0.01	1.80±0.04	467.77±0.02	81.50±0.02
	1.7 (1)	14.5±0.1	12.7±0.04	5.4±0.1	2.29±0.02	2.61±0.01	1.85±0.04	627.89±0.02	69.26±0.02
	1.7(2)	13.8±0.1	9.4±0.04	5.5±0.1	2.23±0.02	3.33±0.01	2.1±0.02	566.37±0.02	72.0±0.02
	3.6	15.3±0.1	13.95±0.03	5.6±0.1	2.09±0.02	2.84±0.01	2.01±0.02	519.85±0.02	90.72±0.02
	CO4	16.3±0.1	13.8±0.04	6.2±0.1	2.46±0.02	3.04±0.02	2.15±0.02	495.21±0.02	92.26±0.02
LRA 1	1.9	11.4±0.1	20.4±0.1	8.1±0.1	1.38±0.02	4.69±0.02	1.95±0.04	305.63±0.02	566.37±0.02
	2.3	11.7±0.1	28.0±0.1	5.8±0.1	2.33±0.02	3.95±0.02	3.13±0.02	231.21±0.02	462.12±0.02
LRA 1(?)	C02	11.4±0.1	17.7±0.1	6.2±0.1	1.44±0.02	5.70±0.01	1.50±0.04	413.64±0.02	792.76±0.02
	C03	12.4±0.1	16.6±0.1	7.4±0.1	1.50±0.02	7.36±0.01	2.48±0.02	393.06±0.02	1040.48±0.02
	C06	13.9±1.1	17.0±0.1	7.2±0.1	2.12±0.02	7.18±0.01	2.63±0.02	348.77±0.02	379.76±0.02
	C07	12.5±0.1	15.80±0.04	7.6±0.1	1.67±0.02	6.93±0.01	3.15±0.02	315.18±0.02	1003.71±0.02
<i>Dolia</i>	4.8	17.3±0.1	16.00±0.04	6.8±0.1	2.19±0.02	6.26±0.02	1.20±0.02	238.18±0.02	183.74±0.02
	4.9	16.3±0.1	18.72±0.1	6.6±0.1	2.54±0.02	6.48±0.02	1.67±0.02	380.67±0.02	269.64±0.02
Red Slip	4.5	49.8±0.1	0.81±0.01	10.2±0.1	2.06±0.02	1.51±0.01	2.04±0.02	294.34±0.02	163.30±0.02
	4.6	23.3±0.1	0.63±0.01	5.0±0.1	1.10±0.02	0.85±0.01	0.59±0.02	170.95±0.02	155.81±0.02
ND	2.4	16.5±0.1	13.60±0.04	6.4±0.1	2.63±0.02	3.08±0.01	1.12±0.02	615.21±0.02	266.89±0.02
	2.9	16.40±0.04	9.30±0.03	7.2±0.1	2.25±0.02	3.03±0.01	1.57±0.04	369.04±0.02	231.45±0.02
Bricks	4.10	14.8±0.1	3.53±0.01	6.6±0.1	1.99±0.02	2.62±0.01	2.81±0.02	562.20±0.02	102.57±0.02
	4.11	17.9±0.1	3.28±0.01	7.5±0.1	2.45±0.02	3.04±0.01	2.85±0.02	694.64±0.02	101.66±0.02
Local	2.5	18.0±0.1	2.98±0.01	7.8±0.1	1.32±0.02	2.98±0.01	1.48±0.01	695.82±0.02	93.43±0.02
	2.6	17.4±0.1	2.18±0.01	7.0±0.1	2.53±0.02	2.83±0.01	2.81±0.02	761.95±0.02	93.69±0.02
	2.7	15.6±0.1	2.73±0.01	8.0±0.1	2.73±0.02	2.80±0.01	2.33±0.02	829.35±0.02	103.84±0.02
	2.8	17.8±0.1	2.71±0.01	7.1±0.1	2.92±0.02	3.19±0.01	2.97±0.02	771.61±0.02	97.51±0.02
	Name	Al ₂ O ₃ (wt%)	CaO(wt%)	Fe ₂ O ₃ (wt%)	K ₂ O(wt%)	MgO(wt%)	Na ₂ O(wt%)	Ba(ppm)	Cr(ppm)
Raw	F1	15.3±0.1	5.5± 0.02	6.4±0.1	2.07±0.02	2.42±0.01	3.05±0.02	659.54±0.02	84.16±0.02
Clay	F2	16.5±0.1	1.67±0.01	7.1±0.1	2.45±0.02	2.94±0.01	2.79±0.02	569.61±0.02	97.31±0.02

H1	13.4±0.1	5.93±0.02	6.0±0.1	1.61±0.02	2.63±0.01	3.33±0.02	529.09±0.02	81.97±0.02
H2	11.9±0.1	6.83±0.02	5.0±0.1	1.46±0.02	2.56±0.01	3.11±0.02	548.80±0.02	80.55±0.02
M1	18.5±0.1	3.28±0.01	9.0±0.1	2.25±0.02	3.64±0.01	2.14±0.02	741.35±0.02	117.43±0.02
M2	19.6±0.1	3.09±0.01	9.3±0.1	2.36±0.02	3.68±0.01	2.22±0.02	902.16±0.02	105.21±0.02

Class	Name	La(ppm)	Rb(ppm)	Sc(ppm)	Sr(ppm)	Y(ppm)	Yb(ppm)	Zr(ppm)
Ayla	1.3(2)	43.08±0.02	78.98±0.02	12.10±0.02	488.49±0.02	27.72±0.02	6.81±0.02	237.40±0.02
	1.4 (2)	35.51±0.02	50.82±0.02	6.22±0.02	478.99±0.02	24.11±0.02	5.63±0.02	194.88±0.02
	1.5	40.25±0.02	50.49±0.02	6.99±0.02	463.68±0.02	26.44±0.02	6.32±0.02	176.67±0.02
	1.7 (1)	36.38±0.02	68.37±0.02	8.95±0.02	512.82±0.02	24.49±0.02	6.86±0.02	16.09±0.02
	1.7(2)	38.94±0.02	62.96±0.02	10.64±0.02	505.19±0.02	24.89±0.02	6.59±0.02	226.72±0.02
	3.6	39.80±0.02	58.43±0.02	12.17±0.02	485.99±0.02	25.25±0.02	7.17±0.02	164.75±0.02
	CO4	42.62±0.02	70.68±0.02	12.33±0.02	497.59±0.02	26.92±0.02	7.04±0.02	181.71±0.02
LRA 1	1.9	13.09±0.02	46.81±0.02	10.15±0.02	533.16±0.02	17.98±0.02	6.87±0.02	99.64±0.02
	2.3	24.21±0.02	68.28±0.02	14.78±0.02	470.22±0.02	19.60±0.02	6.78±0.02	149.31±0.02
LRA1(?)	C02	17.76±0.02	52.33±0.02	9.18±0.02	448.68±0.02	17.79±0.02	5.81±0.02	120.86±0.02
	C03	22.07±0.02	43.39±0.02	19.77±0.02	448.79±0.02	19.57±0.02	8.01±0.02	149.87±0.02
	C06	20.67± 0.02	67.56±0.02	15.05±0.02	398.49±0.02	18.02±0.02	7.37±0.02	121.86±0.02
	C07	18.50±0.02	45.05±0.02	18.69±0.02	542.19±0.02	23.82±0.02	8.79±0.02	138.72±0.02
<i>Dolia</i>	4.8	28.83±0.02	64.50±0.02	17.63±0.02	358.49±0.02	21.21±0.02	8.07±0.02	151.47±0.02
	4.9	26.73±0.02	68.92±0.02	17.22±0.02	505.97±0.02	21.27±0.02	7.43±0.02	144.26±0.02
Red Slipped	4.5	58.99±0.02	88.06±0.02	26.45±0.02	176.65±0.02	35.13±0.02	6.25±0.02	471.09±0.02
	4.6	52.73±0.02	43.80±0.02	23.44±0.02	188.78±0.02	31.37±0.02	5.71±0.02	223.89±0.02
ND	2.4	49.53±0.02	111.10±0.02	14.31±0.02	331.59±0.02	27.00±0.02	7.20±0.02	127.19±0.02
	Name	La(ppm)	Rb(ppm)	Sc(ppm)	Sr(ppm)	Y(ppm)	Yb(ppm)	Zr(ppm)
	2.9	29.50±0.02	109.60±0.02	9.15±0.02	312.99±0.02	20.27±0.02	6.46±0.02	149.05±0.02
Bricks	4.10	20.38±0.02	47.99±0.02	17.36±0.02	337.12±0.02	25.52±0.02	7.43±0.02	155.97±0.02

	4.11	25.87±0.02	61.25±0.02	20.30±0.02	344.23±0.02	31.73±0.02	8.70±0.02	195.10±0.02
Local	2.5	23.09±0.02	40.58±0.02	20.87±0.02	296.58±0.02	25.62±0.02	8.93±0.02	156.31±0.02
	2.6	29.51±0.02	51.44±0.02	18.48±0.02	321.31±0.02	34.55±0.02	7.91±0.02	230.68±0.02
	2.7	38.20±0.02	64.77±0.02	18.72±0.02	257.64±0.02	35.01±0.02	9.15±0.02	201.18±0.02
	2.8	33.73±0.02	60.09±0.02	19.33±0.02	340.67±0.02	35.07±0.02	8.31±0.02	255.85±0.02
Raw Clay	F1	22.27±0.02	58.03±0.02	15.63±0.02	250.19±0.02	30.75±0.02	7.38±0.02	189.73±0.02
	F2	23.75±0.02	57.47±0.02	18.32±0.02	283.64±0.02	30.44±0.02	8.35±0.02	206.90±0.02
	H1	17.94±0.02	39.82±0.02	14.75±0.02	564.77±0.02	23.14±0.02	6.64±0.02	141.25±0.02
	H2	14.28±0.02	37.73±0.02	13.31±0.02	726.75±0.02	21.23±0.02	6.04±0.02	132.21±0.02
	M1	25.31±0.02	53.64±0.02	21.95±0.02	245.95±0.02	28.13±0.02	10.22±0.02	155.16±0.02
	M2	23.91 ±0.02	57.77±0.02	21.72±0.02	254.33±0.02	27.27±0.02	10.04±0.02	160.92±0.02

Appendix 13: Information on LOI of Samples

Sample	Crucible	Sample	Crucible + sample 105°C	Sample 105°C	Weight loss 105°C - %	Crucible + sample 1000°C	Sample 1000°C	Weight loss 1000°C - %
F1	10.1	0.1	10.2	0.1	-2.1	10.2	0.1	-7.9
F2	13.2	0.1	13.3	0.1	-1.7	13.3	0.1	-6.6
H1	15.7	0.1	15.8	0.1	-1.6	15.8	0.1	-9.2
H2	9.5	0.1	9.6	0.1	-1.7	9.6	0.1	-13.2
M1	10.0	0.1	10.1	0.1	-1.4	10.1	0.1	-9.6
M2	10.0	0.1	10.1	0.1	-1.4	10.1	0.1	-8.7
C02	10.1	0.1	10.2	0.1	-0.4	10.2	0.1	-7.3
C03	9.8	0.1	9.9	0.1	-0.6	9.9	0.1	-7.8
C04	9.6	0.1	9.7	0.1	-0.7	9.7	0.1	-3.3
C06	10.0	0.1	10.1	0.1	-0.2	10.1	0.1	-9.4
C07	12.5	0.1	12.6	0.1	-0.6	12.6	0.1	-8.9
1.3(2)	9.7	0.1	9.8	0.1	0.00	9.8	0.1	-3.2
1.4(2)	14.3	0.1	14.4	0.1	-1.1	14.4	0.1	-2.8
1.5	9.8	0.1	9.9	0.1	-0.4	9.9	0.1	-0.7
1.7(1)	9.2	0.1	9.3	0.1	-0.4	9.3	0.1	-8.5
1.7(2)	12.2	0.1	12.3	0.1	-0.9	12.3	0.1	-2.1
1.9	12.5	0.1	12.6	0.1	0.00	12.6	0.1	-11.2
2.3	10.9	0.1	11.0	0.1	-1.4	11.0	0.1	-19.4
2.4	9.5	0.1	9.6	0.1	-0.1	9.6	0.1	-4.6
2.5	13.2	0.1	13.3	0.1	1.2	13.3	0.1	0.7
2.6	9.3	0.1	9.5	0.1	-0.1	9.4	0.1	-2.4
2.7	12.5	0.1	12.6	0.1	-0.9	12.6	0.1	-4.1
2.8	9.3	0.1	9.4	0.1	1.1	9.4	0.1	-1.5
2.9	9.8	0.1	9.9	0.1	-0.3	9.9	0.1	-3.4

Sample	Crucible	Sample	Crucible + sample 105°C	Sample 105°C	Weight loss 105°C - %	Crucible + sample 1000°C	Sample 1000°C	Weight loss 1000°C - %
3.6	12.5	0.1	12.6	0.1	-1.0	12.63	0.1	-3.7
4.5	9.2	0.1	9.3	0.1	-0.6	9.28	0.1	-3.2
4.6	9.3	0.1	9.4	0.1	-0.4	9.39	0.1	-1.5
4.8	15.7	0.1	15.8	0.1	0.7	15.78	0.1	-5.2
4.9	10.7	0.1	10.8	0.1	-0.4	10.77	0.1	-11.4
4.10	16.9	0.1	17.0	0.1	0.1	16.96	0.1	-0.4
4.11	9.7	0.1	9.8	0.1	-0.6	9.76	0.1	-3.4

Sample	Initial weight	Weight loss 1000°C - %	Final weight
C02	0.1	-7.3	0.1
1.4 (2)	0.1	-2.8	0.1
1.5	0.1	-0.7	0.1
1.7 (1)	0.1	-8.5	0.1
1.9	0.1	-11.2	0.1
2.9	0.1	-3.4	0.1
F1	0.1	-7.9	0.1
F2	0.1	-6.6	0.1
H1	0.1	-9.2	0.1
H2	0.1	-13.2	0.1
M1	0.1	-9.6	0.1
M2	0.1	-8.7	0.1
CO3	0.1	-7.8	0.1
CO4	0.1	-3.3	0.1
CO6	0.1	-9.4	0.1

CO7	0.1	-8.9	0.1
1.3(2)	0.1	-3.2	0.1
1.7(2)	0.1	-2.1	0.1
2.3	0.1	-19.4	0.1
2.4	0.1	-4.6	0.1
2.5	0.1	0.7	0.1
2.6	0.1	-2.4	0.1
2.7	0.1	-4.1	0.1
2.8	0.1	-1.5	0.1
3.6	0.1	-3.7	0.1
4.5	0.1	-3.2	0.1
4.6	0.1	-1.5	0.1
4.8	0.1	-5.2	0.1
4.9	0.1	-11.4	0.1
4.10	0.1	-0.4	0.1
4.11	0.1	-3.4	0.1

Appendix 14: ICP-OES Data on Certified Materials

	Al ₂ O ₃ (wt%)	MIN	MAX	CaO (wt%)	MIN	MAX	Fe ₂ O ₃ (wt%)	MIN	MAX	K ₂ O (wt%)	MIN	MAX	MgO (wt%)	MIN	MAX
SARM69 (cert)	14.4	14.2	14.5	2.4	2.3	2.4	7.2	7.1	7.3	2.0	1.9	2.0	1.9	1.8	1.9
SARM69 t0	13.7	13.6	13.7	2.4	2.4	2.5	6.8	6.8	6.9	1.8	1.7	1.8	1.9	1.9	1.9
SARM69 t1	13.7	13.7	13.8	2.4	2.3	2.4	6.6	6.5	6.6	1.7	1.6	1.7	1.9	1.9	1.9
SARM69 t2	13.5	13.4	13.6	2.4	2.4	2.4	6.7	6.7	6.8	1.7	1.7	1.7	1.8	1.8	1.8
SARM69 BIS t0	12.5	12.5	12.6	2.1	2.1	2.1	6.1	6.1	6.2	1.4	1.4	1.5	1.7	1.7	1.7
SARM69 BIS t1	11.8	11.7	12.0	2.2	2.2	2.2	5.9	5.8	5.9	1.5	1.5	1.6	1.7	1.7	1.7

	MnO (wt%)	MIN	MAX	Na ₂ O (wt%)	MIN	MAX	TiO ₂ (wt%)	MIN	MAX	Ba (ppm)	MIN	MAX	Cr (ppm)	MIN	MAX
SARM69 (cert)	0.1	0.1	0.1	0.8	0.8	0.8	0.8	0.8	0.8	518.0	499.0	537.0	223.0	215.0	230.0
SARM69 t0	0.1	0.1	0.1	0.8	0.8	0.8	0.7	0.7	0.7	476.0	454.0	498.0	210.0	207.0	214.0
SARM69 t1	0.1	0.1	0.1	0.8	0.8	0.8	0.7	0.7	0.7	464.0	446.0	482.0	212.0	206.0	218.0
SARM69 t2	0.1	0.1	0.1	0.8	0.8	0.8	0.7	0.7	0.7	468.0	449.0	486.0	229.0	83.0	375.0
SARM69 BIS t0	0.1	0.1	0.1	0.7	0.7	0.7	0.6	0.6	0.7	437.0	421.0	453.0	206.0	200.0	211.0
SARM69 BIS t1	0.1	0.1	0.1	0.7	0.7	0.8	0.6	0.6	0.6	412.0	395.0	429.0	214.0	80.0	348.0

	Cu (ppm)	MIN	MAX	Rb (ppm)	MIN	MAX	Sr (ppm)	MIN	MAX	Sc (ppm)	MIN	MAX
SARM69 (cert)	46.0	43.0	48.0	66.0	65.0	67.0	109.0	108.0	110.0	20.0	19.0	21.0
SARM69 t0	41.0	39.0	43.0	60.0	57.0	63.0	110.0	108.0	112.0	9.0	-1.0	19.0
SARM69 t1	<LOQ			59.0	57.0	61.0	110.0	109.0	111.0	17.0	16.0	18.0
SARM69 t2	44.0	27.0	60.0	60.0	52.0	68.0	109.0	108.0	110.0	17.0	16.0	18.0
SARM69 BIS t0	52.0	44.0	60.0	52.0	50.0	54.0	106.0	105.0	107.0	15.0	14.0	16.0
SARM69 BIS t1	50.0	35.0	65.0	49.0	42.0	56.0	102.0	101.0	103.0	16.0	15.0	17.0

	V (ppm)	MIN	MAX	Y (ppm)	MIN	MAX	Zr (ppm)	MIN	MAX
SARM69 (cert)	157.0	156.0	158.0	29.0	28.0	30.0	271.0	270.0	272.0
SARM69 t0	<LOQ			25.0	24.0	26.0	267.0	264.0	270.0
SARM69 t1	<LOQ			25.0	24.0	26.0	272.0	270.0	274.0
SARM69 t2	<LOQ			25.0	24.0	26.0	264.0	263.0	266.0
SARM69 BIS t0	<LOQ			22.0	21.0	23.0	257.0	243.0	270.0
SARM69 BIS t1	<LOQ			23.0	22.0	24.0	236.0	224.0	249.0

	Al (wt%)	MIN	MAX	Ca (wt%)	MIN	MAX	Fe (wt%)	MIN	MAX	K (wt%)	MIN	MAX	Mg (wt%)	MIN	MAX
98B (cert)	14.3	14.1	14.5	0.1	0.1	0.1	1.2	1.2	1.2	2.8	2.7	2.9	0.4	0.4	0.4
98B t0	14.4	14.3	14.4	0.1	0.1	0.1	1.2	1.1	1.2	2.9	2.8	2.9	0.4	0.4	0.4

98B t1	14.3	14.3	14.4	0.1	0.1	0.1	1.1	1.1	1.2	2.6	2.5	2.6	0.4	0.4	0.4
98B t2	13.4	13.4	13.5	0.1	0.1	0.1	1.1	1.0	1.1	2.7	2.7	2.7	0.4	0.4	0.4
98B BIS t0	14.8	14.8	14.8	0.1	0.1	0.1	1.2	1.1	1.2	2.6	2.5	2.6	0.4	0.4	0.4
98B BIS t1	13.7	13.6	13.8	0.1	0.1	0.1	1.1	1.1	1.2	2.7	2.7	2.7	0.4	0.4	0.4

	Mn (wt%)	MIN	MAX	Na (wt%)	MI N	MAX	Ti (wt%)	MIN	MAX	Ba (wt%)	MIN	MAX	Cr (wt%)	MIN	MAX
98B (cert)	0.0	0.0	0.0	0.2	0.1	0.2	0.8	0.8	0.8	0.1	0.1	0.1	0.0	0.	0.01
98B t0	0.0	0.0	0.0	0.2	0.2	0.2	0.8	0.8	0.8	0.1	0.0	0.1	0.0	-0.0	0.0
98B t1	0.0	0.0	0.0	0.1	0.1	0.2	0.8	0.8	0.8	0.1	0.0	0.1	0.0	-0.0	0.0
98B t2	0.0	0.0	0.0	0.2	0.2	0.2	0.8	0.8	0.8	0.1	0.0	0.1	0.0	-0.0	0.0
98B BIS t0	0.0	0.0	0.0	0.1	0.1	0.2	0.8	0.8	0.8	0.1	0.0	0.1	0.0	-0.0	0.0
98B BIS t1	0.0	0.0	0.0	0.2	0.1	0.2	0.8	0.8	0.8	0.1	0.0	0.1	0.0	-0.0	0.0

	Eu (ppm)	Rb (wt %)	MIN	MAX	Sc (ppm)	MIN	MAX	Sr (wt%)	MIN	MAX	Zr (wt%)	MIN	MAX
98B (cert)	1.3	0.0	0.0	0.0	22.0	21.0	23.0	0.0	0.0	0.0	0.0	0.0	0.0
98B t0	<LOQ	0.0	-0.0	0.0	11.0	11.0	21.0	0.0	0.00	0.0	0.0	0.00	0.0
98B t1	<LOQ	0.0	-0.0	0.0	21.0	20.0	22.0	0.0	0.00	0.0	0.0	0.00	0.0
98B t2	<LOQ	0.0	-0.0	0.0	21.0	20.0	22.0	0.0	0.00	0.0	0.0	0.00	0.0
98B BIS t0	<LOQ	0.0	-0.0	0.0	21.0	20.0	22.0	0.0	0.00	0.0	0.0	0.01	0.1
98B BIS t1	<LOQ	0.0	-0.0	0.0	21.0	20.0	22.0	0.0	0.00	0.0	0.0	0.00	0.0